MMV008138 and Analogs: Potential Novel Antimalarial Agents for *P. falciparum*

LIXUAN LIU

Thesis submitted to the faculty of the Virginia Polytechnic Institute and State University in partial fulfillment of the requirements for the degree of

Master of Science

In

Chemistry

Paul R. Carlier, (Chairman)

David G. I. Kingston

James M. Tanko

April 10th 2018

Blacksburg, VA

Keywords: malaria, antimalarial, *P. falciparum*, MEP pathway, IspD, MMV008138, structure-activity relationship

MMV008138 and Analogs: Potential Novel Antimalarial Agents for *P. falciparum*

LIXUAN LIU

ABSTRACT

Malaria is a severe and deadly mosquito-borne disease. Although treatable, the continuous emergence of multi-drug resistant parasite strains urgently calls for the development of novel antimalarial agents. *P. falciparum* parasites synthesize essential isoprenoid precursors, isopentenyl pyrophosphate (IPP) and dimethylallyl pyrophosphate (DMAPP), via a non-mevalonate pathway: the methylerythritol phosphate (MEP) pathway. This pathway is not utilized by humans. Thus, compounds that target the MEP pathway and disrupt isoprenoid biosynthesis in *P. falciparum* hold promise as potent and safe new antimalarial agents, that engage new targets.

Previously, we and others identified MMV008138 from the Malaria Box as a MEP pathway targeting compound. Later work revealed that it targets the IspD enzyme within the MEP pathway. Work in the Carlier group has established preliminary structure-activity relationship (SAR) of MMV008138: 1) (1*R*,3*S*)-configuration is required; 2) 2', 4'-disubstitution of the D-ring with small, electronegative substituents; 3) functional importance of carboxylate acid at C3.

In this work, I aim to gain further insight into the C3 SAR and A-ring SAR of lead compound MMV008138. Synthesized acid bioisosteres and A-ring analogs of MMV008138 were evaluated in their ability to inhibit *P. falciparum* parasite growth. We showed that the C3 substituent of MMV008138 has a very tight SAR, and likely interacts with a very constricted pocket within the *Pf*IspD enzyme. A-ring modifications are limited to certain positions of MMV001838 and need to be sterically small. However, we have yet to identify a modification that significantly improves drug lead potency.

Future work will continue towards understanding the A-ring SAR of MMV008138, as well as D-ring SAR and C1-SAR. Efforts will also be directed towards finding analogs with improved potency, transport and metabolic stability.

MMV008138 and Analogs: Potential Novel Antimalarial Agents for *P. falciparum*

LIXUAN LIU

GENERAL ABSTRACT

Malaria is a severe and deadly mosquito-borne disease, caused by malaria parasites. Although treatable, the continuous emergence of drug resistance urgently calls for the development of novel antimalarial agents. Research in the Carlier group is aimed at finding drug molecules that can selectively target and kill the malarial parasite, and at the same time be safe to humans. The Carlier group has identified MMV008138 from the Malaria Box as a promising drug lead. In this work, I aim to understand the how the structure of MMV008138 play a role in its ability to kill malaria parasites. These results will help identify modification strategies that may significantly improve drug lead potency.

Acknowledgements

I would like to start by thanking my research advisor Dr. Paul R. Carlier, for his support, patience and encouragement in the past three years. His knowledge, insight and understanding of scientific research is and will always be a personal inspiration and a goal I hope to achieve in my future career. I still remember the beginning of my research when Dr. Carlier would carefully guide me through procedures, techniques and understanding data. His mentorship is crucial to getting me to where I am today, and I greatly appreciate all his effort in my education. I would also like to thank my committee members, Dr. David Kingston and Dr. James Tanko, for their insights and feedback during this process.

I want to give thanks to my colleagues in the Carlier group, Mr. Sha Ding, Ms. Kristyn Cagasova, Mr. Jeremy Cunningham and Ms. Maryam Ghavami, for all the help that they offered to me these past 3 years. I would also like acknowledge our collaborator Dr. Belen Cassera, for the invaluable biological data on our compounds. And, I want to give special thanks to Dr. Zhongke Yao for all his help with my synthesis and tips on lab works. He gave me valuable assistance in starting as an organic chemist.

Finally, I want to thank my parents, for their constructive advice, and more importantly, for standing by me with each decision I make.

Table of contents

List of Figures

List of Tables

List of Contributors

Dr. Maria Belen Cassera: *P. falciparum* Dd2 strain and *Pf*IspD growth inhibition assays; IPP rescue assays; and other biological studies.

Dr. Zhongke Yao: Synthesis of compounds **27a**, *ent*-**27a**, **28a**, *ent*-**28a**, **30a**, *ent*-**30a**, *ent*-**29a**, **29a-j**, (±)-**32**, **33-41** and **48-51**.

Maryam Ghavami: Synthesis of compounds **29k-29ab**. Established synthesis of racemic substituted tryptophan methyl esters (Figure26).

Kristyna Cagasova: Identification of trace impurities in MMV008138 (**29a**) analog ^{1}H NMRs.

Chapter 1: Malaria Treatment and Utilizing the MEP Pathway for Novel Antimalarial Development

1.1 Malaria

1.1.1 Malaria and Malaria Parasites

Malaria is a mosquito-borne infectious disease caused by malaria parasites that belong to the genus *Plasmodium*. Parasites are transmitted to humans via the bites of infected female *Anopheles* mosquitoes, which are called "malaria vectors". On rare occasions, the disease can also be transmitted via blood transfusion.

There are five species of *Plasmodium* parasites that are known to cause malaria in humans: *P. vivax, P. ovale, P. malariae, P. knowlesi* and *P. falciparum*.[3] Of these five, *P. falciparum* is the most prevalent species and accounts for the majority of malaria-related deaths, especially in sub-Saharan Africa.[4]

1.1.2 Malaria Parasite Life Cycle

Understanding of the life cycle of the *Plasmodium* parasites (Figure 1) is important to gaining insight into the transmission and infection of malaria. An infected female *Anopheles* mosquito acts as the malaria vector, causing human infection by a bite (blood-feeding). Humans are initially infected with the parasites in the form of sporozoites, which travel through the blood stream and migrate to the liver. Sporozoites will invade the liver cells where they develop into thousands of merozoites, rupture the liver cells, and return to the bloodstream and begin a human blood cell cycle known as asexual replication. It is this stage of the cycle that results in the clinically observed symptoms of malaria infection. Ultimately, a portion of the merozoites develop into gametocytes, which are the sexual form of the malaria parasite. Gametocytes are the transmissible form of *Plasmodium sp*.; when taken up with blood through a mosquito bite, they can enter the sporogenic cycle within the mosquito, forming new sporozoites. Disease transmission occurs when such an infected mosquito bites an uninfected human.[3]

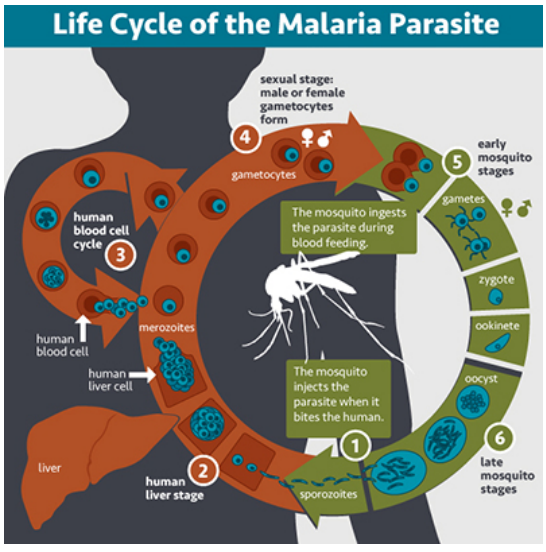

Figure 1. Life cycle of the malaria parasite.[2]

1.1.3 Global Status of Malaria

Malaria has long been a severe health concern worldwide. Through decades of effort, malaria has become preventable and treatable, and a great decline in global malaria burden is seen since 2000. However, over 3 billion of the world's population, spread over 106 countries and territories, still live in areas at

risk of malaria transmission. Malaria continues to be one of the leading causes of death each year, particularly in low-income economies.

Malaria occurrence is very dependent on climatic factors, especially temperature. *P. falciparum*, for example, cannot complete its life cycle in host mosquitos at temperatures lower than 20°C (68°F), and as a result malaria cannot be transmitted in that environment. Thus, malaria is transmitted mainly in tropical and subtropical areas. Transmission is most intense in a broad band around the equator, in areas of the Americas, many parts of Asia, and much of Africa, particularly Sub-Saharan Africa (Figure 2). As we move up the latitude into cooler regions, malaria occurrence is more scarce and seasonal. There, *P. vivax* can be more prevalent than *P. falciparum*, due to its tolerance of lower ambient temperatures.

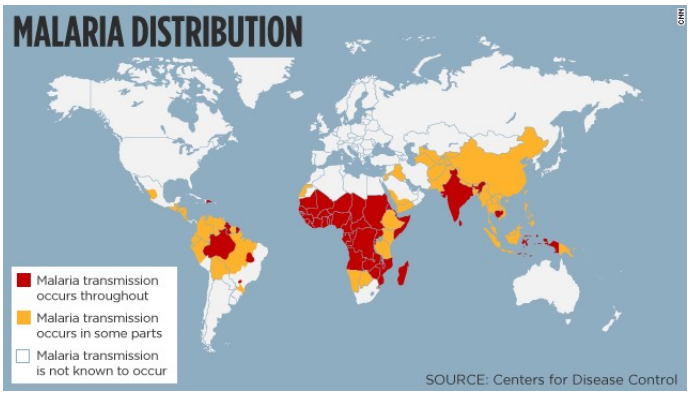

Figure 2. World malaria map.[1]

According to *World Malaria Report 2017*,[4] an estimated 216 million cases of malaria occurred globally in 2016, which is 5 million more than 2015. Of these cases, 96% were caused by *P. falciparum*. Malaria-related deaths were estimated to be 407,000 globally in 2016, which reflects a small reduction from the estimated 446, 000 cases in 2015. Among the malaria endemic areas, Africa carries the majority of the global malaria burden. It is home to approximately 90% of all malaria cases and 91% of malaria deaths, in 2016. Overall, malaria remains a world-wide health threat and concern. Much effort is still needed towards its control, reduction and ultimate elimination.

1.1.4 Malaria Control

In our battle to control malaria, two important points of focus are: prevention and treatment. Preventive methods for malaria include: medication, vector control and prevention of mosquito bites. There are several preventive drugs available, many of which are also used in malaria treatment, such as chloroquine, mefloquine and doxycycline (Figure 3). Due to drug costs, side effects and difficulty in obtaining drugs in poorer countries, preventive medication is impractical for those residing in malaria endemic countries, and are primarily only used in travelers and pregnant women. Drug safety is obviously of paramount concern for pregnant women, who cannot take doxycycline due to its association with the disruption of fetal tooth and bone development.[5-6]

Vector control, which refers to methods that decrease malaria by reducing transmission by mosquitos, is the main and most effective way towards prevention and reduction of malaria transmission. Currently, the most widely adopted methods are use of insecticide-treated mosquito nets (ITNs) and indoor residual spraying (IRS). ITNs are mosquito nets treated with insecticides and are usually retreated every six month. IRS, on the other hand, is the process of spraying a dilute solution of insecticide indoors to kill mosquitos. Effective vector control has greatly alleviated the malaria burden, however, both methods face the problem of insecticide resistance.[7-8]

Yet, for people already infected with malaria, it is too late for vector control, and effective treatment is essential. Not only does it cure the illness and prevent related deaths, it also contributes to reducing malaria transmission. Antimalarial development is critical to the fight against this disease and is a main research focus in the Carlier group.

1.2 Malaria Treatment

Malaria treatment has a long history: attempts to specifically treat malaria can be tracked back to the early 18th century, and it has come a long way since then. Some clinically and historically important antimalarial agents include: quinine, chloroquine, mefloquine and artemisinin (Figure 3).[9-10]

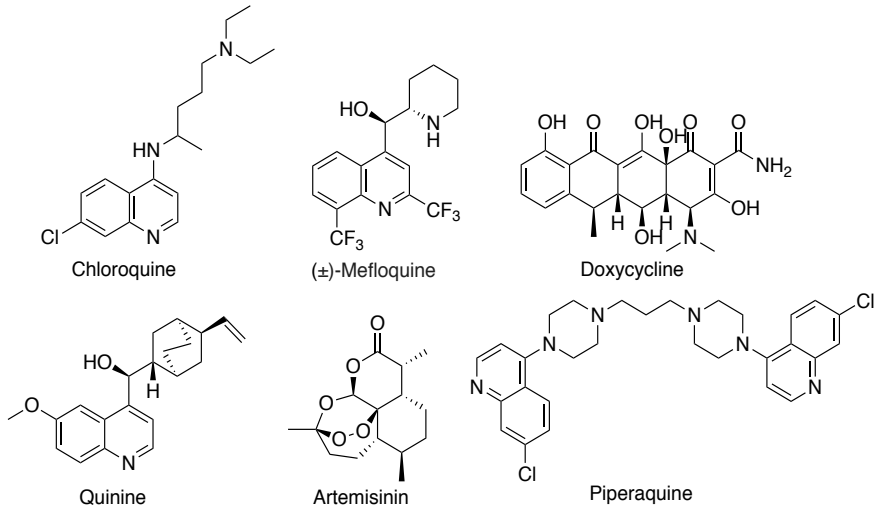

Figure 3. Clinically important antimalarial agents.

Quinine (Figure 3), first isolated from the Cinchona tree bark in 1820, is one of the earliest compounds used in malaria treatment.[11] Though the mechanism of action of quinine is not fully understood, it is hypothesized to be toxic to the parasite by interfering with its ability to take up hemoglobin.[12] Compared to other antimalarials currently available, quinine has relatively low efficacy and tolerability. However, despite this, it remains important in the treatment of multi-resistant malaria and acute cases of severe malaria caused by *P. falciparum*. Quinine has good solubility and can be prepared for intravenous use; thus, it is often the only option for treatment in cases of severe malaria where patients cannot tolerate oral medication.

Chloroquine (Figure 3), is one of the earliest commercially available antimalarial agents, and is the prototype of the 4-aminoquinoline class of antimalarials. Since its use in 1946, it has proven to be the most effective and successful single drug for the prophylaxis and treatment of malaria.[13] Chloroquine is safe to use, even during pregnancy, and affordable. Its efficacy played a crucial role in global reduction of malaria. The toxicity of chloroquine towards malaria parasites is believed to rise from its ability to inhibit the crystallization process of free heme to hemozoin in the parasite's acidic food vacuole.[11] Chloroquine resistant parasite strains began to emerge in the 1960s, no doubt due to widespread distribution of the drug as preventive medication. Resistance became widespread in the 1970s, and today chloroquine-resistant strains of *P. falciparum* are common in all malaria-endemic areas. Some strains of *P. vivax* are still sensitive to chloroquine, but in areas of Asia and Southern America resistant strains are found to be over 50%. Due to the challenge posed by chloroquine resistance in parasites, new antimalarial agents were urgently sought, resulting in the development of mefloquine.[9, 14-15]

Mefloquine (Figure 3), used in its *erythro* racemate form, is structurally similar to quinine (a so-callled "quinoline methanol"). It was developed for use against multi-drug resistant *P. falciparum*. Mefloquine has a long half-life and is highly active against most chloroquine resistant *Plasmodium* strains. Its mechanism of action was originally believed to be similar to chloroquine. However, recent findings suggest that mefloquine kills parasites by inhibiting hemoglobin endocytosis.[16-17] Widespread use of this drug, particularly in Asia, has resulted in significant reduction of efficacy as a monotherapy. Mefloquine use also may present severe side effects such as insomnia, depression and panic attacks. Thus, although mefloquine is a highly effective antimalarial, it is strictly used for resistant strains.[9]

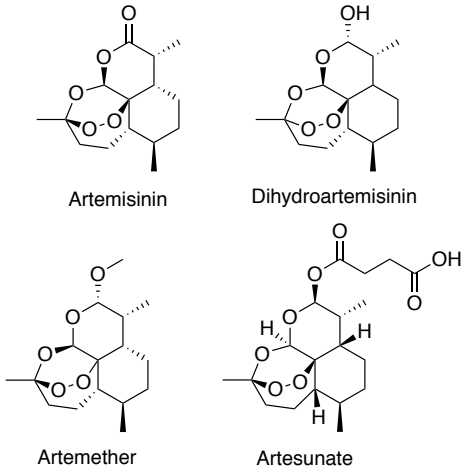

Figure 4. Artemisinin and its derivatives.

Artemisinin (Figure 4) and its derivatives are a large group of drugs used for treatment of *P. falciparum* malaria. Artemisinin was isolated by Chinese scientist Youyou Tu (co-awardee of the 2015 Nobel Prize in Chemistry), from an herb used in Chinese traditional medicine called *Artemisia annua*. Upon administration of the drug, artemisinin and its derivatives metabolize to dihydroartemisinin (Figure 4), which is the main bioactive compound. Artemisinin act faster than other available malaria treatment, and it is active against gametocytes (sexual stage of parasite), which are responsible for disease transmission. It is often used in combination with a partner antimalarial drug that has a

longer half-life, such as piperaquine (Figure 3). This is intended to reduce treatment duration and more importantly prevent development of resistance. Starting in the early 21st century, artemisinin-based combination therapy(ACT) has been adopted worldwide as first-line malaria therapy for *P. falciparum* malaria, and has seen significant results.[4, 9, 13] ACT is by far the most effective malaria treatment available for *P. falciparum* malaria, and is also increasingly being used in *P. vivax* malaria.

Artemether and artesunate (Figure 4) are the most widely used hemi-synthetic derivatives of arteminisin.[9] Artemether is more lipophilic, allowing for oral administration. Artesunate is a relatively unstable drug and rapidly releases dihydroartemisinin upon administration. However, its free carboxylate moiety makes the drug water soluble, allowing for intravenous administration to treat severe and acute cases of malaria.

Resistance is a serious and ever existing problem. Resistance to artemisinin derivatives was first documented in Cambodia and is now widely detected in Southeast Asia, including Thailand, Viet Nam, Myanmar, etc.[18-20] The continuous and emerging resistance to current antimalarials poses a great challenge for malaria control. Moreover, there are rising concerns that *P. falciparum* malaria will be increasingly more difficult to treat as multi-drug resistant strains arise. Thus, there is a pressing need to develop new antimalarial agents that are of high activity and safe to administer. As we have noted, resistance to antimalarial drugs can arise from mutations in the antimalarial target, or by upregulation of enzymes that efflux drug from the parasite (or its food vacuole). It is the goal of current research in the Carlier group to synthesize new, potent and safe antimalarial agents that engage new targets, in hope that they can circumvent these existing resistance mechanisms.

1.3 The MEP pathway – A New Target for Antimalarial Agents

1.3.1 The Apicoplast of *P. falciparum*

In the 20th century, it was discovered that *P. falciparum* carries a plastid organelle, the apicoplast.[21] In the late 20th century and the early 21st century, it was established that this relic chloroplast is prokaryotic in origin, has "plant-like" characteristics, and contains non-mammalian metabolic pathways that have no counterpart in the human host. Such biologically fascinating features made it an attractive therapeutic target.[21-23]

One interesting observation related to the apicoplast is a unique "delayed-death" phenomenon.[24] This phenomenon is observed when parasites are treated with drugs that interfere with its basic housekeeping processes. In experiments conducted by Dahl *et al*.,[24] parasites were treated with antibiotics, such as doxycycline, which inhibit prokaryotic transcription, specifically blocking the expression of the apicoplast genome. Parasites in the first life-

cycle appeared unaffected by the loss of apicoplast-encoded gene products, however, in the second life cycle following antibiotic treatment, the apicoplast genome failed to replicate and parasite death was observed within 96 hours. In contrast, when parasites are treated with drugs that instead interrupt the biosynthesis of fatty acids and isoprenoids, for example, relatively rapid parasite death is observed (24-48 h). These results, taken together, indicate that the anabolic products of the apicoplast are essential for parasite growth and demonstrate that the apicoplast plays a crucial role in the parasite. It was also later established that the apicoplast functions are necessary for *P. falciparum* development in the human host.[25-27] This essentiality of the apicoplast has greatly motivated researchers to investigate the possibility of its component metabolic pathways as antimalarial drug targets.[22-23]

Though the metabolic pathways of the apicoplast have not been fully characterized, a few that have been identified include: fatty acid biosynthesis, isoprenoid precursor biosynthesis, and iron-sulfur cluster biosynthesis. Among these, the MEP pathway employed by *P. falciparum* for isoprenoid precursor biosynthesis attracted the attention of researchers and ushered in new prospects in antimalarial drug development for two main reasons:
1) Isoprenoids are a large family of compounds with diverse structures and chemical properties that fulfill a range of functions of great biological importance.[28] For example, vitamins A, D, E and K are essential nutrients; cholesterol is an essential component of animal cell membranes; steroids are important signaling molecules; and farnesylated proteins participate in signal transduction as well as cell cycle regulation.[28-29] Yet, despite their striking diversity, all isoprenoids have universal precursors: isopentenyl pyrophosphate (IPP, **1**) and dimethylallyl pyrophosphate (DMAPP, **2**). Thus, the biosynthesis pathway of isoprenoid precursors has significant importance in all organisms.
2) The MEP pathway is essential in plants, apicomplexan protozoa such as *P. falciparum*, and most Gram-negative bacteria; in archaea, animals and human hosts the mevalonate pathway provides IPP and DMAPP.[30-31]

1.3.2 The MEP Pathway - Isoprenoid Precursor Biosynthesis in *P. falciparum*

The mevalonate pathway for biosynthesis of IPP (**1**) and DMAPP (**2**) originating from acetyl-coenzyme A(CoA), in yeast and animal cells, was established by studies conducted in the Bloch, Cornforth and Lynen groups.[32-33] It was believed to be the only metabolic pathway employed by all organisms and the sole source of isoprenoid precursors. It was not until the early 1990s that Rohmer and Arigoni independently recognized biosynthetic data that contradicted with the sole operation of the mevalonate pathway.[34-36] Further investigations ultimately led to the discovery of a non-mevalonate pathway, also known as the MEP pathway, which occurs in plants, algae, certain types of bacteria and apicomplexan parasites.

The MEP pathway (Figure 5) utilizes pyruvate (**3**) and D-glyceraldehyde 3-phosphate (G3P, **4**) as building blocks for isoprenoid precursor synthesis, it contains eight reaction steps catalyzed by seven enzymes, as shown in Figure 5.[37-41]

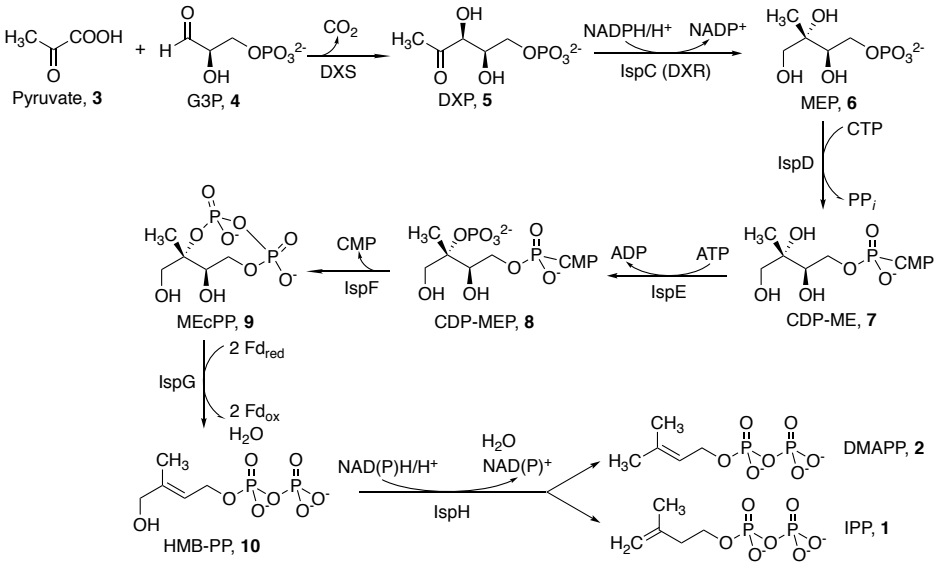

Figure 5. The MEP pathway for IPP (**1**) and DMAPP (**2**) biosynthesis.

1.4 Targeting the MEP Pathway

1.4.1 Prospects of the MEP Pathway as Antimalarial Target

From previous research regarding the MEP pathway, it has been established that the malaria parasite utilizes this pathway for biosynthesis of isoprenoid precursors, and that this pathway is essential to parasite survival and growth. The pathway employs seven different enzymes, all of which can be possible targets for antimalarial agents.[42] Moreover, human hosts do not use the MEP pathway for supply of isoprenoid precursors. These traits have made the MEP pathway an interesting target for antimalarial development in the Carlier group. It is also important to note that some beneficial bacteria in the human body also utilize the MEP pathway, and so selectivity for the parasite over these bacteria would be a beneficial feature of a malaria drug. The unique characteristics of the MEP pathway have encouraged the promise of antimalarial development by targeting MEP pathway enzymes.[43-44] To facilitate the rational development of such antimalarial agents, it is worthwhile to learn about current inhibitors for the MEP pathway enzymes.

1.4.2 Established MEP Pathway Enzyme Inhibitors

The HTS method of hit discovery is often the go-to choice for researchers to identify MEP pathway targeting molecules, since hits can be later rationally modified into leads. In recent years, growing numbers of crystal structures of MEP pathway enzymes have been characterized, which is greatly beneficial to efforts in lead discovery and drug development, particularly structure based drug design. Up to now, inhibitors have been reported for every

enzyme of the MEP pathway, mostly in Gram-negative bacteria (e.g. *E. coli*), plants, and *Mycobacterium tuberculosis*.[43] Here, I will focus on IspC and IspD enzyme inhibitors as they are, respectively, the most studied and most relevant to my research.

1.4.2.1 Inhibitors of 1-Deoxy-D-xylulose 5-phosphate reductoisomerase (IspC)

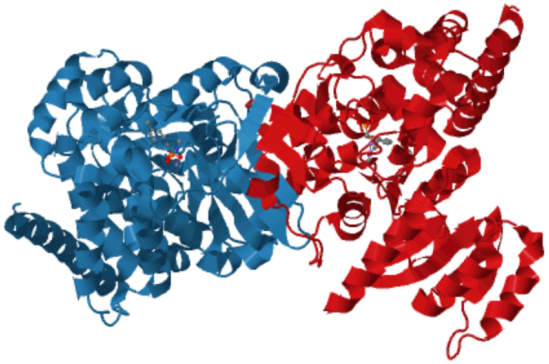

Figure 6. Structure of 3D7 strain *P. falciparum* IspC in complex with FOS analogue and manganese (PBD ID: 4Y6S).

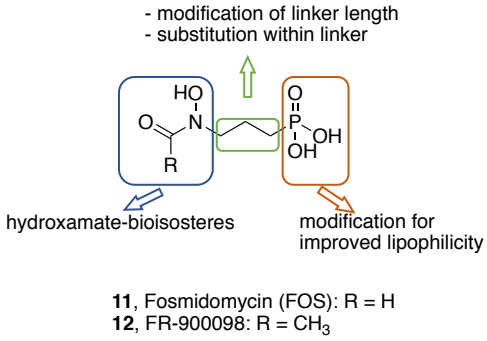

11, Fosmidomycin (FOS): R = H
12, FR-900098: R = CH_3

Figure 7. Fosmidomycin (**11**), FR-900098 (**12**) and positions for modification in scaffold.

P. falciparum Strain	IC_{50} (nM)	
	FOS (**11**)	FR-900098 (**12**)
HB3	350 ± 170	170 ± 100
A2	370 ± 45	170 ± 45
Dd2	290 ± 130	90 ± 20

Table 1. Growth inhibition data of IspC inhibitors FOS (**11**) and FR900098 (**12**)

IspC is by far the best understood enzyme of the MEP pathway with over 30 known (co)crystal structures from different organisms including *P. falciparum* (Figure 6). It catalyzes the second step in the MEP pathway, which is the conversion of DXP (**5**) to MEP (**6**).

Flexibility exists within the structure of IspC and this allows conformational change when the enzyme binds to ligands.[45] This kind of rearrangement shields the enzyme active site from bulk solvent and protects reactive intermediates from being solvent-exposed. Yet, it poses a great challenge in terms of drug design.

The most well-known IspC inhibitor is undoubtedly Fosmidomycin (FOS, **11**). Most IspC inhibitors developed so far are analogs of FOS or of its acetyl analog (FR-900098, **12**).[46-48] FOS (**11**) has been a MEP pathway targeting drug candidate for several years, and entered clinical trials as potential antimalarial agent. From Table 1, we can see that it displays good inhibitory activity against various strains of *P. falciparum*, but clinical evaluation showed FOS to exhibit undesired characteristics, of which the most significant is low bioavailability.[49] Thus, attention has been focused on modifications of FOS (**11**) and FR-900098 (**12**).[50] As illustrated in Figure 7, there are

three main modification approaches to produce analogs: 1) replacement of the hydroxamic acid moiety, 2) modification of the linker and 3) modification of the phosphate group.

Hydroxamates have very good metal chelating ability, making them strong inhibitors of enzymes that need metal cations as cofactor. So, it comes as no surprise that the hydroxamate moiety in FOS (**11**), FR-900098 (**12**) and their reverse hydroxamate analogs (Figure 8, **13** & **14**) are shown to be crucial for chelating divalent cations (Mg^{2+}) present in IspC active site.[51-52] Yet, the chelating ability of hydroxamates is not selective enough. They have good binding affinity for many metal cations besides Mg^{2+}. Also, pre-clinical studies of hydroxamates have shown that they are usually rapidly hydrolyzed or degraded *in vivo*, giving them poor pharmacokinetic and toxicological profiles.[53] Thus, to overcome the inherent limitations of the hydroxamate group, numerous attempts have been made to synthesize hydroxamate-bioisosteres of FOS and explore their inhibition properties.

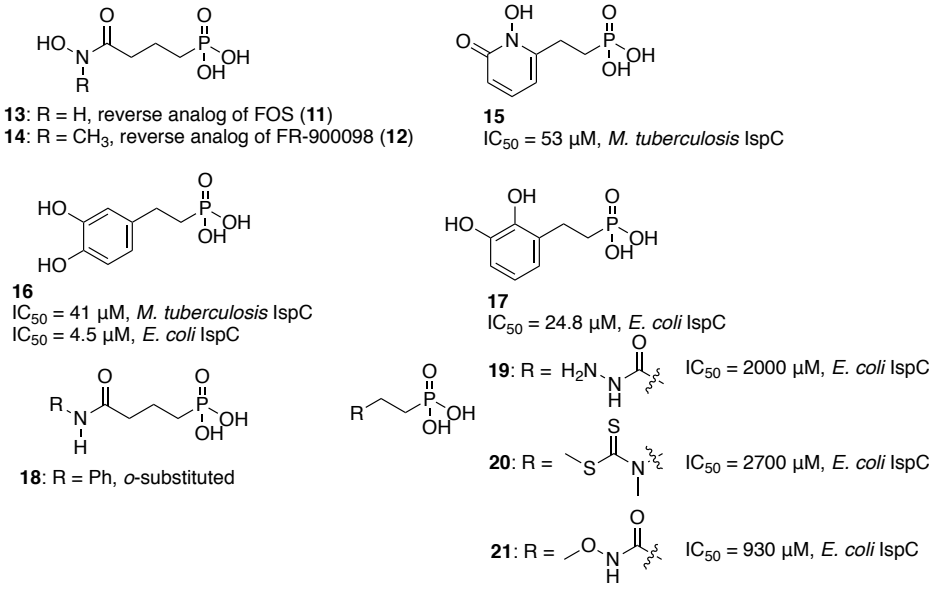

Figure 8: FOS (**11**) and FR-900098 (**12**) analogs with modified hydroxamate moieties.

Larhed *et al.* replaced the hydroxamate group of FR-90098 with a range of bulky heteroaryl and aryl rings to provide a more suitable chelating group and increase overall lipophilicity of the drug.[54] Two new active FOS analogs were identified (**15** & **16**), but unfortunately showed less than satisfactory results upon further enzyme assay study. It was hypothesized that this may be due to unwanted steric interactions of the aromatic ring with a narrow hydroxamate binding pocket.

It was previously established that a *cis*-geometry of the two oxygen atoms in the hydroxamate is required for metal chelation.[55] Song *et al.* further demonstrated that the position of chelating atoms, relative to the phosphate

group, is also important for inhibitory activity. This is reflected in assay data of **16** and **17**, where **16** (IC_{50} = 4.5 μM, *E. coli* IspC) is more potent than **17** (IC_{50} = 24.8 μM, *E. coli* IspC).[56]

van Calenbergh *et al.* made analogs that have the generic formula **18**, where the -R substituent is an *ortho*-substituted aryl ring.[57] It was expected that the aromatic ring would improve lipophilicity and the *ortho*-substituents (e.g. –OMe, -Ac, $-NMe_2$, etc) would take part in chelation of metal ions. Lipophilicity is undoubtedly improved; unfortunately, although majority of the *ortho*-substituents they selected are anions (at physiological pH) or simple Lewis bases, none of the analogs were found active against *P. falciparum* K1 in human erythrocytes (IC_{50} > 64 μM). The authors proposed that the poor flexibility of the amide bond results in lack of binding and inhibitory activity.

The Rohmer group also investigated hydroxamate-bioisosteres based on hydrazines (**19**), dithiocarbamates (**20**), and O-methyl hydroxamates (**21**). Unfortunately, none were found to have good inhibitory activity.[58] Current research results show the possibility that hydroxamate-bioisosteres of FOS and FR-900098 can lead to active inhibitors. But, identification of a good replacement for the hydroxamate moiety have proven difficult overall, and other modifications may be worth investigating.

Modification of the FOS and FR-900098 linker involves two strategies: modification of linker length and introduction of substituent group(s). Bodill, Kaye and others have identified the ideal linker length to be C3.[59-60] Addition of a double bond in the C3 linker (Figure 9, **22**) of FR-900098 (IC_{50} = 2.39 μM) showed improved potency with respect to **13** (IC_{50} = 1.07 μM) against *M. tuberculosis* IspC.

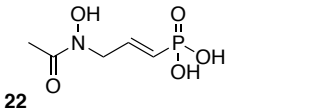

22
IC_{50} = 2.39 μM, *M. tuberculosis* IspC

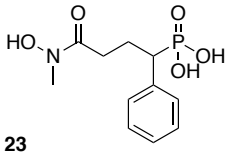

23
IC_{50} = 3.1 μM, *P. falciparum* IspC

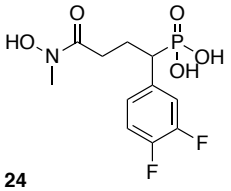

24
IC_{50} = 3.0 μM, *P. falciparum* IspC

Figure 9: FOS (**11**) and FR-900098 (**12**) analogs with modified linker.

The C3 linker of FOS and FR-900098 proves to be quite suitable for derivatization. Several studies show that incorporation of phenyl groups on the α-carbon to the phosphonate group of the reverse analogs (**23** & **24**) can increase their potency toward *P. falciparum* IspC with respect to the parent compounds. For example, compound **23** has an IC_{50} of 3.1 nM against *P. falciparum* IspC, while its parent compound FR-900098 has an IC_{50} of 15 nM; compound **24** has an IC_{50} of 3.0 nM against *P. falciparum* IspC, which is 10-fold higher than that of FOS.[61-62]

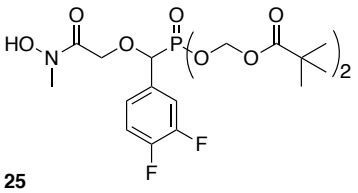

25
IC_{50} = 0.022 μM, *P. falciparum* IspC Dd2 strain

FOS (**11**)
IC_{50} = 0.81 μM, *P. falciparum* IspC Dd2 strain

Figure 10: FOS (**11**) based IspC inhibitor with modified phosphate group.

Modifications of the phosphonate group in FOS (**11**) and FR-900098 (**12**) have also been explored. One new IspC inhibitor found with a modified phosphonate group is compound **25,** reported by the Kurz group (Figure 10).[63] Compound **25** is a functionalized lipophilic ester prodrug. In growth inhibition assays on *P. falciparum* strain Dd2, compound **25** exhibited significantly better IC_{50} values than FOS. This suggests that masking the phosphonate group to make a lipophilic ester prodrug is a strategy worth further investigation. For one thing, such prodrugs would have better permeability across biological membranes. In addition, because ionization of the phosphonate group in FOS is thought to be behind its low bioavailability, its modification may overcome this problem. The discovery and identification of FOS and FR-900098 have indeed been encouraging. However, the suboptimal results from FOS clinical studies and FOS analog research pushes for investigation into other enzymes of the MEP pathway and other possible leads.

1.4.2.2 Inhibitors of 4-Diphosphocytidyl-2C-methyl-D-erythritol 4-phosphate Synthase (IspD)

As mentioned previously, IspD is the third enzyme in the MEP pathway, which catalyzes the transfer of a diphosphocytidyl group from cytidine triphosphate (CTP) to 2C-methyl-D-erythritol 4-phosphate (MEP, **6**), forming CDP-ME (**7**). This catalytic process requires the presence of Mg^{2+} to help the enzyme bind the substrates.

Our understanding of *P. falciparum* IspD is limited: up to now there are only 38 reported IspD crystal structures, including thirteen from *A. thaliana* IspD (*At*IspD), six from *E. coli* IspD (*Ec*IspD), and four from *M. tuberculosis* IspD (*Mt*IspD). No *P. falciparum* IspD crystal structures have been reported. However, primary sequence comparison shows that it has remarkable differences from plant and bacterial IspDs, in the sense that it is much larger. [64] This could be why *Pf*IspD has not yet been crystalized.

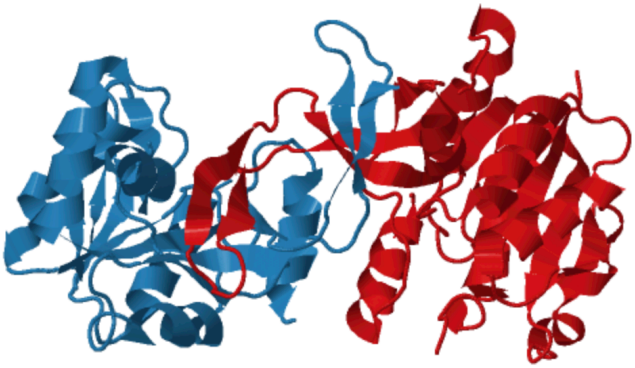

Figure 11. Crystal structure of *E. coli* IspD enzyme (PBD ID: 1VGU).

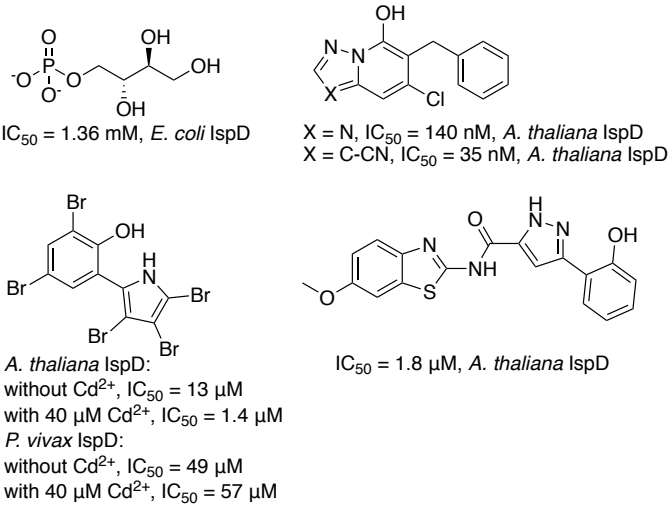

Figure 12. IspD enzyme inhibitors.

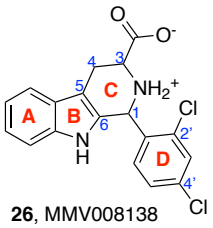

Figure 13. MMV008138 (**26**)

All IspD crystal structures known so far crystalize as homodimers. Figure 11 shows the crystal structure of the IspD enzyme in *E. coli*. Though IspD inhibitors are much less studied than IspC inhibitors, high throughput screening has identified new inhibitors for this enzyme, indicating the druggability of IspD. Figure 12 shows some of the reported inhibitors for IspD in *E. coli, A. thaliana*, and *P. vivax*.[44, 65-67] Worth to note, is the trihydroxybutyl phosphate *E. coli* IspD inhibitor, which is very similar to MEP (**6**) in structure (it is "desmethyl MEP"). Based on its close resemblance to MEP, this compound was found to be a weak MEP-competitive inhibitor of *E. coli* IspD.[66] Potent *A. thaliana* IspD inhibitors were also discovered. Pyrazolo[1,5-*a*]pyridine derivatives, reported by Witschel *et al.* are potent *A. thaliana* IspD inhibitors with IC_{50} in the nanomolar range.[44] Overall, IspD inhibitors reported thus far generally display activity in the millimolar range, and *P. falciparum* IspD inhibitors were rarely studied.

We and others have reported studies on an antimalarial compound MMV008138 (Figure 13, **26**).[68] Our collaborator Prof. Cassera (now of the University of Georgia) was the first to identify MMV008138 (**26**) as an inhibitor of the MEP pathway in *P. falciparum*. Later research by another group identified IspD as the target for MMV008138 (**26**). This compound and its analogs are a current research focus in the Carlier group, as well as a major focus of my master's research, and will be discussed below in further detail.

1.5 MMV008138 and Analogs as Potential Novel antimalarial

1.5.1 Discovery of MMV008138

As mentioned above, MMV008138 (**26**) was identified by our collaborator Prof. Belen Cassera, who applied a phenotypic screen to the Malaria Box. The Malaria Box was an open access library assembled by the Medicines for Malaria Venture (MMV) and Scynexis Inc. as an attempt to catalyze new antimalarial drug development.[69] MMV has since expanded its disease focus and now offers the Pathogen Box (pathogenbox.org). The Malaria Box comprised 400 compounds that were selected from phenotypic screening of over 4 million compounds based on factors including low toxicity, oral bioavailability, chemical diversity, etc. Though all 400 compounds were confirmed to have inhibitory activity against susceptible strains of asexual intraerythrocytic stages of *P. falciparum*, the mechanism of action of each individual compound is unknown.[69]

Because of the already established importance of the MEP pathway, our collaborator Prof. Cassera aimed to design a phenotypic screening method to identify any compounds in the Malaria Box that target this pathway. In 2011, a report by Profs. Yeh and DeRisi (UCSF and Stanford, respectively) demonstrated success in conducting IPP (**1**) chemical rescue of malaria parasites without the apicoplast, and their data show that apicoplast-absent parasites can survive *in vitro* at 200 μM IPP (**1**).[70] This result not only suggests that the MEP pathway is of essential function in this organelle, it also tells us that drugs effective against malaria by interrupting isoprenoid precursor synthesis, may have their effects reversed by IPP supplementation. Important also to note is that in parasites retaining their apicoplast, growth inhibition by FOS (**11**) can be rescued with IPP supplementation. Thus, a reversal of growth inhibition by IPP supplementation was proposed as the method for MEP pathway-targeting lead identification.[68] Based on these findings, Cassera designed the following screening method: compounds in the Malaria Box were first screened against asexual blood-stages of *P. falciparum* Dd2 strain. The Dd2 strain was chosen because it is a readily available (CDC) multiple-resistant parasite strain. Compounds that showed high inhibitory activity were followed by IPP supplementation rescue of drug-treated parasites, to identify MEP pathway inhibitors. Cassera set as her criterion a >95% growth inhibition at 5 μM of inhibitor and >60% reverse growth inhibition with 200 μM IPP supplementation. Only 18 compounds in the MalariaBox displayed >95% growth inhibition at 5 μM of inhibitor. Of these, MMV008138 (**26**) is the only compound that had its growth inhibition reversed with 200 μM IPP supplementation.[68]

1.5.2 Identifying the target of MMV008138

Upon identification of MMV008138 (**26**) as a compound that disrupts isoprenoid precursor synthesis, its target and mechanism of action came into question. The first step would be to narrow down whether MMV008138 (**26**) directly targets the MEP pathway, like FOS **(11)**, or whether it indirectly interferes with isoprenoid precursor synthesis, like doxycycline (DOX). As previously mentioned, some antibiotics are known to kill parasites via disruption of basic housekeeping processes of the organelles. Such is the case with DOX,[24, 71] which blocks protein translation in the apicoplast, indirectly interfering with isoprenoid precursor synthesis, and eventually results in parasite death. Like all such other antibiotics, a pronounced delayed-death phenotype will be observed during drug inhibition study with DOX. In contrast, inhibitors that directly target the MEP pathway, such as FOS (**11**), will display rapid onset of action. These statements are corroborated by data from an *in vitro* activity study of DOX, FOS (**11**) and MMV008138 (**26**) against asexual stages in different *P. falciparum* strains conducted by Cassera and Carlier *et al*. (Table 2).[68] By comparing the three data sets, we can see MMV008138 (**26**) displays a similar data pattern to that of FOS (**11**), in the sense that IC_{50} values at 72 h and 96 h are within two-fold of each other. However, DOX displays a delayed-death phenotype since there is a greater than five-fold decrease in IC_{50} between 72 and 96 h. This observation led Cassera *et al*. to propose that MMV008138 (**26**) has a mechanism of action that is more comparable to FOS (**11**) than DOX and that this drug directly targets the MEP pathway.

Compound	IC_{50} (nM) against:			
	Dd2[a]		NF54[b]	
	72 h	96 h	72 h	96 h
DOX	> 4,500	900 ± 180	2,370 ± 410	380 ± 60
FOS (**11**)	880 ± 70	430 ± 50	980 ± 60	ND
MMV008138 (**26**)	350 ± 50	180 ± 30	300 ± 10	ND

[a] *P. falciparum* Dd2 strain is a multi-resistant strain, including chloroquine-resistant.
[b] *P. falciparum* NF54 strain is chloroquine-sensitive. ND: not determined

Table 2. *In vitro* activity study of DOX, FOS (**11**), and MMV008138 (**26**) against different strains of asexual stage *P. falciparum*.

To verify their hypothesis, the effects of DOX, FOS (**11**) and MMV008138 (**26**) on apicoplast development were studied. In short, both FOS (**11**) and DOX are shown to inhibit apicoplast elongation and disturb mitochondrial membrane potential. Both effects can be fully reversed by IPP supplementation in FOS (**11**)-inhibited parasites, while in DOX inhibited parasites, only mitochondrial membrane potential can be restored.[68] As expected, when they conducted the same assay with MMV008138 (**26**), the MMV008138 (**26**) treated parasites displayed both inhibitory effects and both effects were fully reversed upon IPP supplementation. Such a result directly proves that

MMV008138 (**26**) and DOX attack different targets, and is consistent with the hypothesis that MMV008138 (**26**) may act directly on a target within the MEP pathway.

Several questions come to mind. What is the target of MMV008138 (**26**), and is it the same target as FOS (**11**), IspC? To shed light on this, MMV008138 (**26**) was further tested against a FOS-resistant *P. falciparum* strain (FOS^r). Comparing IC_{50} data of FOS^r strain with its parental strain Dd2 (Table 3),[68] we see that MMV008138 (**26**) showed no increase in IC_{50}, while the IC_{50} value for FOS (**11**) increased 4-fold. This is convincing evidence that IspC is unlikely to be the target of MMV008138 (**26**) within the MEP pathway. Later research by Wu *et al*. provided evidence that MMV008138 (**26**) targets IspD, the third enzyme in the MEP pathway.[72]

Compound	IC_{50} (nM) against:	
	Dd2 parasites at 72 h	FOS^r parasites at 72 h
FOS (**11**)	880 ± 70	3,330 ± 150
MMV008138 (**26**)	350 ± 50	250 ± 10

Table 3. IC_{50} data of FOS (**11**) and MMV008138 (**26**) against FOS^r strain and its parental strain Dd2.

Resistant Population	Gene ID[a]	Description[b]
08138R1	PF3D7_0106900	2-C-methyl-D-erythritol 4-phosphate cytidylyltransferase
	PF3D7_1247500	Putative protein kinase
	PF3D7_1456700	Conserved *Plasmodium* protein
08138R2	PF3D7_0106900	2-C-methyl-D-erythritol 4-phosphate cytidylyltransferase
	PF3D7_0302900	Putative exportin
	PF3D7_1478600	*Plasmodium* exported protein
08138R3	PF3D7_0106900	2-C-methyl-D-erythritol 4-phosphate cytidylyltransferase
	PF3D7_1417400	Cyclic nucleotide binding protein pseudogene

[a]PlasmoDB gene identification number. [b]Basic gene description based on PlasmoDB functional assignments.

Table 4. Summary of mutant genes in drug resistant strains.

Wu *et al*. successfully generated and selected three MMV008138-resistant *P. falciparum* strains: 08138R1, 08138R2 and 08138R3, from the parent W2 strain. Whole-genome sequencing was conducted on all four strains, and genomic mutations were identified for each of the mutant strains relative to the parent strain. By parallel comparison of the mutated genes in each drug-resistant strain, PF3D7_0106900 was found to be the only mutated gene shared by all three (Table 4).[72] The PF3D7_0106900 gene is generally believed to encode the IspD enzyme within the MEP pathway. This finding supports the previous hypothesis that potency of MMV008138 (**26**) rises from acting on a target in the MEP pathway and suggests IspD to be the target.

As further corroboration, *in vitro* inhibition of purified *P. falciparum* IspD (*Pf*IspD) by the four stereoisomers of MMV008138 (**26**) was measured. Only the (1*R*,3*S*)-diastereomer was a potent inhibitor with an IC_{50} of 7.0 nM. Note that this result was published just before the Carlier group's manuscript on the stereoisomers (described below) was submitted for review. Based on the above genetic and biochemical data, Wu *et al*. positively identified *Pf*IspD as the molecular target of MMV008138 (**26**).[72]

1.5.3 Active Stereoisomer of MMV008138

The discovery of MMV008138 (**26**) is exciting for several reasons. Structure-wise, the presence of a tetrahydro-β-carboline and pipecolic acid moieties make it an attractive molecule. Both moieties are privileged scaffolds in drug discovery.[73-74] Another notable fact is that MMV008138 (**26**) contains only two stereo centers, giving only four possible diastereomers.[72, 75]

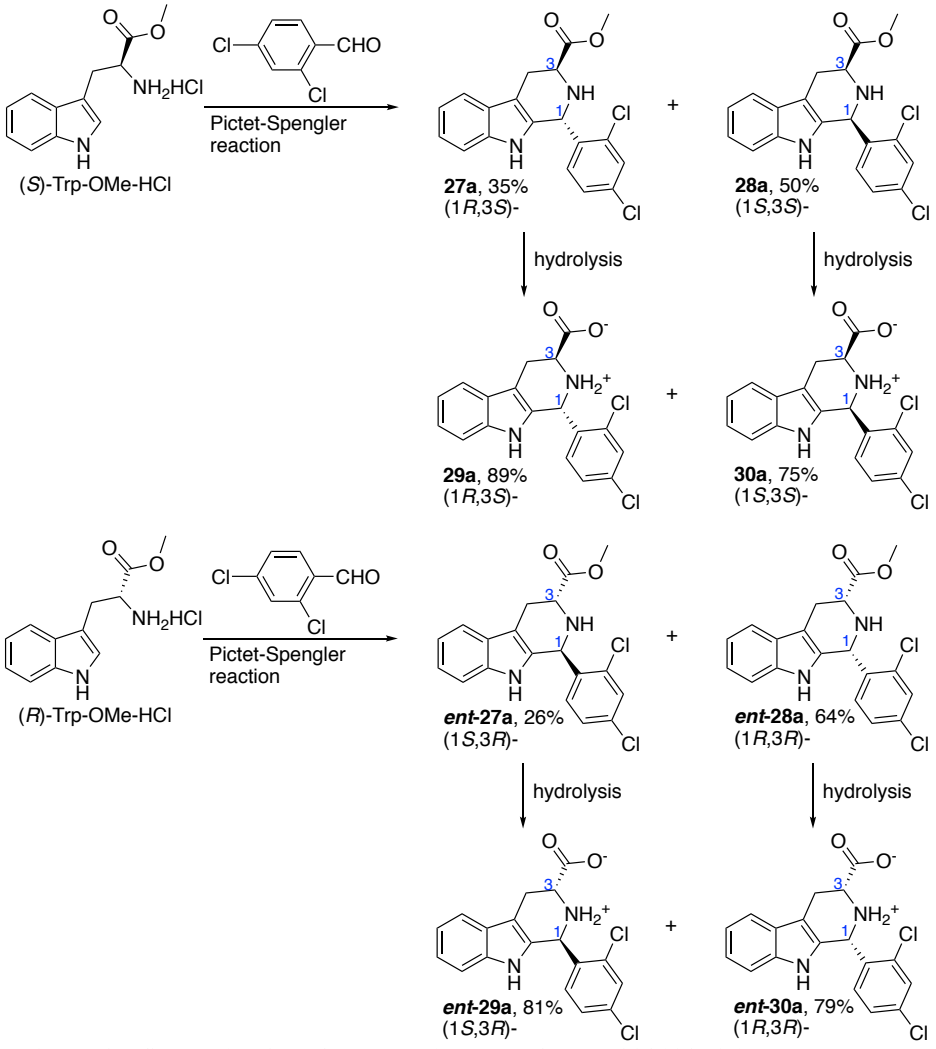

Figure 14. Synthesis of the four stereoisomers of MMV008138 (**26**)

The original HTS that discovered MMV008138 (**26**) was conducted on a stereochemically undefined sample (Figure 13). It is unclear whether MMV008138 (**26**) is a mixture of four or two stereoisomers, or a single stereoisomer. To identify the active stereoisomer of MMV008138 (**26**), Dr. Zhongke Yao from the Carlier group synthesized all four stereoisomers via the Pictet-Spengler reaction (Figure 14).[75] Growth

Compound	*P. falciparum* Dd2 strain IC_{50} (nM)	% rescue with 200 μM IPP
MMV008138 (**26**)	210 ± 90	100
29a	250 ± 70	100
***ent*-29a**	> 10,000	ND
30a	> 10,000	ND
***ent*-30a**	300 ± 200	60

ND: not determined

Table 5. IC_{50} data of MMV008138 (**26**) and its pure stereomers.

inhibition and reverse growth inhibition by IPP supplementation were conducted on all four compounds. From the results shown in Table 5, (1*R*,3*S*)-MMV008138 (**29a**) is the most potent stereoisomer (IC_{50} = 250 ± 70 nM), and like MMV008138, it displayed 100% rescue after IPP supplementation. In comparison, ***ent*-30a** is 10-fold less active, and the other two (**30a** & **ent-29a**) are both inactive. Thus, we concluded that (1*R*,3*S*)-MMV008138 (**29a**) is the active stereoisomer and that MMV008138 (**26**) inhibition of IspD is quite stereoselective. Since the IC_{50} values for **29a** and MMV008138 (**26**) are identical within error, we concluded that MMV008138 (**26**) is the pure (1*R*,3*S*)-diastereomer.[75]

1.5.4 Structure-Activity Relationship Study of MMV008138

To better understand the structural determinants of the activity of (1*R*,3*S*)-MMV008138 **(29a)**, and to assist the structural modification of the lead compound, structure-activity relationships (SAR) of MMV008138 (**26**) were closely studied in the Carlier group. In the previously described screening of the Malaria Box, Carlier and Cassera determined that the carboxylic acid at C3 (i.e., pipecolic acid) is likely of structural importance. The only other tetrahydro-β-carboline moiety-containing compound (Figure 15, **31**) in the Malaria Box has no antiapicoplast activity, and does not contain a carboxylic acid at C3 (i.e., is not a pipecolic acid).[68] Of course, it should be noted that this compound also differs considerably from MMV008183 (**26**) at the C1-aryl group.

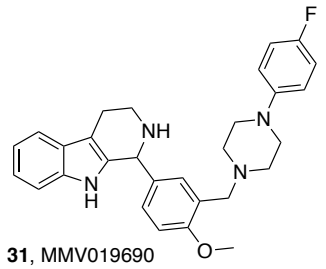

31, MMV019690

Figure 15. MMV019690 (**31**).

To understand the structure-activity relationships in more detail, a series of (1*R*,3*S*)-MMV008138 (**29a**) analogs were synthesized in our group and growth inhibitory assay studies were performed. Table 6 shows the bioassay data of (1*R*,3*S*)-MMV008138 (**29a**) and its D-ring variant analogs.[75-76] By comparing entries 2-4 with entry 1, we can conclude that 2′, 4′-disubstitution is required, as compound **29b** is obviously inactive, and compound **29c** and **29d**

are substantially less potent. The nature of the 2′, 4′-substituents is also revealed to be important.

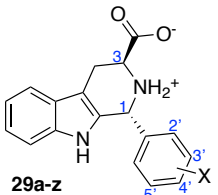

29a-z
(1*R*,3*S*)-

Entry	Compound	X	*P. falciparum* Dd2 strain growth inhibition IC_{50} (nM)	% rescue with 200 μM IPP[b]	*Pf*IspD IC_{50} (nM)[c]	% *E. coli* growth inhibition (18 h)[d]
1	**29a**	2', 4'-Cl_2	250 ± 70	100 @ 2.5 μM	44 ± 15	NI @ 500 μM
2	**29b**	H	> 10,000	ND	> 5,000	NI @ 250 μM
3	**29c**	2'-Cl	3,280 ± 990	60 ± 5 @ 10 μM	~ 1,000	NI @ 250 μM
4	**29d**	4'-Cl	1,170 ± 60	50 ± 7 @ 10 μM	510 ± 90	NI @ 250 μM
5	**29e**	2'-Cl, 4'-Me	410 ± 40	100 @ 2.5 μM	82 ± 10	NI @ 500 μM
6	**29f**	2'-Me, 4'-Cl	700 ± 90	100 @ 2.5 μM	260 ± 50	NI @ 500 μM
7	**29g**	2', 4'-Me_2	70% inhibition @ 10,000	ND	~ 1,000	NI @ 250 μM
8	**29h**	2', 4'-F_2	780 ± 175	100 @ 5 μM	230 ± 10	NI @ 500 μM
9	**29i**	2', 4'-$(OMe)_2$	> 20,000	ND	> 5,000	NI @ 250 μM
10	**29j**	2', 4'-$(CF_3)_2$	> 10,000	ND	> 5,000	NI @ 250 μM
11	**29k**	2'-F, 4'-Cl	860 ± 80	100 @ 5 μM	140 ± 30	NI @ 250 μM
12	**29l**	2'-Cl, 4'-F	433 ± 55	100 @ 10 μM	100 ± 10	NI @ 250 μM
13	**29m**	2'-Cl, 4'-Br	320 ± 60	100 @ 5 μM	34 ± 11	NI @ 250 μM
14	**29n**	2'-Br, 4'-Cl	360 ± 40	100 @ 5 μM	31 ± 4	NI @ 125 μM
15	**29o**	2', 4'-Br_2	590 ± 20	100 @ 10 μM	84 ± 14	NI @ 125 μM
16	**29p**	2'-I, 4'-F	970 ± 180	100 @ 10 μM	140 ± 70	NI @ 250 μM
17	**29q**	2'-F, 4'-I	3,343 ± 496	100 @ 10 μM	130 ± 20	NI @ 125 μM
18	**29r**[a]	2'-Br, 4'-I	1,500 ± 200	80 ± 5 @ 10 μM	ND	ND
19	**29s**	2'-Cl, 4'-OMe	> 5,000	ND	ND	ND
20	**29t**	2'-OMe, 4'-Cl	2,500 ± 600	ND	ND	ND
21	**29u**	2'-Cl, 4'-OH	> 5,000	ND	ND	ND
22	**29v**	2'-Cl, 4'-COOH	0% inhibition @ 10,000	ND	ND	ND
23	**29w**	3', 4'-Cl_2	> 10,000	ND	0% inhibition @ 500 nM	NI @ 250 μM
24	**29x**	2', 6'-F2, 4'-Cl	1,800 ± 150	80 ± 8 @ 10 μM	ND	ND
25	**29y**	2' 3' 4'-F_3	~ 20,000	ND	ND	ND
26	**29z**	2'-Br, 4'-F, 5'-OMe	> 10,000	ND	ND	ND

[a]Tested as approximate 1: 1 mixture of the (1*R*,1*S*) and (1*S*,1*S*)-stereoisomers. [b]Drug at indicated concentration. [c]Recombinant *P. falciparum* IspD IC_{50} values measured at [*Pf*IspD] of 60 nM. [d]Percent growth inhibition at indicated concentration. ND: not determined. NI: no inhibition.

Table 6. Bioassay data of (1*R*,3*S*)-MMV008138 (**29a**) and its D-ring analogs.

Comparison of entry 1 to entries 5-10 showed that, in general, as the substituents get larger and less electronegative, potency of analog decrease drastically. There are exceptions, such as **29o** being more potent than **29h**. But overall, it appears that sterically small and electronegative 2′, 4′-disubstitution of C1-aryl ring is crucial for drug potency.[57] This tight D-ring SAR for **29a** analogs was further confirmed with 17 new D-ring analogs published by Carlier *et al*.[76] From entries 11-15, it is clear that inhibition potency of analogs can be retained with one -Cl substituent either in the 2' or 4' position of D-ring; both -Cl substituents can also be replaced with -Br. However, potency is drastically lost with the absence of -Cl and the replacement with -I and/or -F (entries 8, 16-18). This trend is curious and likely reflects both steric and electronic effects on ligand binding. As Carlier *et al.* noted in their recent publication,[76] the preference for -Cl and -Br at the 2' or 4' position of D-ring could be due to halogen-bonding with backbone carbonyl oxygens of *Pf*IspD, as was seen in co-crystal structures of *At*IspD inhibitors with *At*IspD (PBD ID: 2YC5 and 4NAL).[65, 82] Nevertheless, compounds **29e**, **29f**, **29h**, **29k-29q** still act as MEP pathway inhibitors, as seen with full recovery upon IPP rescue; and possibly still target the IspD enzyme. From entries 9-10, as well as 19-26, it is apparent that electron-donating substituents and bulky electron-withdrawing substituents, e.g. -OMe, -OH, -COOH, are all poor replacement for -Cl. Such analogs are very poor *P. falciparum* growth inhibitors. In conclusion, D-ring analogs of (1*R*,3*S*)-MMV008138 (**29a**) require not only 2', 4'-disubstitution, but also at least one small electron-withdrawing substituent.[76]

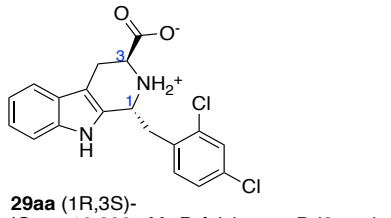

29aa (1R,3S)-
IC_{50} > 10,000 nM, *P. falciparum* Dd2 strain

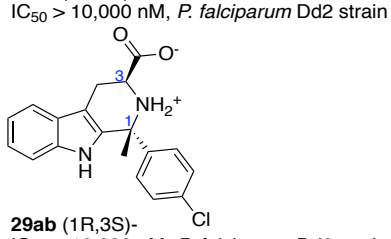

29ab (1R,3S)-
IC_{50} > 10,000 nM, *P. falciparum* Dd2 strain

Figure 16. IC_{50} data of (1*R*,3*S*)-MMV008138 (**29a**) C1-analogs.

Modification at C1 was also recently explored. From the growth inhibition data shown for compounds **29aa** and **29ab** (Figure 16), it is clear that such modification abrogates compound potency.[76] Though the sample number is small, it appears that the C1-position of (1*R*,3*S*)-MMV008138 (**29a**) tolerates little modification.

Because the carboxylic acid group can often be problematic in drug development, we prepared several isosteric and non-isosteric derivatives. Table 7 shows the bioassay data of **29a** and a limited number of its C3-variant analogs.[75-76] Compound (±)-**32**, which lacks a C3-substituent, barely inhibits parasite growth, confirming the significance of a carboxylate group at C3. The methyl ester precursor of **29a**, compound **27a**, also displays very weak inhibitory activity. Amide and hydrazine analogs were more successful, though not as potent as **29a**, indicating that within limits, the carboxylic

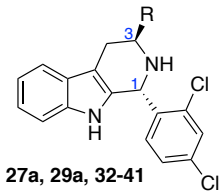

27a, 29a, 32-41

Entry	Compound	R	*P. falciparum* Dd2 strain growth inhibition IC_{50} (nM)	% rescue with 200 μM IPP[a]
1	**29a**	COOH	250 ± 70	100 @ 2.5 μM
2	**27a**	COOMe	6,800 ± 1,400	20 ± 10 @ 20 μM
3	(±)-**32**	H	10,000 ± 1,600	0 @ 20 μM
4	**33**	$CONH_2$	1,200 ± 100	50 ± 7 @ 10 μM
5	**34**	CONHMe	190 ± 30	100 @ 2.5 μM
6	**35**	CONH*i*-Pr	50% inhibition @ 10,000	ND
7	**36**	CONHBu	80% inhibition @ 10,000	ND
8	**37**	CONH*c*-C_6H_{11}	2,830 ± 500	0 @ 10 μM
9	**38**	CONHNHMe	1,940 ± 200	80 @ 10 μM
10	**39**	CONHEt	~ 5,000	ND
11	**40**	$CONMe_2$	> 20,000	ND
12	**41**	CH_2OH	> 10,000	ND

[a]Drug at indicated concentration. ND: not determined

Table 7. Bioassay data of (1*R*,3*S*)-MMV008138 (**29a**) and its C3-analogs.

acid group can be replaced. An important find is the methyl amide analog (**34**), which exhibits comparable growth inhibition IC_{50} data to **29a**, and is significantly better than the 1° amide analog (**33**). Further investigation also showed that the methyl amide analog (**34**), like **29a**, exhibits full rescue with 200 μM IPP, and does not strongly inhibit *E. coli* growth. These findings suggest methyl amide to be a good replacement for the carboxylic acid group at C3. Though the number of C3-analogs investigated is limited, we can conclude with confidence that the carboxylic acid and methyl amide groups at C3 are essential to compound potency and likely play an important role in binding with target enzyme.

As mentioned, MMV008138 (**26**) contains a tetrahydro-β-carboline substructure that is present in many known biologically active compounds and drug molecules. Tetrahydro-β-carbolines have a wide range of molecular targets, raising the possible complication of off-target activity of MMV008138. To assess this, we took (1*R*,3*S*)-MMV008138 (**29a**) and its methyl amide analog (**34**), and investigated their inhibitory activity with 200 μM IPP

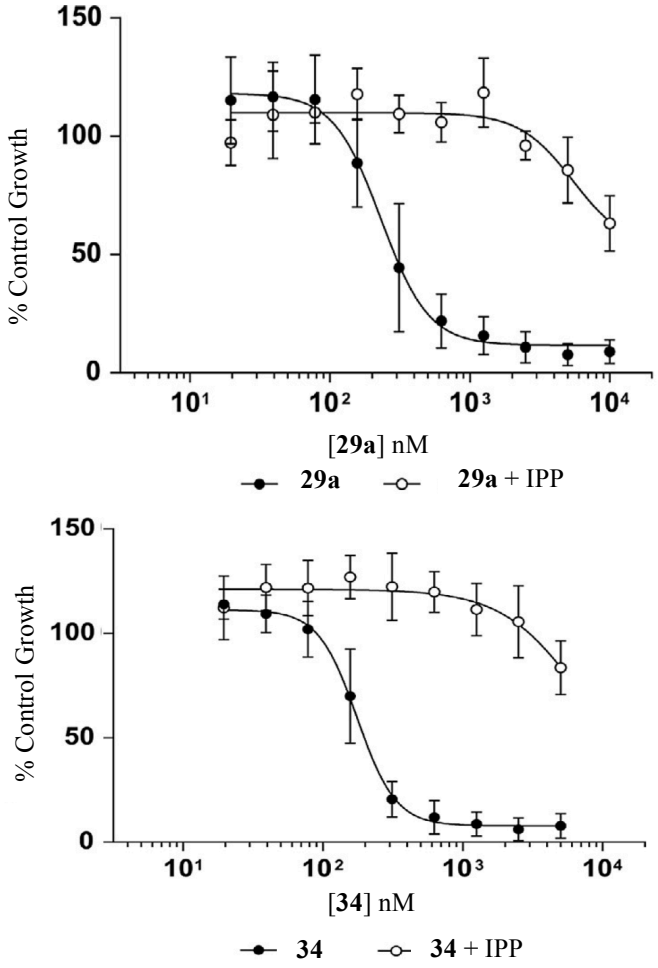

Figure 17. Inhibitory activity of **29a** and **34** in the absence and presence of 200 μM IPP (**1**).

(Figure 17). A roughly 40-fold increase in IC_{50} value is seen. In other words, the off-target effect of (1*R*,3*S*)-MMV008138 (**29a**) and its methyl amide analog (**34**), on *P. falciparum* growth inhibition, does not occur unless their concentrations are 40-fold of what is required to inhibit the MEP pathway.[75]

To sum up, SAR studies revealed to us that the inhibitory activity of MMV008138 (**26**) arises from: (1) (1*R*,3*S*)-configuration; (2) sterically small and electronegative 2′, 4′-disubstitution of the D-ring; and (3) a carboxylate or methyl amide substituent at C3.

1.5.5 Selective Inhibition of the MEP Pathway with MMV008138

Antimalarials targeting the MEP pathway are proposed to be safe and effective, because humans utilize the mevalonate pathway for isoprenoid precursor synthesis. However, we need to address the issue that the MEP pathway is present in bacteria in the human microbiome, and growth inhibition of microbiome flora can bring about undesirable side effects, such as gastrointestinal distress. Thus, selectivity of (1*R*,3*S*)-MMV008138 (**29a**) towards only the *P. falciparum* IspD enzyme is desirable.

Studies of MMV008138 (**26**) on *E. coli, A thaliana,* and *M. tuberculosis* IspD indicated no inhibition, indicating this compound as a species-selective inhibitor of IspD.[77-78] We also tested the inhibitory activity of (1*R*,3*S*)-MMV008138 (**29a**) and its methyl amide analog (**34**) against *E. coli*. No growth inhibition was observed at 500 μM of inhibitor (Table 6).[75] Although humans do not have a functional MEP pathway (MEP itself has not been detected

in humans), there is a low sequence identity (only 11% over only 225 residues) enzyme termed "human IspD" (*h*IspD) that is associated with Walker-Warburg syndrome,[79] a congenital muscular dystrophy. The recent *h*IspD crystal structure (PDB ID: 4CVH) was accompanied by functional studies that demonstrated cytidyltransferase activity toward pentose phosphates, including ribulose 5-phosphate, ribose 5-phosphate, and ribitol 5-phosphate.[80] However, the reported activity toward MEP (using the low signal to noise ratio malachite green assay[81]) did not differ from control (i.e. without a sugar phosphate substrate).

Thus, the question whether *Pf*IspD inhibitors will also target the human IspD enzyme needs to be addressed. Recently, in collaboration with Dr. Cassera, our group showed that (1*R*,3*S*)-MMV008138 (**29a**) at 200 μM does not inhibit human IspD-catalyzed reaction of ribose-5-phosphate and CTP.[76] This further convinced us that species-specific inhibition of *P. falciparum* MEP pathway is achievable and that (1*R*,3*S*)-MMV008138 (**29a**) presents itself as a promising lead as a novel antimalarial. Thus, my current project in the Carlier groups focuses on the structural modification of (1*R*,3*S*)-MMV008138 (**29a**) to further investigate its SAR and provide analogs with potential for preclinical evaluation.

1.6 References for Chapter 1:

1. World malaria map. http://www.cnn.com/2016/04/25/health/world-malaria-day-funding/index.html.

2. Life cycle of malaria parasite. https://www.niaid.nih.gov/diseases-conditions/malaria-parasite.

3. Richie, T. L.; Parekh, F. K., *Malaria*. Elsevier Academic Press Inc: San Diego, 2009; p 1309-1364.

4. WHO, World Malaria Report 2017. **2017**.

5. Nosten, F.; McGready, R.; d'Alessandro, U.; Bonell, A.; Verhoeff, F.; Menendez, C.; Mutabingwa, T.; Brabin, B., Antimalarial drugs in pregnancy: a review. *Current drug safety* **2006,** *1*, 1-15.

6. Ward, S. A.; Sevene, E. J. P.; Hastings, I. M.; Nosten, F.; McGready, R., Antimalarial drugs and pregnancy: Safety, pharmacokinetics, and pharmacovigilance. *Lancet Infect. Dis.* **2007,** *7*, 136-144.

7. Koudou, B. G.; Tano, Y.; Doumbia, M.; Nsanzabana, C.; Cisse, G.; Girardin, O.; Dao, D.; N'Goran, E. K.; Vounatsou, P.; Bordmann, G.; Keiser, J.; Tanner, M.; Utzinger, J., Insecticide-treated bed nets and curtains for preventing malaria. *Med. Vet. Entomol.* **2005,** *19*, 27-37.

8. Langeler, C.; Snow, R. W., From efficacy to effectiveness: Insecticide-treated bednets in Africa. *Bull. World Health Organ.* **1996,** *74*, 325-332.

9. Schlitzer, M., Antimalarial drugs - What is in use and what is in the pipeline. *Arch. Pharm.* **2008,** *341*, 149-163.

10. Wiesner, J.; Ortmann, R.; Jomaa, H.; Schlitzer, M., New antimalarial drugs. *Angew. Chem.-Int. Edit.* **2003,** *42*, 5274-5293.

11. Foley, M.; Tilley, L., Quinoline antimalarials: Mechanisms of action and resistance and prospects for new agents. *Pharmacol. Ther.* **1998,** *79*, 55-87.

12. Bennett, J. M.; Desforges, J. F., Quinine-induced haemolysis - Mechanism of action. *Br. J. Haematol.* **1967,** *13*, 706-+.

13. Schlitzer, M., Malaria chemotherapeutics part 1: History of antimalarial drug development, currently used therapeutics, and drugs in clinical development. *ChemMedChem* **2007,** *2*, 944-986.

14. Fidock, D. A.; Rosenthal, P. J.; Croft, S. L.; Brun, R.; Nwaka, S., Antimalarial drug discovery: Efficacy models for compound screening. *Nat. Rev. Drug Discov.* **2004,** *3*, 509-520.

15. Wells, T. N. C.; van Huijsduijnen, R. H.; Van Voorhis, W. C., Malaria medicines: a glass half full? *Nat. Rev. Drug Discov.* **2015,** *14*, 424-+.

16. Famin, O.; Ginsburg, H., Differential effects of 4-aminoquinoline-containing antimalarial drugs on hemoglobin digestion in *Plasmodium falciparum*-infected erythrocytes. *Biochem. Pharmacol.* **2002,** *63*, 393-398.

17. Ghavami, M.; Dapper, C. H.; Dalal, S.; Holzschneider, K.; Klemba, M.; Carlier, P. R., Parallel inhibition of amino acid efflux and growth of erythrocytic *Plasmodium falciparum* by mefloquine and non-piperidine analogs: Implication for the mechanism of antimalarial action. *Bioorg. Med. Chem. Lett.* **2016,** *26*, 4846-4850.

18. Dondorp, A. M.; Fairhurst, R. M.; Slutsker, L.; MacArthur, J. R.; Breman, J. G.; Guerin, P. J.; Wellems, T. E.; Ringwald, P.; Newman, R. D.; Plowe, C. V., The threat of artemisinin-resistant malaria. *N. Engl. J. Med.* **2011,** *365*, 1073-1075.

19. Dondorp, A. M.; Yeung, S.; White, L.; Nguon, C.; Day, N. P. J.; Socheat, D.; von Seidlein, L., Artemisinin resistance: Current status and scenarios for containment. *Nat. Rev. Microbiol.* **2010,** *8*, 272-280.

20. Fairhurst, R. M.; Dondorp, A. M., Artemisinin-resistant *Plasmodium falciparum* malaria. *Microbiol. Spectr.* **2016,** *4*, 16.

21. McFadden, G. I.; Reith, M. E.; Munholland, J.; LangUnnasch, N., Plastid in human parasites. *Nature* **1996,** *381*, 482-482.

22. McFadden, G. I.; Roos, D. S., Apicomplexan plastids as drug targets. *Trends Microbiol.* **1999,** *7*, 328-333.

23. Wiesner, J.; Reichenberg, A.; Heinrich, S.; Schlitzer, M.; Jomaa, H., The plastid-like organelle of apicomplexan parasites as drug target. *Curr. Pharm. Design* **2008,** *14*, 855-871.

24. Dahl, E. L.; Rosenthal, P. J., Multiple antibiotics exert delayed effects against the *Plasmodium falciparum* anicoplast. *Antimicrob. Agents Chemother.* **2007,** *51*, 3485-3490.

25. Nagaraj, V. A.; Sundaram, B.; Varadarajan, N. M.; Subramani, P. A.; Kalappa, D. M.; Ghosh, S. K.; Padmanaban, G., Malaria parasite-synthesized heme is essential in the mosquito and liver stages and complements host heme in the blood stages of infection. *PLoS Pathog.* **2013,** *9*, 13.

26. van Schaijk, B. C. L.; Kumar, T. R. S.; Vos, M. W.; Richman, A.; van Gemert, G. J.; Li, T.; Eappen, A. G.; Williamson, K. C.; Morahan, B. J.; Fishbaugher, M.; Kennedy, M.; Camargo, N.; Khan, S. M.; Janse, C. J.; Sim, K. L.; Hoffman, S. L.; Kappe, S. H. I.; Sauerwein, R. W.; Fidock, D. A.; Vaughan, A. M., Type II fatty acid biosynthesis is essential for *Plasmodium falciparum* sporozoite development in the midgut of *Anopheles* mosquitoes. *Eukaryot. Cell* **2014,** *13*, 550-559.

27. Wiley, J. D.; Merino, E. F.; Krai, P. M.; McLean, K. J.; Tripathi, A. K.; Vega-Rodriguez, J.; Jacobs-Lorena, M.; Klemba, M.; Cassera, M. B., Isoprenoid precursor biosynthesis is the essential metabolic role of the apicoplast during gametocytogenesis in *Plasmodium falciparum*. *Eukaryot. Cell* **2015,** *14*, 128-139.

28. Gershenzon, J.; Dudareva, N., The function of terpene natural products in the natural world. *Nat. Chem. Biol.* **2007,** *3*, 408-414.

29. Tamanoi, F.; Kato-Stankiewicz, J.; Jiang, C.; Machado, I.; Thapar, N., Farnesylated proteins and cell cycle progression. *J. Cell. Biochem.* **2001,** *84*, 64-70.

30. Bach, T. J., SOme New Aspects of Isoprenoid Biosynthesis in Plants - A Review. *Lipids* **1995,** *30*, 191-202.

31. Odom, A. R., Five questions about non-mevalonate isoprenoid biosynthesis. *PLoS Pathog.* **2011,** *7*, 3.

32. Chang, W. C.; Song, H.; Liu, H. W.; Lu, P. H., Current development in isoprenoid precursor biosynthesis and regulation. *Curr. Opin. Chem. Biol.* **2013,** *17*, 571-579.

33. Miziorko, H. M., Enzymes of the mevalonate pathway of isoprenoid biosynthesis. *Arch. Biochem. Biophys.* **2011,** *505*, 131-143.

34. Arigoni, D.; Eisenreich, W.; Latzel, C.; Sagner, S.; Radykewicz, T.; Zenk, M. H.; Bacher, A., Dimethylallyl pyrophosphate is not the committed precursor of isopentenyl pyrophosphate during terpenoid biosynthesis from 1-deoxyxylulose in higher plants. *PNAS* **1999,** *96*, 1309-1314.

35. Rohmer, M., The discovery of a mevalonate-independent pathway for isoprenoid biosynthesis in bacteria, algae and higher plants. *Nat. Prod. Rep.* **1999,** *16*, 565-574.

36. Rohmer, M.; Seemann, M.; Horbach, S.; BringerMeyer, S.; Sahm, H., Glyceraldehyde 3-phosphate and pyruvate as precursors of isoprenic units in an alternative non-mevalonate pathway for terpenoid biosynthesis. *J. Am. Chem. Soc.* **1996,** *118*, 2564-2566.

37. Eisenreich, W.; Bacher, A.; Arigoni, D.; Rohdich, F., Biosynthesis of isoprenoids via the non-mevalonate pathway. *Cell. Mol. Life Sci.* **2004,** *61*, 1401-1426.

38. Frank, A.; Groll, M., The methylerythritol phosphate pathway to isoprenoids. *Chem. Rev.* **2017,** *117*, 5675-5703.

39. Grawert, T.; Groll, M.; Rohdich, F.; Bacher, A.; Eisenreich, W., Biochemistry of the non-mevalonate isoprenoid pathway. *Cell. Mol. Life Sci.* **2011,** *68*, 3797-3814.

40. Lichtenthaler, H. K., Non-mevalonate isoprenoid biosynthesis: Enzymes, genes and inhibitors. *Biochem. Soc. Trans.* **2000,** *28*, 785-789.

41. Zhao, L. S.; Chang, W. C.; Xiao, Y. L.; Liu, H. W.; Liu, P. H., Methylerythritol Phosphate Pathway of Isoprenoid Biosynthesis. In *Annu. Rev. Biochem., Vol 82*, Kornberg, R. D., Ed. Annual Reviews: Palo Alto, **2013**, *82*, pp 497-+.

42. Masini, T.; Kroezen, B. S.; Hirsch, A. K. H., Druggability of the enzymes of the non-mevalonate-pathway. *Drug Discov. Today* **2013,** *18*, 1256-1262.

43. Masini, T.; Hirsch, A. K. H., Development of Inhibitors of the 2C-Methyl-D-erythritol 4-Phosphate (MEP) Pathway Enzymes as Potential Anti-Infective Agents. *J. Med. Chem.* **2014,** *57*, 9740-9763.

44. Witschel, M. C.; Hoffken, H. W.; Seet, M.; Parra, L.; Mietzner, T.; Thater, F.; Niggeweg, R.; Rohl, F.; Illarionov, B.; Rohdich, F.; Kaiser, J.; Fischer, M.; Bacher, A.; Diederich, F., Inhibitors of the Herbicidal Target IspD: Allosteric Site Binding. *Angew. Chem.-Int. Edit.* **2011,** *50*, 7931-7935.

45. Yajima, S.; Nonaka, T.; Kuzuyama, T.; Seto, H.; Ohsawa, K., Crystal structure of 1-deoxy-D-xylulose 5-phosphate reductoisomerase complexed with cofactors: Implications of a flexible loop movement upon substrate binding. *J. Biochem.* **2002,** *13*, 313-317.

46. Jackson, E. R.; Dowd, C. S., Inhibition of 1-Deoxy-D-Xylulose-5-Phosphate Reductoisomerase (Dxr): A review of the synthesis and biological evaluation of recent inhibitors. *Curr. Top. Med. Chem.* **2012,** *12*, 706-728.

47. Murkin, A. S.; Manning, K. A.; Kholodar, S. A., Mechanism and inhibition of 1-deoxy-D-xylulose-5-phosphate reductoisomerase. *Bioorganic Chem.* **2014,** *57*, 171-185.

48. Zeidler, J.; Schwender, J.; Muller, C.; Wiesner, J.; Weidemeyer, C.; Beck, E.; Jomaa, H.; Lichtenthaler, H. K., Inhibition of the non-mevalonate 1-deoxy-D-xylulose-5-phosphate pathway of plant isoprenoid biosynthesis by fosmidomycin. *Z.Naturforsch.(C)* **1998,** *53*, 980-986.

49. Fernandes, J. F.; Lell, B.; Agnandji, S. T.; Obiang, R. M.; Bassat, Q.; Kremsner, P. G.; Mordmuller, B.; Grobusch, M. P., Fosmidomycin as an antimalarial drug: A meta-analysis of clinical trials. *Future Microbiol.* **2015,** *10*, 1375-1390.

50. Jomaa, H.; Wiesner, J.; Sanderbrand, S.; Altincicek, B.; Weidemeyer, C.; Hintz, M.; Turbachova, I.; Eberl, M.; Zeidler, J.; Lichtenthaler, H. K.; Soldati, D.; Beck, E., Inhibitors of the nonmevalonate pathway of isoprenoid biosynthesis as antimalarial drugs. *Science* **1999,** *285*, 1573-1576.

51. Behrendt, C. T.; Kunfermann, A.; Illarionova, V.; Matheeussen, A.; Pein, M. K.; Grawert, T.; Kaiser, J.; Bacher, A.; Eisenreich, W.; Illarionov, B.; Fischer, M.; Maes, L.; Groll, M.; Kurz, T., Reverse fosmidomycin derivatives against the antimalarial drug target IspC (Dxr). *J. Med. Chem.* **2011,** *54*, 6796-6802.

52. Giessmann, D.; Heidler, P.; Haemers, T.; Van Calenbergh, S.; Reichenberg, A.; Jomaa, H.; Weidemeyerd, C.; Sanderbrand, S.; Wiesner, J.; Link, A., Towards new antimalarial drugs: Synthesis of non-hydrolyzable phosphate mimics as feed for a predictive QSAR study on 1-deoxy-D-xylulose-5-phosphate reductoisomerase inhibitors. *Chem. Biodivers.* **2008,** *5*, 643-656.

53. Muri, E. M. F.; Nieto, M. J.; Sindelar, R. D.; Williamson, J. S., Hydroxamic acids as pharmacological agents. *Curr. Med. Chem.* **2002,** *9*, 1631-1653.

54. Andaloussi, M.; Lindh, M.; Bjorkelid, C.; Suresh, S.; Wieckowska, A.; Iyer, H.; Karlen, A.; Larhed, M., Substitution of the phosphonic acid and hydroxamic acid functionalities of the DXR inhibitor FR900098: An attempt to improve the activity against *Mycobacterium tuberculosis*. *Bioorg. Med. Chem. Lett.* **2011,** *21*, 5403-5407.

55. Umeda, T.; Tanaka, N.; Kusakabe, Y.; Nakanishi, M.; Kitade, Y.; Nakamura, K. T., Molecular basis of fosmidomycin's action on the human malaria parasite *Plasmodium falciparum*. *Sci Rep* **2011,** *1*, 8.

56. Deng, L. S.; Sundriyal, S.; Rubio, V.; Shi, Z. Z.; Song, Y. C., Coordination chemistry based approach to lipophilic inhibitors of 1-deoxy-D-xylulose-5-phosphate reductoisomerase. *J. Med. Chem.* **2009,** *52*, 6539-6542.

57. Chofor, R.; Risseeuw, M. D. P.; Pouyez, J.; Johny, C.; Wouters, J.; Dowd, C. S.; Couch, R. D.; Van Calenbergh, S., Synthetic fosmidomycin analogues with altered chelating moieties do not Inhibit 1-deoxy-D-xylulose5-phosphate reductoisomerase or *Plasmodium falciparum* growth *in vitro*. *Molecules* **2014,** *19*, 2571-2587.

58. Zingle, C.; Kuntz, L.; Tritsch, D.; Grosdemange-Billiard, C.; Rohmer, M., Modifications around the hydroxamic acid chelating group of fosmidomycin, an inhibitor of the metalloenzyme 1-deoxyxylulose 5-phosphate reductoisomerase (DXR). *Bioorg. Med. Chem. Lett.* **2012,** *22*, 6563-6567.

59. Bodill, T.; Conibear, A. C.; Mutorwa, M. K. M.; Goble, J. L.; Blatch, G. L.; Lobb, K. A.; Klein, R.; Kaye, P. T., Exploring DOXP-reductoisomerase binding limits using phosphonated N-aryl and N-heteroarylcarboxamides as DXR inhibitors. *Bioorg. Med. Chem.* **2013,** *21*, 4332-4341.

60. Jackson, E. R.; San Jose, G.; Brothers, R. C.; Edelstein, E. K.; Sheldon, Z.; Haymond, A.; Johny, C.; Boshoff, H. I.; Couch, R. D.; Dowd, C. S., The effect of chain length and unsaturation on Mtb Dxr inhibition and antitubercular killing activity of FR900098 analogs. *Bioorg. Med. Chem. Lett.* **2014,** *24*, 649-653.

61. Behrendt, C. T.; Kunfermann, A.; Illarionova, V.; Matheeussen, A.; Grawert, T.; Groll, M.; Rohdich, F.; Bacher, A.; Eisenreich, W.; Fischer, M.; Maes, L.; Kurz, T., Synthesis and antiplasmodial activity of highly active reverse analogues of the antimalarial drug candidate fosmidomycin. *ChemMedChem* **2010,** *5*, 1673-1676.

62. Kurz, T.; Schluter, K.; Pein, M.; Behrendt, C.; Bergmann, B.; Walter, R. D., Conformationally restrained aromatic analogues of fosmidomycin and FR900098. *Arch. Pharm.* **2007,** *340*, 339-344.

63. Brucher, K.; Illarionov, B.; Held, J.; Tschan, S.; Kunfermann, A.; Pein, M. K.; Bacher, A.; Grawert, T.; Maes, L.; Mordmuller, B.; Fischer, M.; Kurz, T., α-Substituted β-oxa isosteres of fosmidomycin: Synthesis and biological evaluation. *J. Med. Chem.* **2012,** *55*, 6566-6575.

64. Bjorkelid, C.; Bergfors, T.; Henriksson, L. M.; Stern, A. L.; Unge, T.; Mowbray, S. L.; Jones, T. A., Structural and functional studies of mycobacterial IspD enzymes. *Acta Crystallogr. Sect. D-Biol. Crystallogr.* **2011,** *67*, 403-414.

65. Kunfermann, A.; Witschel, M.; Illarionov, B.; Martin, R.; Rottmann, M.; Hoffken, H. W.; Seet, M.; Eisenreich, W.; Knolker, H. J.; Fischer, M.; Bacher, A.; Groll, M.; Diederich, F., Pseudilins: Halogenated, allosteric inhibitors of the non-mevalonate pathway Enzyme IspD. *Angew. Chem.-Int. Edit.* **2014,** *53*, 2235-2239.

66. Lillo, A. M.; Tetzlaff, C. N.; Sangari, F. J.; Cane, D. E., Functional expression and characterization of EryA, the erythritol kinase of Brucella abortus, and enzymatic synthesis of L-erythritol-4-phosphate. *Bioorg. Med. Chem. Lett.* **2003,** *13*, 737-739.

67. Witschel, M.; Rohl, F.; Niggeweg, R.; Newton, T., In search of new herbicidal inhibitors of the non-mevalonate pathway. *Pest Manag. Sci.* **2013,** *69*, 559-563.

68. Bowman, J. D.; Merino, E. F.; Brooks, C. F.; Striepen, B.; Carlier, P. R.; Cassera, M. B., Antiapicoplast and gametocytocidal screening to identify the mechanisms of action of compounds within the malaria box. *Antimicrob. Agents Chemother.* **2014,** *58*, 811-819.

69. Spangenberg, T.; Burrows, J. N.; Kowalczyk, P.; McDonald, S.; Wells, T. N. C.; Willis, P., The open access malaria box: a drug discovery catalyst for neglected diseases. *PLoS One* **2013,** *8*, 8.

70. Yeh, E.; DeRisi, J. L., Chemical Rescue of Malaria Parasites Lacking an Apicoplast Defines Organelle Function in Blood-Stage Plasmodium falciparum. *PLoS. Biol.* **2011,** *9*, 10.

71. Dahl, E. L.; Rosenthal, P. J., Apicoplast translation, transcription and genome replication: Targets for antimalarial antibiotics. *Trends Parasitol.* **2008,** *24*, 279-284.

72. Wu, W.; Herrera, Z.; Ebert, D.; Baska, K.; Cho, S. H.; DeRisi, J. L.; Yeh, E., A chemical rescue screen identifies a *Plasmodium falciparum* apicoplast inhibitor targeting MEP isoprenoid precursor biosynthesis. *Antimicrob. Agents Chemother.* **2015,** *59*, 356-364.

73. Cao, R. H.; Peng, W. L.; Wang, Z. H.; Xu, A. L., β-Carboline alkaloids: Biochemical and pharmacological functions. *Curr. Med. Chem.* **2007,** *14*, 479-500.

74. Welsch, M. E.; Snyder, S. A.; Stockwell, B. R., Privileged scaffolds for library design and drug discovery. *Curr. Opin. Chem. Biol.* **2010,** *14*, 347-361.

75. Yao, Z. K.; Krai, P. M.; Merino, E. F.; Simpson, M. E.; Slebodnick, C.; Cassera, M. B.; Carlier, P. R., Determination of the active stereoisomer of the MEP pathway-targeting antimalarial agent MMV008138, and initial structure-activity studies. *Bioorg. Med. Chem. Lett.* **2015,** *25*, 1515-1519.

76. Ghavami, M.; Merino, E. F.; Yao, Z.-K.; Elahi, R.; Simpson, M. E.; Fernandez-Murga, M. L.; Butler, J. H.; Casasanta, M. A.; Krai, P. M.; Totrov, M. M.; Slade, D. J.; Carlier, P. R.; Cassera, M. B., Biological studies and target engagement of the 2-C-methyl-d-erythritol 4-phosphate cytidylyltransferase (IspD)-targeting antimalarial agent (1R,3S)-MMV008138 and analogs. *ACS Infect. Dis.* **2017**.

77. Imlay, L. S.; Armstrong, C. M.; Masters, M. C.; Li, T.; Price, K. E.; Edwards, R. L.; Mann, K. M.; Li, L. X.; Stallings, C. L.; Berry, N. G.; O'Neill, P. M.; Odom, A. R., *Plasmodium* IspD (2-C-methyl-D-erythritol 4-phosphate cytidyltransferase), an essential and druggable antimalarial target. *ACS Infect. Dis.* **2015,** *1*, 157-167.

78. Xu, G. P.; Gilbertson, S. R., Development of building blocks for the synthesis of N-heterocyclic carbene ligands. *Org. Lett.* **2005,** *7*, 4605-4608.

79. Roscioli, T.; Kamsteeg, E.-J.; Buysse, K.; Maystadt, I.; van Reeuwijk, J.; van den Elzen, C.; van Beusekom, E.; Riemersma, M.; Pfundt, R.; Vissers, L. E. L. M.; Schraders, M.; Altunoglu, U.; Buckley, M. F.; Brunner, H. G.; Grisart, B.; Zhou, H.; Veltman, J. A.; Gilissen, C.; Mancini, G. M. S.; Delree, P.; Willemsen, M. A.; Ramadza, D. P.; Chitayat, D.; Bennett, C.; Sheridan, E.; Peeters, E. A. J.; Tan-Sindhunata, G. M. B.; de Die-Smulders, C. E.; Devriendt, K.; Kayserili, H.; El-Hashash, O. A. E.-F.; Stemple, D. L.; Lefeber, D. J.; Lin, Y.-Y.; van Bokhoven, H., Mutations in ISPD cause Walker-Warburg syndrome and defective glycosylation of α-dystroglycan. *Nat. Genet.* **2012,** *44*, 581-585.

80. Riemersma, M.; Froese, D. S.; van Tol, W.; Engelke, Udo F.; Kopec, J.; van Scherpenzeel, M.; Ashikov, A.; Krojer, T.; von Delft, F.; Tessari, M.; Buczkowska, A.; Swiezewska, E.; Jae, Lucas T.; Brummelkamp, Thijn R.;

Manya, H.; Endo, T.; van Bokhoven, H.; Yue, Wyatt W.; Lefeber, Dirk J., Human IspD is a cytidyltransferase required for dystroglycan O-mannosylation. *Chem. Biol.* **2015,** *22*, 1643-1652.

81. Bernal, C.; Palacin, C.; Boronat, A.; Imperial, S., A colorimetric assay for the determination of 4-diphosphocytidyl-2-C-methyl-d-erythritol 4-phosphate synthase activity. *Analytical Biochemistry* **2005,** *337*, 55-61.

82. Schwab, A.; Illarionov, B.; Frank, A.; Kunfermann, A.; Seet, M.; Bacher, A.; Witschel, M. C.; Fischer, M.; Groll, M.; Diederich, F., Mechanism of allosteric inhibition of the enzyme IspD by three different classes of ligands. *ACS Chem. Biol.* **2017,** *12*, 2132-2138.

Chapter 2: Structure-Activity Relationship Study of MMV008138 Acid Bioisosteres and A-ring Analogs

2.1 Synthesis and biological evaluation of MMV008138 acid bioisosteres

Investigations of acid bioisosteres are an important aspect to understanding SAR of drug lead scaffolds containing a carboxylic acid group, as in the case with (1*R*,3*S*)-MMV008138 (**29a**). The carboxylic acid moiety is a key functionality in biological processes, and has a wide presence in biologically important molecules, such as amino acids, saccharides, vitamins, etc. It also has a significant role in drug design. This is clearly illustrated with the large number (>450) of commercially available carboxylic acid-containing drugs, spanning from common anti-inflammatory drugs, like aspirin, to statins and antibiotics.[1] The intrinsic properties of the carboxylic acid group, such as acidity, electrostatic interactions and hydrogen-bonding characteristics, are often key to drug-target interaction. Yet, for the same reasons, the presence of a carboxylic acid group in drug leads can often be a liability as well. For example, because carboxylates are negatively charged, their ability to passively diffuse across biological membranes is diminished, reducing drug transport and permeability. This is particularly apparent in the development of central nervous system drugs, where the blood-brain barrier presents yet another challenge.[2-3] Studies within the last few years have also shown that carboxylic acid drugs are often associated with idiosyncratic drug toxicity, which is caused by metabolism of the functionality in the liver, and exhibit high chance of drug-induced liver injury.[4] Thus, a suitable replacement for the acid functionality, or an acid bioisostere, is often investigated to circumvent these problems.

Our previous SAR study of (*1R*,*3S*)-MMV008138 (**29a**) has firmly established the functional significance of the carboxylate acid substituent at C3.[5] However, an approximate 6-fold difference between growth inhibition potency (cell-based assay) and enzyme IC_{50} (cell-free assay) was observed during biological studies. This could be due to poor membrane penetration ability caused by carboxylic acid moiety. The methyl amide analog **34**, was previously shown to be comparable to the parent **29a** in terms of growth inhibition, but its inadequate solubility in pH = 7.4 buffer (determined by Pharmaron, data not shown) makes it unsuitable for further *in vivo* studies.[5-6] Thus, it would be beneficial to look further into other acid bioisosteres of the lead compound and investigate the potential of this structural modification strategy.

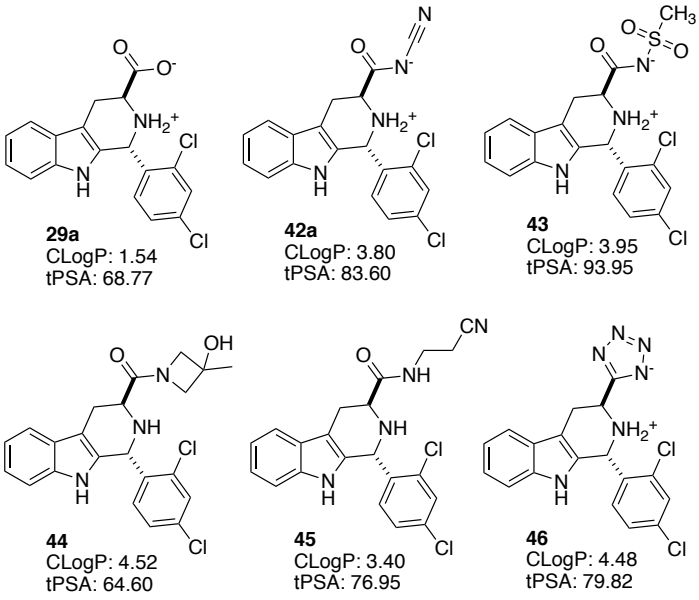

Figure 18. Acid bioisosteres of (1*R*, 3*S*)-MMV008138 (**29a**).

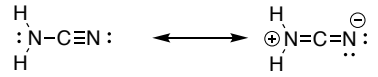

Figure 19. Resonance structures of cyanamide.

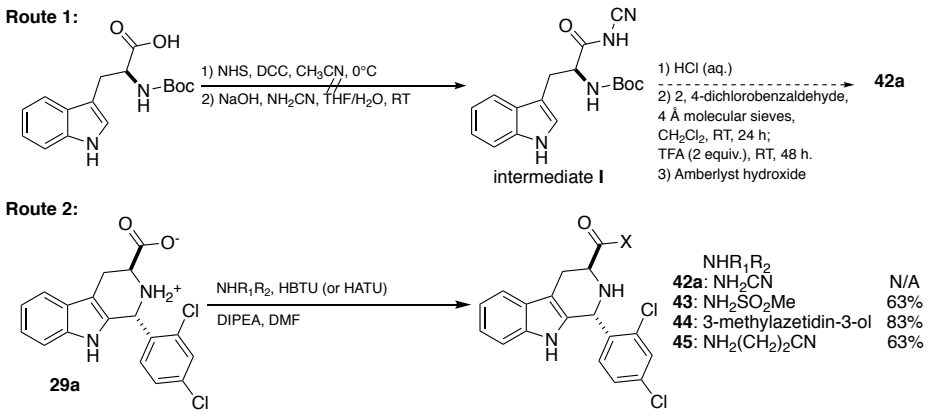

Figure 20. Synthetic route for acid bioisosteres of **29a**.

2.1.1 Synthesis

Combining acid bioisostere research and data by Ballatore *et al*. and Meanwell *et al*.,[2-3, 7] with our acquired inhibition assay data,[5] five acid bioisosteres of **29a** (Figure 18) were selected for further investigation. All five compounds have calculated topological polar surface area (tPSA) values that are relatively close to that of **29a** and are smaller than 140, which indicates good intestinal absorption.

Compound **42a** contains a –CONHCN fragment as replacement for the carboxylic acid, introducing a nitrile group to the main scaffold. Nitriles are a common functional group in pharmaceuticals, thus **42a** is worth investigating to supplement previous SAR data though its CLogP value is larger than that of **29a**,

Previously amide analogs of **29a** (**33**-**40**), were synthesized via substitution reaction of the methyl ester (**27a)** with the corresponding amine.[5] However, due to resonance, the amine nitrogen of cyanamide is partially positively charged (Figure 19), making cyanamide a poor nucleophile. Because no prior successful literature examples of directly reacting cyanamide with amino acid methyl ester derivatives were found, it seems that cyanamide is not nucleophilic enough for reaction with the ester **27a** and calls for new synthetic method. To conclusively determine whether an attempted reaction can give the expected -NHCN containing product, IR spectroscopy was adopted as a characterization

method.[8] This is because the nitrile functional group has a unique, medium intensity IR absorption at around 2200 cm^{-1}, which can easily be observed. From the IR spectrum of cyanamide and *N*-cyanobenzamide (Figure 21, **42b**), we can clearly see a medium intensity, slightly resolved doublet at 2150-2260 cm^{-1} from the -NHCN moiety, confirming viability of IR analysis.

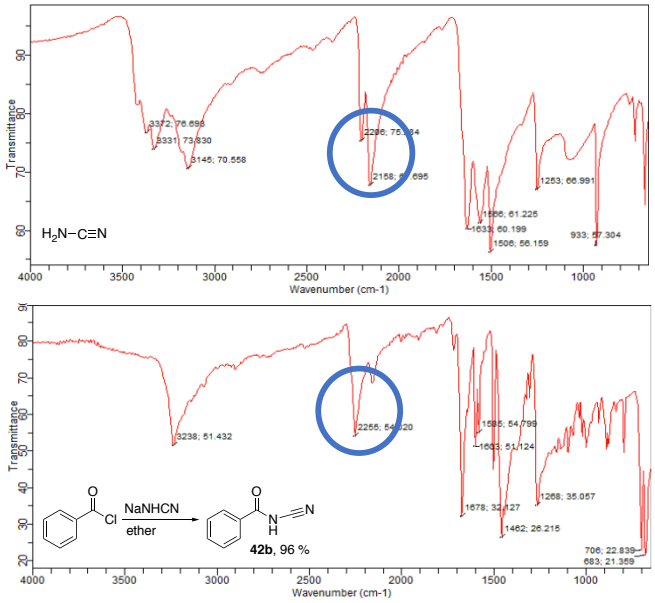

Figure 21. IR absorption of -NHCN.

My initial attempt to synthesize compound **42a** was via Route 1 shown in Figure 20,[9] which introduces the -NHCN fragment to a protected (*S*)-tryptophan prior to ring formation via Pictet-Spengler reaction. IR analysis of intermediate **I** shows no absorption at around 2200 cm^{-1} (Figure 22a), indicating Route 1 was unsuccessful. In a general literature search, work by Kwon *et al.* shows that reacting NH_2CN with an activated protected amino acid under basic conditions often afford cyclization product, iminohydantoins (Figure 22b).[9-10] This may be a possible explanation to why the expected product was not obtained, though the exact structure of intermediate **I** was not elucidated. Direct coupling of NH_2CN with **29a**

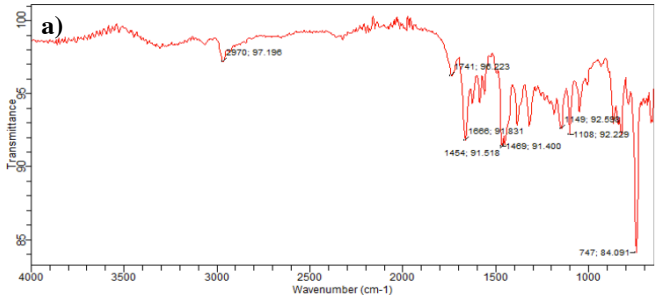

Figure 22. **a)** IR spectra of intermediate **I**. **b)** Iminohydantoin.

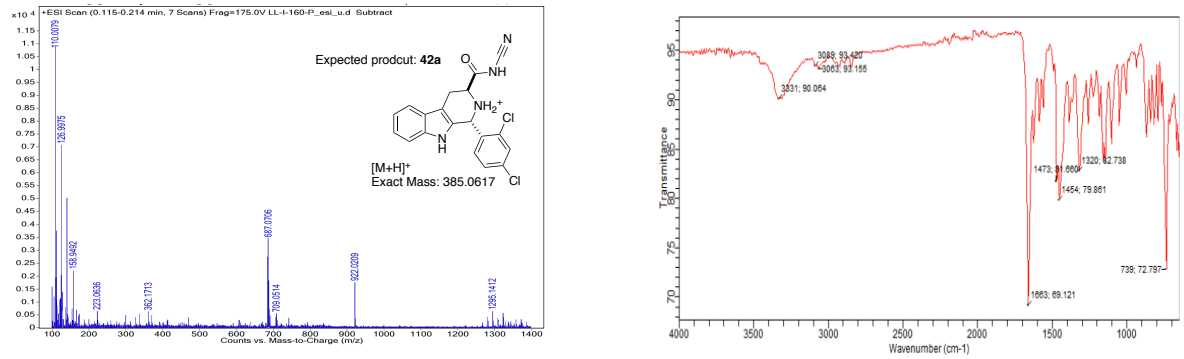

Figure 23. Spectral data of direct coupling product of NH_2CN with **29a**.

was also attempted (Route 2, Figure 20).[11-12] The reaction afforded a product that did not match the expected mass for **42a** ($[M+H]^+$ = 385.0617) by HRMS, and IR analysis showed no -CN triple bond stretch absorption at around 2200 cm^{-1} (Figure 23). The mechanism of coupling reactions using HBTU or HATU, reveal that the acid is first converted to an activated ester. The activated ester is then attacked by the amine reactant to afford the corresponding amide product.[11-12] It appears that cyanamide is not nucleophilic enough to attack even activated esters formed from HBTU or HATU. We are certain that Route 2 cannot afford compound **42a** from spectral evidence in Figure 23. Due to the difficulty in synthesizing **42a**, efforts were put forward to making analogs **43**-**46**.

Compound **43** is an acyl-methylsulfonamide analog of **29a**. Acylsulfonamides, as carboxylic acid group replacements, were among some of the most extensively explored and successful bioisosteres.[2] The pK_a value of acylsulfonamides usually fall within the range of 4-6, which is close to that of carboxylic acids (RCOOH, pK_a = ~4.7). Ballatore *et al.* reported calculated and experimental data of acid bioisosteres that show acylsulfonamides to have higher $logD_{7.4}$ value than that of the parent acid, indicating improved membrane transport ability at physiological pH.[2-3] This trend is also observed with the CLogP prediction of **43** and **29a** (Figure 18). At the same time, calculations by Ballatore also show improved aqueous solubility of roughly 2-fold when the acid group is replaced with an acyl-methylsulfonamide. Moreover, it is believed that the geometry of hydrogen bonding formed by the sulfonamide moiety resembles that of carboxylic acids, as the distance of the two oxygen atoms in both groups are relatively similar.[2-3]

Compound **44**, containing a 3-methylazetidin-3-ol fragment, is a modification suggested to Prof. Carlier at a malaria meeting. This acid bioisostere can be considered as a special amide derivative of **29a**. From computed parameters (Figure 18), compound **44** and **29a** have very close tPSA values, while the CLogP value of **44** is more than double the value for **29a**. This means, if **44** exhibits comparable inhibition ability to **29a**, the 3-methylazetidin-3-ol fragment may resolve transport liability brought about by the carboxylic acid moiety and the hydroxyl group on the azetidine may improve solubility as well.

Another important and interesting acid bioisostere to investigate is the tetrazole analog of **29a**, compound **46**. Tetrazolic acids have properties that closely resemble those of carboxylic acids, such as planarity and acidity. At the same time, they are more lipophilic and have an extended hydrogen-bonding environment compared with the corresponding acid. These factors make tetrazole analogs one of the most frequently used acid bioisoteres. One important and successful example of the employment of tetrazole as carboxylic acid replacement would be the high

blood pressure drug, losartan (Cozaar). Losartan, compared with its carboxylic acid parent, both have pK_a around 5 and exhibit high potency *in vitro*. *In vitro* studies revealed losartan to be 10-fold more potent than the parent at the AT1 receptor (data not shown). Besides target potency, transport is also improved with the replacement of carboxylic acid with a tetrazole. Upon oral administration, losartan was found to be 20 times more potent than the parent.[2] Compound **45** was made as a precursor in the synthesis of compound **46** and it is an amide acid bioisostere of **29a**, its biological activity was also investigated.

Synthesis of compounds **43**-**45** was successfully conducted via Route 2 as shown in Figure 20.[11-12] Compound (1*R*,3*S*)-MMV008138 (**29a)** was successfully synthesized by repeating Dr. Z. K. Yao's two-step procedure (Figure 14).[5] Direct coupling of amine to **29a**, by HBTU or HATU, was easily conducted at ambient temperature in DMF overnight. The selection of coupling reagent, in this case, is based on availability of the chemical. Either coupling agent work well in this coupling, affording compound **43**, **44**, **45** in 63%, 83% and 63% yields respectively (Figure 20).

Synthesis and purification of the tetrazole analog **46** was more complicated. It is expected that compound **46** would be highly polar due to the four nitrogen atoms present in the tetrazole ring. Parth Vaghani, a previous undergraduate researcher in our group, successfully synthesized a small quantity of **46** as a mixture of stereoisomers; HRMS showed a molecular mass that matched the expected result. However, due to the high polarity of compound **46**, he was unable to purify and separate its *cis*- and *trans*- diastereomers. To resolve the difficulty in separation caused by its high polarity, we hypothesized synthesizing a protected tetrazole (**47**) first, and finally deprotecting to acquire compound **46**. Based on methods for tetrazole synthesis published by Duncia *et al*.,[13] the synthetic route shown in Figure 24 was proposed. Unfortunately, the attempt to synthesize compound **47** directly from compound **45** failed, and starting material was recovered via flash chromatography. This could be the result of steric hindrance from the bulky tetrahydro- β-carboline scaffold.

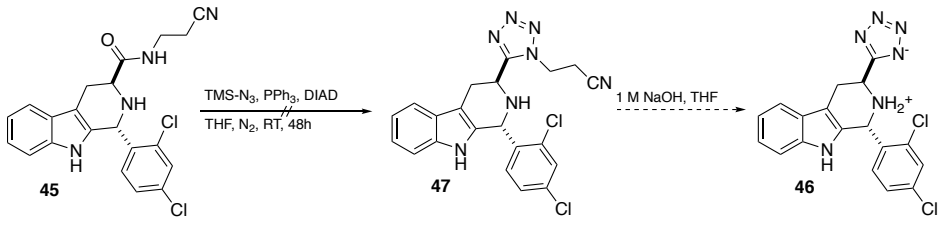

Figure 24. Attempted direct synthesis of compound **46**.

To overcome the difficulty of late-stage introduction of a protected tetrazole group at C3, an indirect synthetic route starting

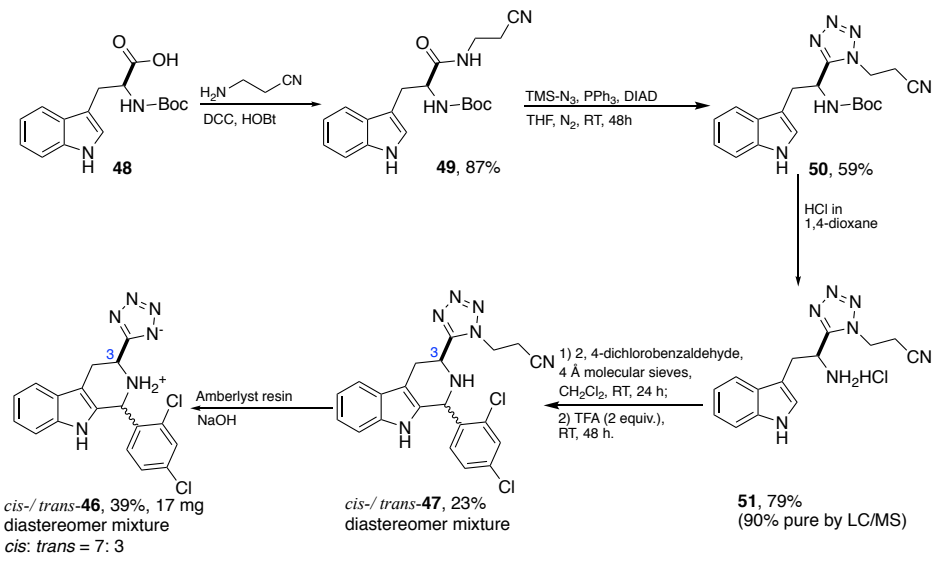

Figure 25. Indirect synthesis of compound **46**.

from Boc-Trp-OH was undertaken (Figure 25). Coupling of $NH_2(CH_2)_2CN$ with Boc-Trp-OH by DCC and HOBt afforded compound **49** in 87% yield. *N*-Boc-Trp-tetrazole analog **50** was also successfully synthesized in this case by Duncia's two-step literature procedure in 59% yield.[13] Acidic deprotection (HCl in dioxane) afforded **51** in 79% yield, while leaving the $-(CH_2)_2CN$ intact; only a slight impurity was visible by LC/MS and NMR. The subsequent Pictet-Spengler reaction of compound **51** with 2, 4-dichlorobenzaldehyde proceeded as hoped, but with a low yield (23%). Unfortunately, despite multiple attempts with various solvent systems, separation of the *cis*- and *trans*-diastereomers via flash chromatography was unsuccessful. It appears that the presence of the $-(CH_2)_2CN$ protecting group on tetrazole is insufficient to reduce the polarity of compound **47**, and cannot enable effective separation of the *cis*- and *trans*- diastereomers. The Pictet-Spengler adduct was obtained as a diastereomer mixture, *cis-/ trans*-**47**. The final step to remove the $-(CH_2)_2CN$ group was conduct under basic conditions with Amberlyst hydroxide resin. HRMS confirmed that the expected product was formed ($[M+H]^+$, calculated 385.0730, found 385.0714). NMR of the product showed the presence of significant impurities, yet due to the polarity of *cis-/ trans*-**46**, purification was difficult. Eventually, we resorted to HPLC (assistance from the Josan group and M. Ghavami) to remove most of the impurity and obtain *cis-/ trans*-**46** in 39% yield as a mixture of diastereomers (*cis* : *trans* = 3 : 7).

2.1.2 Biological study and results

Compounds **43**-**45** and *cis-/ trans*-**46** were studied in biological assays, performed by our collaborator Prof. M.B. Cassera at the University of Georgia. *P. falciparum* growth inhibition (IC_{50}) assays were conducted on all four compounds to assess their inhibitory activity. Inhibition studies were conducted with the inhibitor against *P. falciparum* Dd2 strain, by SYBR Green I assay. In short, ring stage parasite cultures were grown for 72 h under

controlled conditions, in the presence of increasing concentrations of the inhibitor. After 72 h, parasite growth can be quantified by SYBR Green I assay, where SYBR Green I is a dye that binds double-strand DNA to form a fluorescent adduct. The level of fluorescence is proportional to the concentration of double-strand DNA, which itself reflects the extent to which asexual reproduction of the parasite has occurred.[14] The half-maximum growth inhibition concentrations (IC_{50}) were calculated using nonlinear regression curve fitting with GraphPad Prism (GraphPad Software, Inc.).[6, 14-15]

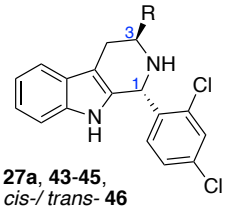

27a, **43-45**, *cis-/ trans-* **46**

Entry	Compound	R	*P. falciparum* Dd2 strain growth inhibition IC_{50} (nM)
1	**29a**	-COOH	250 ± 70
2	**43**	$-CONHSO_2Me$	3,000 – 5,000 ± 1,000
3	**44**	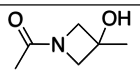	> 5,000
4	**45**	$-CONH(CH_2)_2CN$	> 5,000
5	*cis-/ trans-* **46**[a]		1,250 – 2,500

[a]cis : trans = 3 : 7.

Table 8. Growth inhibition data of acid bioisosteres of MMV008138.

From the growth inhibition data shown in Table 8, all four acid bioisosteres (**43-45**, *cis-/ trans*-**46**) show weak potency towards *P. falciparum* Dd2 strain; none have IC_{50} value comparable to the parent (**29a**) nor are they within the nanomolar range. It is important to note that compound *cis-/ trans*-**46** was assayed as a mixture of the *cis*- and *trans*- diastereomer (*cis* : *trans* = 3 : 7), thus the actual IC_{50} value for the effective *trans*- isomer would be smaller than the value reported in Table 8. From the ratio of *cis*- and *trans*- isomer in the diastereomer mixture, we know that the *trans*-isomer (**46**) is approximately 70 %. Thus, the IC_{50} value for **46** would be roughly between 875 – 1750 nM. However, even with this in consideration, the tetrazole analog did not exhibit improved inhibitory activity towards *P. falciparum*. It is therefore not an excellent bioisosteric replacement for the carboxylic acid group. Because none of the four analogs (**43-45**, *cis-/ trans*-**46**) exhibited good inhibitory activity towards parasite growth, IPP reversal of growth inhibition was deemed unnecessary and therefore not conducted.

The biological assay results revealed that methylsulfonamide, $-NH(CH_2)_2CN$, 3-methylazetidin-3-ol, and tetrazole (**46**) are bad or poor replacements for the carboxylic acid group of our lead compound (1*R*,3*S*)-

MMV008138 (**29a**). This indicates a very tight C3 substituent SAR for analogs of **29a**. Together with the data from previously investigated C3 analogs (Table 7), it seems that only small amides (e.g. methyl amide) can serve as good carboxylic acid surrogate.[5-6] It is reasonable to hypothesize that the C3 substituent of **29a** must be interacting with a very constricted pocket within the *Pf*IspD enzyme. Thus, an appropriate substituent at C3, in terms of electron-withdrawing property, hydrogen-bonding ability, and more importantly size, is critical to compound potency.

Despite the unsuccessful attempts in acid bioisostere investigation with **43**-**45** & *cis*-/ *trans*-**46**, our current knowledge of C3 SAR for analogs of **29a**, complemented with preliminary drug metabolism study results, suggest that acid bioisosteres may remain a viable approach for structural modification. However, further investigation of C3 analogs of **29a** should be directed to the search of small, heteroatom-containing isosteric replacements for the carboxylic acid moiety.

2.2 Synthesis and biological evaluation of MMV008138 A-ring analogs

A-ring analogs of (1*R*,3*S*)-MMV008138 (**29a**) is a lead analog series less explored in our ongoing research, albeit crucial to the thorough understanding of the SAR regarding drug lead **29a**.

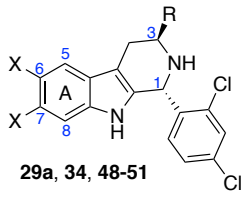

29a, **34**, **48-51**

Entry	Compound	R	X	*P. falciparum* Dd2 strain growth inhibition IC_{50} (nM)
1	**29a**	COOH	H	250 ± 70
2	**34**	CONHMe	H	190 ± 30
3	**48**	COOH	F	73 % inhibition @ 10,000
4	**49**	COOH	Cl	>10,000
5	**50**	CONHMe	F	1,189 ± 95
6	**51**	CONHMe	Cl	74 % inhibition @ 10,000

Table 9. Growth inhibition data of di-substituted (1*R*,3*S*)-MMV008138 (**29a)** A-ring analogs.

In the initial effort to probe the A-ring SAR of **29a**, four di-substituted A-ring analogs (Table 9, **48**-**51**) were synthesized by Dr. Z. K. Yao.[16] From growth inhibition shown in Table 9, it is apparent that neither 6, 7-Cl_2 nor 6, 7-F_2 are potent analogs, as their ability to inhibit parasite growth is reduced by at least 4-fold in comparison to **29a** and **34**. It appears that 6, 7- disubstitution is an unfavorable structural modification strategy to improve drug lead properties. However, due to the lack of understanding and insight into A-ring SAR of **29a**, it would be presumptuous to assume that the A-ring moiety of **29a** can tolerate no modification. Two important questions are yet to be addressed regarding A-ring modification: 1) Which position(s)

can tolerate modification to improve drug properties; 2) what functional groups can be used? Thus, a larger library of A-ring analogs must by synthesized and assayed to gain further sight. To better elucidate biological assay data and understand SAR, it is beneficial to probe the A-ring positions one at a time and one functionality at a time. These findings in turn, will better direct us in future analog investigation and lead optimization.

2.2.1 Synthesis

A-ring modification of (1*R*,3*S*)-MMV008138 (**29a**) is very difficult to execute directly from **29a**. Even if viable, purification would be an ever-rising challenge when taking into consideration the polarity of the (1*R*,3*S*)-MMV008138 (**29a**) scaffold. Thus, a more feasible approach would be to synthesize substituted (*S*)-tryptophan methyl ester analogs, and employ them as starting materials in following synthesis to afford target molecules.

2.2.1.1 Synthesis of substituted (*S*)-tryptophan methyl ester analogs

Preparation of (1*R*,3*S*)-MMV008138 (**29a**) A-ring analogs from substituted (*S*)-tryptophan methyl ester precursors follow the same synthesis depicted in Figure 14.[5] However, asymmetric synthesis to afford enantiopure substituted (*S*)-tryptophan methyl esters have proven challenging. The synthesis implemented by Dr. Z. K. Yao, though successful, was a complex and time-consuming process; he used used a Pd-catalyzed route to prepare the requisite indoles, and then used a Schöllkopf chiral auxiliary method to prepare the corresponding enantioenriched tryptophans.[16]

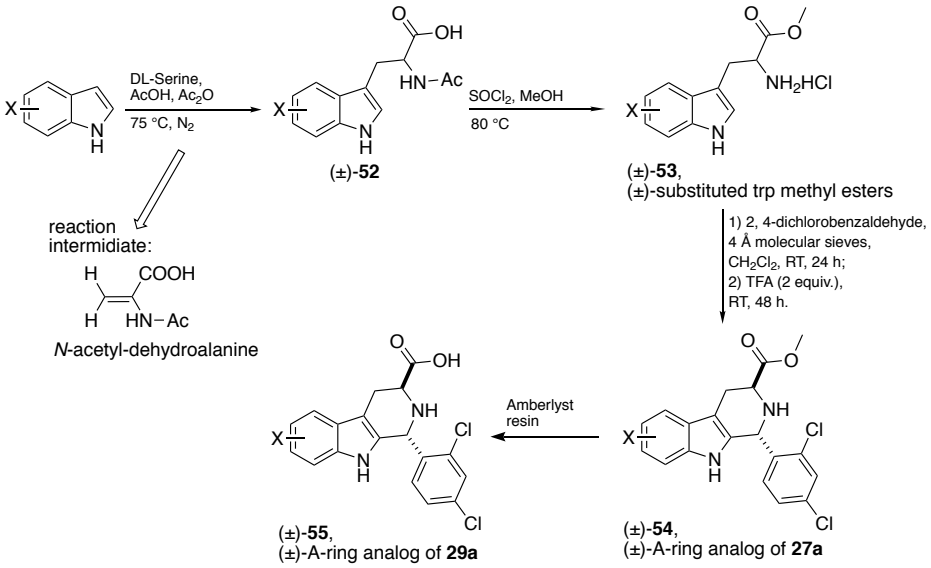

Figure 26. Synthesis of racemic tryptophan derivatives and racemic MMV008138 A-ring analogs.

To circumvent the problem of complicated synthesis, a synthetic route to give racemic substituted tryptophan methyl esters (Figure 26, (±)-**53**) has been successfully implemented by M. Ghavami in our group (Figure 26). Presumably the reaction proceeds via formation of the *O*,*N*-

diacetylserine, which then eliminates to give *N*-acetyl-dehydroalanine (Figure 26). Michael addition of the indole to this intermediate and proton transfer steps give the desired *N*-acetyl tryptophan ((±)-**52**).[17-19] Of course it must be noted that the A-ring analogs of **29a** ((±)-**55**) synthesized from racemic substituted tryptophan methyl esters ((±)-**53**) are racemic mixtures as well. The racemic mixture is a 1: 1 ratio of the expected **29a** analog with (1*R*,3*S*)-stereochemistry and its enantiomer with (1*S*,3*R*)-stereochemistry. Though not as ideal as running biological assays on stereochemically pure A-ring analog samples, assays on racemic samples can be a good strategy for time economy. From the IC_{50} data obtained on racemic samples, we can get an estimated IC_{50} of the corresponding (1*R*,3*S*)-analog by cutting the obtained value by half. Though this is only an approximation, it does help us understand the inhibitory activity of a certain A-ring analog and decide whether the adopted modification strategy merits preparation of the pure (1*R*,3*S*)-stereoisomer. From the synthetic scheme shown in Figure 26, we can see it only requires two steps to the substituted tryptophan methyl ester precursor (±)-**53**, greatly improving the efficiency in probing A-ring SAR.

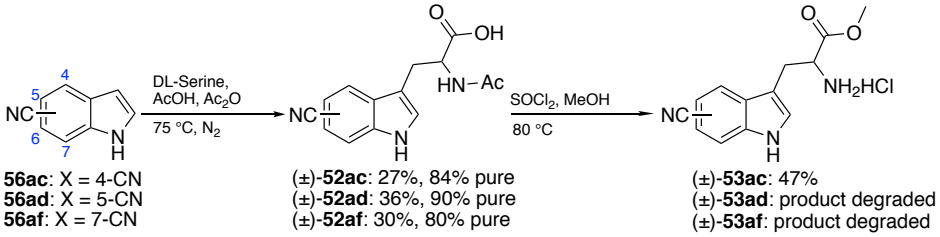

Figure 27. Synthesis of (±)-**53ac**, **ad**, **af**.

As Ms. M. Ghavami was already working on various halogenated indoles, I turned my attention to cyano-indoles. The cyano group is small in size, stable to metabolism and is present in over 30 approved pharmaceuticals.[20] In addition, the strong electron-withdrawing nature of the cyano group could reduce the likelihood of oxidative metabolism of the benzo-ring of the indole. However, despite the success of the synthetic route in Figure 26 to provide racemic halogenated A-ring variants of **29a**, problems quickly began to emerge when it was applied to cyanoindoles **56ac**, **ad**, **af** (Figure 27).

Cyanoindoles **56ac**, **ad**, **af** were purchased from Astatech and Arkpharm. Cyano-substituted tryptophans (±)-**52ac**, **ad**, **af** were successfully synthesized, but in lower than desired yields (27 – 36%). Although the synthesis of acetyl protected tryptophan derivatives from monosubstituted indoles and serine is well established in previous literature,[17-19] this method gives good to excellent yields (70 – 98%) only with indole starting materials bearing a halogen or an electron donating group (EDG, e.g. -Me, -OMe). When monosubstituted indoles with an electron

withdrawing group (EWG), e.g. nitroindoles are used, the yields of the corresponding acetyl protected tryptophan derivatives were significantly lower, only 40 – 60% depending on the position of the substituent.[17] From these literature data, a general trend can be observed: the smaller the Hammett subtituent constant (σ) of the indole substituent, the higher the yield of the corresponding product. This trend can be well explained through a mechanistic standpoint. As described above, this sequence depends upon a Michael addition, where the substituted indole acts as the Michael donor (nucleophile). Because any factor that can increase nucleophilicity of the Michael donor will also facilitate the reaction, it is reasonable that this particular reaction will proceed well with EDG- or halogen-substituted indoles, but not with EWG-substituted indoles.[21] An additional problem with this reaction method is product purification. Acetyl protected tryptophan derivatives are acidic polar compounds that have serious tailing when conducting flash chromotography. Thus, 1 – 2 % acetic acid has to be added to a polar eluant system to reduce dragging and move the product. However, this in turn introduced the problem of inefficient removal of acetic acid and high boiling point solvent, which contributed to (±)-**52ac, ad, af** being only 80 – 90 % pure.

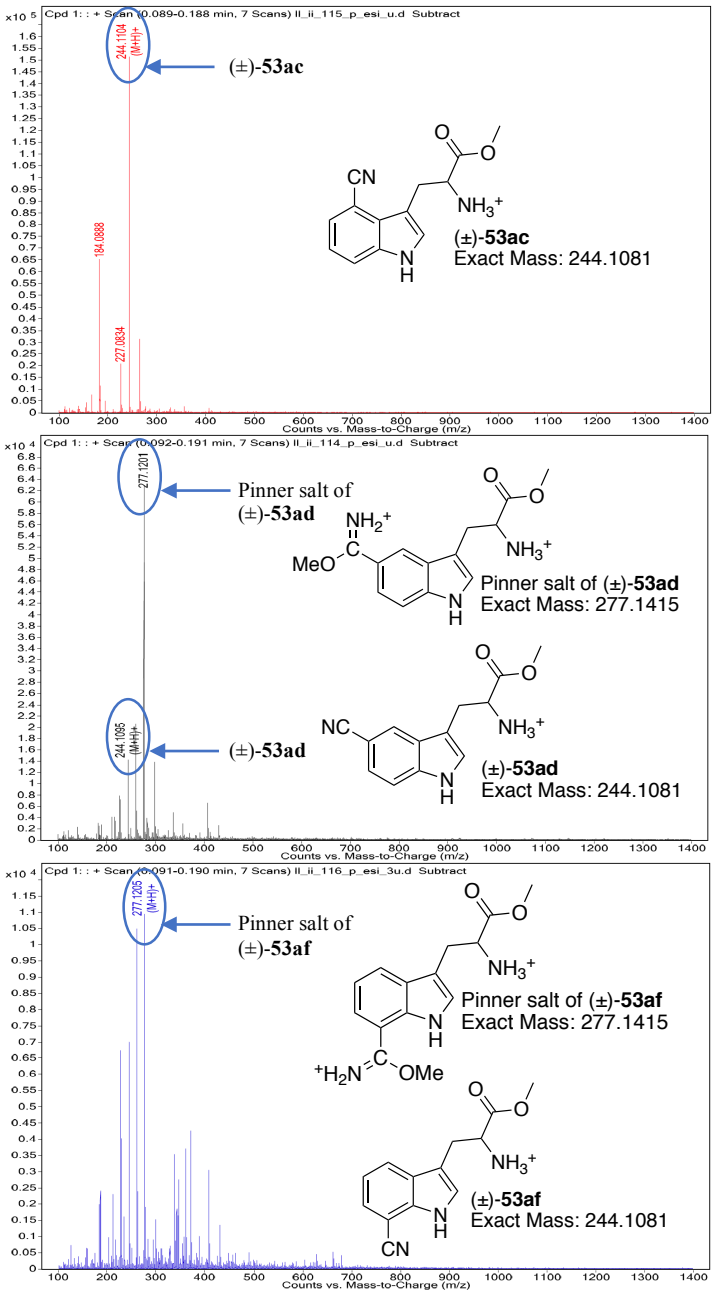

Figure 28. HRMS of (±)-**53ac**, **ad**, **af**.

The second step to synthesize (±)-**53ac**, **ad**, **af**, which is acetyl deprotection and acid methylation, presented the even more critical problem of product degradation. The one-pot synthesis of substituted (±)-Trp-OMe-HCl by refluxing acetyl protected tryptophan derivatives with $SOCl_2$ and MeOH is efficient and easy to work-up (the product precipitates as HCl salt). However, the acidic and protic reaction condiction is not well tolerated by functional groups like -CN, which are prone to side-reactions under such condition.[22-23] As can be seen in Figure 27, only (±)-**53ac** was obtained in 47 % yield. Both (±)-**53ad** and (±)-**53af** were a mixture by NMR, of which the majority is degraded product based on HRMS analysis (Figure 28).

Nitriles can undergo alcoholysis under acidic conditions, namely the Pinner reaction, to form an imino ester salt, or Pinner salt (Figure 29).[23] The Pinner salt itself is quite reactive and can also further react with various nucleophiles (e.g. H_2O). As acetyl deprotection and acid methylation reactions progress, HCl is generated and accumulated in the reaction system. In the presence of MeOH at 80°C, the chance of product degradation via the Pinner reaction will greatly increase. Two solutions to this problem would be: 1) track and control reaction time to quench prior to product degradation; 2) isolate the expected product, substituted (±)-Trp-OMe-HCl, from the Pinner salt, if this were indeed possible without substantial hydrolysis to the methyl ester or carboxylic acid. But neither of these approaches seemed feasible.Without an effective solution to circumvent the complications mentioned above, in addition to the fact that asymmetric synthesis of (*S*)-tryptophan methyl ester precursors is prefered, a new synthetic route needs to be established.

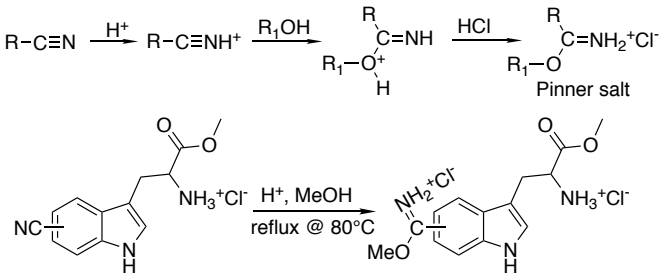

Figure 29. The Pinner reaction.

Advances in nickel-catalyzed reductive cross-coupling, particularly research by Liu *et al.*, provided us with a new approach to asymmetric synthesis of substituted (*S*)-tryptophan derivatives.[24-25] Liu *et al.* provided 29 examples of his method to synthesize enantioenriched amino acids from iodoarenes and Boc-β-iodo-Ala-OMe. High enantiopurity (>99% ee) was demonstrated for protected L-phenylalanine derivatives (e.g. (*S*)-4-methoxy-Boc-Phe-O*t*Bu, (*S*)-4-bromo-Cbz-Phe-OBn and (*S*)-4-cyano-Cbz-Phe-OBn) and the method was also applied to the asymmetric synthesis of one Trp derivative, (*S*)-5-fluoro-Boc-Trp-OMe. I thus applied this method by Liu *et al*., to the synthesis of substituted (*S*)-Trp-OMe-HCl analogs.[24] This route also uses substituted indoles as the initial starting material and consists of three major synthetic steps, the details of which are depicted in Figure 30. The first

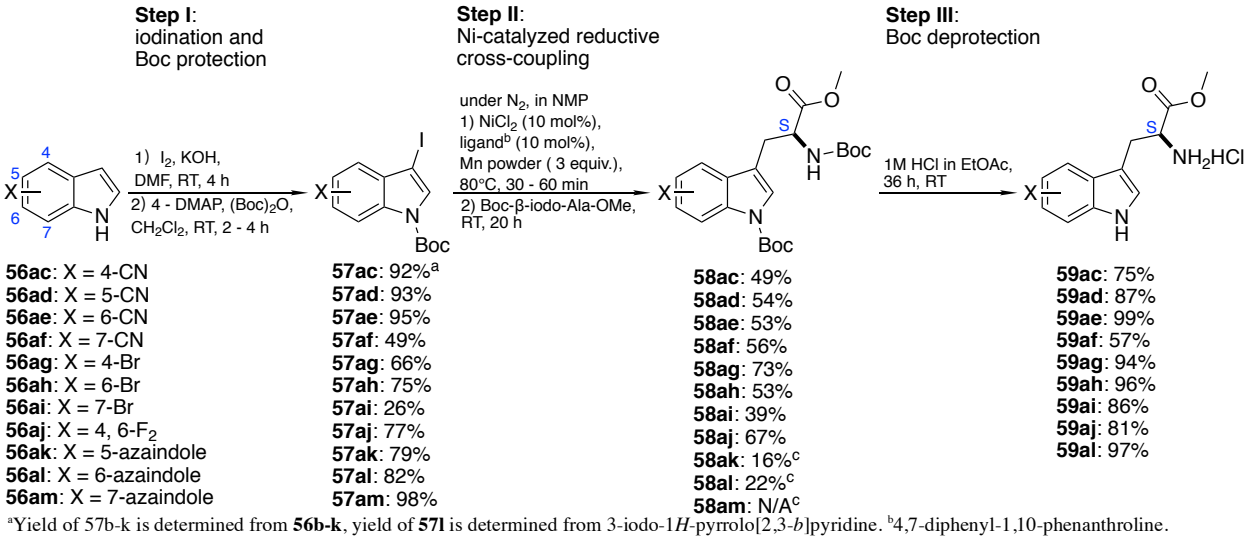

[a]Yield of 57b-k is determined from **56b-k**, yield of **57l** is determined from 3-iodo-1*H*-pyrrolo[2,3-*b*]pyridine. [b]4,7-diphenyl-1,10-phenanthroline.
[c]Coupling reaction temperature of second step is at 45°C. N/A, signifies "not applicable", meaning the expected product is not afforded.

Figure 30. Asymmetric synthesis of (*S*)-Trp-OMe-HCl analogs via Ni-catalyzed reductive cross-coupling.

step is the iodination of monosubstituted indoles (**56ac-am**) under basic conditions, followed by 4-DMAP catalyzed Boc protection to give the corresponding *tert*-butyl 3-iodo-1*H*-indole-1-carboxylate derivative (**57ac-am**). Yields for this sequence ranged from 26 – 95%. The low yields observed for **57af** (49%, 7-cyano) and **57ai** (26%, 7-bromo) is likely due to steric hindrance for the installation of the Boc group. The second and key step of this synthetic route is the Nickel-catalyzed reductive cross-coupling of **57ac-am** to Boc-β-iodo-Ala-OMe to give (*S*)-Boc-Trp(Boc)-OMe analog, **58b-l**.[24] Under inert atmosphere (N_2) at 80°C, the bidentate ligand 4,7-diphenyl-1,10-phenanthroline (**L**) and $NiCl_2$ form an (**L**)$Ni^{II}Cl_2$ complex which is reduced by Mn powder to first generate ligated-Ni(0) complex *in situ* (**a** in Figure 31 below).[26] The reaction is allowed to cool to room temperature after 30 – 60 minutes, and the two reactants are added simutaneously to allow for cross-coupling reaction overnight. The corresponding product (**58ac-al)**, can be easily isolated and purified via flash chromatography. Yields for cyano- or halogen-substituted products (**58ac-aj**) are good, ranging from 39 – 73%; while yields for azaindole analogs **58ak-am** are much lower, only 16 – 22% or no reaction. The final step is acid deprotection of the two Boc groups in **58ac-al**. The final product, substituted (*S*)-Trp-OMe-HCl (**59ac-al**), was obtained via filtration with moderate to excellent yields (57 – 97%).

Reviewing the yields for the Ni-catalyzed reductive cross-coupling products **58ac-am**, it is clear that the reaction works well for 3-iodoindoles **57ac-aj** that bear weak (-Br) to strong electron-withdrawing groups (-CN, or 4,6-F_2). These results also show good cross-coupling selectivity for I vs Br or F, although the position of halogen substitution on the indole nucleus also varies in this comparison. From reactions I performed, in conjunction with

similar successful examples from the literature, it is reasonable to infer that this reaction can be compatible with a large range of starting materials.[24-25] The benzo substituent on **57** derivatives can included halogens, carboxylates, -OMe, and -CF_3. However, as Figure 30 also shows, reactions with 3-iodoazaindole derivatives (**57al-am**) proceed in significantly lower yields (**58ak**, **al**), and in the case of **57am**, no desired **58am** was obtained.

Ni-catalyzed reductive cross-coupling of Ar-I and Alkyl-I is widely accepted to occur via a radical chain mechanism.[26] For our particular reaction (Figure 30, Step II), a detailed proposed mechanism is shown in Figure 31 and Figure 32. Selectivity for cross-coupling product (Ar-Alkyl) rises from: 1) selective oxidative addition of Ar-I over Alkyl-I; 2) selective formation of the more stable alkyl radicals over aryl radicals.[26-27] From the reaction mechanism, we can see that selective oxidative addition of Ar-I (**57ac-am**) to ligated Ni(0) complex **a** generates a (**L**)Ni^{II}(Ar)I complex **b**. The starting Boc-β-iodo-Ala-OMe is reduced by ligated Ni(I) iodide **d** to form the alanine radical **f**. This radical **f** then adds to intermediate **b** to give Ni(III) intermediate **c**. Reductive elimination gives the desired product **58ac-al** and ligated Ni(I) iodide **d**. Single-electron transfer (SET) from complex **d** to the Boc-β-

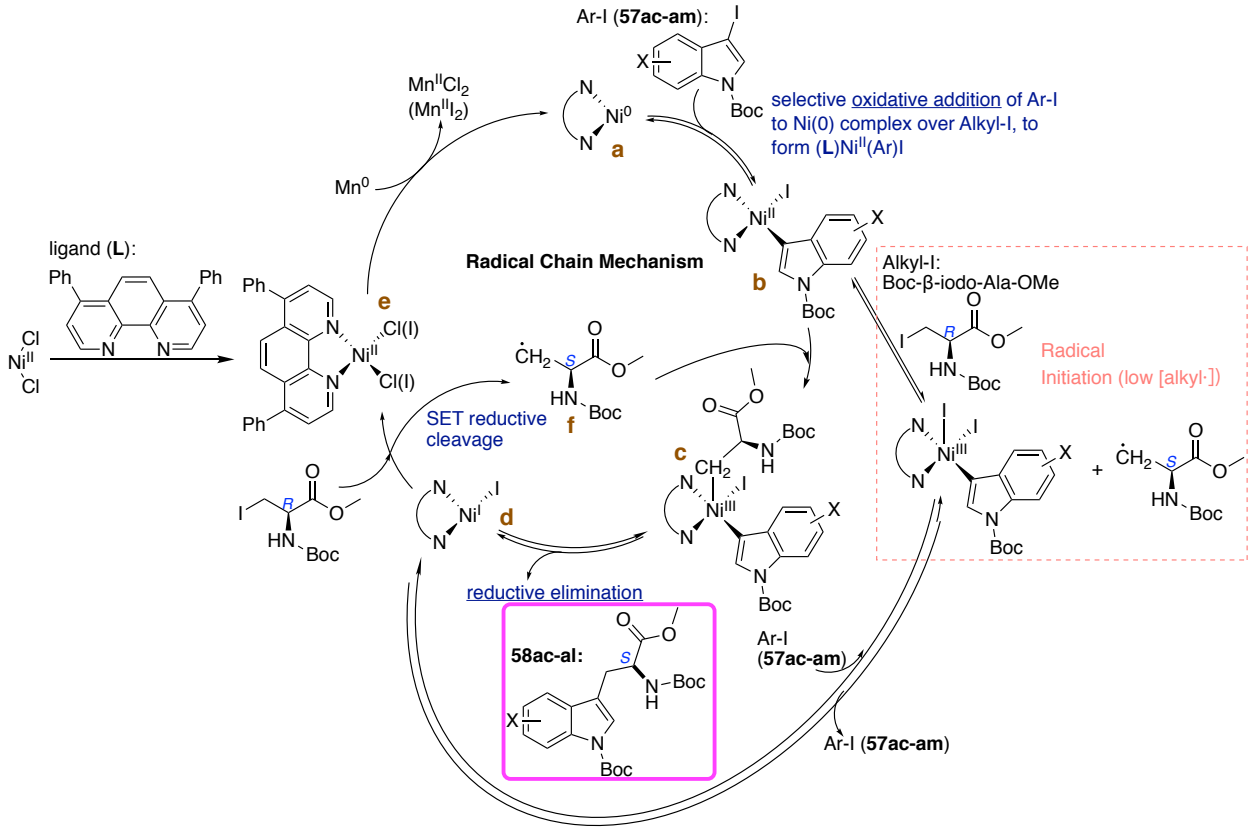

Figure 31. Radical chain mechanism of Ni-catalyzed reductive cross-coupling.

iodo-Ala-OMe generates the aforementioned alanine radical **f** and ligated Ni(II) dichloride **e**. Reduction of **e** by one equivalent of Mn metal generates $MnCl_2$ and regenerates the catalyst **a** in its resting state.

Selectivity, in the initial oxidative addition, to form exclusively the (**L**)Ni^{II}(Ar)I complex **b** and not the alternative (**L**)Ni^{II}(Alkyl)I complex is essential to forming cross-coupling product. This selectivity rises from the subtle differences in reactivity between $Ar^{\delta+}$-$I^{\delta-}$ and $Alkyl^{\delta+}$-$I^{\delta-}$.[26-27] Thus poorly reactive aryl halides (e.g. iodomesitylene) and highly reactive alkyl halides (e.g. benzyl bromide) will produce low yields for the cross-coupled product. Recent mechanistic studies also revealed that the oxidative addition rate and stability of the resulting (**L**)Ni^{II}(Ar)I complex play important roles in reaction outcome. Fast oxidative reaction rate is preferred, and any factor that causes Ar-I to undergo this step slowly, such as steric hinderance, is likely to cause unfavorable results. Stable (**L**)Ni^{II}(Ar)I complex is desired. Unstable (**L**)Ni^{II}(Ar)I complexes are susceptible to deleterious side reactions like disproportionation, conproportionation, and/ or hydrogen abstraction, and increase the chance of competing mechanisms to generate homocoupled and/ or Ar-H by-products.[28]

These mechanistic observations can provide plausible explanations to the difficulty in forming cross-coupled products, **58ak-am**. Possible reasons are: 1) reactivity difference between **57ak-am** ($Ar^{\delta+}$-$I^{\delta-}$) and Boc-β-iodo-Ala-OMe ($Alkyl^{\delta+}$-$I^{\delta-}$) is too small, causing slow oxidative addition; and/ or, 2) the (**L**)Ni^{II}(Ar)I complex formed is unstable. Because the hydrodeiodination products 1-(*tert*-butyloxycarbonyl)-5-azaindole and 1-(*tert*-butyloxycarbonyl)-6-azaindole were isolated as by-products of **57ak** and **57al**, and no homocoupled by-products were isolated, I believe the second reason is the more likely explanation.

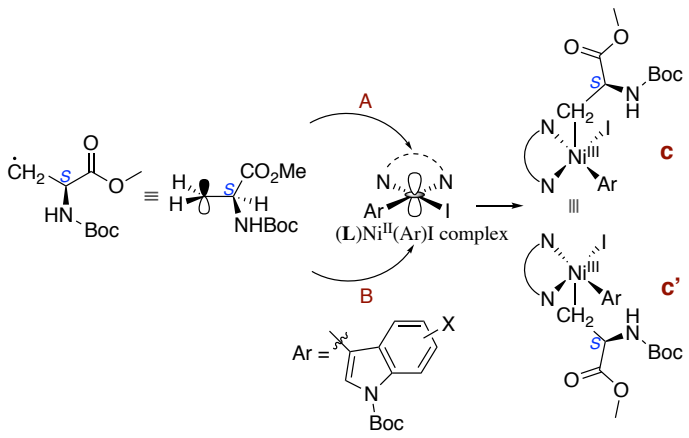

Figure 32. Addition of alkyl radical with (**L**)Ni^{II}(Ar)I complex.

Figure 32 provides an explanation to the feasibilty of asymmetric synthesis of substituted (*S*)-Trp-OMe-HCl (**59ac-al**). The alkyl radical generated from Boc-β-iodo-Ala-OMe can attack the (**L**)Ni^{II}(Ar)I complexe via approach A or approach B. Because the radical center is not chiral, the two diastereomeric (**L**)Ni^{III}(Ar)(Alkyl)I complexes **c** and **c'** can be formed. These two complexes differ only in the configuration at the Ni(III) center, but reductive

elimination from both **c** and **c'** will yield the desired product **58ac-al** with the original chiral center in Boc-β-iodo-Ala-OMe left unchanged. β-Hydride elimination in metal catalysis, frequent in palladium chemistry, is often detrimental to asymmetric coupling. Fortunately, the energy required to enable Ni-C bond rotation of (**L**)Ni^{III}(Ar)(Alkyl)I prior to β-hydride elimination is often much higher than comparable palldium intermediates. Thus, β-hydride elimination is less likely in Ni-catalysis and often not a problem.[25, 27] Under reaction conditions similar to those described in Figure 30 Step II, Liu *et al.* have successfully conducted asymmetric synthesis of a diverse range of enantiopure L- or D-amino acid derivatives, supported by rotation and *ee* measurements (*ee* > 99%).[24] To evalute enantiopurity of **59ac-aj, al**, optical rotation measurements were conducted (supporting info). With comparison to available literature data, I am confident that **59ac-aj, al** are highly enantioenriched. Follow up determination of *ee* values will verify whether or not **59ac-aj, al** are enantiopure.

In summary, asymmetric synthesis of (*S*)-Trp-OMe-HCl analogs via Ni-catalyzed reductive cross-coupling, as depicted in Figure 30, is an effective and simple method to obtain highly enantioenriched compounds for use in (1*R*,3*S*)-MMV008138 (**29a**) A-ring analog synthesis. This new synthetic route, albeit with one more step than the previous approach, have the following advantages: 1) intermediates synthesized and the final product are all easy to isolate and purify via flash chromatography or filtration; 2) reaction conditions are mild; 3) applicable to a wide and diverse range of substituted indole starting materials, except for azaindoles; 4) the final products, (*S*)-Trp-OMe-HCl analogs, are highly enantioenriched.

2.2.1.2 Synthesis of MMV008138 A-ring analogs

Synthesis of (1*R*,3*S*)-MMV008138 (**29a**) A-ring analogs from the corresponding substituted (*S*)-Trp-OMe-HCl (Figure 33) follows the same protocol in Figure 14, which is Pictet-Spengler reaction followed by hydrolysis.[5]

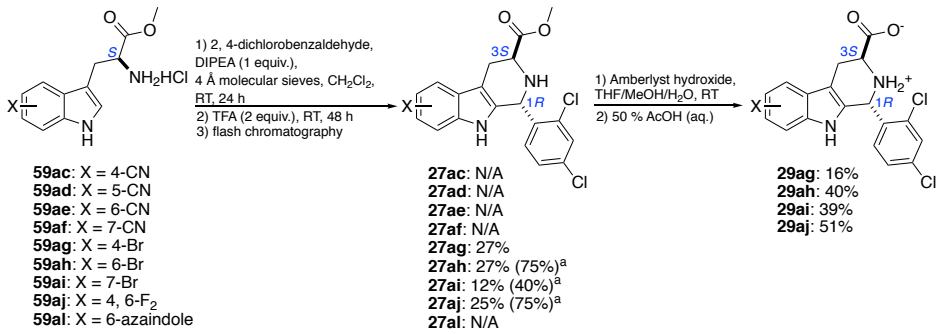

[a]First yield is of the (1*R*,3*S*)-product, yield in parenthesis is the total yield of (1*R*,3*S*)- and (1*S*,3*S*)-product. N/A signifies "not applicable", meaning the expected product did not form.

Figure 33. Synthesis of (1*R*,3*S*)-MMV008138 (**29a**) A-ring analogs.

Halogen substituted (*S*)-Trp-OMe-HCl (**59ag-aj**)

underwent the Pictet-Spengler reaction and subsequent hydrolysis smoothly. The *trans*-isomer (**27ag-aj**) from each step was successfully isolated and purified based on prior protocol established by Dr. Z. K. Yao. The ratio of the *trans*-isomers (**27ag-aj**) and the *cis*-isomer were within the expected range of 1: 2 to 1: 3.[5] We did encounter purification difficulties with the final products (A-ring analogs). There were traces of impurity present on NMR even after repeating purification work-up multiple times. The need to repeatedly conduct purification work-up largely contributes to the low yields of **29ag-aj**. The impurity was later identified by K. Cagasova to be gamma-hydroxybutyric acid, which we traced to the oxidative degradation of THF. Switching to dry THF and conducting a N_2 purge prior to the hydrolysis reaction resolved this problem.

Unfortunately, synthesis of **27ac-af** & **al** were unsuccessful. To understand why these reactions failed, we need to first examine the mechanism of the Pictet-Spengler reaction (Figure 34).[29-32] The Pictet-Spengler reaction is believed to occur in three to four steps. The first step is acid-catalyzed formation of iminium ion **a** from amine and aldehyde. The second step is nucleophilic attack of the iminium ion by the aryl group. This can happen one of two ways: pathway B directly forms a six-membered ring intermediate **c** and undergoes proton loss to give the Pictet-Spengler adduct **d** (three steps); pathway A generates a spiroindolenine intermediate **b** instead, which quickly undergoes a 1,2-sigmatropic shift to give the six-membered ring intermediate **c**, which then loses a proton to afford **d**.[29-32]

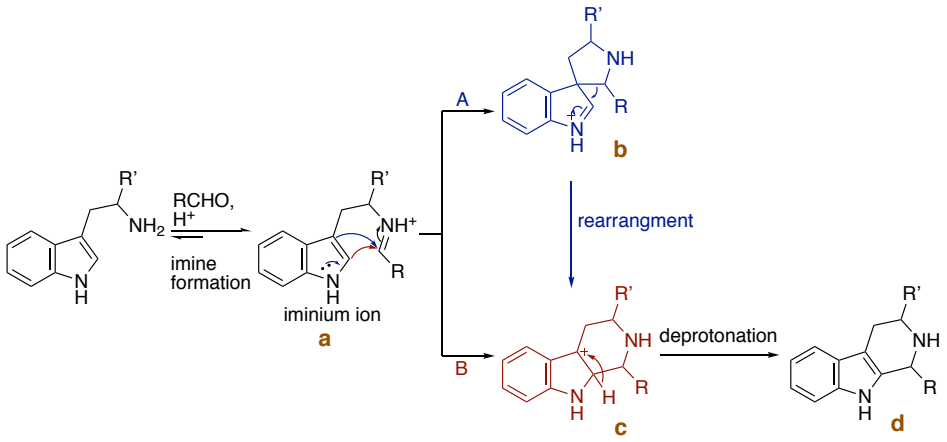

Figure 34. Mechanism of the Pictet-Spengler reaction.

As judged by thin-layer chromatography (TLC), imine formation occurred smoothly (**59ac-af**) in most cases, and we suspect the problem for no **27ac-af** formation lay in the slow conversion of imine to intermediates **b**/**c**. The efficiency of nucleophilic attack is dependent on the reactivity of the aryl group, which acts as the nucleophile (Nu^-). The higher the electron density at the position of attack, the easier the reaction. Thus, electron-donating groups (EDG) on the aryl ring can benefit the reaction. Examples of Pictet-Spengler reaction where the starting material

bears benzo substituents like -N_3, -OMe, -OH, even halogens, have been reported.[33-36] However, to the best of my knowledge, there are no prior examples where the aromatic substituent is strongly electron withdrawing (EWG). The failed attempts to synthesize **27ac-af** suggest that the presence of a strong EWG, like nitrile, can significantly decrease nucleophilic reactivity of the aryl group and hinder ring formation.

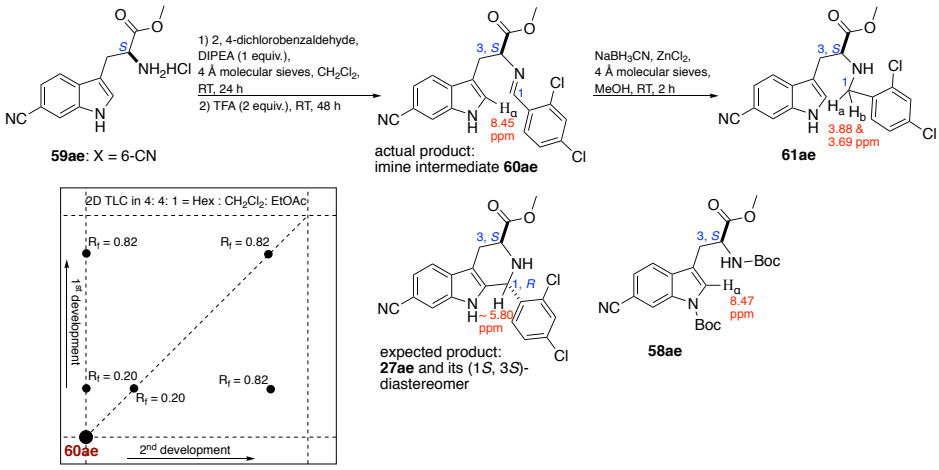

Figure 35. Synthesis and characterization of **60ae**.

This hypothesis is confirmed by the characterization of the isolated reaction products following attempted Pictet-Spengler reaction of **59ac-af**. To be concise, the isolated product (**60ae**) from **59ae** is used as an example (Figure 35). I initially suspected **60ae** to be the imine intermediate and

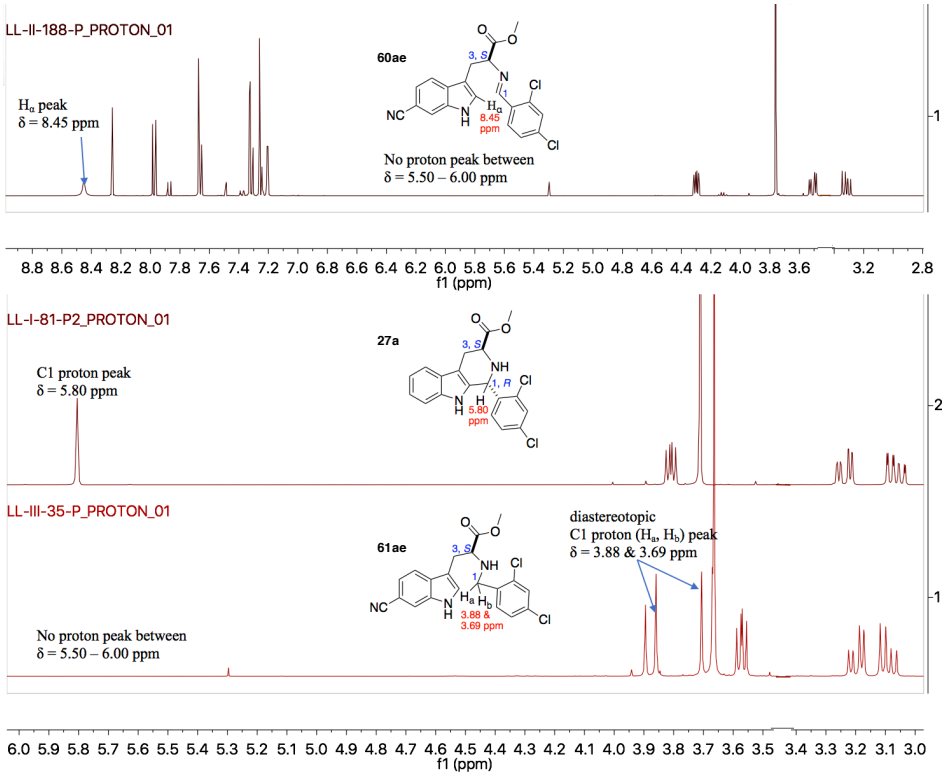

Figure 36. ^{1}H NMR comparison of **60ae**, **61ae** and **27a**.

not the expected product (**27ae**), based on two observations: 1) fractions of **60ae** from flash chromatography always contain traces of 2, 4-dichlorobenzaldehyde based on TLC R_f value comparison; 2) 2D TLC showed that purified **60ae** degrades on silica, giving one spot with $R_f \approx 0$ and one with large R_f close to 2, 4-dichlorobenzaldehyde. Close

examination of the ^{1}H NMR of **60ae** shows that it has no peak between δ = 5.50 – 6.00 ppm, which is where the peak for C1 proton usually appear. It also has an extra peak at δ = 8.45 ppm that integrates to 1, which should not be present in the ^{1}H NMR of cyclized Pictet-Spengler product (**27ae**). The chemical shift of δ = 8.45 ppm matches well with H_α in **58ae** (δ = 8.45 ppm), so it is most likely from H_α in **60ae**. This NMR observation proves that ring formation via nucleophilic attack did not occur due to low nucleophilicity caused by the electron withdrawing effect of -CN. To further validate that compound **60ae** is the imine intermediate, imine reduction by $NaBH_3CN$ was conducted. If **60ae** is in fact an imine, it will be reduced to **61ae** by $NaBH_3CN$. Comparison of ^{1}H NMR between **61ae** and **27a** will show significant difference in the peaks for C1 proton(s). Indeed, **60ae** can be reduced to afford **61ae** in 91% yield. Compound **61ae** has no proton peak between δ = 5.50 – 6.00 ppm. At the same time, it exhibits two diastereotopic proton peaks that are coupled to each other and have significantly lower chemical shifts than C1 proton in **27a**. These observations are consistent with my predictions and further confirm that compound **60ae** is the imine intermediate.

The above investigations show that imine formation is not a problem, but in the presence of strong electron withdrawing aromatic substituents (e.g. -CN), the following cyclization cannot proceed to afford the Pictet-Spenger reaction product. Though only the synthesis of **27al** was attempted (**27ak** not attempted), its failed synthesis may be due to similar reasons. Azaindoles are π-deficient heterocycles, thus they may not be nucleophilic enough to attack the iminium ion and form the expected cyclized product.

2.2.2 Biological study and results

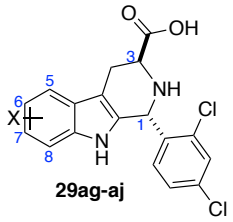

29ag-aj

Entry	Compound	X	*P. falciparum* Dd2 strain growth inhibition IC_{50} (nM)
1	**29a**	H	250 ± 70
2	**29ag**	5-Br	no inhibition @ 10,000
3	**29ah**	7-Br	4,280 ± 610
4	**29ai**	8-Br	~ 10,000
5	**29aj**	5, 7-F_2	964 ± 63

Table 10. Growth inhibition data of (1*R*,3*S*)-MMV008138 (**29a)** A-ring analogs.

Four new (1*R*,3*S*)-MMV008138 (**29a**) A-ring analogs (**29ag-aj**) were successfully synthesized for biological studies, corresponding growth inhibition data is presented in Table 10.

IC_{50} values of bromo-substituted A-ring analogs (**29ag-ai**), show that these analogs have low or no inhibitory activity. Thus, it is apparent that addition of -Br to the A-ring of **29a** is an

unfavorable modification. It is possible the binding pocket for **29a** in *Pf*IspD makes very close contact with the carbons of the benzo-ring and that no further substitution can be tolerated. However, 5,7-difluorinated compound **29aj** does have inhibitory activity towards parasite growth, being roughly 4 times less potent than **29a**. Most importantly, it is much more potent than **48** (Table 9, 73 % inhibition @ 10,000), which is 6,7-difluorinated.

2.2.3 Future Research Directions

Based on my results with brominated derivatives **29ag-ai**, future exploration of the A-ring should explore installation of small substituents. Fluorine atoms have unique properties, which led to its widespread application in medicinal chemistry as a hydrogen isostere. Fluorine atoms and hydrogen atoms are similar in size. Fluorination of metabolically labile sites within a drug lead is a common method to improve metabolic stability, on the condition that the presence of fluorine will not impair drug-target binding. The high electronegativity of fluorine has a strong effect on the pKa of nearby functionalities.[7] It also greatly polarizes the C-F bond, forming strong electrostatic interactions with nearby hydrogens. These interactions can greatly affect the activity of a drug molecule. The above reasons may contribute to the promising IC_{50} result of mono-fluorinated A-ring analogs: 5-F-analog and 7-F-analog, yet these benefiting influences do not appear to be additive as (1*R*,3*S*)-5, 7-F_2-analog **29aj** loses potency. It seems that single fluorination of the A-ring is worth further pursuit.

The series of mono-substituted nitrile A-ring analogs of **29a** are still of interest. Investigation into these compounds will reveal whether installation of the nitrile group is a viable modification strategy to the A-ring. It will also provide with some insight into how a strong electron-withdrawing group on the A-ring will affect the performance of our lead compound. Due to the difficulties encountered in running Pictet-Spengler reactions with nitrile substituted (*S*)-Trp-OMe-HCl (**59ac-af**), we should try pursuing cyanation of bromo substituted A-ring analogs. Such as cyanation with $K_4[Fe(CN)_6]$ using a $Pd(PPh_3)_4$/ DBU catalytic system.[37]

With more insight into the SAR of (1*R*,3*S*)-MMV008183 (**29a**) we will gain better understanding of drug behavior, drug ligand interaction, as well as how the drug lead can be modified in various substructures to improve its overall performance.

2.3 References for Chapter 2:

1. Kalgutkar, A. S.; Daniels, J. S., Carboxylic acids and their bioisosteres. In *Metabolism, Pharmacokinetics and Toxicity of Functional Groups: Impact of the Building Blocks of Medicinal Chemistry on Admet*, Smith, D. A., Ed. 2010; pp 99-167.

2. Ballatore, C.; Huryn, D. M.; Smith, A. B., Carboxylic acid (bio)isosteres in drug design. *ChemMedChem* **2013,** *8*, 385-395.

3. Lassalas, P.; Gay, B.; Lasfargeas, C.; James, M. J.; Tran, V.; Vijayendran, K. G.; Brunden, K. R.; Kozlowski, M. C.; Thomas, C. J.; Smith, A. B.; Huryn, D. M.; Ballatore, C., Structure property relationships of carboxylic acid isosteres. *J. Med. Chem.* **2016,** *59*, 3183-3203.

4. Lassila, T.; Hokkanen, J.; Aatsink, S. M.; Mattila, S.; Turpeinen, M.; Tolonen, A., Toxicity of carboxylic acid-containing drugs: The role of acyl migration and CoA conjugation investigated. *Chem. Res. Toxicol.* **2015,** *28*, 2292-2303.

5. Yao, Z. K.; Krai, P. M.; Merino, E. F.; Simpson, M. E.; Slebodnick, C.; Cassera, M. B.; Carlier, P. R., Determination of the active stereoisomer of the MEP pathway-targeting antimalarial agent MMV008138, and initial structure-activity studies. *Bioorg. Med. Chem. Lett.* **2015,** *25*, 1515-1519.

6. Ghavami, M.; Merino, E. F.; Yao, Z.-K.; Elahi, R.; Simpson, M. E.; Fernandez-Murga, M. L.; Butler, J. H.; Casasanta, M. A.; Krai, P. M.; Totrov, M. M.; Slade, D. J.; Carlier, P. R.; Cassera, M. B., Biological studies and target engagement of the 2-C-methyl-D-erythritol 4-phosphate cytidylyltransferase (IspD)-targeting antimalarial agent (1*R*,3*S*)-MMV008138 and analogs. *ACS Infect. Dis.* **2017**.

7. Meanwell, N. A., Synopsis of some recent tactical application of bioisosteres in drug design. *J. Med. Chem.* **2011,** *54*, 2529-2591.

8. Duvernay, F.; Chiavassa, T.; Borget, F.; Aycard, J. P., Experimental study of water-ice catalyzed thermal isomerization of cyanamide into carbodiimide: Implication for prebiotic chemistry. *J. Am. Chem. Soc.* **2004,** *126*, 7772-7773.

9. Kwon, C. H.; Nagasawa, H. T.; Demaster, E. G.; Shirota, F. N., Acyl, N-protected α-aminoacyl, and peptidyl derivatives as prodrug forms of the alcohol deterrent agent cyanamide. *J. Med. Chem.* **1986,** *29*, 1922-1929.

10. Sun, Z. Y.; Kwon, C. H.; Wurpel, J. N. D., Structure-activity study of 5-substituted 1-carbobenzoxy-2-iminohydantoins as potential anticonvulsant agents. *J. Med. Chem.* **1994,** *37*, 2841-2845.

11. El-Faham, A.; Albericio, F., Peptide coupling reagents, more than a letter soup. *Chem. Rev.* **2011,** *111*, 6557-6602.

12. Valeur, E.; Bradley, M., Amide bond formation: Beyond the myth of coupling reagents. *Chem. Soc. Rev.* **2009,** *38*, 606-631.

13. Duncia, J. V.; Pierce, M. E.; Santella, J. B., 3 Synthetic routes to a sterically hindred tetrazole - a new one - step mild coversion of an amide into a tetrazole. *J. Org. Chem.* **1991,** *56*, 2395-2400.

14. Smilkstein, M.; Sriwilaijaroen, N.; Kelly, J. X.; Wilairat, P.; Riscoe, M., Simple and inexpensive fluorescence-based technique for high-throughput antimalarial drug screening. *Antimicrob. Agents Chemother.* **2004,** *48*, 1803-1806.

15. Bowman, J. D.; Merino, E. F.; Brooks, C. F.; Striepen, B.; Carlier, P. R.; Cassera, M. B., Antiapicoplast and gametocytocidal screening to identify the mechanisms of action of compounds within the malaria box. *Antimicrob. Agents Chemother.* **2014,** *58*, 811-819.

16. Carlier, P. R.; Cassera, M. B.; Merino, E. F.; Yao, Z. K.; Ghavami, M., Compositions and formulations of methylerthritol phosohate pathway inhibitors and uses there of. **2015,** VTIP 15-044, PCT/US2015/058157.

17. Blaser, G.; Sanderson, J. M.; Batsanov, A. S.; Howard, J. A. K., The facile synthesis of a series of tryptophan derivatives. *Tetrahedron Lett.* **2008,** *49*, 2795-2798.

18. Konda-Yamada, Y.; Okada, C.; Yoshida, K.; Umeda, Y.; Arima, S.; Sato, N.; Kai, T.; Takayanagi, H.; Harigaya, Y., Convenient synthesis of 7 ' and 6 '-bromo-D-tryptophan and their derivatives by enzymatic optical resolution using D-aminoacylase. *Tetrahedron* **2002,** *58*, 7851-7861.

19. Yokoyama, Y.; Hikawa, H.; Mitsuhashi, M.; Uyama, A.; Hiroki, Y.; Murakami, Y., Total synthesis without protection: Three-step synthesis of optically active clavicipitic acids by a biomimetic route. *Eur. J. Org. Chem.* **2004,** 1244-1253.

20. Fleming, F. F.; Yao, L.; Ravikumar, P. C.; Funk, L.; Shook, B. C., Nitrile-containing pharmaceuticals: efficacious roles of the nitrile pharmacophore. *J. Med. Chem.* **2010,** *53*, 7902-7917.

21. Yokoyama, Y.; Nakakoshi, M.; Okuno, H.; Sakamoto, Y.; Sakurai, S., Mechanism for the direct synthesis of tryptophan from indole and serine: A useful NMR technique for the detection of a reactive intermediate in the reaction mixture. *Magn. Reson. Chem.* **2010,** *48*, 811-817.

22. Krieble, V. K.; Noll, C. I., The hydrolysis of nitriles with acids. *J. Am. Chem. Soc.* **1939,** *61*, 560-563.

23. Robinson, B., A non-catalytic alcoholysis of nitriles. *J. Chem. Soc.* **1963,** 2417-&.

24. Lu, X.; Yi, J.; Zhang, Z. Q.; Dai, J. J.; Liu, J. H.; Xiao, B.; Fu, Y.; Liu, L., Expedient synthesis of chiral α-amino acids through nickel-catalyzed reductive cross-coupling. *Chem.-Eur. J.* **2014,** *20*, 15339-15343.

25. Tasker, S. Z.; Standley, E. A.; Jamison, T. F., Recent advances in homogeneous nickel catalysis. *Nature* **2014,** *509*, 299-309.

26. Biswas, S.; Weix, D. J., Mechanism and selectivity in nickel-catalyzed cross-electrophile coupling of aryl halides with alkyl halides. *J. Am. Chem. Soc.* **2013,** *135*, 16192-16197.

27. Weix, D. J., Methods and mechanisms for cross-electrophile coupling of Csp(2) halides with alkyl electrophiles. *Accounts Chem. Res.* **2015,** *48*, 1767-1775.

28. Bajo, S.; Laidlaw, G.; Kennedy, A. R.; Sproules, S.; Nelson, D. J., Oxidative addition of aryl electrophiles to a prototypical nickel(0) complex: Mechanism and structure/reactivity relationships. *Organometallics* **2017,** *36*, 1662-1672.

29. Dalpozzo, R., The chiral pool in the Pictet-Spengler reaction for the synthesis of β-carbolines. *Molecules* **2016,** *21*, 18.

30. Jackson, A. H.; Smith, A. E., Electrophilic substitution in indoles. 2. Formation of 3,3-spirocyclic indole derivatives from tryptamines and their rearrangement to beta-carbolines. *Tetrahedron* **1968,** *24*, 403-&.

31. Liu, J. J.; Nakagawa, M.; Ogata, K.; Hino, T., The Pictet-Spengler reaction of NB-hydroxytryptamines and cysteinal. 2. Tempurature effects, stereochemistry and mechanism. *Chem. Pharm. Bull.* **1991,** *39*, 1672-1676.

32. Ungemach, F.; Cook, J. M., Spiroindolenine intermediate - review. *Heterocycles* **1978,** *9*, 1089-1119.

33. Czerwinski, K. M.; Deng, L.; Cook, J. M., Mechanism driven trans stereospecificity in the Pictet-Spengler reaction - stereospecific formation of trans-1,2,3-trisubstituted-tetrahydro beta-carbolines by condensation of NB-diphenylmethyl tryptophan isopropyl esters with aldehydes. *Tetrahedron Lett.* **1992,** *33*, 4721-4724.

34. Friedrich, A.; Brase, S.; O'Connor, S. E., Synthesis of 4-, 5-, 6-, and 7-azidotryptamines. *Tetrahedron Lett.* **2009,** *50*, 75-76.

35. McCoy, E.; Galan, M. C.; O'Connor, S. E., Substrate specificity of strictosidine synthase. *Bioorg. Med. Chem. Lett.* **2006,** *16*, 2475-2478.

36. Trujillo, J. I.; Meyers, M. J.; Anderson, D. R.; Hegde, S.; Mahoney, M. W.; Vernier, W. F.; Buchler, I. P.; Wu, K. K.; Yang, S.; Hartmann, S. J.; Reitz, D. B., Novel tetrahydro-beta-carboline-1-carboxylic acids as inhibitors

of mitogen activated protein kinase-activated protein kinase 2 (MK-2) (vol 17, pg 4657, 2007). *Bioorg. Med. Chem. Lett.* **2009,** *19*, 2365-2365.

37. Zhang, D.; Sun, H.; Zhang, L.; Zhou, Y.; Li, C.; Jiang, H.; Chen, K.; Liu, H., An expedient Pd/DBU mediated cyanation of aryl/heteroaryl bromides with K-4 Fe(CN)(6). *Chem. Commun.* **2012,** *48*, 2909-2911.

Chapter 3: Experimental

3.1 General

NMR spectra were performed on Agilent U4-DD2 (400 MHz) or Agilent MR4 (500 MHz). ^{1}H NMR spectra were recorded at 400MHz. ^{13}C NMR spectra were correspondingly recorded at 101 MHz. ^{19}F NMR spectra were correspondingly recorded at 376 MHz. Chemical shifts for ^{1}H and ^{13}C are presented in ppm with tetramethylsilane (TMS) as the internal standard and ^{19}F NMR used hexafluorobenzene as a reference. All deuterated solvents were purchased from Cambridge Isotope Laboratories. The following abbreviations are used to show coupling in the spectra: s (singlet), d (doublet), t (triplet), q(quartet), qt (quintet), br s (broad singlet), and m (multiplet).

High resolution mass spectroscopy (HRMS) was performed, by Bill Debout and Mehdi Ashraf-Khorassani, on an Agilent 6220 LC/MS time-of-flight mass spectrometer using either electrospray ionization (ESI) or atmospheric pressure chemical ionization (APCI). Liquid chromatography–mass spectrometry (LC/MS) was performed, by Mehdi Ashraf-Khorassani, on a Thermo Electron TSQ LC/MS triple quad spectrometer using electrospray ionization (ESI). Column chromatography was performed with flash grade silica gel (SiO_2, 32-63 μm) from Fisher Scientific. Thin layer chromatography (TLC) was performed on Sorbent Technologies Inc Silica G TLC plates (SiO_2, 60 Å). Optical rotation was performed on a Jasco P-2000 digital polarimeter using a cylindrical glass cell (3.5 mm D x 100 mm L). Infrared spectroscopy was measured on a Cary 630 FTIR with Diamond ATR from Agilent. Melting points were measured on a BUCHI Melting Point M-560.

Starting materials were purchased from Sigma-Aldrich, Fisher Scientific, Acros, Astatech, Arkpharm and Combi-block, and were used without further purification. Our group's literature procedure[1] was followed to prepare (1*R*,3*S*)-methyl-1-(2,4-dichlorophenyl)-2,3,4,9-tetrahydro-1*H*-pyrido[3,4-*b*]indole-3-carboxylate (**27a**) and (1*R*,3*S*)-1-(2,4-dichlorophenyl)-2,3,4,9-tetrahydro-1*H*-pyrido[3,4-*b*]indole-3-carboxylic acid (**29a**).

3.2 Procedures

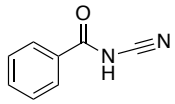

***N*-cyanobenzamide (42b)**: A literature procedure was followed.[2] Sodium hydrogencyanamide (0.640g, 10.0 mmol) was added to a round bottom flask with Et_2O (10 mL) and cooled to 0 ºC in ice bath. Benzyl chloride (581 µL, 5.0 mmol, in 10 mL Et_2O) was then added dropwise to the above solution. The reaction mixture was warmed to room temperature and stirred for 12 hours. The precipitate formed was filtered and washed with Et_2O (3×10 mL) and dissolved in minimal H_2O. The resulting solution was acidified to pH = 1 with 1 M HCl to form a white precipitate. The precipitate was filtered and washed with H_2O (3×10 mL) to afford the crude product. The filtrate was extracted with EtOAc (3×15 mL). The combined organic layers were dried with Na_2SO_4, concentrated in vacuo to afford the crude product. The combined crude product was recrystallized with EtOAc and petroleum ether to obtain **42b** (705 mg, 96%) as a clear-white solid.

^{1}H NMR (400 MHz, Methanol-d_4) δ 7.88 (app dd, J = 8.4, 1.3 Hz, 2H), 7.67 (tt, J = 7.5, 1.2 Hz, 1H), 7.53 (app t, J = 7.7 Hz, 2H), 4.92 (br s, 1H). ^{13}C NMR (101 MHz, Methanol-d_4) δ 168.5 135.0, 131.6, 130.0, 129.2, 109.2. IR (solid): 3238 (br, m), 2255 (m, C≡N), 1678 (s, C=O), 1603 (m), 1585 (m), 1462 (s), 1268 (m), 706 (s), 683 (s) cm^{-1}. mp 132-133 °C (lit mp 134-137 °C)[9]

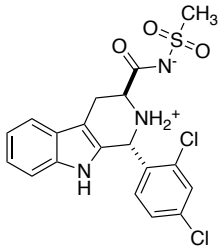

(1*R*,3*S*)-1-(2,4-dichlorophenyl)-*N*-(methylsulfonyl)-2,3,4,9-tetrahydro-1*H*-pyrido[3,4-*b*]indole-3-carboxamide (43): A standard procedure for acid and amine coupling was followed.[3] To a solution of **29a** (181 mg, 0.5 mmol) in DMF (2 mL), was added methanesulfonamide (57 mg, 0.6 mmol), HBTU (379 mg, 1.0 mmol) and Et_3N (0.25 mL, 1.8 mmol). The reaction mixture was stirred in a sealed tube at room temperature for 12 hours. Cold H_2O (20 mL) was added to the reaction mixture to form a precipitate. The precipitate was filtered and dissolved in MeOH (0.5 mL), followed by addition of Et_2O (5 mL), CH_2Cl_2 (10 mL) and hexanes (15 mL). The mixture was stirred in ice

bath for 15 minutes and then filtered. The solid was washed with CH_2Cl_2 to afford **43** (138 mg, 63%) as a light yellow solid.

^{1}H NMR (400 MHz, DMSO-d_6) δ 11.09 (s, 1H), 7.73 (d, J = 2.2 Hz, 1H), 7.50 (d, J = 7.8 Hz, 1H), 7.39 – 7.32 (m, 2H), 7.15 (br s, 1H), 7.13 (app ddd, J = 8.2, 7.0, 1.2) 7.03 (ddd, J = 8.0, 7.1, 1.0 Hz, 1H), 6.85 (d, J = 8.4 Hz, 1H), 4.26 (dd, J = 12.0, 4.8 Hz, 1H), 3.41 – 3.35 (m, 1H), 3.33 (s, 3H), 2.98 (ddd, J = 15.8, 12.0, 1.3 Hz, 1H). ^{13}C NMR (101 MHz, DMSO-d_6) δ 165.5, 136.2, 134.5, 134.2, 134.1, 132.7, 129.7, 129.6, 127.5, 125.9, 122.1, 119.1, 118.5, 111.5, 107.6, 54.9, 51.9, 48.6, 27.6. HRMS (ESI) $[M+H]^+$ calculated for $C_{19}H_{18}C_{l2}N_3O_3S^+$: 438.0440, found 438.0409.

mp decomp at 190 °C

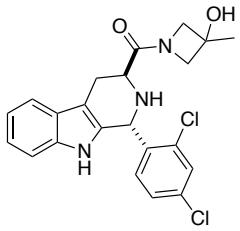

((1*R*,3*S*)-1-(2,4-dichlorophenyl)-2,3,4,9-tetrahydro-1*H*-pyrido[3,4-*b*]indol-3-yl)(3-hydroxy-3-methylazetidin-1-yl)methanone (44): A standard procedure for acid and amine coupling was followed.[3] To a solution of **29a** (200 mg, 0.55 mmol) in DMF (2 mL), was added 3-methylazetidin-3-ol hydrochloride (102 mg, 0.8 mmol), HBTU (412 mg, 1.1 mmol) and DIPEA (0.38 mL, 2.2 mmol). The reaction mixture was stirred in a sealed tube at room temperature for 12 hours. Cold H_2O (20 mL) was added to the reaction mixture to form a precipitate. The precipitate was filtered and dissolved in MeOH (0.5 mL), followed by addition of Et_2O (5 mL), CH_2Cl_2 (10 mL) and hexanes (15 mL). The mixture was stirred in ice bath for 15 minutes and then filtered. The solid was washed with CH_2Cl_2 to afford **43** (183 mg, 83%) as a pale yellow solid.

^{1}H NMR (400 MHz, DMSO-d_6) δ 10.72 (s, 1H), 7.70 (t, J = 2.4 Hz, 1H), 7.49 (d, J = 7.4 Hz, 1H), 7.29 (dd, J = 8.3, 2.2 Hz, 1H), 7.24 (dd, J = 7.9, 1.0 Hz, 1H), 7.06 (ddt, J = 8.1, 7.0, 1.1 Hz, 1H), 6.99 (ddt, J = 8.1, 7.0, 1.1 Hz, 1H), 6.69 (d, J = 8.3 Hz, 1H), 5.56 (d, J = 2.6 Hz, 1H), 5.52 (t, J = 5.1 Hz, 1H), 3.80 – 3.71 (m, 1H), 3.71 – 3.57 (m, 3H), 3.45 – 3.35 (m, 1H), 3.09 (dt, J = 13.0, 5.6 Hz, 1H), 2.88 – 2.71 (m, 2H), 1.294, 1.285 (both s, together 3H - resulting from two amide rotamers). ^{13}C NMR (101 MHz, DMSO-d_6) δ 172.10, 172.06, 138.88, 138.80, 136.08, 134.60, 134.54, 132.65, 132.63, 132.52, 132.47, 131.35, 131.25, 129.02, 129.00, 126.71, 126.65, 126.64, 126.62,

121.14, 118.44, 118.42, 117.82, 111.11, 109.27, 109.26, 67.01, 66.88, 64.05, 64.01, 61.98, 61.76, 50.82, 50.78, 48.29, 47.94, 26.25, 26.21, 23.99, 23.83 (Note: chemical shifts reported to 0.01 ppm to allow peaks of the two amide rotamers to be distinguished: 40 resonances of a possible 44 were detected). HRMS (ESI) $[M+H]^+$ calculated for $C_{22}H_{22}Cl_2N_3O_2^+$: 430.1084, found 430.1087.

mp 159-168 °C. $[\alpha]_D^{23}$ = -39.4 (c = 0.84, MeOH).

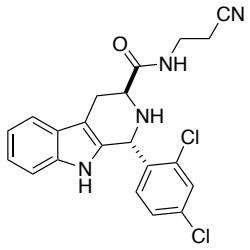

(1*R*,3*S*)-*N*-(2-cyanoethyl)-1-(2,4-dichlorophenyl)-2,3,4,9-tetrahydro-1*H*-pyrido[3,4-*b*]indole-3-carboxamide (45): A standard procedure for acid and amine coupling was followed.[3] To a solution of **29a** (231 mg, 0.6 mmol) in DMF (3 mL), was added 3-aminopropanenitrile (71 µL, 0.9 mmol), HBTU (729 mg, 1.8 mmol) and DIPEA (0.39 mL, 2.1 mmol). The reaction mixture was stirred in a sealed tube at room temperature for 12 hours. Cold H_2O (20 mL) was added to the reaction mixture to form a precipitate. The precipitate was filtered, dissolved in CH_2Cl_2 (15 mL) and concentrated in vacuo. The residue was purified using flash chromatography on silica gel (CH_2Cl_2 : EtOAc = 7 : 3) to yield **45** (168 mg, 63%) as an off-white solid.

^{1}H NMR (400 MHz, DMSO-d_6) δ 10.72 (s, 1H), 8.17 (t, *J* = 5.9 Hz, 1H), 7.69 (d, *J* = 2.2 Hz, 1H), 7.47 (dt, *J* = 7.7, 0.7 Hz, 1H), 7.31 (ddd, *J* = 8.3, 2.2, 0.3 Hz, 1H), 7.24 (dt, *J* = 8.0, 0.9 Hz, 1H), 7.06 (ddd, *J* = 8.1, 7.0, 1.3 Hz, 1H), 6.99 (ddd, *J* = 7.7, 7.1, 1.1 Hz, 1H), 6.70 (d, *J* = 8.3 Hz, 1H), 5.58 (d, *J* = 4.9 Hz, 1H), 3.49 – 3.37 (m, 1H), 3.31 – 3.23 (m, 1H), 3.11 (dd, *J* = 9.2, 5.1 Hz, 1H), 3.01 (dd, *J* = 15.2, 4.6 Hz, 1H), 2.72 (ddd, *J* = 15.2, 9.8, 1.4 Hz, 1H), 2.65 (td, *J* = 6.5, 1.1 Hz, 2H). ^{13}C NMR (101 MHz, DMSO-d_6) δ 173.0, 138.8, 136.2, 134.5, 132.6, 131.3, 129.1, 126.8, 126.5, 121.2, 119.2, 119.1, 118.5, 117.7, 111.2, 108.9, 51.5, 50.6, 34.7, 25.2, 17.5. HRMS (ESI) $[M+H]^+$ calculated for $C_{21}H_{19}Cl_2N_4O^+$: 419.0930, found 413.0920.

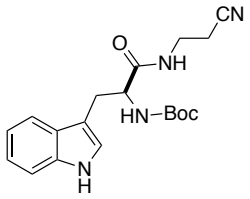

***tert*-butyl (*S*)-(1-((2-cyanoethyl)amino)-3-(1*H*-indol-3-yl)-1-oxopropan-2-yl)carbamate (49)**: A standard procedure for acid and amine coupling was followed.[3] To a solution of (*tert*-butoxycarbonyl)-*L*-tryptophan (2.50 g mg, 8.2 mmol) in DMF (10 mL) at 0 ºC, was added hydroxybenzotriazole (1.11 g, 8.2 mmol), *N,N′*-dicyclohexylcarbodiimide (1.70 g, 8.2 mmol) and 3-aminopropanenitrile (0.6 mL, 8.2 mmol). The reaction mixture was stirred in a sealed flask at 0 ºC for 48 hours, and then stored in the fridge for 12 hours. The precipitate was filtered. Cold H_2O (20 mL) was added to the reaction mixture to form a precipitate. The precipitate was filtered, washed with cold Et_2O. The resulting solid was recrystallized with CH_2Cl_2 to afford **49** (2.53 g, 87%) as a white solid.

^{1}H NMR (400 MHz, Methanol-d_4) δ 7.57 (d, J = 7.9 Hz, 1H), 7.32 (d, J = 8.7 Hz, 1H), 7.11 (s, 1H), 7.09 (t, J = 7.7 Hz, 1H), 7.02 (t, J = 7.2 Hz, 1H), 4.29 (t, J = 7.3 Hz, 1H), 3.42 – 3.34 (m, 1H), 3.29 – 3.18 (m, 2H), 3.12 – 3.03 (m, 1H), 2.56 – 2.26 (m, 2H), 1.38 (s, 9H). ^{13}C NMR (101 MHz, Methanol-d_4) δ 175.3, 157.6, 138.0, 128.8, 124.6, 122.4, 119.8, 119.4, 119.2, 112.3, 110.9, 80.7, 57.2, 36.5, 29.3, 28.6, 18.0. HRMS (ESI) $[M+Na]^+$ calculated for $C_{19}H_{24}N_4NaO_3^+$: 379.1741, found 379.1724.

mp 147-152 °C. $[\alpha]_D^{22}$ = -2.0 (c = 2.09, MeOH).

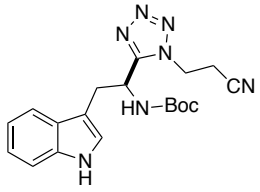

***tert*-butyl (*S*)-(1-(1-(2-cyanoethyl)-1*H*-tetrazol-5-yl)-2-(1*H*-indol-3-yl)ethyl)carbamate (50)**: A standard literature procedure for tetrazole synthesis was followed.[4] **49** (0.75 g, 2.1 mmol), triphenylphosphine (1.38 g, 5.3 mmol) was added to a Schlenk tube equipped with a stir bar. The vessel was evacuated and filled with nitrogen (three cycles). THF (20 mL) was added to the flask, the resulting mixture was then cooled to 0 ºC. At 0 ºC, azidotrimethylsilane (0.7 mL, 5.3 mmol) was added dropwise, followed by diisopropyl azodicarboxylate (1.0 mL, 5.3 mmol). The reaction mixture was warmed to room temperature and stirred for 60 hours. At 0 ºC, a 5.5% aqueous

solution of $(NH_4)_2Ce(NO_3)_6$ was added dropwise to quench reaction. Minimal THF was added to dissolve precipitate. The solution was extracted with EtOAc (3×20 mL). The combined organic layer was washed with $NaHCO_3$ (sat. aq.), brine; dried over Na_2SO_4 and concentrated in vacuo. The residue was purified using flash chromatography on silica gel (CH_2Cl_2 : EtOAc = 7 : 3) to yield **50** (0.47 g, 59%) as a white solid.

^{1}H NMR (400 MHz, Methanol-d_4) δ 7.42 (dt, J = 7.9, 1.0 Hz, 1H), 7.33 (d, J = 8.2 Hz, 1H), 7.11 (td, J = 7.7, 1.1 Hz, 1H), 7.01 (td, J = 8.2, 7.5, 1.2 Hz, 1H), 6.93 (br s, 1H), 5.18 (dd, J = 9.0, 6.3 Hz, 1H), 4.33 – 4.24 (m, 1H), 4.23 – 4.14 (m, 1H), 3.58 – 3.37 (m, 2H), 2.44 (m, 2H), 1.37 (s, 9H). ^{13}C NMR (101 MHz, Methanol-d_4) δ 158.4, 157.7, 137.9, 128.1, 125.0, 122.8, 120.4, 118.8, 117.4, 112.6, 110.0, 81.0, 47.8, 43.5, 30.6, 28.6, 18.0. HRMS (ESI) $[M+Na]^+$ calculated for $C_{19}H_{23}N_7NaO_2^+$: 404.1805, found 404.1825.

mp 166-171 °C. $[\alpha]_D^{23}$ = +44.2 (c = 1.04, MeOH).

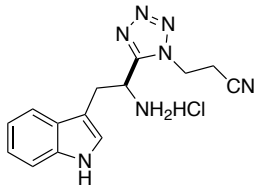

(*S*)-3-(5-(1-amino-2-(1*H*-indol-3-yl)ethyl)-1*H*-tetrazol-1-yl)propanenitrile hydrochloride (51): To a solution of **50** (750 mg, 1.9 mmol) in 1,4-dioxane (10 mL), was added 4 M HCl in 1,4-dioxane (13 mL, in excess). The reaction mixture was stirred at room temperature for 12 hours. The solvents were removed in vacuo to afford **51** (550 mg, 79%, 90% purity) as a lightly colored solid.

^{1}H NMR (400 MHz, Methanol-d_4) δ 7.39 (app d, J = 8.2 Hz, 1H), 7.23 – 7.11 (m, 2H), 7.07 (s, 1H), 7.00 (ddd, J = 8.2, 7.2, 1.0 Hz, 1H), 5.13 (dd, J = 10.5, 4.5 Hz, 1H), 4.07 – 3.97 (m, 1H), 3.77 – 3.68 (m, 1H), 3.44 (dd, J = 14.5, 11.1 Hz, 2H), 2.40 (ddd, J = 17.1, 7.9, 6.9 Hz, 1H), 2.21 (ddd, J = 17.1, 6.6. 5.8, 1H). ^{13}C NMR (101 MHz, Methanol-d_4) δ 154.6, 137.9, 127.6, 125.8, 123.4, 121.0, 118.2, 117.4, 113.0, 107.3, 47.5, 43.7, 30.9, 17.8. HRMS (ESI) calculated for $C_{14}H_{16}N_7^+$: 282.1462, found 282.1463.

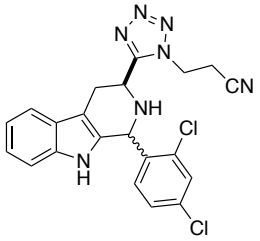

(1*S*, 3*S*) and (1*R*,3*S*)-3-(5-(1-(2,4-dichlorophenyl)-2,3,4,9-tetrahydro-1*H*-pyrido[3,4-*b*]indol-3-yl)-1*H*-tetrazol-1-yl)propanenitrile (*cis*- and *trans*-47): A standard literature procedure for Pictet-Spengler reaction was followed.[1] To a solution of **50** (500 mg, 1.6 mmol) in CH_2Cl_2 (6 mL) was added 4 Å molecular sieves (1.00 g), 2,4 dichlorobenzaldehyde (276 mg, 1.6 mmol). The reaction mixture was stirred at room temperature for 24 hours. Trifluoroacetic acid (250 μL, 3.2 mmol) was then added dropwise. The resulting mixture was stirred at room temperature for another 48 hours. An aqueous solution of $NaHCO_3$ (2.40 g, 30.0 mmol, in 20 mL H2O) was added dropwise at 0 °C, followed by an addition of EtOAc (80 mL). The mixture was stirred for 15 minutes. The phases were separated and the aqueous layer was extracted with EtOAc (3×20 mL). The combined organic layers were washed with brine, dried over Na_2SO_4, concentrated, then purified by flash chromatography (3 : 1 : 1 CH_2Cl_2/ hexanes / EtOAc) to give a mixture of *cis*- and *trans*-**47** (163 mg, 23%) , in 4 : 6 ratio as measured from the indole NH peaks (10.5-11 ppm) and the C1 peaks (5.5 – 5.8 ppm). Where diastereomeric peaks can be resolved, they are listed separately below with the corresponding fractional integral.

^{1}H NMR (400 MHz, DMSO-d_6) δ 10.84 (s, 0.6 H, *cis*-), 10.61 (s, 0.4 H, *trans*-), 7.71 (d, J = 2.1 Hz, 1H), 7.58 (d, J = 7.7 Hz, 0.6 H, *cis*-), 7.53 (d, J = 7.7 Hz, 0.4 H, *trans*-), 7.37 (dd, J = 8.6, 2.5 Hz, 1H), 7.30 (dt, J = 7.9, 1.0 Hz, 0.6 H, *cis*-), 7.26 (dt, J = 7.9, 1.0 Hz, 0.4 H, *trans*-), 7.14 – 6.98 (m, 1H), 6.77 (d, J = 8.3 Hz, 1H), 5.79 (d, J = 9.3 Hz, 0.4 H, *trans*-), 5.52 (d, J = 5.8 Hz, 0.6 H, *cis*-), 4.88 – 4.73 (m, 1H), 4.57 (m, 1H), 4.40 – 4.24 (m, 1H), 3.83 (dd, J = 12.2, 5.6 Hz, 1H), 3.31 – 3.16 (m, 2H), 2.94 (s, 1H). ^{13}C NMR (101 MHz, DMSO-d_6) δ 155.98, 137.93, 137.50, 136.20, 136.11, 134.72, 134.37, 133.41, 133.08, 133.00, 132.19, 131.53, 129.40, 128.84, 127.46, 127.03, 126.62, 126.48, 121.43, 121.18, 118.68, 118.62, 118.04, 117.92, 117.80, 117.51, 111.24, 109.17, 108.75, 54.92, 51.17, 47.85, 42.99, 42.92, 42.67, 25.33, 24.92, 17.88, 17.51. (Note: chemical shifts reported to 0.01 ppm to allow peaks of the two diastereomers to be distinguished: 39 resonances of a possible 42 were detected). HRMS (ESI) $[M+Na]^+$ calculated for $C_{21}H_{17}Cl_2N_7Na^+$: 460.0815, found 460.0823.

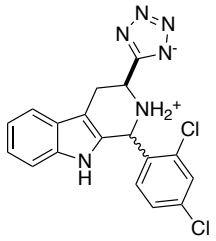

(*S*)-5-(1-(2,4-dichlorophenyl)-2,3,4,9-tetrahydro-1*H*-pyrido[3,4-*b*]indol-2-ium-3-yl)tetrazol-1-ide (*cis*- and *trans*-46): To a solution of *cis- and trans*-**47** (described above, 110 mg, 0.25 mmol) in THF (8 mL) and MeOH (2 mL) was added an aqueous solution of 1 M NaOH (0.4 mL, 0.4 mmol). The reaction mixture was stirred at room temperature for 12 hours. The mixture was then acidified to pH = 4 with 1 M HCl and extracted with EtOAc (3×20 mL). The combined organic layers were washed with $NaHCO_3$ (sat. aq.), brine, dried over Na_2SO_4, and concentrated in vacuo. The residue, as a sodium salt, was dissolved in THF / MeOH / H_2O (2 mL / 2 mL / 2 mL) and Amberlyst hydroxide resin (3 g, Aldrich, loading: 4.2 mmol/g) was added. The mixture was stirred at room temperature for 12 hours, to allow for ion exchange. The resin was filtered and washed with MeOH and CH_2Cl_2 alternatively (4 × 10 mL). An aqueous solution of AcOH (50%) (20 mL) was added to cleave the product from the resin, the cleaving solution was collected by filtration. The cleavage step was repeated for other 3 times. The combined cleaving solutions were condensed under vacuum. The residue was dissolved in MeOH (1 mL), followed by addition of Et_2O (10 mL) and hexane (25 mL). The mixture was stirred for 15 minutes in ice bath and then filtered. The solid was washed with hexane, dried and purified via HPLC (28 – 32 % CH_3CN in H_2O, performed by M. Ghavami using the Josan group HPLC) to give a mixture of *cis*- and *trans*-**46** (17 mg, 39%) as a light yellow solid, in 3 : 7 ratio as measured by ^{1}H NMR of the C1-H peaks (5.5 – 5.8 ppm).

^{1}H NMR (400 MHz, Methanol-d_4) δ 7.65 (d, J = 2.1 Hz, 0.7 H, *cis*-), 7.63 (d, J = 2.1 Hz, 0.3 H, *trans*-), 7.56 (dt, J = 7.7, 1.1 Hz, 0.7 H, *cis*-), 7.53 (dt, J = 7.7, 1.1 Hz, 0.3 H, *trans*-), 7.38 – 7.24 (m, 2H), 7.17 – 7.00 (m, 3H), 6.24 (s, 0.3 H, *trans*-), 6.08 (s, 0.7 H, *cis*-), 5.01 (dd, J = 10.1, 5.3 Hz, 0.3 H, *trans*-), 4.80 (dd, J = 9.2, 4.8 Hz, 0.7 H, *cis*-), 3.50 (d, J = 4.9 Hz, 0.3 H, *trans*-), 3.47 (d, J = 4.8 Hz, 0.7 H, *cis*-), 3.44 – 3.34 (m, 1H). ^{13}C NMR (101 MHz, Methanol-d_4) δ 166.85, 137.08, 136.49, 136.49, 136.47, 136.45, 135.34, 135.27, 134.58, 131.82, 129.51, 129.29, 128.60, 127.58, 127.20, 126.09, 121.98, 121.71, 118.96, 118.94, 117.72, 117.58, 113.07, 110.83, 108.41, 107.97, 51.70, 45.77, 25.78. (Note: chemical shifts reported to 0.01 ppm to allow peaks of the two diastereomers to be distinguished: 29 resonances of a possible 36 were detected). HRMS (ESI) $[M+H]^+$ calculated for $C_{18}H_{15}Cl_2N_6^+$: 385.0730, found 385.0714.

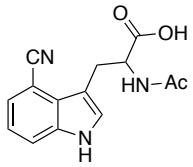

2-acetamido-3-(4-cyano-1*H*-indol-3-yl)propanoic acid ((±)-52ac): A literature procedure was followed.[5-6] 4-cyano-*1H*-indole (500 mg, 3.5 mmol) was added to a Schlenk tube equipped with a stir bar. The vessel was evacuated and filled with nitrogen (three cycles). A solution of DL-serine (740 mg, 7.04 mmol) in AcOH (8.0 mL, 140.8 mmol) and Ac_2O (2.8 mL, 28.2 mmol) was added to the flask. The reaction mixture was heated to 75 °C and stirred for 3 hours. The mixture was then cooled to room temperature, diluted with Et_2O (50 mL), and adjusted to pH = 11 with 30% NaOH (20 mL). The water layer was further washed with diethyl ether (3 × 50 mL), then ice-cooled. The organic layer was further extracted with 1M NaOH (3 × 20 mL) and combined with the previous aqueous phase. A small amount of $Na_2S_2O_4$ was added to the combined alkali solution, which was then adjusted to pH = 3 with concentrated HCl. The mixture was extracted with EtOAc (3 × 50 mL). The combined organic layers were washed with brine, dried over Na_2SO_4, concentrated, then purified by flash chromatography (9 : 1 CH_2Cl_2/ MeOH with 2% AcOH) to give (±)-**52ac** (256 mg, 27%, 84% purity) as tan colored solid.

^{1}H NMR (400 MHz, Methanol-d_4) δ 7.65 (dd, J = 8.2, 0.9 Hz, 1H), 7.42 (dd, J = 7.4, 0.9 Hz, 1H), 7.33 (s, 1H), 7.18 (dd, J = 8.2, 7.4 Hz, 1H), 4.84 (dd, J = 8.8, 5.6 Hz, 1H), 3.60 (ddd, J = 15.0, 5.6, 0.9 Hz, 1H), 3.37 – 3.28 (m, 2H), 1.92 (s, 3H). HRMS (ESI) $[M+Na]^+$ calculated for $C_{14}H_{13}N_3NaO_3^+$: 294.0849, found 294.0859.

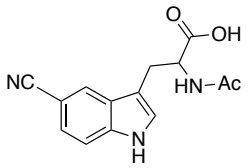

2-acetamido-3-(5-cyano-1*H*-indol-3-yl)propanoic acid ((±)-52ad): A literature procedure was followed.[5-6] 5-cyano-*1H*-indole (500 m g, 3.5 mmol) was added to a Schlenk tube equipped with a stir bar. The vessel was evacuated and filled with nitrogen (three cycles). A solution of DL-serine (740 mg, 7.04 mmol) in AcOH (8.0 mL, 140.8 mmol) and Ac_2O (2.8 mL, 28.2 mmol) was added to the flask. The reaction mixture was heated to 75 °C and stirred for 3 hours. The mixture was then cooled to room temperature, diluted with Et_2O (50 mL), and adjusted to pH = 11 with 30% NaOH (20 mL). The water layer was further washed with diethyl ether (3 × 50 mL), then ice-cooled.

The organic layer was further extracted with 1M NaOH (3 × 20 mL) and combined with the previous aqueous phase. A small amount of $Na_2S_2O_4$ was added to the combined alkali solution, which was then adjusted to pH = 3 with concentrated HCl. The mixture was extracted with EtOAc (3 × 50 mL). The combined organic layers were washed with brine, dried over Na_2SO_4, concentrated, then purified by flash chromatography (9 : 1 CH_2Cl_2/ MeOH with 2% AcOH) to give (±)-**52ad** (340 mg, 36%, 90% purity) as tan colored solid.

^{1}H NMR (400 MHz, Methanol-d_4) δ 8.01 (dd, J = 1.6, 0.7 Hz, 1H), 7.47 (dd, J = 8.5, 0.7 Hz, 1H), 7.37 (dd, J = 8.5, 1.6 Hz, 1H), 7.28 (br s, 1H), 4.72 (dd, J = 7.9, 5.3 Hz, 1H), 3.35 (ddd, J = 14.8, 5.3, 0.8 Hz, 1H), 3.19 (ddd, J = 14.8, 7.9, 0.8 Hz, 1H), 1.91 (s, 3H). HRMS (ESI) $[M+Na]^+$ calculated for $C_{14}H_{13}N_3NaO_3^+$: 294.0849, found 294.0856.

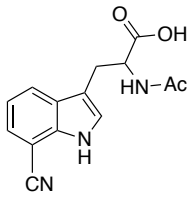

2-acetamido-3-(7-cyano-1*H*-indol-3-yl)propanoic acid ((±)-52af): A literature procedure was followed.[5-6] 7-cyano-*1H*-indole (500 m g, 3.5 mmol) was added to a Schlenk tube equipped with a stir bar. The vessel was evacuated and filled with nitrogen (three cycles). A solution of DL-serine (740 mg, 7.04 mmol) in AcOH (8.0 mL, 140.8 mmol) and Ac_2O (2.8 mL, 28.2 mmol) was added to the flask. The reaction mixture was heated to 75 °C and stirred for 3 hours. The mixture was then cooled to room temperature, diluted with Et_2O (50 mL), and adjusted to pH = 11 with 30% NaOH (20 mL). The water layer was further washed with diethyl ether (3 × 50 mL), then ice-cooled. The organic layer was further extracted with 1M NaOH (3 × 20 mL) and combined with the previous aqueous phase. A small amount of $Na_2S_2O_4$ was added to the combined alkali solution, which was then adjusted to pH = 3 with concentrated HCl. The mixture was extracted with EtOAc (3 × 50 mL). The combined organic layers were washed with brine, dried over Na_2SO_4, concentrated, then purified by flash chromatography (9 : 1 CH_2Cl_2/ MeOH with 2% AcOH) to give (±)-**52af** (285 mg, 30%, 80% purity) as tan colored solid.

^{1}H NMR (400 MHz, Methanol-d_4) δ 7.90 (dd, J = 8.0, 1.0 Hz, 1H), 7.49 (ddd, J = 7.4, 1.0, 0.4 Hz, 1H), 7.25 (br s, 1H), 7.15 (dd, J = 8.0, 7.4 Hz, 1H), 4.73 (dd, J = 8.0, 5.2 Hz, 1H), 3.36 (ddd, J = 14.8, 5.2, 0.8 Hz, 1H), 3.18 (ddd, J = 14.8, 8.0, 0.8 Hz, 1H), 1.90 (s, 3H). HRMS (ESI) $[M+H]^+$ calculated for $C_{14}H_{14}N_3O_3^+$: 271.1030, found 272.1049.

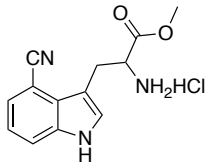

methyl 2-amino-3-(4-cyano-1*H*-indol-3-yl)propanoate hydrochloride ((±)-53ac): To a solution of (±)-**52ac** (310 mg, 1.2 mmol) in MeOH (5 mL) was added thionyl chloride (0.8 mL, 12.0 mmol). The reaction mixture was brought to reflux and stirred for 24 hours. After cooling to room temperature, Et_2O was added in excess to form precipitate. The precipitate was filtered and dried to afford (±)-**53ac** (112 mg, 47%) as a light tan solid.

^{1}H NMR (400 MHz, Methanol-d_4) δ 7.74 (dd, J = 8.3, 0.9 Hz, 1H), 7.51 (dd, J = 7.4, 0.9 Hz, 1H), 7.47 (br s, 1H), 7.28 (dd, J = 8.3, 7.4 Hz, 1H), 4.41 (dd, J = 9.0, 6.3 Hz, 1H), 3.78 (s, 3H), 3.77 – 3.72 (m, 1H), 3.43 (ddd, J = 15.1, 9.0, 0.6 Hz, 1H). ^{13}C NMR (101 MHz, Methanol-d_4) δ 170.6, 138.7, 129.7, 127.4, 127.2, 122.7, 120.6, 118.3, 107.9, 101.8, 55.0, 53.6, 27.5. HRMS (ESI) $[M+H]^+$ calculated for $C_{13}H_{14}N_3O_2^+$: 244.1081, found 244.1104.

mp decomp at 200 °C.

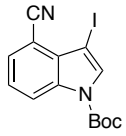

***tert*-butyl 4-cyano-3-iodo-1*H*-indole-1-carboxylate (57ac)**: A literature procedure for synthesis of *tert*-butyl 3-iodo-1*H*-indole-1-carboxylate was followed.[7] To a solution of 4-cyano-*1H*-indole (1.42 g, 10.0 mmol) in DMF (25 mL) was added iodine (3.80 g, 15.0 mmol) and potassium hydroxide (1.40 g, 25.0 mmol). The reaction mixture was stirred at room temperature for 4 hours. The reaction mixture was then poured into 400 mL of ice water containing 0.5% ammonia and 0.1% sodium thiosulfate. The mixture was placed in an ice bath for 2 hours to ensure the complete precipitation. The precipitate was filtered, washed with ice water and dried in vacuo to obtain crude product as a yellow solid. It was used in the next step without further purification. The obtained solid was dissolved in CH_2Cl_2 (20 mL). 4-Dimethylaminopyridine (122 mg, 1.0 mmol, 10 mol%) and di-tert-butyl dicarbonate (3.27 g, 15.0 mmol) was then added to the solution. The reaction mixture was stirred at room temperature for 12 hours. The mixture was then washed with 1 M HCl (200 mL) and the aqueous phase was extracted with CH_2Cl_2 (3 x 30 mL). The combined organic layers were dried over Na_2SO_4 and concentrated in vacuo. The residue was purified by flash chromatography (1:1 CH_2Cl_2/ hexanes) to give **57ac** (3.46 g, 92% over two steps) as a white solid.

^{1}H NMR (400 MHz, Chloroform-*d*) δ 8.48 (d, *J* = 8.4 Hz, 1H), 7.87 (br s, 1H), 7.64 (dd, *J* = 7.6, 1.0 Hz, 1H), 7.40 (ddd, *J* = 8.4, 7.6, 0.4 Hz, 1H), 1.67 (s, 9H). ^{13}C NMR (101 MHz, Chloroform-*d*) δ 148.0, 135.3, 134.1, 130.2, 129.6, 125.0, 120.04, 116.6, 105.0, 85.7, 60.7, 28.2. (Note: A $^{5}J_{HH}$ = 0.4 ~ 0.6 Hz is observed between H2 of indole and H4 or H7 of indole throughout 57**ac**-57**am**). HRMS (ESI) $[M+H]^+$ calculated for $C_{14}H_{14}IN_2O_2^+$: 369.0094, found 369.0096.

mp 156-157 °C.

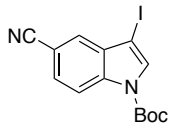

***tert*-butyl 5-cyano-3-iodo-*1H*-indole-1-carboxylate (57ad)**: A literature procedure for synthesis of *tert*-butyl 3-iodo-1*H*-indole-1-carboxylate was followed.[7] To a solution of 5-cyano-*1H*-indole (0.80 g, 5.6 mmol) in DMF (15 mL) was added iodine (2.13 g, 8.4 mmol) and potassium hydroxide (0.56 g, 14.0 mmol). The reaction mixture was stirred at room temperature for 4 hours. The reaction mixture was then poured into 400 mL of ice water containing 0.5% ammonia and 0.1% sodium thiosulfate. The mixture was placed in an ice bath for 2 hours to ensure the complete precipitation. The precipitate was filtered, washed with ice water and dried in vacuo to obtain crude product as a yellow solid. It was used in the next step without further purification. The obtained solid was dissolved in CH_2Cl_2 (20 mL). 4-Dimethylaminopyridine (65 mg, 0.5 mmol, 10 mol%) and di-tert-butyl dicarbonate (1.83 g, 8.4 mmol) was then added to the solution. The reaction mixture was stirred at room temperature for 12 hours. The mixture was then washed with 1 M HCl (200 mL) and the aqueous phase was extracted with CH_2Cl_2 (3 x 30 mL). The combined organic layers were dried over Na_2SO_4 and concentrated in vacuo. The residue was purified by flash chromatography (1 : 1 CH_2Cl_2/ hexanes) to give **57ad** (1.91 g, 93% over two steps) as a white solid.

^{1}H NMR (400 MHz, Chloroform-*d*) δ 8.24 (d, *J* = 8.7 Hz, 1H), 7.82 (br s, 1H), 7.75 (dd, *J* = 1.6, 0.7 Hz, 1H), 7.61 (ddd, *J* = 8.7, 1.6, 0.4 Hz, 1H), 1.68 (s, 9H). ^{13}C NMR (101 MHz, Chloroform-*d*) δ 148.1, 137.1, 132.6, 132.4, 128.5, 126.7, 119.4, 116.2, 107.1, 85.8, 64.5, 28.2. HRMS (ESI) $[M+H]^+$ calculated for $C_{14}H_{14}IN_2O_2^+$: 369.0094, found 369.0106.

mp 150-156 °C.

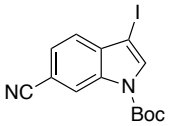

***tert*-butyl 6-cyano-3-iodo-1*H*-indole-1-carboxylate (57ae)**: A literature procedure for synthesis of *tert*-butyl 3-iodo-1*H*-indole-1-carboxylate was followed.[7] To a solution of 6-cyano-*1H*-indole (0.27 g, 1.9 mmol) in DMF (10 mL) was added iodine (0.72 g, 2.8 mmol) and potassium hydroxide (0.19 g, 4.8 mmol). The reaction mixture was stirred at room temperature for 2 hours. The reaction mixture was then poured into 400 mL of ice water containing 0.5% ammonia and 0.1% sodium thiosulfate. The mixture was placed in an ice bath for 2 hours to ensure the complete precipitation. The precipitate was filtered, washed with ice water and dried in vacuo to obtain crude product as a yellow solid. It was used in the next step without further purification. The obtained solid was dissolved in CH_2Cl_2 (10 mL). 4-Dimethylaminopyridine (21 mg, 0.2 mmol, 10 mol%) and di-tert-butyl dicarbonate (0.61 g, 2.8 mmol) was then added to the solution. The reaction mixture was stirred at room temperature for 12 hours. The mixture was then washed with 1 M HCl (100 mL) and the aqueous phase was extracted with CH_2Cl_2 (3 x 15 mL). The combined organic layers were dried over Na_2SO_4 and concentrated in vacuo. The residue was purified by flash chromatography (1 : 1 CH_2Cl_2/ hexanes) to give **57ae** (0.65 g, 95% over two steps) as a white solid.
^{1}H NMR (400 MHz, Chloroform-*d*) δ 8.50 (s, 1H), 7.88 (br s, 1H), 7.55 (dd, *J* = 8.2, 1.4 Hz, 1H), 7.50 (dd, *J* = 8.2, 0.7 Hz, 1H), 1.68 (s, 9H). ^{13}C NMR (101 MHz, Chloroform-*d*) δ 148.1, 135.5, 134.1, 133.5, 126.5, 122.6, 119.8, 119.7, 108.60, 85.9, 64.8, 28.2. HRMS (ESI) $[M+H]^+$ calculated for $C_{14}H_{14}IN_2O_2^+$: 369.0094, found 369.0109.
mp 155-158 °C.

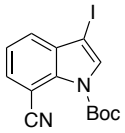

***tert*-butyl 7-cyano-3-iodo-1*H*-indole-1-carboxylate (57af)**: A literature procedure for synthesis of *tert*-butyl 3-iodo-1*H*-indole-1-carboxylate was followed.[7] To a solution of 7-cyano-*1H*-indole (0.78 g, 5.5 mmol) in DMF (15 mL) was added iodine (2.09 g, 8.3 mmol) and potassium hydroxide (0.55 g, 13.8 mmol). The reaction mixture was stirred at room temperature for 4 hours. The reaction mixture was then poured into 400 mL of ice water containing 0.5% ammonia and 0.1% sodium thiosulfate. The mixture was placed in an ice bath for 2 hours to ensure the complete precipitation. The precipitate was filtered, washed with ice water and dried in vacuo to obtain crude

product as a yellow solid. It was used in the next step without further purification. The obtained solid was dissolved in CH_2Cl_2 (20 mL). 4-Dimethylaminopyridine (62 mg, 0.6 mmol, 10 mol%) and di-tert-butyl dicarbonate (1.80 g, 8.3 mmol) was then added to the solution. The reaction mixture was stirred at room temperature for 12 hours. The mixture was then washed with 1 M HCl (200 mL) and the aqueous phase was extracted with CH_2Cl_2 (3 x 20 mL). The combined organic layers were dried over Na_2SO_4 and concentrated in vacuo. The residue was purified by flash chromatography (1 : 1 CH_2Cl_2/ hexanes) to give **57af** (1.73 g, 49% over two steps) as a white solid.

^{1}H NMR (400 MHz, Chloroform-*d*) δ 7.78 (ddd, *J* = 7.6, 1.2, 0.4 Hz, 1H), 7.78 (d, *J* = 0.4 Hz, 1H), 7.67 (dd, *J* = 8.0, 1.2 Hz, 1H), 7.39 (dd, *J* = 8.0, 7.6 Hz, 1H), 1.70 (s, 9H). ^{13}C NMR (101 MHz, Chloroform-*d*) δ 147.7, 134.1, 133.1, 132.8, 132.7, 127.0, 123.5, 117.9, 100.0, 86.6, 65.0, 28.1. HRMS (ESI) $[M+H]^+$ calculated for $C_{14}H_{14}IN_2O_2^+$: 369.0094, found 369.0112.

mp 133-137 °C.

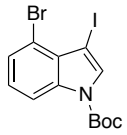

***tert*-butyl 4-bromo-3-iodo-1*H*-indole-1-carboxylate (56ag)**: A literature procedure for synthesis of *tert*-butyl 3-iodo-1*H*-indole-1-carboxylate was followed.[7] To a solution of 4-bromo-*1H*-indole (1.9 mL, 15.0 mmol) in DMF (15 mL) was added iodine (5.71 g, 22.5 mmol) and potassium hydroxide (2.10 g, 37.5 mmol). The reaction mixture was stirred at room temperature for 4 hours. The reaction mixture was then poured into 400 mL of ice water containing 0.5% ammonia and 0.1% sodium thiosulfate. The mixture was placed in an ice bath for 2 hours to ensure the complete precipitation. The precipitate was filtered, washed with ice water and dried in vacuo to obtain crude product as a yellow solid. It was used in the next step without further purification. The obtained solid was dissolved in CH_2Cl_2 (20 mL). 4-Dimethylaminopyridine (183 mg, 1.5 mmol, 10 mol%) and di-tert-butyl dicarbonate (4.91 g, 22.5 mmol) was then added to the solution. The reaction mixture was stirred at room temperature for 12 hours. The mixture was then washed with 1 M HCl (300 mL) and the aqueous phase was extracted with CH_2Cl_2 (3 x 30 mL). The combined organic layers were dried over Na_2SO_4 and concentrated in vacuo. The residue was purified by flash chromatography (1 : 1 CH_2Cl_2/ hexanes) to give **57ag** (4.19 g, 66% over two steps) as a white solid.

^{1}H NMR (400 MHz, Chloroform-*d*) δ 8.26 (d, *J* = 8.3 Hz, 1H), 7.81 (br s, 1H), 7.43 (dd, *J* = 7.8, 0.9 Hz, 1H), 7.16 (dd, *J* = 8.3, 7.8 Hz, 1H), 1.66 (s, 9H). ^{13}C NMR (101 MHz, Chloroform-*d*) δ 148.2, 135.8, 133.4, 128.5, 126.7, 125.9, 115.4, 114.9, 85.1, 61.3, 28.2. HRMS (ESI) $[M+H]^+$ calculated for $C_8H_6BrIN^+$ ($C_{13}H_{14}BrINO_2^+$ - CO_2, - CH_2=$C(CH_3)_2$): 321.8723, found 321.8720.

mp decomp at 125 °C.

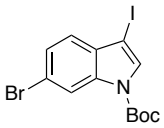

***tert*-butyl 6-bromo-3-iodo-1*H*-indole-1-carboxylate (57ah)**: A literature procedure for synthesis of *tert*-butyl 3-iodo-1*H*-indole-1-carboxylate was followed.[7] To a solution of 6-bromo-*1H*-indole (2.94 g, 15.0 mmol) in DMF (15 mL) was added iodine (5.71 g, 22.5 mmol) and potassium hydroxide (2.10 g, 37.5 mmol). The reaction mixture was stirred at room temperature for 4 hours. The reaction mixture was then poured into 400 mL of ice water containing 0.5% ammonia and 0.1% sodium thiosulfate. The mixture was placed in an ice bath for 2 hours to ensure the complete precipitation. The precipitate was filtered, washed with ice water and dried in vacuo to obtain crude product as a yellow solid. It was used in the next step without further purification. The obtained solid was dissolved in CH_2Cl_2 (20 mL). 4-Dimethylaminopyridine (183 mg, 1.5 mmol, 10 mol%) and di-tert-butyl dicarbonate (4.91 g, 22.5 mmol) was then added to the solution. The reaction mixture was stirred at room temperature for 12 hours. The mixture was then washed with 1 M HCl (300 mL) and the aqueous phase was extracted with CH_2Cl_2 (3 x 30 mL). The combined organic layers were dried over Na_2SO_4 and concentrated in vacuo. The residue was purified by flash chromatography (1 : 3 CH_2Cl_2/ hexanes) to give **57ah**(4.76 g, 75% over two steps) as a white solid.

^{1}H NMR (400 MHz, Chloroform-*d*) δ 8.35 (br s, 1H), 7.68 (br s, 1H), 7.42 (dd, *J* = 8.4, 1.7 Hz, 1H), 7.25 (dd, *J* = 8.4, 0.6 Hz, 2H), 1.66 (s, 9H). ^{13}C NMR (101 MHz, Chloroform-*d*) δ 148.4, 135.5, 131.2, 130.7, 126.7, 122.8, 119.5, 118.4, 85.1, 65.0, 28.2 (^{1}H NMR and ^{13}C NMR match literature data)[10]. HRMS (ESI) $[M-H]^-$ calculated for $C_8H_4BrIN^-$ ($C_{13}H_{12}BrINO_2^-$ - CO_2, - CH_2=$C(CH_3)_2$): 319.8577, found 319.8556.

mp 149-152 °C.

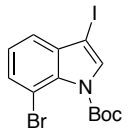

***tert*-butyl 7-bromo-3-iodo-1*H*-indole-1-carboxylate (57ai)**: A literature procedure for synthesis of *tert*-butyl 3-iodo-1*H*-indole-1-carboxylate was followed.[7] To a solution of 7-bromo-*1H*-indole (2.94 g, 15.0 mmol) in DMF (15 mL) was added iodine (5.71 g, 22.5 mmol) and potassium hydroxide (2.10 g, 37.5 mmol). The reaction mixture was stirred at room temperature for 4 hours. The reaction mixture was then poured into 400 mL of ice water containing 0.5% ammonia and 0.1% sodium thiosulfate. The mixture was placed in an ice bath for 2 hours to ensure the complete precipitation. The precipitate was filtered, washed with ice water and dried in vacuo to obtain crude product as a yellow solid. It was used in the next step without further purification. The obtained solid was dissolved in CH_2Cl_2 (20 mL). 4-Dimethylaminopyridine (183 mg, 1.5 mmol, 10 mol%) and di-tert-butyl dicarbonate (4.91 g, 22.5 mmol) was then added to the solution. The reaction mixture was stirred at room temperature for 12 hours. The mixture was then washed with 1 M HCl (300 mL) and the aqueous phase was extracted with CH_2Cl_2 (3 x 30 mL). The combined organic layers were dried over Na_2SO_4 and concentrated in vacuo. The residue was purified by flash chromatography (1 : 4 CH_2Cl_2/ hexanes) to give **57ai** (1.61 g, 26% over two steps) as a white solid.
^{1}H NMR (400 MHz, Chloroform-*d*) δ 7.65 (br s, 1H), 7.60 (ddd, *J* = 7.7, 1.1, 0.4 Hz, 1H), 7.39 (dd, *J* = 7.7, 1.1 Hz, 1H), 7.19 (t, *J* = 7.7 Hz, 1H), 1.66 (s, 9H). ^{13}C NMR (101 MHz, Chloroform-*d*) δ 147.6, 135.5, 133.6, 133.5, 131.0, 124.71, 121.1, 107.6, 85.2, 64.4, 28.1.

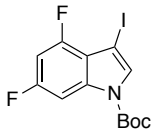

***tert*-butyl 4,6-difluoro-3-iodo-1*H*-indole-1-carboxylate (57aj)**: A literature procedure for synthesis of *tert*-butyl 3-iodo-1*H*-indole-1-carboxylate was followed.[7] To a solution of 4,6-difluoro-*1H*-indole (1.00 g, 6.5 mmol) in DMF (10 mL) was added iodine (1.74 g, 6.88 mmol) and potassium hydroxide (0.92 g, 16.3 mmol). The reaction mixture was stirred at room temperature for 4 hours. The reaction mixture was then poured into 400 mL of ice water containing 0.5% ammonia and 0.1% sodium thiosulfate. The mixture was placed in an ice bath for 2 hours to ensure the complete precipitation. The precipitate was filtered, washed with ice water and dried in vacuo to obtain crude product as a yellow solid. It was used in the next step without further purification. The obtained solid was dissolved

in CH_2Cl_2 (20 mL). 4-Dimethylaminopyridine (80 mg, 0.7 mmol, 10 mol%) and di-tert-butyl dicarbonate (1.32 g, 6.5 mmol) was then added to the solution. The reaction mixture was stirred at room temperature for 12 hours. The mixture was then washed with 1 M HCl (300 mL) and the aqueous phase was extracted with CH_2Cl_2 (3 x 30 mL). The combined organic layers were dried over Na_2SO_4 and concentrated in vacuo. The residue was purified by flash chromatography (1 : 4 CH_2Cl_2/ hexanes) to give **57aj**(1.91 g, 77% over two steps) as a white solid.

^{1}H NMR (400 MHz, Chloroform-*d*) δ 7.73 (br d, $^3J_{HF}$ = 9.4 Hz, 1H), 7.61 (s, 1H), 6.73 (ddd, $^3J_{HF}$ = 10.6, $^3J_{HF}$ = 9.4, $^4J_{HH}$ = 2.2 Hz, 1H), 1.66 (s, 9H). ^{19}F NMR (376 MHz, Chloroform-*d*) δ -112.80 (m), -122.45 (dd, $^3J_{HF}$ = 10.6 Hz, $^4J_{FF}$ = 4.5 Hz). ^{13}C NMR (101 MHz, Chloroform-*d*) δ 160.8 (dd, $^1J_{CF}$= 242.7, $^3J_{CF}$ = 11.0 Hz), 155.4 (dd, $^1J_{CF}$ = 255.1, $^3J_{CF}$ = 14.2 Hz), 148.1, 137.0 (dd, $^3J_{CF}$ = 13.9, 8.5 Hz), 131.3 (d, $^3J_{CF}$ = 4.0 Hz), 116.5 (dd, $^2J_{CF}$ = 16.7, $^4J_{CF}$ = 2.9 Hz), 99.2 (dd, $^2J_{CF}$ = 28.4, 23.0 Hz), 99.0 (dd, $^2J_{CF}$ = 28.9, $^4J_{CF}$ = 5.1 Hz), 85.4, 55.4, 28.2.

mp 140-146 °C.

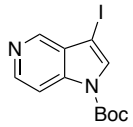

***tert*-butyl 3-iodo-1*H*-pyrrolo[3,2-*c*]pyridine-1-carboxylate (57ak)**: A literature procedure for synthesis of *tert*-butyl 3-iodo-1*H*-indole-1-carboxylate was followed.[7] To a solution of 1*H*-pyrrolo[3,2-*c*]pyridine (1.18 g, 10.0 mmol) in DMF (10 mL) was added iodine (2.67 g, 10.5 mmol) and potassium hydroxide (1.40 g, 25.0 mmol). The reaction mixture was stirred at room temperature for 4 hours. The reaction mixture was then poured into 400 mL of ice water containing 0.5% ammonia and 0.1% sodium thiosulfate. The mixture was placed in an ice bath for 2 hours to ensure the complete precipitation. The precipitate was filtered, washed with ice water and dried in vacuo to obtain crude product as a yellow solid. It was used in the next step without further purification. The obtained solid was dissolved in CH_2Cl_2 (20 mL). 4-Dimethylaminopyridine (122 mg, 1.0 mmol, 10 mol%) and di-tert-butyl dicarbonate (2.29 g, 10.5 mmol) was then added to the solution. The reaction mixture was stirred at room temperature for 12 hours. The mixture was then washed with 1 M HCl (300 mL) and the aqueous phase was extracted with CH_2Cl_2 (3 x 30 mL). The combined organic layers were dried over Na_2SO_4 and concentrated in vacuo. The residue was purified by flash chromatography (3 : 1 hexanes/ EtOAc) to give **57ak**(2.73 g, 79% over two steps) as a white solid.

^{1}H NMR (400 MHz, Chloroform-*d*) δ 8.92 (s, 1H), 8.58 (d, *J* = 6.6 Hz, 1H), 8.53 (d, *J* = 6.6 Hz, 1H), 8.04 (s, 1H), 1.71 (s, 9H). ^{13}C NMR (101 MHz, Chloroform-*d*) δ 146.7, 143.1, 136.9, 135.8, 134.9, 130.0, 112.6, 88.8, 62.2, 28.1

(^{1}H NMR and ^{13}C NMR similar to literature data)[11-12]. HRMS (ESI) $[M+H]^+$ calculated for $C_{12}H_{14}IN_2O_2^+$: 345.0094, found 345.0121 (HRMS match literature data)[11-12].

mp decomp at 140 °C (lit mp 127-128°C)[12].

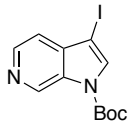

***tert*-butyl 3-iodo-1*H*-pyrrolo[2,3-*c*]pyridine-1-carboxylate (57al)**: A literature procedure for synthesis of *tert*-butyl 3-iodo-1*H*-indole-1-carboxylate was followed.[7] To a solution of 1*H*-pyrrolo[2,3-*c*]pyridine (1.18 g, 10.0 mmol) in DMF (10 mL) was added iodine (2.67 g, 10.5 mmol) and potassium hydroxide (1.40 g, 25.0 mmol). The reaction mixture was stirred at room temperature for 4 hours. The reaction mixture was then poured into 400 mL of ice water containing 0.5% ammonia and 0.1% sodium thiosulfate. The mixture was placed in an ice bath for 2 hours to ensure the complete precipitation. The precipitate was filtered, washed with ice water and dried in vacuo to obtain crude product as a yellow solid. It was used in the next step without further purification. The obtained solid was dissolved in CH_2Cl_2 (20 mL). 4-Dimethylaminopyridine (122 mg, 1.0 mmol, 10 mol%) and di-tert-butyl dicarbonate (2.29 g, 10.5 mmol) was then added to the solution. The reaction mixture was stirred at room temperature for 12 hours. The mixture was then washed with 1 M HCl (300 mL) and the aqueous phase was extracted with CH_2Cl_2 (3 x 30 mL). The combined organic layers were dried over Na_2SO_4 and concentrated in vacuo. The residue was purified by flash chromatography (3 : 1 hexanes/ EtOAc) to give **57al**(2.83 g, 82% over two steps) as a white solid.

^{1}H NMR (400 MHz, Chloroform-*d*) δ 9.50 (br s, 1H), 8.55 (dd, *J* = 6.3, 0.6 Hz, 1H), 8.29 (br s, 1H), 7.85 (dd, *J* = 6.3, 0.8 Hz, 1H), 1.71 (s, 9H). ^{13}C NMR (101 MHz, Chloroform-*d*) δ 146.3, 143.4, 140.3, 132.9, 131.1, 129.8, 118.9, 89.1, 63.4, 28.1(^{1}H NMR and ^{13}C NMR similar to literature data)[11]. HRMS (ESI) $[M+H]^+$ calculated for $C_{12}H_{14}IN_2O_2^+$: 345.0094, found 345.0106 (HRMS match literature data)[11].

mp decomp at 125°C (lit mp 149-150°C)[11].

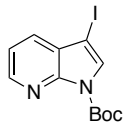

***tert*-butyl 3-iodo-1*H*-pyrrolo[2,3-*b*]pyridine-1-carboxylate (57am)**: A literature procedure for synthesis of *tert*-butyl 3-iodo-1*H*-indole-1-carboxylate was followed.[7] To a solution of 3-iodo-1*H*-pyrrolo[2,3-*b*]pyridine (1.95 g, 8.0 mmol) in CH_2Cl_2 (20 mL), was added 4-dimethylaminopyridine (98 mg, 0.8 mmol, 10 mol%) and di-tert-butyl dicarbonate (1.78 g, 8.2 mmol). The reaction mixture was stirred at room temperature for 12 hours. The mixture was then washed with 1 M HCl (300 mL) and the aqueous phase was extracted with CH_2Cl_2 (3 x 30 mL). The combined organic layers were dried over Na_2SO_4 and concentrated in vacuo. The residue was purified by flash chromatography (3 : 1 hexanes/ EtOAc) to give **57am**(2.71 g, 98% over two steps) as a white solid.
^{1}H NMR (400 MHz, Chloroform-*d*) δ 8.53 (ddd, *J* = 4.8, 1.6, 0.4 Hz, 1H), 7.79 (d, *J* = 0.4 Hz, 1H), 7.71 (dd, *J* = 7.7, 1.6 Hz, 1H), 7.28 (dd, *J* = 7.7, 4.8 Hz, 1H), 1.67 (s, 9H). ^{13}C NMR (101 MHz, Chloroform-*d*) δ 147.6, 147.0, 146.4, 130.8, 130.0, 125.4, 119.4, 84.9, 62.0, 28.2.

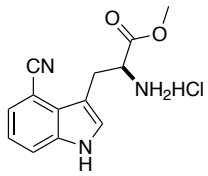

methyl (*S*)-2-amino-3-(4-cyano-1*H*-indol-3-yl)propanoate hydrochloride (59ac): A literature procedure for Nickel catalyzed aryl halide and alkyl halide cross-coupling was followed.[7] $NiCl_2$ (92 mg, 0.7 mmol, 10 mol%), 4,7-diphenyl-1,10-phenanthroline (234 mg, 0.7 mmol, 10 mol%) and Mn powder (1.16 g, 21.0 mmol) were added to a Schlenk tube equipped with a stir bar. The vessel was evacuated and filled with nitrogen (three cycles). To these solids, 1-methyl-2-pyrrolidinone (15 mL) was added under nitrogen atmosphere. The reaction mixture was stirred at 80 °C for 45 minutes. After cooling the reaction mixture to room temperature, **57ac** (2.58 g, 7.0 mmol) and Boc-β-iodo-Ala-OMe (2.77 g, 8.4 mmol) in 1-methyl-2-pyrrolidinone (8 mL) was added under a positive flow of nitrogen. The reaction mixture was stirred at room temperature for 20 hours. To remove the 1-methyl-2-pyrrolidinone, the reaction mixture was poured into 250 mL of ice water and the resulting mixture was extracted with ethyl acetate (4 x 30 mL). The combined organic layer was dried over Na_2SO_4, filtered and concentrated in vacuo. The residue was purified by column chromatography (1 : 1 hexanes/ CH_2Cl_2) to give **58ac** (1.53 g, 49%) as a white solid. **58ac** (1.33 g, 3.0 mmol)

was then dissolved in 1 M HCl in EtOAc (30 mL) and stirred at room temperature for 36 hours. The precipitate was filtered and recrystallized with MeOH/ EtOAc to give **59ac** (629 mg, 75%) as a white solid.

^{1}H NMR (400 MHz, Methanol-d_4) δ 7.74 (dd, J = 8.3, 0.9 Hz, 1H), 7.51 (dd, J = 7.4, 0.9 Hz, 1H), 7.46 (s, 1H), 7.28 (dd, J = 8.3, 7.4 Hz, 1H), 4.41 (dd, J = 9.0, 6.3 Hz, 1H), 3.78 (s, 3H), 3.77 – 3.71 (m, 1H), 3.42 (ddd, J = 15.1, 9.0, 0.7 Hz, 1H). ^{13}C NMR (101 MHz, Methanol-d_4) δ 170.7, 138.7, 129.7, 127.4, 127.2, 122.7, 120.7, 118.3, 107.9, 101.9, 55.0, 53.6, 27.5. HRMS (ESI) $[M+H]^+$ calculated for $C_{13}H_{14}N_3O_2^+$: 244.1081, found 244.1086.

mp 228-232 °C (decomp). $[\alpha]_D^{22}$ = -9.1 (c = 2.61, MeOH).

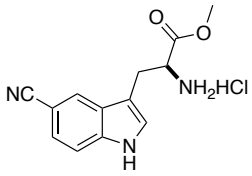

methyl (*S*)-2-amino-3-(5-cyano-1*H*-indol-3-yl)propanoate hydrochloride (59ad): A literature procedure for Nickel catalyzed aryl halide and alkyl halide cross-coupling was followed.[7] $NiCl_2$ (78 mg, 0.6 mmol, 10 mol%), 4,7-diphenyl-1,10-phenanthroline (199 mg, 0.6 mmol, 10 mol%) and Mn powder (989 mg, 18.0 mmol) were added to a Schlenk tube equipped with a stir bar. The vessel was evacuated and filled with nitrogen (three cycles). To these solids, 1-methyl-2-pyrrolidinone (10 mL) was added under nitrogen atmosphere. The reaction mixture was stirred at 80 °C for 45 minutes. After cooling the reaction mixture to room temperature, **57ad** (2.21 g, 6.0 mmol) and Boc-β-iodo-Ala-OMe (2.37 g, 7.2 mmol) in 1-methyl-2-pyrrolidinone (5 mL) was added under a positive flow of nitrogen. The reaction mixture was stirred at room temperature for 20 hours. To remove the 1-methyl-2-pyrrolidinone, the reaction mixture was poured into 250 mL of ice water and the resulting mixture was extracted with ethyl acetate (4 x 30 mL). The combined organic layer was dried over Na_2SO_4, filtered and concentrated in vacuo. The residue was purified by column chromatography (10 : 10 : 1 hexanes/ CH_2Cl_2/ EtOAc) to give **58ad** (1.45 g, 49%, $[\alpha]_D^{23}$ = +37.5 (c = 2.44, $CHCl_3$) as a white solid. **58ad** (1.34 g, 3.0 mmol) was then dissolved in 1 M HCl in EtOAc (30 mL) and stirred at room temperature for 36 hours. The precipitate was filtered and recrystallized with MeOH/ EtOAc to give **59ad** (735 mg, 87%) as a white solid.

^{1}H NMR (400 MHz, Methanol-d_4) δ 8.32 (dd, J = 8.7, 0.7 Hz, 1H), 8.05 (dd, J = 1.6, 0.7 Hz, 1H), 7.81 (s, 1H), 7.68 (dd, J = 8.7, 1.6 Hz, 1H), 4.46 (dd, J = 7.3, 5.9 Hz, 1H), 3.82 (s, 3H), 3.46 (ddd, J = 15.2, 5.9, 0.8 Hz, 1H), 3.37 (ddd,

J = 15.2, 7.3, 0.8 Hz, 1H). ^{13}C NMR (101 MHz, Methanol-d_4) δ 168.9, 129.8, 127.62, 127.56, 123.6, 119.0, 116.0, 112.7, 105.85, 85.1, 52.4, 52.3, 26.8. HRMS (ESI) $[M+H]^+$ calculated for $C_{13}H_{14}N_3O_2^+$: 244.1081, found 244.1087. mp decomp at 150 °C. $[\alpha]_D^{22}$ = +23.6 (c = 2.93, MeOH).

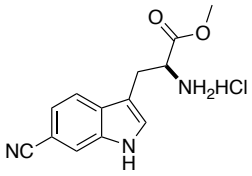

methyl (*S*)-2-amino-3-(6-cyano-1*H*-indol-3-yl)propanoate hydrochloride (59ae): A literature procedure for Nickel catalyzed aryl halide and alkyl halide cross-coupling was followed.[7] $NiCl_2$ (65 mg, 0.5 mmol, 10 mol%), 4,7-diphenyl-1,10-phenanthroline (166 mg, 0.5 mmol, 10 mol%) and Mn powder (830 mg, 15.0 mmol) were added to a Schlenk tube equipped with a stir bar. The vessel was evacuated and filled with nitrogen (three cycles). To these solids, 1-methyl-2-pyrrolidinone (10 mL) was added under nitrogen atmosphere. The reaction mixture was stirred at 80 °C for 45 minutes. After cooling the reaction mixture to room temperature, **57ae** (1.84 g, 5.0 mmol) and Boc-β-iodo-Ala-OMe (1.98 g, 6.0 mmol) in 1-methyl-2-pyrrolidinone (5 mL) was added under a positive flow of nitrogen. The reaction mixture was stirred at room temperature for 20 hours. To remove the 1-methyl-2-pyrrolidinone, the reaction mixture was poured into 250 mL of ice water and the resulting mixture was extracted with ethyl acetate (4 x 30 mL). The combined organic layer was dried over Na_2SO_4, filtered and concentrated in vacuo. The residue was purified by column chromatography (5 : 5 : 1 hexanes/ CH_2Cl_2/ EtOAc) to give **58ae** (1.15 g, 53%) as a white solid. **58ae** (1.11 g, 2.5 mmol) was then dissolved in 1 M HCl in EtOAc (30 mL) and stirred at room temperature for 36 hours. The precipitate was filtered and recrystallized with MeOH/ EtOAc to give **59ae** (690 mg, 99%) as a white solid.

^{1}H NMR (400 MHz, Methanol-d_4) δ 7.82 (s, 1H), 7.70 (d, J = 8.2 Hz, 1H), 7.48 (s, 1H), 7.36 (dd, J = 8.2, 1.4 Hz, 1H), 4.34 (dd, J = 7.1, 5.9 Hz, 1H), 3.79 (s, 3H), 3.46 (dd, J = 15.2, 5.9 Hz, 1H), 3.39 (dd, J = 15.2, 7.1 Hz, 1H). ^{13}C NMR (101 MHz, Methanol-d_4) δ 170.8, 137.0, 131.5, 130.1, 123.0, 121.4, 120.2, 117.7, 109.0, 105.1, 54.6, 53.7, 27.1. HRMS (ESI) $[M+H]^+$ calculated for $C_{13}H_{14}N_3O_2^+$: 244.1081, found 244.1085.

mp 235-237 °C (decomp). $[\alpha]_D^{23}$ = +27.8 (c = 1.12, MeOH).

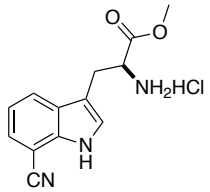

methyl (*S*)-2-amino-3-(7-cyano-1*H*-indol-3-yl)propanoate hydrochloride (59af): A literature procedure for Nickel catalyzed aryl halide and alkyl halide cross-coupling was followed.[7] $NiCl_2$ (60 mg, 0.5 mmol, 10 mol%), 4,7-diphenyl-1,10-phenanthroline (153 mg, 0.5 mmol, 10 mol%) and Mn powder (764 mg, 13.8 mmol) were added to a Schlenk tube equipped with a stir bar. The vessel was evacuated and filled with nitrogen (three cycles). To these solids, 1-methyl-2-pyrrolidinone (10 mL) was added under nitrogen atmosphere. The reaction mixture was stirred at 80 °C for 45 minutes. After cooling the reaction mixture to room temperature, **57af** (1.69 g, 4.6 mmol) and Boc-β-iodo-Ala-OMe (1.82 g, 5.5 mmol) in 1-methyl-2-pyrrolidinone (5 mL) was added under a positive flow of nitrogen. The reaction mixture was stirred at room temperature for 20 hours. To remove the 1-methyl-2-pyrrolidinone, the reaction mixture was poured into 250 mL of ice water and the resulting mixture was extracted with ethyl acetate (4 x 30 mL). The combined organic layer was dried over Na_2SO_4, filtered and concentrated in vacuo. The residue was purified by column chromatography (5 : 5 : 1 hexanes/ CH_2Cl_2/ EtOAc) to give **58af** (1.14 g, 56%, $[\alpha]_D^{23}$ = +29.2 (c = 2.60, $CHCl_3$) as a white solid. **58af** (968 mg, 2.5 mmol) was then dissolved in 1 M HCl in EtOAc (30 mL) and stirred at room temperature for 36 hours. The precipitate was filtered and washed with EtOAc to give **59af** (403 mg, 57%, <90% purity) as an off-white solid.

^{1}H NMR (400 MHz, Methanol-d_4) δ 7.88 (dd, J = 8.0, 1.0 Hz, 1H), 7.56 (dd, J = 7.5, 1.0 Hz, 1H), 7.37 (s, 1H), 7.22 (t, J = 7.7 Hz, 1H), 4.36 (dd, J = 7.2, 5.8 Hz, 1H), 3.79 (s, 3H), 3.48 – 3.39 (m, 2H). ^{13}C NMR (101 MHz, Methanol-d_4) δ 170.6, 131.2, 131.1, 128.60, 128.3, 128.0, 125.2, 125.2, 120.4, 109.3, 54.5, 53.7, 26.9. HRMS (ESI) $[M+H]^+$ calculated for $C_{13}H_{14}N_3O_2^+$: 244.1081, found 244.1086.

mp decomp at 110 °C. $[\alpha]_D^{22}$ = +20.7 (c = 1.65, MeOH).

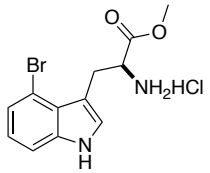

methyl (*S*)-2-amino-3-(4-bromo-1*H*-indol-3-yl)propanoate hydrochloride (59ag): A literature procedure for Nickel catalyzed aryl halide and alkyl halide cross-coupling was followed.[7] $NiCl_2$ (65 mg, 0.5 mmol, 10 mol%), 4,7-diphenyl-1,10-phenanthroline (166 mg, 0.5 mmol, 10 mol%) and Mn powder (830 mg, 13.8 mmol) were added to a Schlenk tube equipped with a stir bar. The vessel was evacuated and filled with nitrogen (three cycles). To these solids, 1-methyl-2-pyrrolidinone (10 mL) was added under nitrogen atmosphere. The reaction mixture was stirred at 80 °C for 45 minutes. After cooling the reaction mixture to room temperature, **57ag** (2.11 g, 5.0 mmol) and Boc-β-iodo-Ala-OMe (1.98 g, 6.0 mmol) in 1-methyl-2-pyrrolidinone (5 mL) was added under a positive flow of nitrogen. The reaction mixture was stirred at room temperature for 20 hours. To remove the 1-methyl-2-pyrrolidinone, the reaction mixture was poured into 250 mL of ice water and the resulting mixture was extracted with ethyl acetate (4 x 30 mL). The combined organic layer was dried over Na_2SO_4, filtered and concentrated in vacuo. The residue was purified by column chromatography (5 : 5 : 1 hexanes/ CH_2Cl_2/ EtOAc) to give **58ag** (1.81 g, 73%) as a white solid. **58ag** (1.67 g, 3.4 mmol) was then dissolved in 1 M HCl in EtOAc (30 mL) and stirred at room temperature for 36 hours. The precipitate was filtered and recrystallized with MeOH/ EtOAc to give **59ag** (1.05 g, 94%) as a white solid.

^{1}H NMR (400 MHz, Methanol-d_4) δ 7.41 (dd, J = 8.0, 0.8 Hz, 1H), 7.27 (s, 1H), 7.24 (dd, J = 7.6, 0.8 Hz, 1H), 7.03 (t, J = 8.0, 7.6 Hz, 1H), 4.44 (dd, J = 9.8, 5.7 Hz, 1H), 3.88 (ddd, J = 14.8, 5.7, 0.7 Hz, 1H), 3.81 (s, 3H), 3.25 (ddd, J = 14.8, 9.8, 0.7 Hz, 1H). ^{13}C NMR (101 MHz, Methanol-d_4) δ 170.9, 140.0, 128.1, 126.1, 124.7, 124.0, 114.0, 112.4, 108.6, 56.0, 53.6, 28.8. HRMS (ESI) $[M+H]^+$ calculated for $C_{12}H_{14}BrN_2O_2^+$: 297.0233, found 297.0232.

mp 126-127 °C (decomp). $[\alpha]_D^{23}$ = -16.3 (c = 0.59, MeOH).

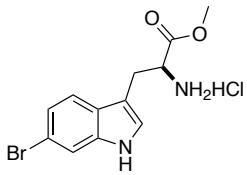

methyl (*S*)-2-amino-3-(6-bromo-1*H*-indol-3-yl)propanoate hydrochloride (59ah): A literature procedure for Nickel catalyzed aryl halide and alkyl halide cross-coupling was followed.[7] $NiCl_2$ (65 mg, 0.5 mmol, 10 mol%), 4,7-

diphenyl-1,10-phenanthroline (166 mg, 0.5 mmol, 10 mol%) and Mn powder (830 mg, 13.8 mmol) were added to a Schlenk tube equipped with a stir bar. The vessel was evacuated and filled with nitrogen (three cycles). To these solids, 1-methyl-2-pyrrolidinone (10 mL) was added under nitrogen atmosphere. The reaction mixture was stirred at 80 °C for 45 minutes. After cooling the reaction mixture to room temperature, **57ah** (2.11 g, 5.0 mmol) and Boc-β-iodo-Ala-OMe (1.98 g, 6.0 mmol) in 1-methyl-2-pyrrolidinone (5 mL) was added under a positive flow of nitrogen. The reaction mixture was stirred at room temperature for 20 hours. To remove the 1-methyl-2-pyrrolidinone, the reaction mixture was poured into 250 mL of ice water and the resulting mixture was extracted with ethyl acetate (4 x 30 mL). The combined organic layer was dried over Na_2SO_4, filtered and concentrated in vacuo. The residue was purified by column chromatography (5 : 5 : 1 hexanes/ CH_2Cl_2/ EtOAc) to give **58ah** (1.32 g, 53%) as a white solid. **58ah** (1.10 g, 2.2 mmol) was then dissolved in 1 M HCl in EtOAc (30 mL) and stirred at room temperature for 36 hours. The precipitate was filtered and recrystallized with MeOH/ EtOAc to give **59ah** (707 mg, 96%) as a white solid.

^{1}H NMR (400 MHz, Methanol-d_4) δ 7.56 (dd, J = 1.8, 0.5 Hz, 1H), 7.45 (dd, J = 8.5, 0.5 Hz, 1H), 7.22 (s, 1H), 7.18 (dd, J = 8.5, 1.8 Hz, 1H), 4.33 (dd, J = 7.3, 5.6 Hz, 1H), 3.79 (s, 3H), 3.43 (ddd, J = 15.2, 5.6, 0.8 Hz, 1H), 3.36 (ddd, J = 15.2, 7.3, 0.8 Hz, 1H). ^{13}C NMR (101 MHz, Methanol-d_4) δ 170.7, 139.1, 127.2, 126.6, 123.5, 120.4, 116.4, 115.54, 108.0, 54.5, 53.7, 27.3. HRMS (ESI) $[M+H]^+$ calculated for $C_{12}H_{14}BrN_2O_2^+$: 297.0233, found 297.0231.

$[\alpha]_D^{23}$ = +13.9 (c = 1.20, MeOH).

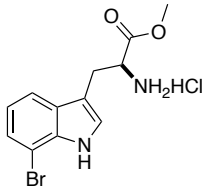

methyl (*S*)-2-amino-3-(6-bromo-1*H*-indol-3-yl)propanoate hydrochloride (59ai): A literature procedure for Nickel catalyzed aryl halide and alkyl halide cross-coupling was followed.[7] $NiCl_2$ (48 mg, 0.4 mmol, 10 mol%), 4,7-diphenyl-1,10-phenanthroline (123 mg, 0.4 mmol, 10 mol%) and Mn powder (610 mg, 11.1 mmol) were added to a Schlenk tube equipped with a stir bar. The vessel was evacuated and filled with nitrogen (three cycles). To these solids, 1-methyl-2-pyrrolidinone (10 mL) was added under nitrogen atmosphere. The reaction mixture was stirred at 80 °C for 45 minutes. After cooling the reaction mixture to room temperature, **57ai** (1.56 g, 3.7 mmol) and Boc-β-iodo-Ala-OMe (1.46 g, 4.4 mmol) in 1-methyl-2-pyrrolidinone (5 mL) was added under a positive flow of nitrogen. The reaction

mixture was stirred at room temperature for 20 hours. To remove the 1-methyl-2-pyrrolidinone, the reaction mixture was poured into 250 mL of ice water and the resulting mixture was extracted with ethyl acetate (4 x 30 mL). The combined organic layer was dried over Na_2SO_4, filtered and concentrated in vacuo. The residue was purified by column chromatography (3 : 1 hexanes/ EtOAc) to give **58ai** (713 mg, 39%) as a white solid. **58ai** (1.217 g, 2.5 mmol) was then dissolved in 1 M HCl in EtOAc (30 mL) and stirred at room temperature for 36 hours. The precipitate was filtered and recrystallized with MeOH/ EtOAc to give **59ai** (704 mg, 86%) as a white solid.

^{1}H NMR (400 MHz, Methanol-d_4) δ 7.54 (d, J = 7.8 Hz, 1H), 7.33 (d, J = 7.8 Hz, 1H), 7.29 (s, 1H), 7.00 (t, J = 7.8 Hz, 1H), 4.34 (dd, J = 7.2, 5.6 Hz, 1H), 3.79 (s, 3H), 3.48 – 3.32 (m, 2H). ^{13}C NMR (101 MHz, Methanol-d_4) δ 170.7, 136.7, 129.8, 126.8, 125.6, 121.6, 118.4, 109.0, 105.9, 54.5, 53.7, 27.5. HRMS (ESI) $[M+H]^+$ calculated for $C_{12}H_{14}BrN_2O_2^+$: 297.0233, found 297.0231.

$[\alpha]_D^{23}$ = +14.6 (c = 1.00, MeOH).

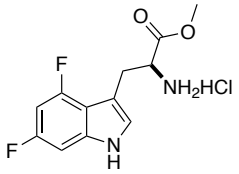

methyl (*S*)-2-amino-3-(4,6-difluoro-1*H*-indol-3-yl)propanoate hydrochloride (59aj): A literature procedure for Nickel catalyzed aryl halide and alkyl halide cross-coupling was followed.[7] $NiCl_2$ (46 mg, 0.4 mmol, 10 mol%), 4,7-diphenyl-1,10-phenanthroline (116 mg, 0.4 mmol, 10 mol%) and Mn powder (577 mg, 10.5 mmol) were added to a Schlenk tube equipped with a stir bar. The vessel was evacuated and filled with nitrogen (three cycles). To these solids, 1-methyl-2-pyrrolidinone (10 mL) was added under nitrogen atmosphere. The reaction mixture was stirred at 80 °C for 45 minutes. After cooling the reaction mixture to room temperature, **57aj** (1.33 g, 3.5 mmol) and Boc-β-iodo-Ala-OMe (1.38 g, 4.2 mmol) in 1-methyl-2-pyrrolidinone (5 mL) was added under a positive flow of nitrogen. The reaction mixture was stirred at room temperature for 20 hours. To remove the 1-methyl-2-pyrrolidinone, the reaction mixture was poured into 250 mL of ice water and the resulting mixture was extracted with ethyl acetate (4 x 30 mL). The combined organic layer was dried over Na_2SO_4, filtered and concentrated in vacuo. The residue was purified by column chromatography (10 : 10 : 1 hexanes/ CH_2Cl_2/ EtOAc) to give **58aj** (1.06 g, 67%) as a white solid. **58aj** (1.05 g, 2.3 mmol) was then dissolved in 1 M HCl in EtOAc (30 mL) and stirred at room temperature for 36 hours. The precipitate was filtered and recrystallized with MeOH/ EtOAc to give **59aj** (539 mg, 86%) as a white solid.

^{1}H NMR (400 MHz, Methanol-d_4) δ 7.17 (s, 1H), 6.96 (dd, $^{3}J_{HF}$ = 9.6, $^{4}J_{HH}$ = 2.1 Hz, 1H), 6.64 (ddd, $^{3}J_{HF}$ = 11.8, 9.6, $^{4}J_{HH}$ = 2.1 Hz, 1H), 4.27 (dd, J = 8.7, 5.7 Hz, 1H), 3.81 (s, 3H), 3.49 (ddd, J = 14.7, 5.7, 0.9 Hz, 1H), 3.29 – 3.24 (m, 1H). ^{19}F NMR (376 MHz, Methanol-d_4) δ -120.99 (td, $^{3}J_{HF}$ = 9.6, $^{4}J_{FF}$ = 4.1 Hz), -123.80 (dd, $^{3}J_{HF}$ = 11.5, $^{4}J_{FF}$ = 4.1 Hz). ^{13}C NMR (101 MHz, Methanol-d_4) δ 170.8, 159.5 (dd, $^{1}J_{CF}$ = 237.7, $^{3}J_{CF}$ = 11.6 Hz), 156.1 (dd, $^{1}J_{CF}$ = 243.5, $^{3}J_{CF}$ = 15.5 Hz), 140.2 (t, $^{3}J_{CF}$ = 13.9 Hz), 126.6 (d, $^{4}J_{CF}$ = 2.3 Hz), 113.3 (dd, $^{2}J_{CF}$ = 19.6, $^{4}J_{CF}$ = 1.4 Hz), 106.7 (d, $^{3}J_{CF}$ = 2.7 Hz), 95.6 (dd, $^{2}J_{CF}$ = 28.8, 23.9 Hz), 95.2 (dd, $^{2}J_{CF}$ = 25.9, $^{4}J_{CF}$ = 4.6 Hz), 55.0, 53.6, 28.8.
HRMS (ESI) $[M+H]^+$ calculated for $C_{12}H_{13}F_2N_2O_2^+$: 255.0940, found 255.0956.
mp decomp at 200 °C. $[\alpha]_D^{23}$ = +5.5 (c = 1.39, MeOH).

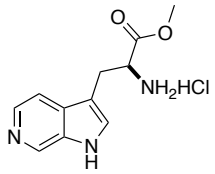

methyl (*S*)-2-amino-3-(1*H*-pyrrolo[2,3-*c*]pyridin-3-yl)propanoate hydrochloride (59al): A literature procedure for Nickel catalyzed aryl halide and alkyl halide cross-coupling was followed.[7] $NiCl_2$ (98 mg, 0.8 mmol, 10 mol%), 4,7-diphenyl-1,10-phenanthroline (249 mg, 0.8 mmol, 10 mol%) and Mn powder (1.25 g, 22.5 mmol) were added to a Schlenk tube equipped with a stir bar. The vessel was evacuated and filled with nitrogen (three cycles). To these solids, 1-methyl-2-pyrrolidinone (10 mL) was added under nitrogen atmosphere. The reaction mixture was stirred at 80 °C for 45 minutes. After cooling the reaction mixture to room temperature, **57al** (2.58 g, 7.5 mmol) and Boc-β-iodo-Ala-OMe (2.96 g, 9.0 mmol) in 1-methyl-2-pyrrolidinone (5 mL) was added under a positive flow of nitrogen. The reaction mixture was stirred at room temperature for 20 hours. To remove the 1-methyl-2-pyrrolidinone, the reaction mixture was poured into 250 mL of ice water and the resulting mixture was extracted with ethyl acetate (4 x 30 mL). The combined organic layer was dried over Na_2SO_4, filtered and concentrated in vacuo. The residue was purified by column chromatography (1 : 1 hexanes/ EtOAc) to give **58aj** (679 mg, 22%) as a white solid. **58al** (645 mg, 1.5 mmol) was then dissolved in 1 M HCl in EtOAc (30 mL) and stirred at room temperature for 36 hours. The precipitate was filtered and recrystallized with MeOH/ EtOAc to give **59al** (380 mg, 97%) as a white solid.
^{1}H NMR (400 MHz, Methanol-d_4) δ 9.11 (t, J = 0.8 Hz, 1H), 8.29 (dd, J = 6.5, 0.8 Hz, 1H), 8.19 (s, 1H), 8.18 (dd, J = 6.5, 0.8 Hz, 1H), 4.49 (t, J = 6.5 Hz, 1H), 3.81 (s, 3H), 3.60 (ddd, J = 14.2, 6.5, 0.6 Hz, 1H), 3.55 (ddd, J = 14.2,

6.5, 0.6 Hz, 1H). ^{13}C NMR (101 MHz, Methanol-d_4) δ 170.3, 140.1, 138.2, 133.12, 129.3, 128.7, 116.8, 111.3, 54.3, 53.9, 26.2. HRMS (ESI) $[M+H]^+$ calculated for $C_{11}H_{14}N_3O_2^+$: 220.1081, found 297.1097.

m.p. 212-218 °C (decomp). $[\alpha]_D^{23}$ = +25.1 (c = 0.65, MeOH).

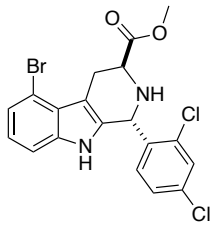

methyl (1*R*,3*S*)-5-bromo-1-(2,4-dichlorophenyl)-2,3,4,9-tetrahydro-1*H*-pyrido[3,4-*b*]indole-3-carboxylate (27ag): A standard literature procedure for Pictet-Spengler reaction was followed.[1] To a solution of **59ag** (530 mg, 1.6 mmol) in CH_2Cl_2 (6 mL) was added 4 Å molecular sieves (1.00 g), 2,4 dichlorobenzaldehyde (278 mg, 1.6 mmol) and DIPEA (276 µL, 1.6 mmol). The reaction mixture was stirred at room temperature for 24 hours. Trifluoroacetic acid (244 µL, 3.2 mmol) was then added dropwise. The resulting mixture was stirred at room temperature for another 48 hours. An aqueous solution of $NaHCO_3$ (2.40 g, 30.0 mmol, in 20 mL H2O) was added dropwise at 0 °C, followed by an addition of EtOAc (80 mL). The mixture was stirred for 15 minutes. The phases were separated and the aqueous layer was extracted with EtOAc (3×20 mL). The combined organic layers were washed with brine, dried over Na_2SO_4, concentrated, then purified by flash chromatography (3 : 1 hexanes/ EtOAc) to give **27ag** (192 mg, 27%) as a white solid.

^{1}H NMR (400 MHz, Chloroform-*d*) δ 7.77 (s, 1H), 7.47 (d, *J* = 2.2 Hz, 1H), 7.27 (dd, *J* = 7.5, 0.8 Hz, 1H), 7.18 (dd, *J* = 8.1, 0.8 Hz, 1H), 7.12 (ddd, *J* = 8.3, 2.2, 0.4 Hz, 1H), 6.99 (d, *J* = 8.0 Hz, 1H), 6.94 (d, *J* = 8.0 Hz, 1H), 5.83 (s, 1H), 3.82 (dd, *J* = 7.7, 5.0 Hz, 1H), 3.75 (s, 3H), 3.66 (ddd, *J* = 15.9, 5.0, 1.4 Hz, 1H), 3.42 (ddd, *J* = 15.9, 7.7, 1.4 Hz, 1H). ^{13}C NMR (101 MHz, Chloroform-*d*) δ 173.9, 137.6, 137.2, 134.7, 134.5, 132.8, 131.0, 130.0, 127.4, 125.9, 123.8, 123.3, 114.1, 110.4, 110.3, 52.4, 52.2, 51.2, 26.6.

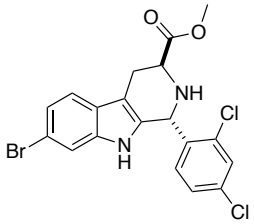

methyl (1*R*,3*S*)-7-bromo-1-(2,4-dichlorophenyl)-2,3,4,9-tetrahydro-1*H*-pyrido[3,4-*b*]indole-3-carboxylate (27ah): A standard literature procedure for Pictet-Spengler reaction was followed.[1] To a solution of **59ah** (500 mg, 1.5 mmol) in CH_2Cl_2 (6 mL) was added 4 Å molecular sieves (1.00 g), 2,4 dichlorobenzaldehyde (263 mg, 1.5 mmol) and DIPEA (260 µL, 1.5 mmol). The reaction mixture was stirred at room temperature for 24 hours. Trifluoroacetic acid (230 µL, 3.0 mmol) was then added dropwise. The resulting mixture was stirred at room temperature for another 48 hours. An aqueous solution of $NaHCO_3$ (2.40 g, 30.0 mmol, in 20 mL H2O) was added dropwise at 0 °C, followed by an addition of EtOAc (80 mL). The mixture was stirred for 15 minutes. The phases were separated and the aqueous layer was extracted with EtOAc (3×20 mL). The combined organic layers were washed with brine, dried over Na_2SO_4, concentrated, then purified by flash chromatography (8 : 8 : 1 hexanes/ CH_2Cl_2/ EtOAc) to give **27ah** (186 mg, 27%) as a white solid.

^{1}H NMR (400 MHz, Chloroform-*d*) δ 7.67 (s, 1H), 7.48 (d, *J* = 2.0 Hz, 1H), 7.44 – 7.36 (m, 2H), 7.24 (dd, *J* = 8.4, 1.7 Hz, 1H), 7.13 (ddd, *J* = 8.4, 2.1, 0.5 Hz, 1H), 6.92 (d, *J* = 8.4 Hz, 1H), 5.83 (s, 1H), 3.85 (dd, *J* = 7.4, 5.1 Hz, 1H), 3.73 (s, 3H), 3.22 (ddd, *J* = 15.4, 5.1, 1.4 Hz, 1H), 3.07 (ddd, *J* = 15.4, 7.4, 1.4 Hz, 1H). ^{13}C NMR (101 MHz, Chloroform-*d*) δ 173.7, 137.6, 137.1, 134.7, 134.5, 132.4, 130.9, 130.0, 127.4, 125.9, 123.2, 119.7, 115.9, 114.1, 109.9, 52.4, 52.4, 51.2, 24.7.

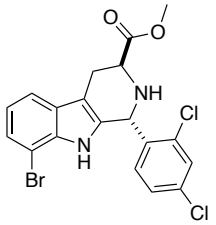

methyl (1*R*,3*S*)-8-bromo-1-(2,4-dichlorophenyl)-2,3,4,9-tetrahydro-1*H*-pyrido[3,4-*b*]indole-3-carboxylate (27ai): A standard literature procedure for Pictet-Spengler reaction was followed.[1] To a solution of **59ai** (500 mg, 1.5 mmol) in CH_2Cl_2 (6 mL) was added 4 Å molecular sieves (1.00 g), 2,4 dichlorobenzaldehyde (263 mg, 1.5 mmol) and DIPEA (260 µL, 1.5 mmol). The reaction mixture was stirred at room temperature for 24 hours.

Trifluoroacetic acid (230 μL, 3.0 mmol) was then added dropwise. The resulting mixture was stirred at room temperature for another 48 hours. An aqueous solution of $NaHCO_3$ (2.40 g, 30.0 mmol, in 20 mL H2O) was added dropwise at 0 °C, followed by an addition of EtOAc (80 mL). The mixture was stirred for 15 minutes. The phases were separated and the aqueous layer was extracted with EtOAc (3×20 mL). The combined organic layers were washed with brine, dried over Na_2SO_4, concentrated, then purified by flash chromatography (8 : 8 : 1 hexanes/ CH_2Cl_2/ EtOAc) to give **27ai** (79 mg, 12%) as a white solid.

^{1}H NMR (400 MHz, Chloroform-*d*) δ 7.81 (s, 1H), 7.54 – 7.45 (m, 2H), 7.34 (dd, *J* = 7.8, 1.0 Hz, 1H), 7.14 (ddd, *J* = 8.4, 2.1, 0.4 Hz, 1H), 7.03 (t, *J* = 7.8 Hz, 1H), 6.90 (d, *J* = 8.4 Hz, 1H), 5.88 (s, 1H), 3.83 (dd, *J* = 7.9, 4.9 Hz, 1H), 3.74 (s, 3H), 3.24 (ddd, *J* = 15.4, 4.9, 1.3 Hz, 1H), 3.08 (ddd, *J* = 15.4, 7.9, 1.3 Hz, 1H). ^{13}C NMR (101 MHz, Chloroform-*d*) δ 173.6, 137.4, 135.1, 134.8, 134.6, 132.4, 130.9, 130.1, 128.1, 127.4, 124.9, 121.1, 117.7, 111.2, 104.7, 52.5, 52.1, 51.3, 25.1.

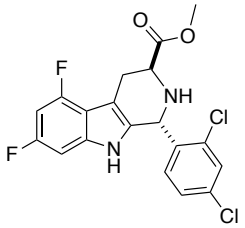

methyl (1*R*,3*S*)-5,7-difluoro-1-(2,4-dichlorophenyl)-2,3,4,9-tetrahydro-1*H*-pyrido[3,4-*b*]indole-3-carboxylate (27aj): A standard literature procedure for Pictet-Spengler reaction was followed.[1] To a solution of **59ai** (290 mg, 1.0 mmol) in CH_2Cl_2 (6 mL) was added 4 Å molecular sieves (0.50 g), 2,4 dichlorobenzaldehyde (175 mg, 1.0 mmol) and DIPEA (174 μL, 1.0 mmol). The reaction mixture was stirred at room temperature for 24 hours. Trifluoroacetic acid (153 μL, 2.0 mmol) was then added dropwise. The resulting mixture was stirred at room temperature for another 48 hours. An aqueous solution of $NaHCO_3$ (2.40 g, 30.0 mmol, in 20 mL H2O) was added dropwise at 0 °C, followed by an addition of EtOAc (80 mL). The mixture was stirred for 15 minutes. The phases were separated and the aqueous layer was extracted with EtOAc (3×20 mL). The combined organic layers were washed with brine, dried over Na_2SO_4, concentrated, then purified by flash chromatography (5 : 1 hexanes/ EtOAc) to give **27aj** (101 mg, 25%) as a white solid.

^{1}H NMR (400 MHz, Chloroform-*d*) δ 7.71 (s, 1H), 7.48 (d, *J* = 2.1 Hz, 1H), 7.16 (ddd, *J* = 8.3, 2.1, 0.5 Hz, 1H), 6.99 (d, *J* = 8.4 Hz, 1H), 6.75 (ddd, $^3J_{HF}$ = 9.2, $^4J_{HH}$ = 2.0, 0.4 Hz, 1H), 6.60 (ddd, $^3J_{HF}$ = 10.6, 10.0, $^4J_{HH}$ = 2.0 Hz,

1H), 5.82 (s, 1H), 3.85 (dd, *J* = 7.6, 5.2 Hz, 1H), 3.74 (s, 3H), 3.37 (ddd, *J* = 15.6, 5.2, 1.4 Hz, 1H), 3.22 (ddd, *J* = 15.6, 7.6, 1.4 Hz, 1H). ^{19}F NMR (376 MHz, Chloroform-*d*) δ -118.06 (td, $^{3}J_{HF}$ = 9.2, $^{4}J_{FF}$ = 4.1 Hz), -121.36 (ddd, $^{3}J_{HF}$ = 10.2, $^{4}J_{FF}$ = 4.1, $^{5}J_{HF}$ = 2.2 Hz). ^{13}C NMR (101 MHz, Chloroform-*d*) δ 173.7, 165.0 (d, $^{1}J_{CF}$ = 264.3 Hz), 157.4 (d, $^{1}J_{CF}$ = 265.0 Hz), 141.4, 137.5, 134.7, 134.4, 131.7, 130.9, 130.0, 127.5, 118.0, 107.9, 94.0, 93.8, 53.6, 52.4, 51.0, 25.8.

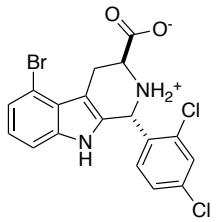

(1*R*,3*S*)-5-bromo-1-(2,4-dichlorophenyl)-2,3,4,9-tetrahydro-1*H*-pyrido[3,4-*b*]indol-2-ium-3-carboxylate (29ag): A modification of an Amberlyst resin-mediated catch and release protocol was followed.[8] To a solution of **27ag** (192 mg, 0.4 mmol) in THF / MeOH / H2O (2.0 mL / 1.0 mL / 1.0 mL) was added Amberlyst hydroxide resin (3.00 g, Aldrich, loading: 4.2 mmol/g). The reaction mixture was stirred at room temperature for 24 hours. The resin was filtered and washed with MeOH and CH_2Cl_2 alternatively (4 × 10 mL). An aqueous solution of AcOH (50%) (20 mL) was added to cleave the product from the resin, the cleaving solution was collected by filtration. The cleavage step was repeated for another 3 times. The combined cleaving solutions were condensed under vacuum. The residue was added MeOH (0.5 mL), followed by addition of Et2O (10 mL) and hexane (25 mL). The mixture was stirred for 15 minutes in ice bath and then filtered. The solid was washed with hexane to afford **29ag** (29 mg, 16%) as a pale yellow solid.

^{1}H NMR (400 MHz, Methanol-d_4) δ 7.71 (d, *J* = 2.1 Hz, 1H), 7.38 (dd, *J* = 8.4, 2.1 Hz, 1H), 7.25 (dd, *J* = 8.1, 0.8 Hz, 1H), 7.22 (dd, *J* = 7.7, 0.8 Hz, 1H), 7.07 – 6.94 (m, 2H), 6.34 (s, 1H), 4.00 – 3.87 (m, 1H), 3.63 – 3.52 (m, 1H). ^{13}C NMR (101 MHz, Methanol-d_4) δ 173.6, 139.7, 137.7, 137.2, 133.5, 133.5, 131.1, 129.6, 129.1, 126.1, 124.6, 124.4, 114.7, 111.8, 110.4, 54.6, 52.3, 26.2. HRMS (ESI) $[M+H]^+$ calculated for $C_{18}H_{14}BrCl_2N_2O_2^+$: 438.9610, found 438.9581.

m.p. decomp at 170 °C. $[\alpha]_D^{23}$ = -95.0 (c = 0.66, MeOH).

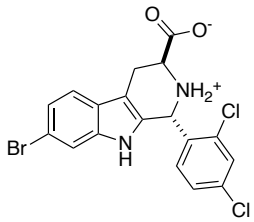

(1*R*,3*S*)-7-bromo-1-(2,4-dichlorophenyl)-2,3,4,9-tetrahydro-1*H*-pyrido[3,4-*b*]indol-2-ium-3-carboxylate (29ah): A modification of an Amberlyst resin-mediated catch and release protocol was followed.[8] To a solution of **27ah** (154 mg, 0.3 mmol) in THF / MeOH / H2O (2.0 mL / 1.0 mL / 1.0 mL) was added Amberlyst hydroxide resin (3.00 g, Aldrich, loading: 4.2 mmol/g). The reaction mixture was stirred at room temperature for 24 hours. The resin was filtered and washed with MeOH and CH_2Cl_2 alternatively (4 × 10 mL). An aqueous solution of AcOH (50%) (20 mL) was added to cleave the product from the resin, the cleaving solution was collected by filtration. The cleavage step was repeated for another 3 times. The combined cleaving solutions were condensed under vacuum. The residue was added MeOH (0.5 mL), followed by addition of Et_2O (10 mL) and hexane (25 mL). The mixture was stirred for 15 minutes in ice bath and then filtered. The solid was washed with hexane to afford **29ah** (50 mg, 40%) as a light yellow solid.

^{1}H NMR (400 MHz, Methanol-d_4) δ 7.72 (d, J = 2.1 Hz, 1H), 7.49 (dd, J = 8.4, 0.5 Hz, 1H), 7.44 (dd, J = 1.7, 0.5 Hz, 1H), 7.38 (dd, J = 8.4, 2.1 Hz, 1H), 7.20 (dd, J = 8.4, 1.7 Hz, 1H), 7.03 (d, J = 8.4 Hz, 1H), 6.38 (s, 1H), 3.97 (dd, J = 8.1, 5.5 Hz, 1H), 3.45 (ddd, J = 16.2, 5.5, 1.3 Hz, 1H), 3.24 (ddd, J = 16.2, 8.1, 1.3 Hz, 1H). ^{13}C NMR (101 MHz, Methanol-d_4) δ 173.4, 139.4, 137.8, 137.3, 133.5, 133.3, 131.1, 129.1, 129.0, 126.2, 123.8, 120.8, 117.1, 115.2, 110.0, 54.9, 52.3, 23.8. HRMS (ESI) $[M+H]^+$ calculated for $C_{18}H_{14}BrCl_2N_2O_2^+$: 438.9610, found 438.9621. m.p. decomp at 170 °C. $[\alpha]_D^{23}$ = +0.4 (c = 1.59, MeOH).

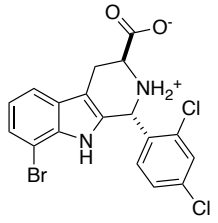

(1*R*,3*S*)-8-bromo-1-(2,4-dichlorophenyl)-2,3,4,9-tetrahydro-1*H*-pyrido[3,4-*b*]indol-2-ium-3-carboxylate (29ai): A modification of an Amberlyst resin-mediated catch and release protocol was followed.[8] To a solution of **27ai** (79 mg, 0.2 mmol) in THF / MeOH / H_2O (1.0 mL / 0.5 mL / 0.5 mL) was added Amberlyst hydroxide resin (1.50 g,

Aldrich, loading: 4.2 mmol/g). The reaction mixture was stirred at room temperature for 24 hours. The resin was filtered and washed with MeOH and CH_2Cl_2 alternatively (4 × 10 mL). An aqueous solution of AcOH (50%) (20 mL) was added to cleave the product from the resin, the cleaving solution was collected by filtration. The cleavage step was repeated for another 3 times. The combined cleaving solutions were condensed under vacuum. The residue was added MeOH (0.5 mL), followed by addition of Et_2O (10 mL) and hexane (25 mL). The mixture was stirred for 15 minutes in ice bath and then filtered. The solid was washed with hexane to afford **29ai** (30 mg, 39%) as an off-white solid.

^{1}H NMR (400 MHz, Methanol-d_4) δ 7.71 (d, J = 2.1 Hz, 1H), 7.57 (d, J = 7.7 Hz, 1H), 7.35 (dd, J = 8.4, 2.1 Hz, 1H), 7.34 (d, J = 7.7 Hz, 1H), 7.02 (t, J = 7.7 Hz, 1H), 6.96 (d, J = 8.4 Hz, 1H), 6.33 (s, 1H), 3.91 (s, 1H), 3.56 – 3.42 (m, 1H), 3.25 – 3.09 (m, 1H). ^{13}C NMR (101 MHz, Methanol-d_4) δ 168.7, 137.5, 137.3, 137.3, 133.4, 131.0, 129.3, 128.9, 128.8, 126.4, 121.9, 118.8, 113.5, 111.3, 105.6, 52.7, 32.8, 23.7. HRMS (ESI) $[M+H]^+$ calculated for $C_{18}H_{14}BrCl_2N_2O_2^+$: 438.9610, found 438.9609.

m.p. decomp at 160 °C. $[\alpha]_D^{23}$ = +61.6 (c = 0.88, MeOH).

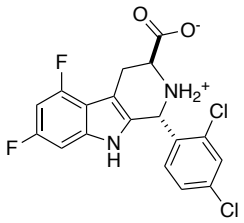

(1*R*,3*S*)-5,7-difluoro-1-(2,4-dichlorophenyl)-2,3,4,9-tetrahydro-1*H*-pyrido[3,4-*b*]indol-2-ium-3-carboxylate (29aj): A modification of an Amberlyst resin-mediated catch and release protocol was followed.[8] To a solution of **27aj** (100 mg, 0.2 mmol) in THF / MeOH / H2O (1.0 mL / 0.5 mL / 0.5 mL) was added Amberlyst hydroxide resin (2.00 g, Aldrich, loading: 4.2 mmol/g). The reaction mixture was stirred at room temperature for 24 hours. The resin was filtered and washed with MeOH and CH_2Cl_2 alternatively (4 × 10 mL). An aqueous solution of AcOH (50%) (20 mL) was added to cleave the product from the resin, the cleaving solution was collected by filtration. The cleavage step was repeated for another 3 times. The combined cleaving solutions were condensed under vacuum. The residue was added MeOH (0.5 mL), followed by addition of Et_2O (10 mL) and hexane (25 mL). The mixture was stirred for 15 minutes in ice bath and then filtered. The solid was washed with hexane to afford **29aj** (49 mg, 51%) as an off-white solid.

^{1}H NMR (400 MHz, Methanol-d_4) δ 7.71 (d, J = 2.1 Hz, 1H), 7.38 (dd, J = 8.4, 2.1 Hz, 1H), 7.05 (d, J = 8.4 Hz, 1H), 6.83 (dd, J = 9.3, 2.0 Hz, 1H), 6.64 (ddd, J = 10.8, 10.1, 2.0 Hz, 1H), 6.33 (s, 1H), 3.96 (s, 1H), 3.64 – 3.48 (m, 1H), 3.42 – 3.34 (m, 1H). ^{19}F NMR (376 MHz, Methanol-d_4) δ -119.82 (td, $^{3}J_{HF}$ = 9.7, $^{4}J_{FF}$ = 3.8 Hz), -123.72 (dd, $^{3}J_{HF}$ = 10.7, $^{4}J_{FF}$ = 3.8). ^{13}C NMR (101 MHz, Methanol-d_4) δ 173.4, 161.0 (dd, $^{1}J_{CF}$ = 238.4, $^{3}J_{CF}$ = 11.8 Hz), 157.5 (dd, $^{1}J_{CF}$ = 247.2, $^{3}J_{CF}$ = 15.0 Hz), 140.2 (t, $^{3}J_{CF}$ = 14.4 Hz), 137.7, 137.2, 133.4, 131.1, 129.1, 128.8 (d, $^{4}J_{CF}$ =2.8 Hz), 112.8 (d, $^{2}J_{CF}$ =20.3 Hz), 108.0, 95.8 (dd, $^{2}J_{CF}$ =29.2, 23.4 Hz), 95.0 (dd, $^{2}J_{CF}$ =26.4, $^{4}J_{CF}$ =4.4 Hz), 54.9, 52.2, 25.1 (two Cl-bearing carbons in D ring are accidentally equivalent). HRMS (ESI) $[M+H]^+$ calculated for $C_{18}H_{13}Cl_2F_2N_2O_2^+$: 397.0317, found 397.0283.

m.p. decomp at 170 °C. $[\alpha]_D^{23}$ = -38.8 (c = 1.18, MeOH).

3.3 References for Chapter 3

1. Yao, Z. K.; Krai, P. M.; Merino, E. F.; Simpson, M. E.; Slebodnick, C.; Cassera, M. B.; Carlier, P. R., Determination of the active stereoisomer of the MEP pathway-targeting antimalarial agent MMV008138, and initial structure-activity studies. *Bioorg. Med. Chem. Lett.* **2015,** *25*, 1515-1519.

2. Hegarty, A. F.; Hegarty, C. N., Kinetics and mechanism of hydrolysis of amidinating agent, 1-(N1-benzoylamidino)-3,5-dimethylpyrazole. *Journal of the Chemical Society-Perkin Transactions 2* **1973**, 2054-2060.

3. El-Faham, A.; Albericio, F., Peptide Coupling Reagents, More than a Letter Soup. *Chem. Rev.* **2011,** *111*, 6557-6602.

4. Duncia, J. V.; Pierce, M. E.; Santella, J. B., 3 Synthetic routes to a sterically hindered tetrazole - a new one-step mild conversion of an amide into a tetrazole. *J. Org. Chem.* **1991,** *56*, 2395-2400.

5. Yokoyama, Y.; Hikawa, H.; Mitsuhashi, M.; Uyama, A.; Hiroki, Y.; Murakami, Y., Total synthesis without protection: Three-step synthesis of optically active clavicipitic acids by a biomimetic route. *Eur. J. Org. Chem.* **2004**, 1244-1253.

6. Yokoyama, Y.; Nakakoshi, M.; Okuno, H.; Sakamoto, Y.; Sakurai, S., Mechanism for the direct synthesis of tryptophan from indole and serine: a useful NMR technique for the detection of a reactive intermediate in the reaction mixture. *Magn. Reson. Chem.* **2010,** *48*, 811-817.

7. Lu, X.; Yi, J.; Zhang, Z. Q.; Dai, J. J.; Liu, J. H.; Xiao, B.; Fu, Y.; Liu, L., Expedient Synthesis of Chiral alpha-Amino Acids through Nickel-Catalyzed Reductive Cross-Coupling. *Chem.-Eur. J.* **2014,** *20*, 15339-15343.

8. Dandapani, S.; Lan, P.; Beeler, A. B.; Beischel, S.; Abbas, A.; Roth, B. L.; Porco, J. A., Jr.; Panek, J. S., Convergent synthesis of complex diketopiperazines derived from pipecolic acid scaffolds and parallel screening against GPCR targets. *J. Org. Chem.* **2006,** *71*, 8934-8945.

9. Ridge, D. N.; Hanifin, J. W.; Harten, L. A.; Johnson, B. D.; Menschik, J.; Nicolau, G.; Sloboda, A. E.; Watts, D. E., Potential anti-arthritic agents .2. benzoylacetonitriles and beta-aminocinnamonitriles. *J. Med. Chem.* **1979,** *22*, 1385-1389.

10. Fong, H. K. H.; Brunel, J. M.; Longeon, A.; Bourguet-Kondracki, M.-L.; Barker, D.; Copp, B. R., Synthesis and biological evaluation of the ascidian blood-pigment halocyamine A. *Org. Biomol. Chem.* **2017**, 15, 6194-6204.

11. Merkul, E.; Klukas, F.; Dorsch, D.; Graedler, U.; Greiner, H. E.; Mueller, T. J. J., Rapid preparation of triazolyl substituted NH-heterocyclic kinase inhibitors via one-pot Sonogashira coupling-TMS-deprotection-CuAAC sequence. *Org. Biomol. Chem.* **2011**, 9, 5129-5136.

12. Lefoix, M.; Daillant, J. P.; Routier, S.; Merour, J. Y.; Gillaizeau, I.; Coudert, G., Versatile and convenient methods for the synthesis of C-2 and C-3 functionalised 5-azaindoles. *Synthesis-Stuttgart* **2005**, 3581-3588.

Appendix:

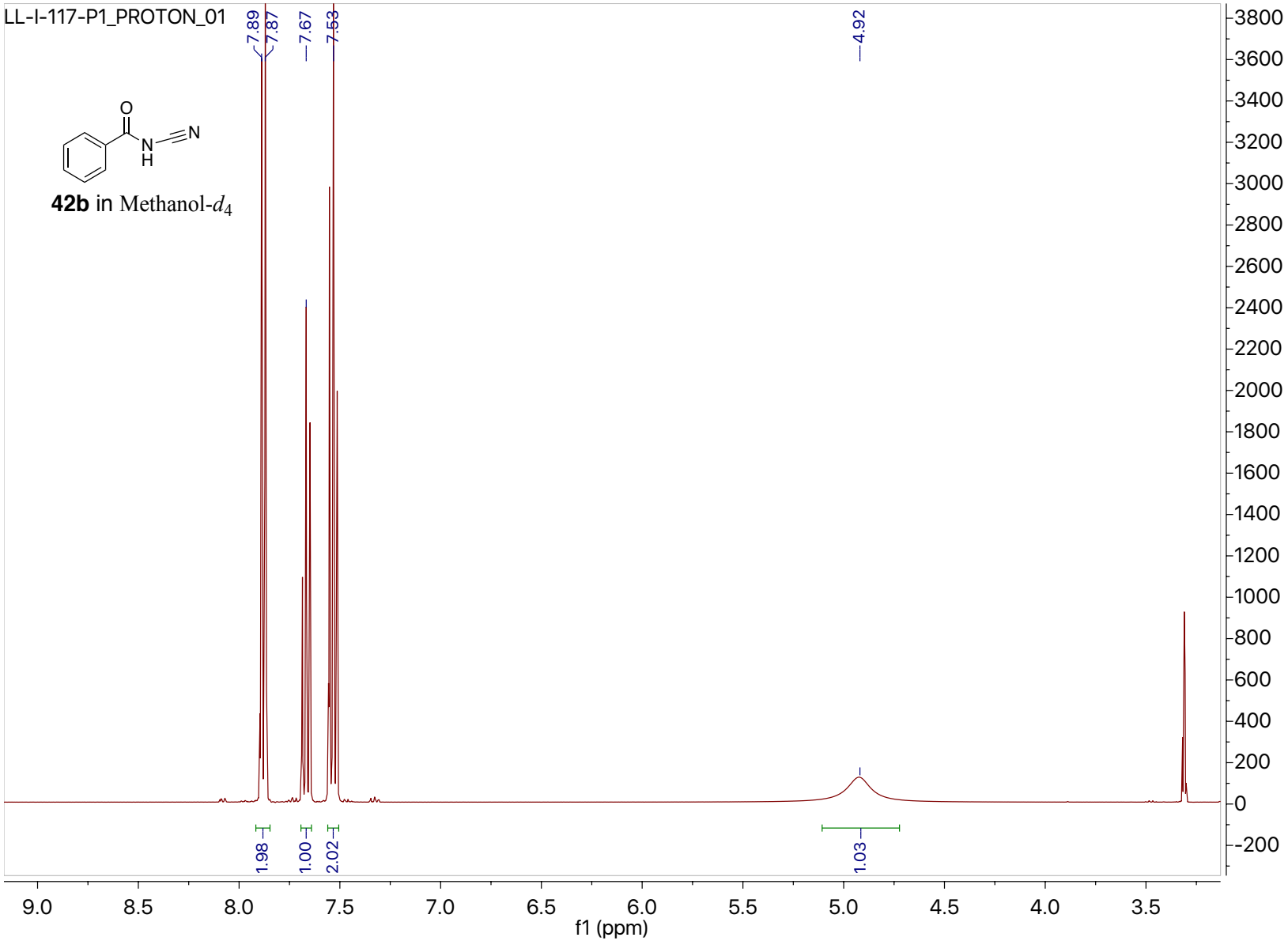
LL-I-117-P1_PROTON_01
7.89
7.87
7.67
7.53
4.92
O
N
H
N
42b in Methanol-d_4
1.98
1.00
2.02
1.03
9.0
8.5
8.0
7.5
7.0
6.5
6.0
5.5
5.0
4.5
4.0
3.5
f1 (ppm)
3800
3600
3400
3200
3000
2800
2600
2400
2200
2000
1800
1600
1400
1200
1000
800
600
400
200
0
-200

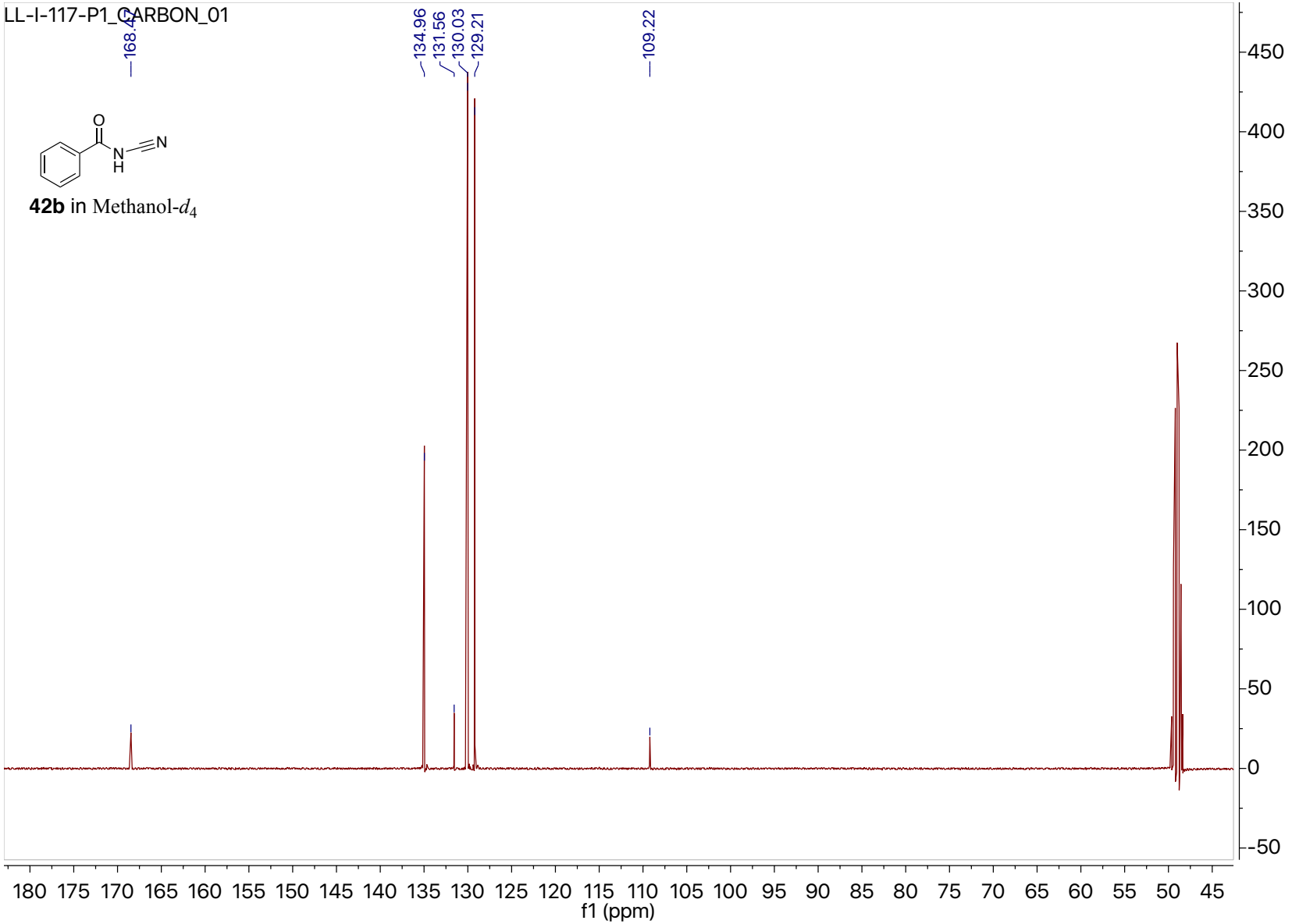
LL-I-117-P1_CARBON_01
168.42
134.96
131.56
130.03
129.21
109.22
O
N
N
H
42b in Methanol-d_4
450
400
350
300
250
200
150
100
50
0
-50
180 175 170 165 160 155 150 145 140 135 130 125 120 115 110 105 100 95 90 85 80 75 70 65 60 55 50 45
f1 (ppm)

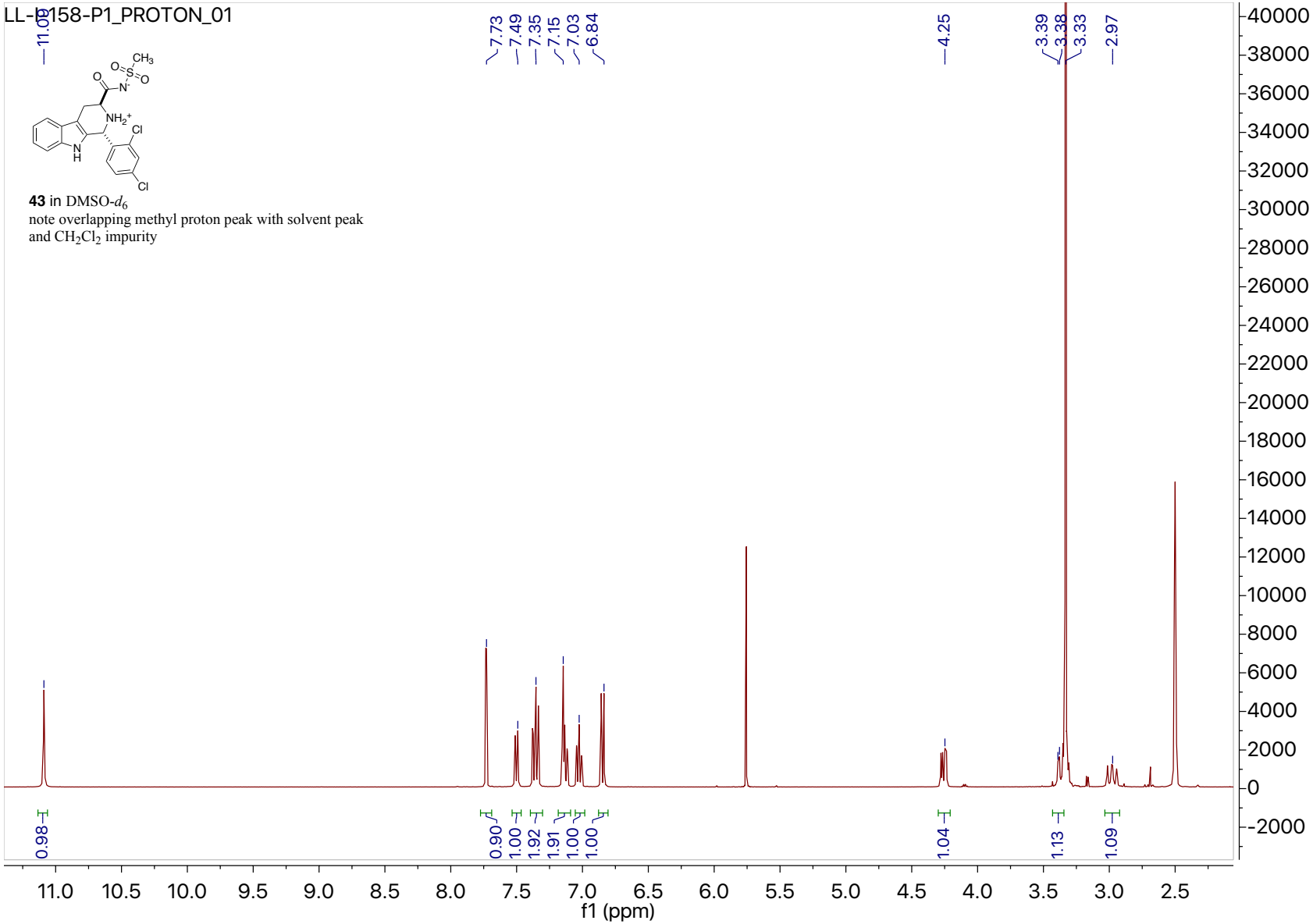

43 in DMSO-d_6
note overlapping methyl proton peak with solvent peak
and CH_2Cl_2 impurity

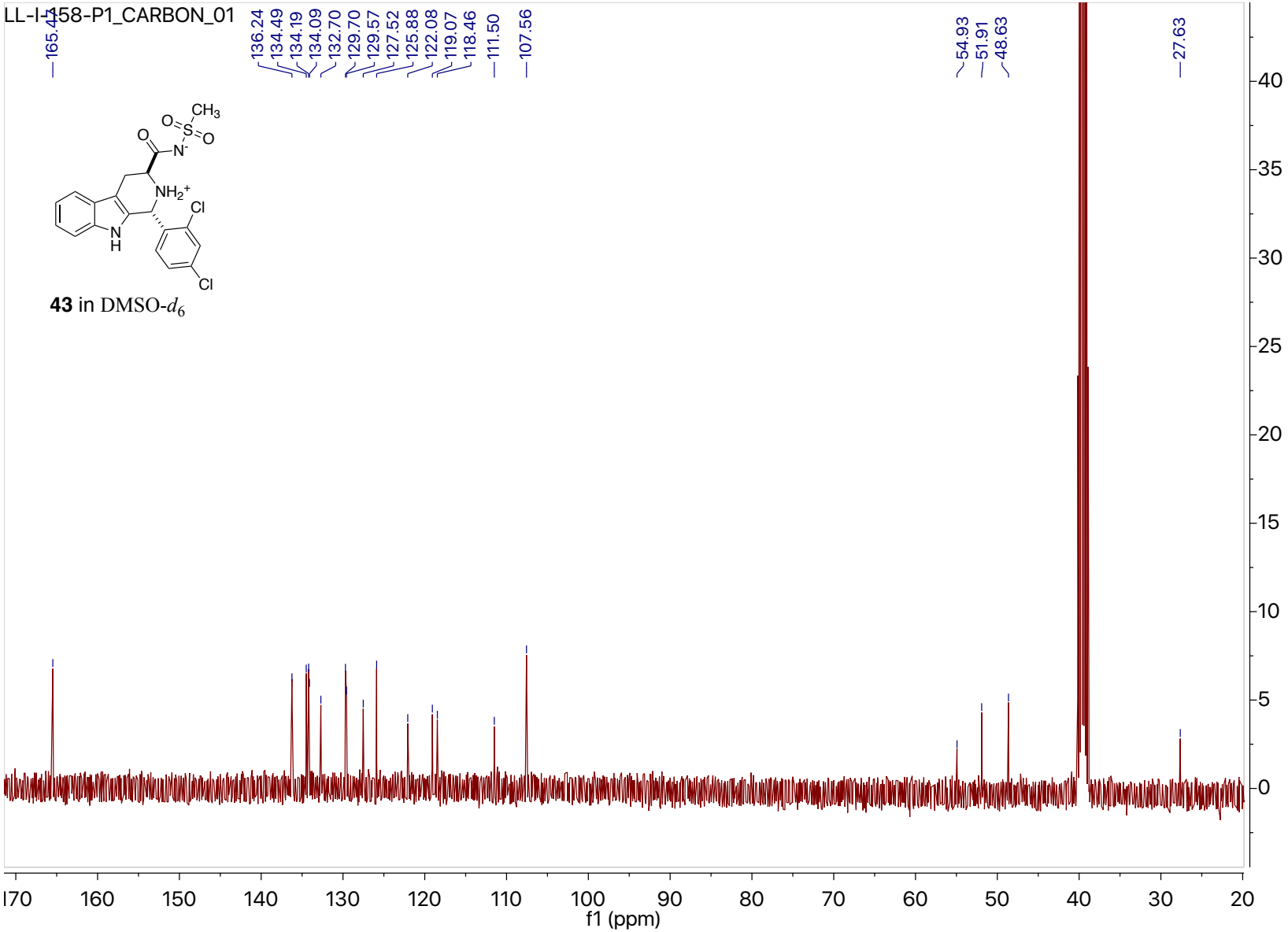
LL-I-158-P1_CARBON_01
165.42
136.24
134.49
134.19
134.09
132.70
129.70
129.57
127.52
125.88
122.08
119.07
118.46
111.50
107.56
54.93
51.91
48.63
27.63
CH3
O
S
O
O
N
NH2+
Cl
N
H
Cl
43 in DMSO-d6
40
35
30
25
20
15
10
5
0
170
160
150
140
130
120
110
100
90
80
70
60
50
40
30
20
f1 (ppm)

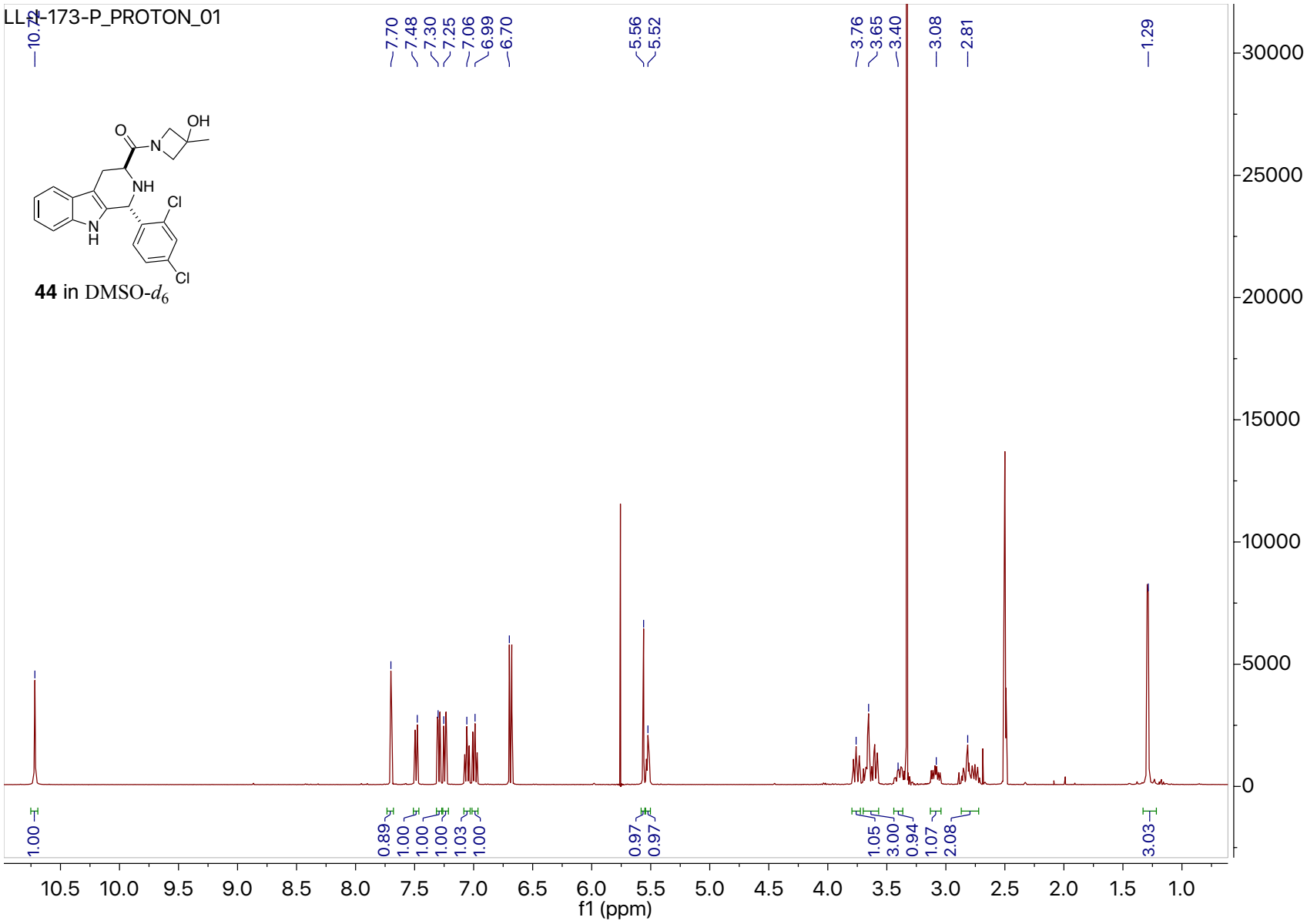
LL-I-173-P_PROTON_01
10.72
7.70
7.48
7.30
7.25
7.06
6.99
6.70
5.56
5.52
3.76
3.65
3.40
3.08
2.81
1.29
OH
O
N
NH
N
H
Cl
Cl
44 in DMSO-d6
30000
25000
20000
15000
10000
5000
0
1.00
0.89
1.00
1.00
1.00
1.03
1.00
0.97
0.97
1.05
3.00
0.94
1.07
2.08
3.03
10.5 10.0 9.5 9.0 8.5 8.0 7.5 7.0 6.5 6.0 5.5 5.0 4.5 4.0 3.5 3.0 2.5 2.0 1.5 1.0
f1 (ppm)

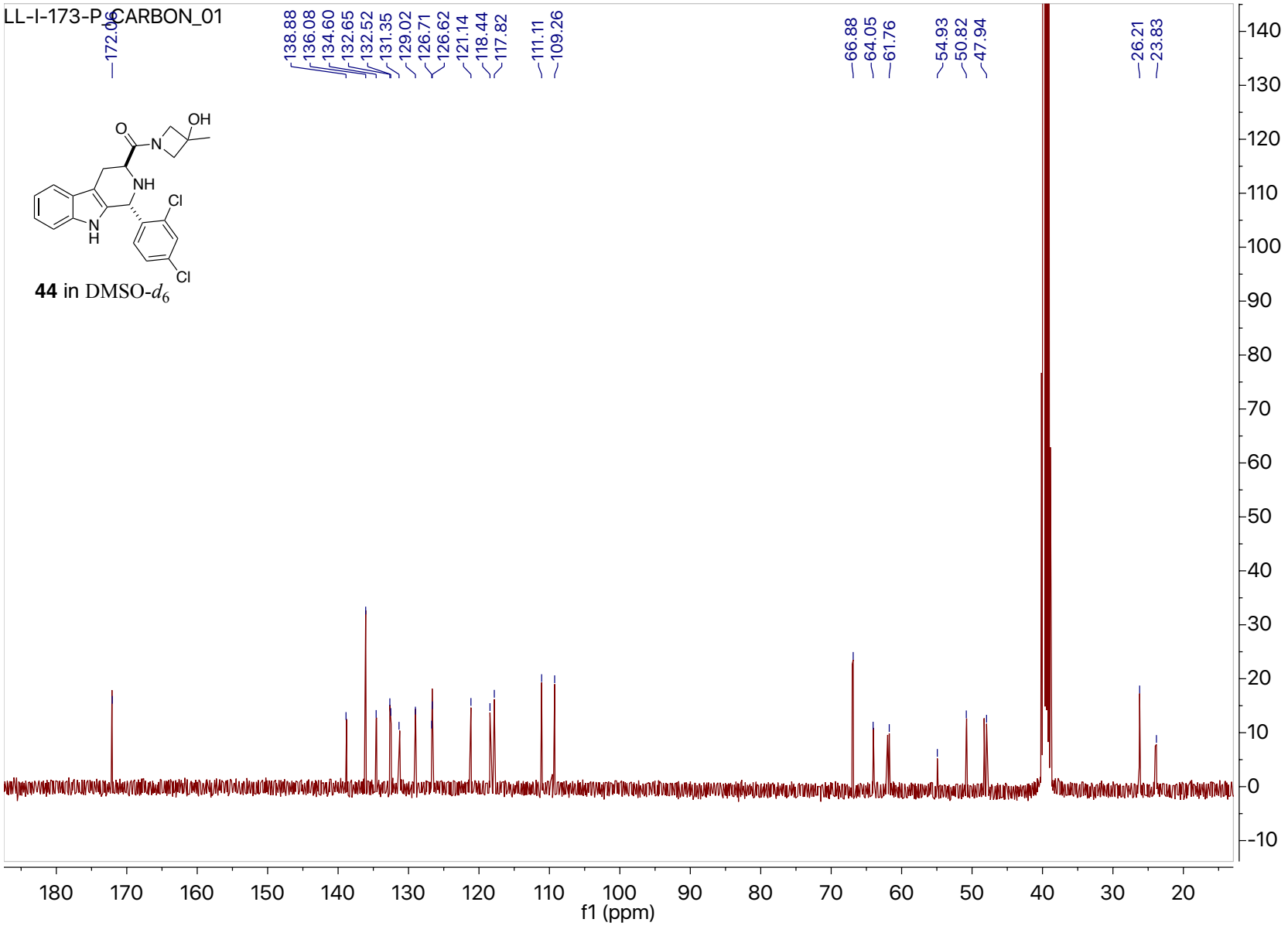
LL-I-173-P CARBON_01
172.06
138.88
136.08
134.60
132.65
132.52
131.35
129.02
126.71
126.62
121.14
118.44
117.82
111.11
109.26
66.88
64.05
61.76
54.93
50.82
47.94
26.21
23.83
OH
O
N
NH
N
H
Cl
Cl
44 in DMSO-d6
f1 (ppm)

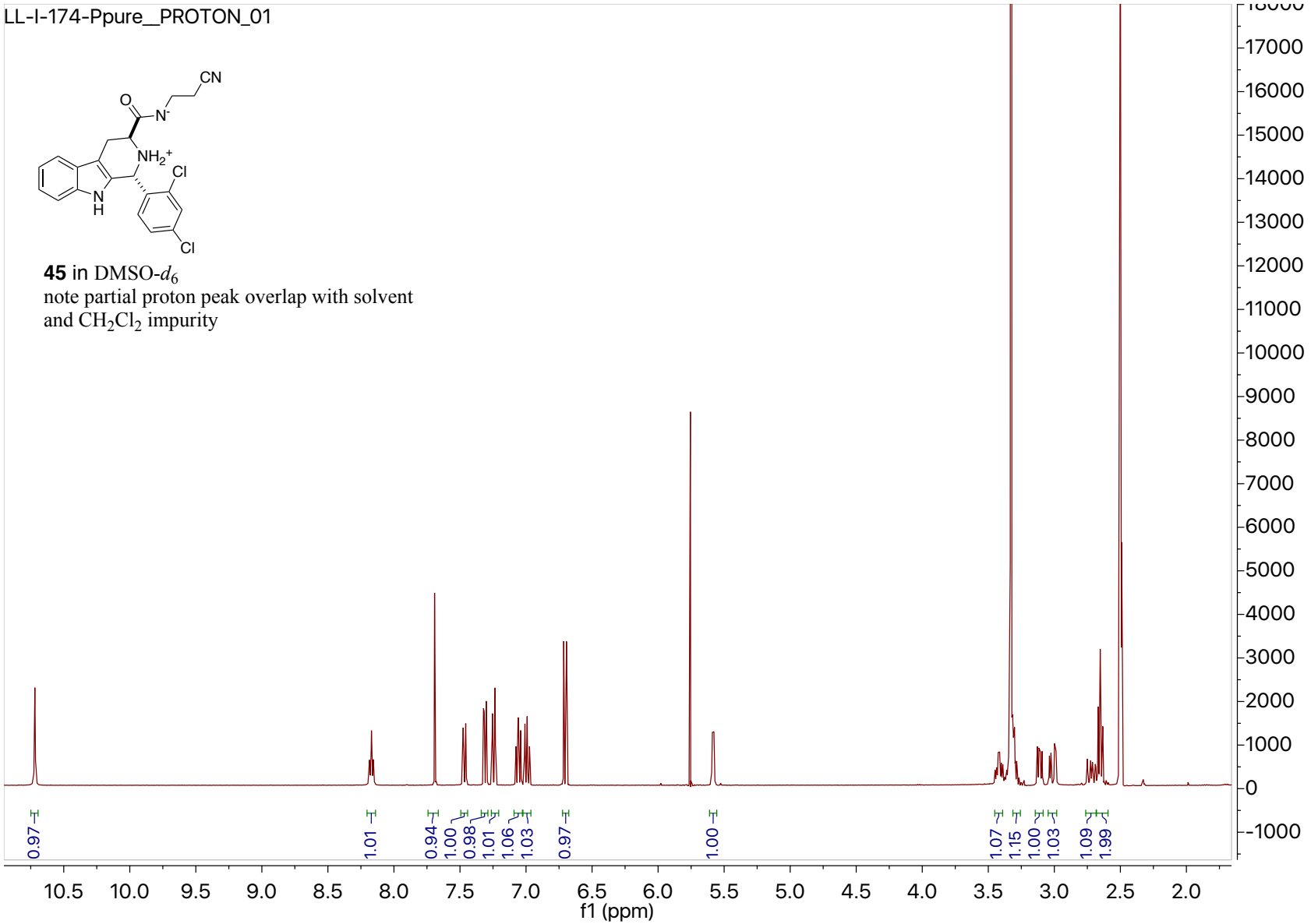
LL-I-174-Ppure__PROTON_01
CN
O
N
NH2+
Cl
N
H
Cl
45 in DMSO-d6
note partial proton peak overlap with solvent
and CH2Cl2 impurity
17000
16000
15000
14000
13000
12000
11000
10000
9000
8000
7000
6000
5000
4000
3000
2000
1000
0
-1000
0.97
1.01
0.94
1.00
0.98
1.01
1.06
1.03
0.97
1.00
1.07
1.15
1.00
1.03
1.09
1.99
10.5
10.0
9.5
9.0
8.5
8.0
7.5
7.0
6.5
6.0
5.5
5.0
4.5
4.0
3.5
3.0
2.5
2.0
f1 (ppm)

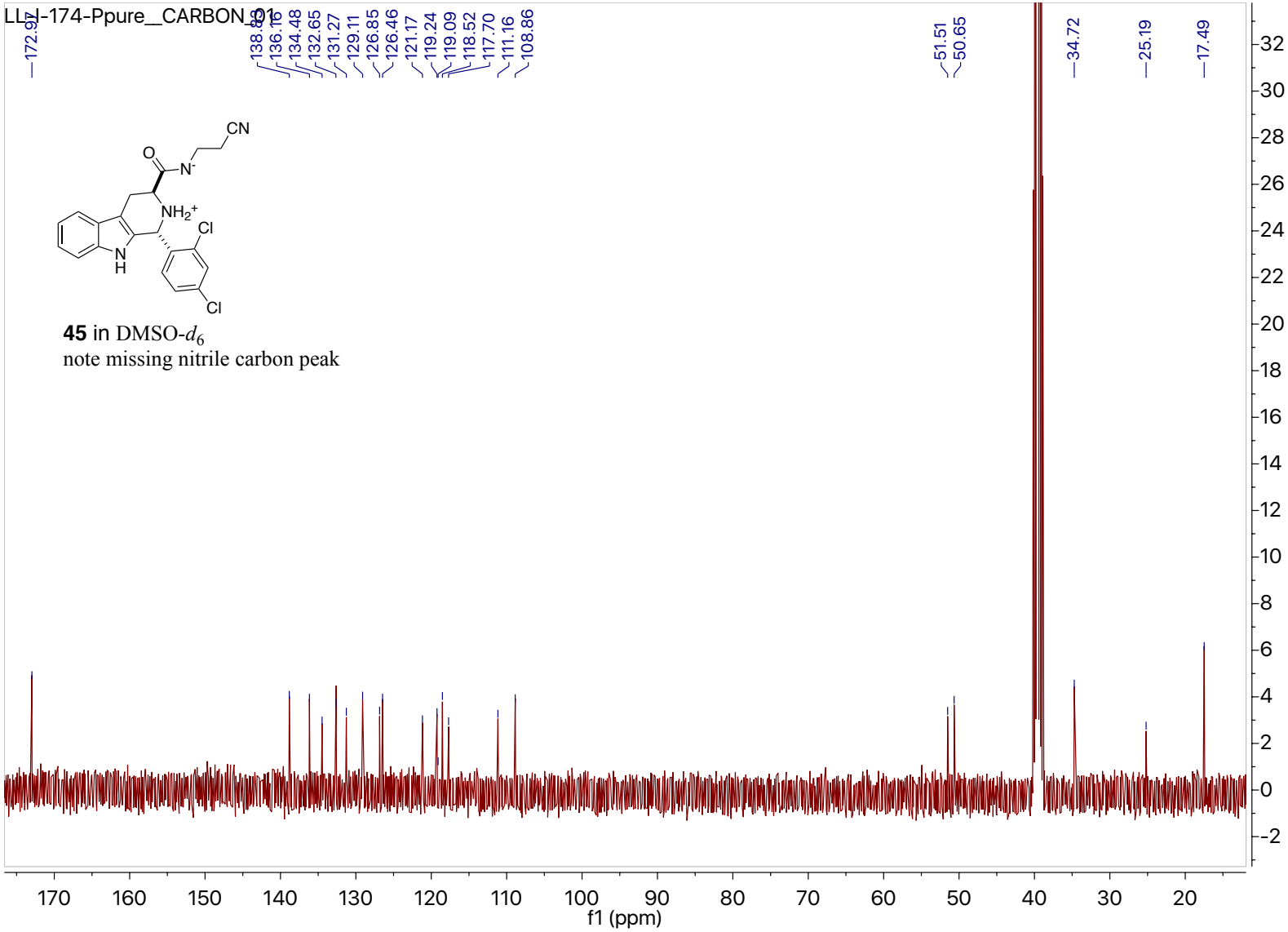

45 in DMSO-d_6
note missing nitrile carbon peak

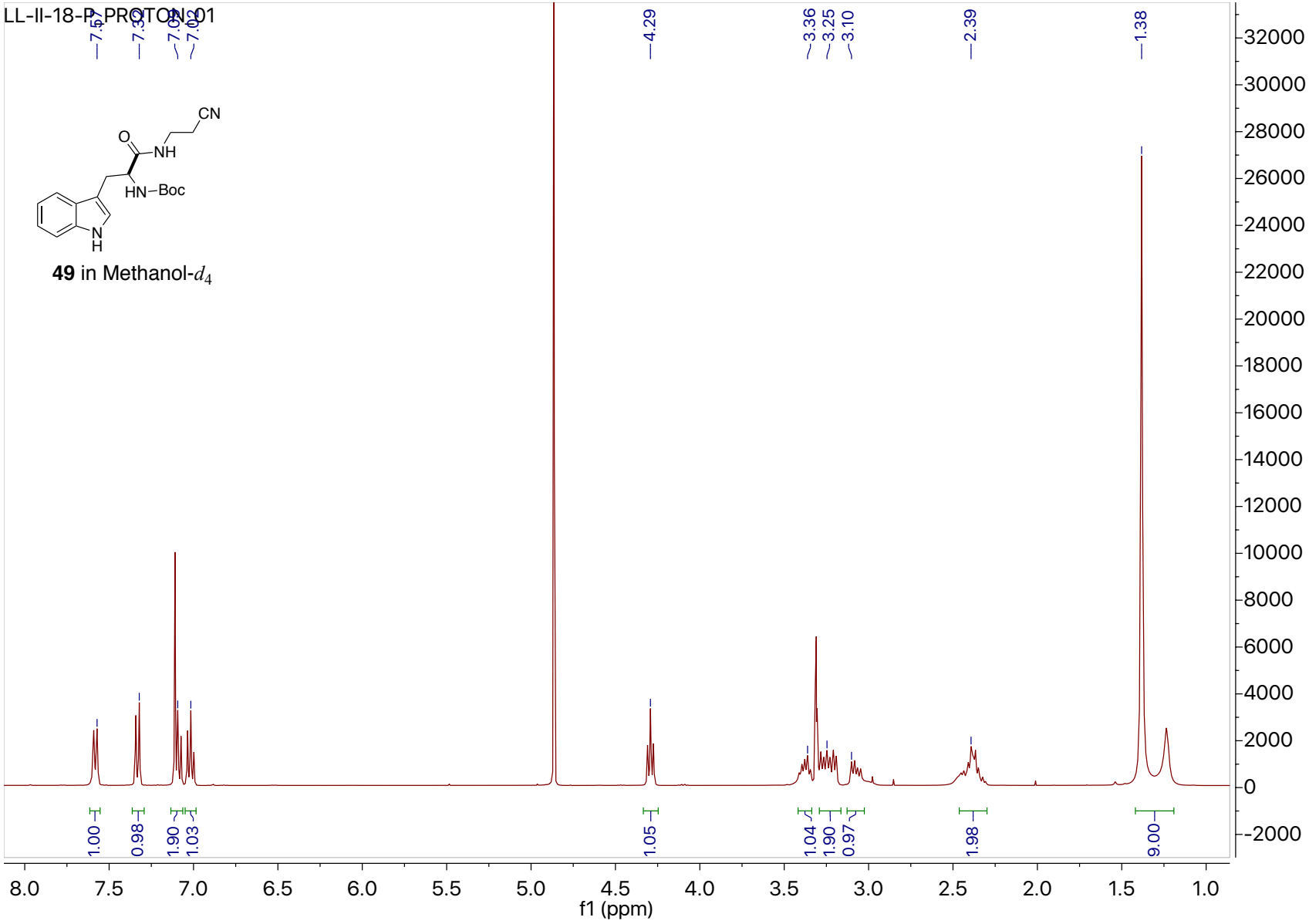
LL-II-18-P PROTON-01
7.57
7.33
7.09
7.02
4.29
3.36
3.25
3.10
2.39
1.38
CN
O
NH
HN–Boc
N
H
49 in Methanol-d_4
1.00
0.98
1.90
1.03
1.05
1.04
1.90
0.97
1.98
9.00
32000
30000
28000
26000
24000
22000
20000
18000
16000
14000
12000
10000
8000
6000
4000
2000
0
-2000
8.0
7.5
7.0
6.5
6.0
5.5
5.0
4.5
4.0
3.5
3.0
2.5
2.0
1.5
1.0
f1 (ppm)

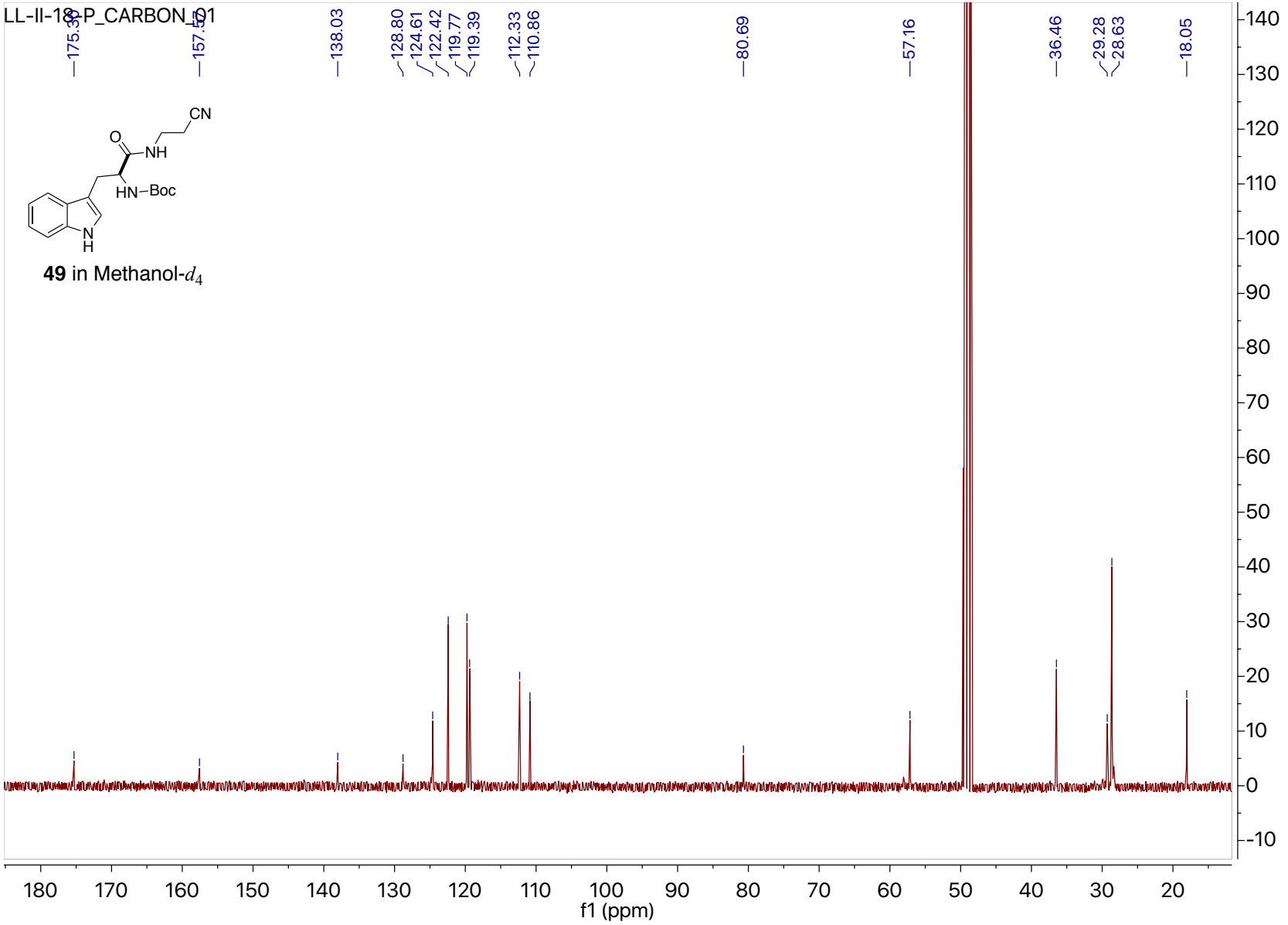
LL-II-18-P_CARBON_01
175.30
157.55
138.03
128.80
124.61
122.42
119.77
119.39
112.33
110.86
80.69
57.16
36.46
29.28
28.63
18.05
CN
O
NH
HN–Boc
N
H
49 in Methanol-d_4
f1 (ppm)

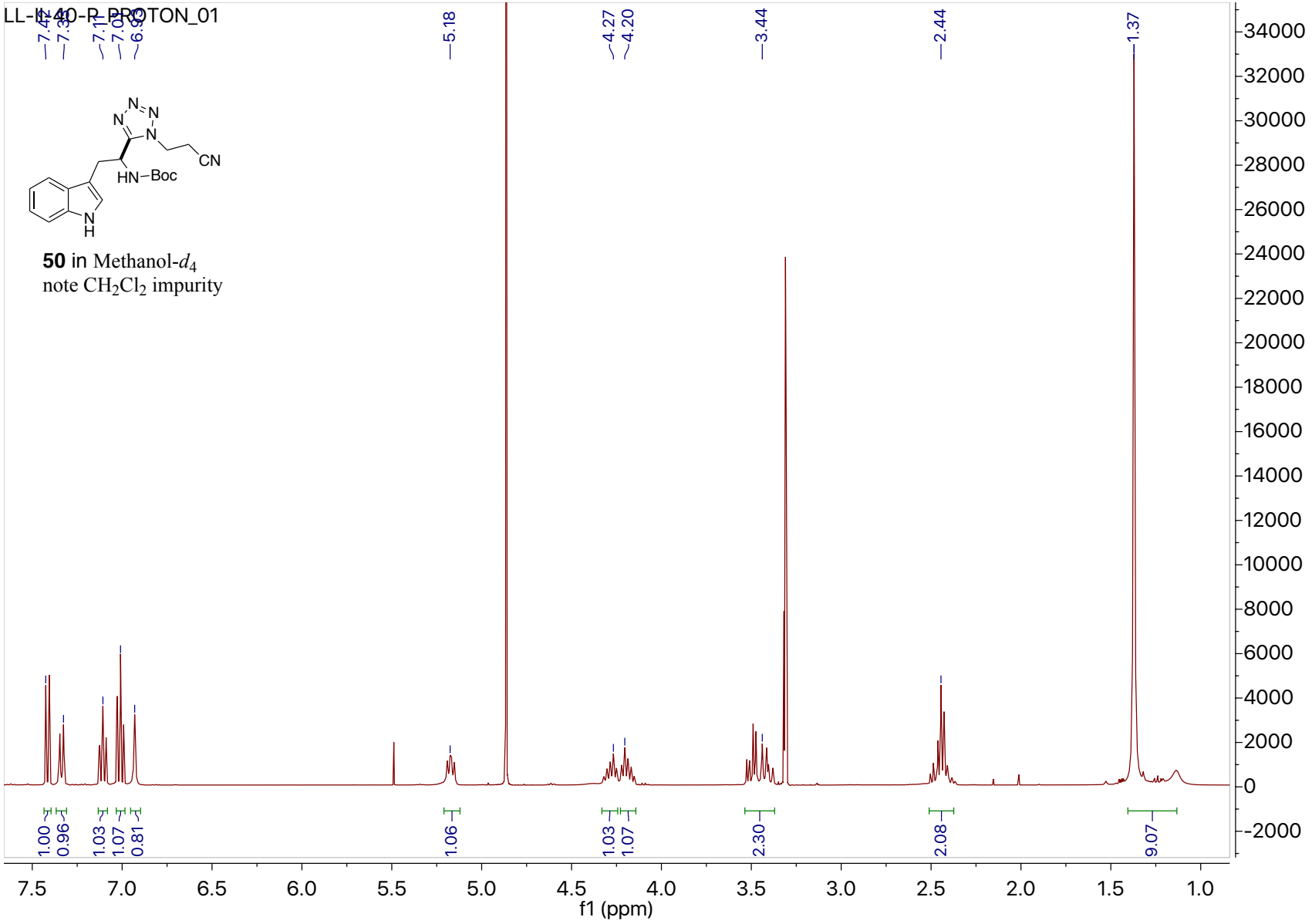
LL-IL40-P_PROTON_01
7.42
7.39
7.11
7.09
6.97
5.18
4.27
4.20
3.44
2.44
1.37
HN–Boc
CN
N
H
50 in Methanol-d4
note CH2Cl2 impurity
1.00
0.96
1.03
1.07
0.81
1.06
1.03
1.07
2.30
2.08
9.07
f1 (ppm)

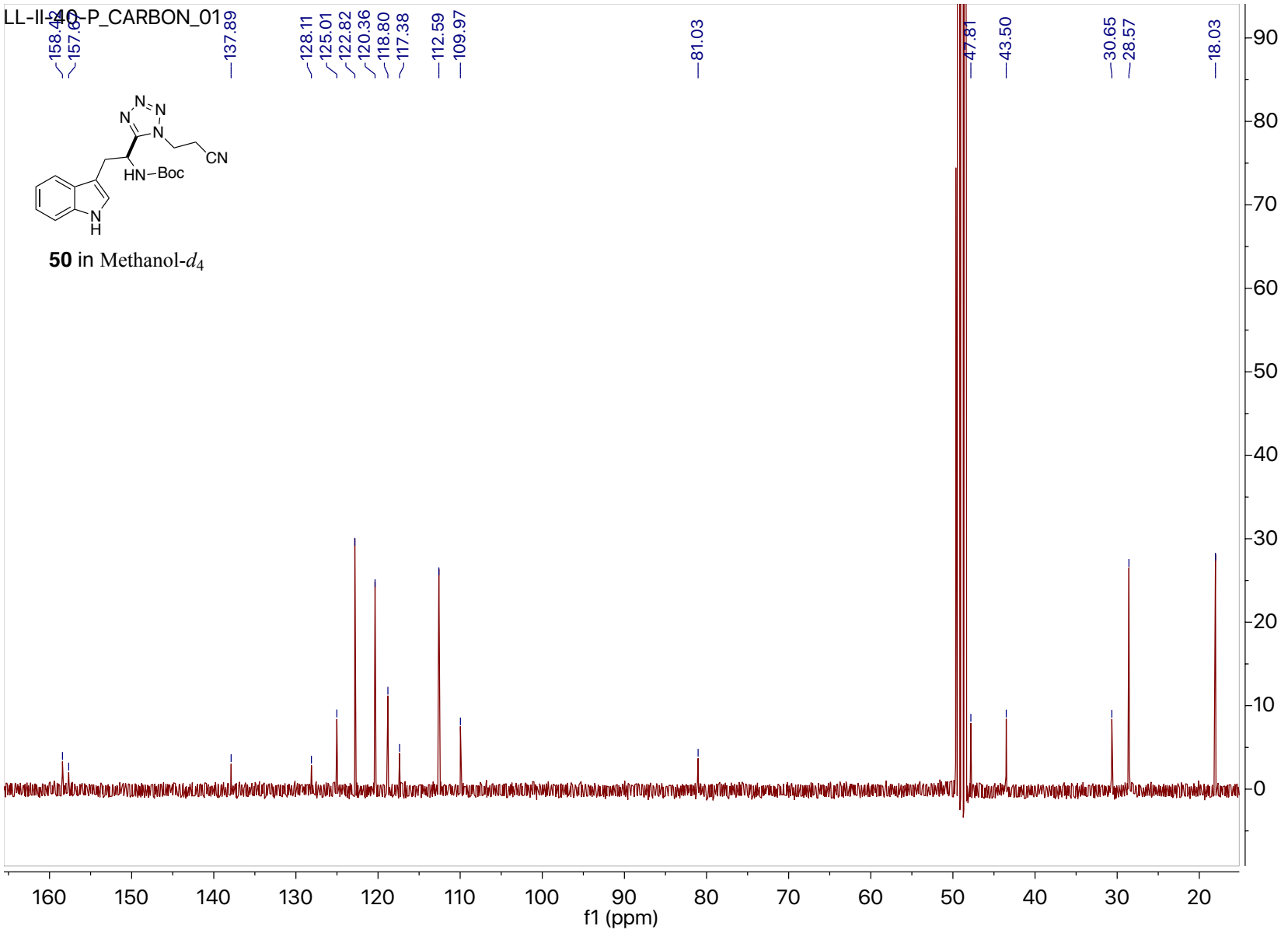

50 in Methanol-d_4

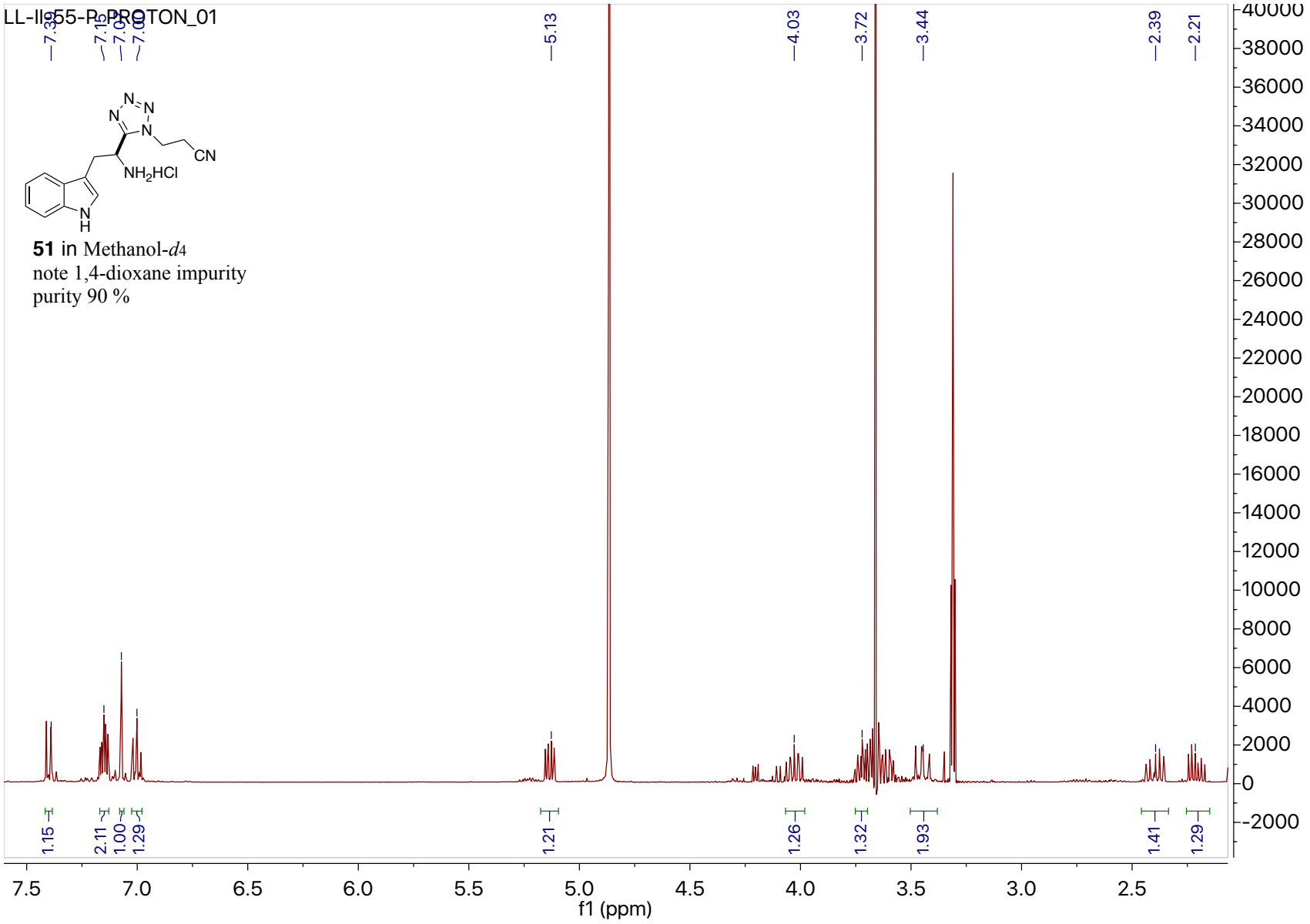
LL-II-55-P-PROTON_01
7.39
7.15
7.03
7.00
5.13
4.03
3.72
3.44
2.39
2.21
N
N
N
N
CN
NH2HCl
N
H
51 in Methanol-d4
note 1,4-dioxane impurity
purity 90 %
1.15
2.11
1.00
1.29
1.21
1.26
1.32
1.93
1.41
1.29
40000
38000
36000
34000
32000
30000
28000
26000
24000
22000
20000
18000
16000
14000
12000
10000
8000
6000
4000
2000
0
-2000
7.5
7.0
6.5
6.0
5.5
5.0
4.5
4.0
3.5
3.0
2.5
f1 (ppm)

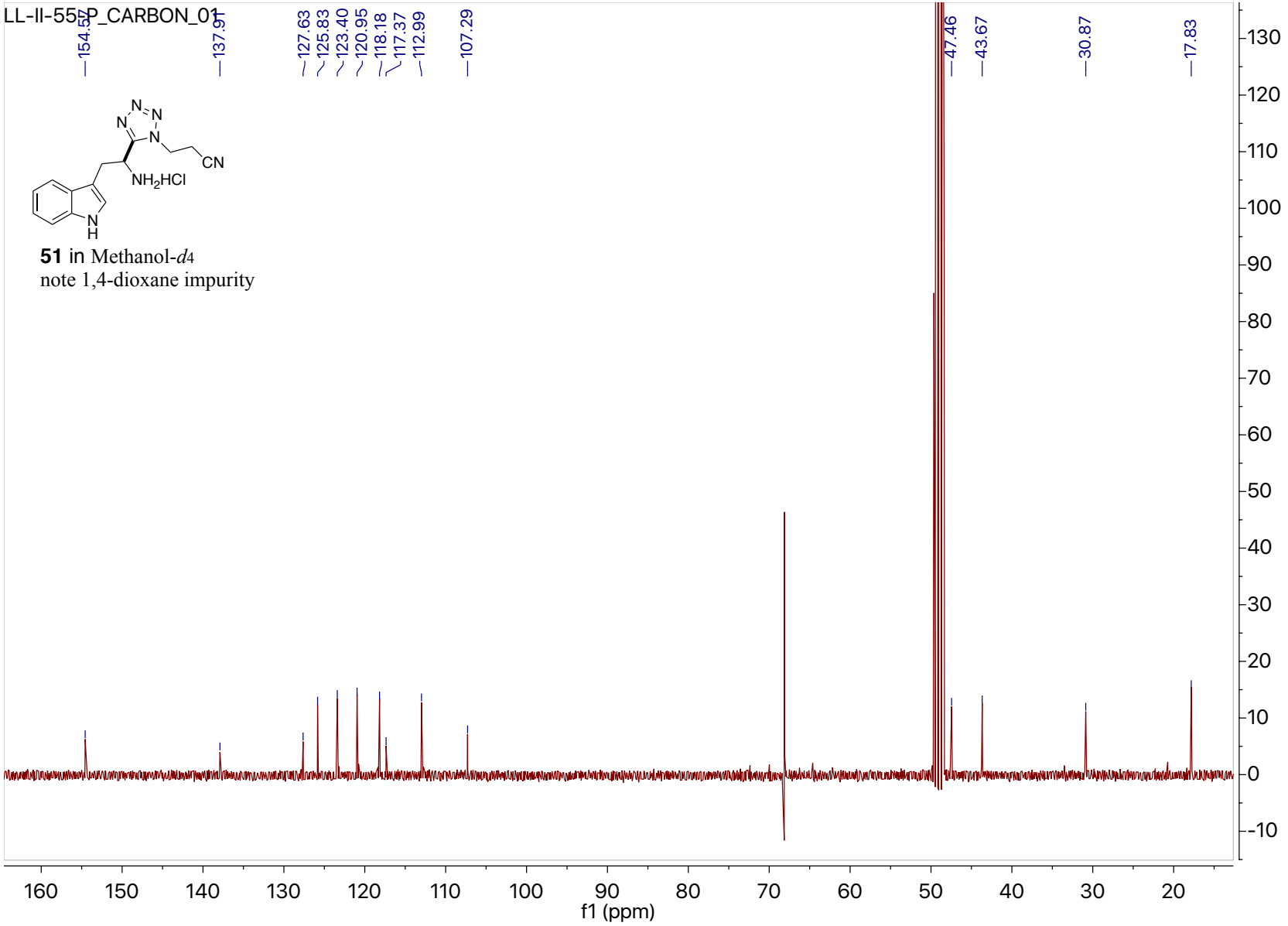
LL-II-55-P_CARBON_01
154.57
137.91
127.63
125.83
123.40
120.95
118.18
117.37
112.99
107.29
47.46
43.67
30.87
17.83
CN
NH2HCl
51 in Methanol-d4
note 1,4-dioxane impurity
f1 (ppm)

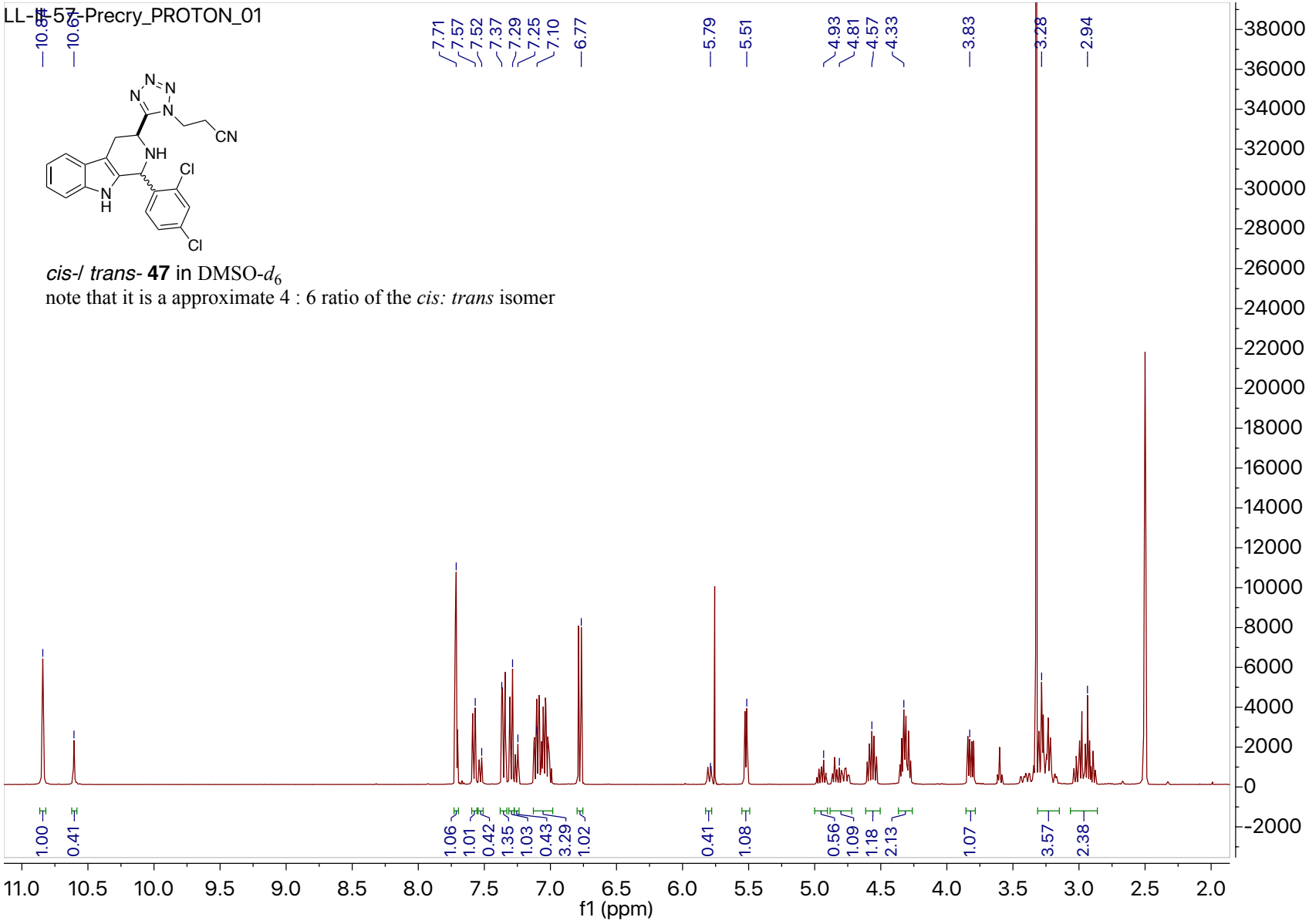
LL-#-57-Precry_PROTON_01
10.87
10.67
7.71
7.57
7.52
7.37
7.29
7.25
7.10
6.77
5.79
5.51
4.93
4.81
4.57
4.33
3.83
3.28
2.94
N
N
N
N
CN
NH
Cl
N
H
Cl
cis-/ trans- 47 in DMSO-d6
note that it is a approximate 4 : 6 ratio of the cis: trans isomer
1.00
0.41
1.06
1.01
0.42
1.35
1.03
0.43
3.29
1.02
0.41
1.08
0.56
1.09
1.18
2.13
1.07
3.57
2.38
38000
36000
34000
32000
30000
28000
26000
24000
22000
20000
18000
16000
14000
12000
10000
8000
6000
4000
2000
0
-2000
11.0
10.5
10.0
9.5
9.0
8.5
8.0
7.5
7.0
6.5
6.0
5.5
5.0
4.5
4.0
3.5
3.0
2.5
2.0
f1 (ppm)

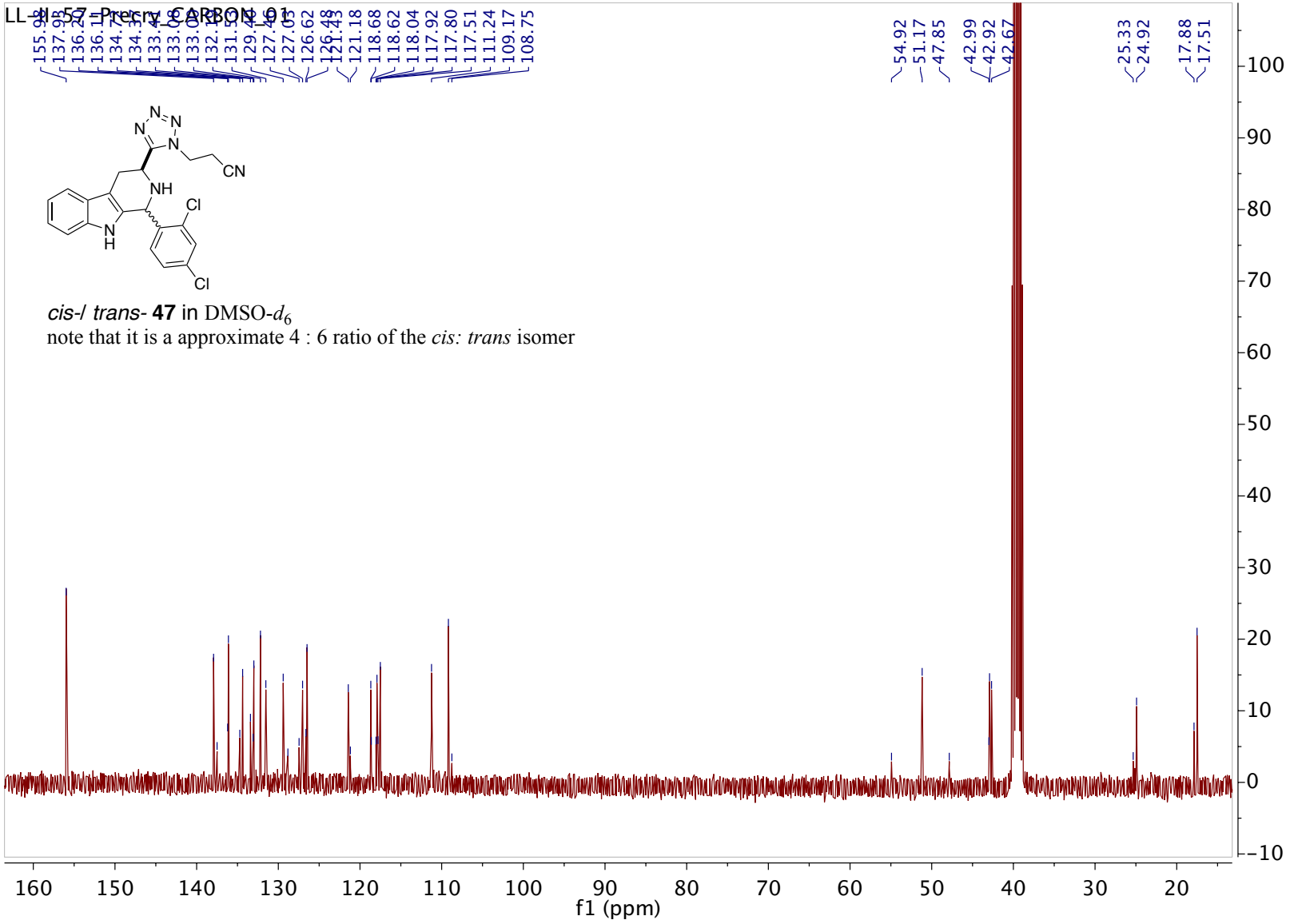

cis-/ trans- **47** in DMSO-d_6
note that it is a approximate 4 : 6 ratio of the *cis: trans* isomer

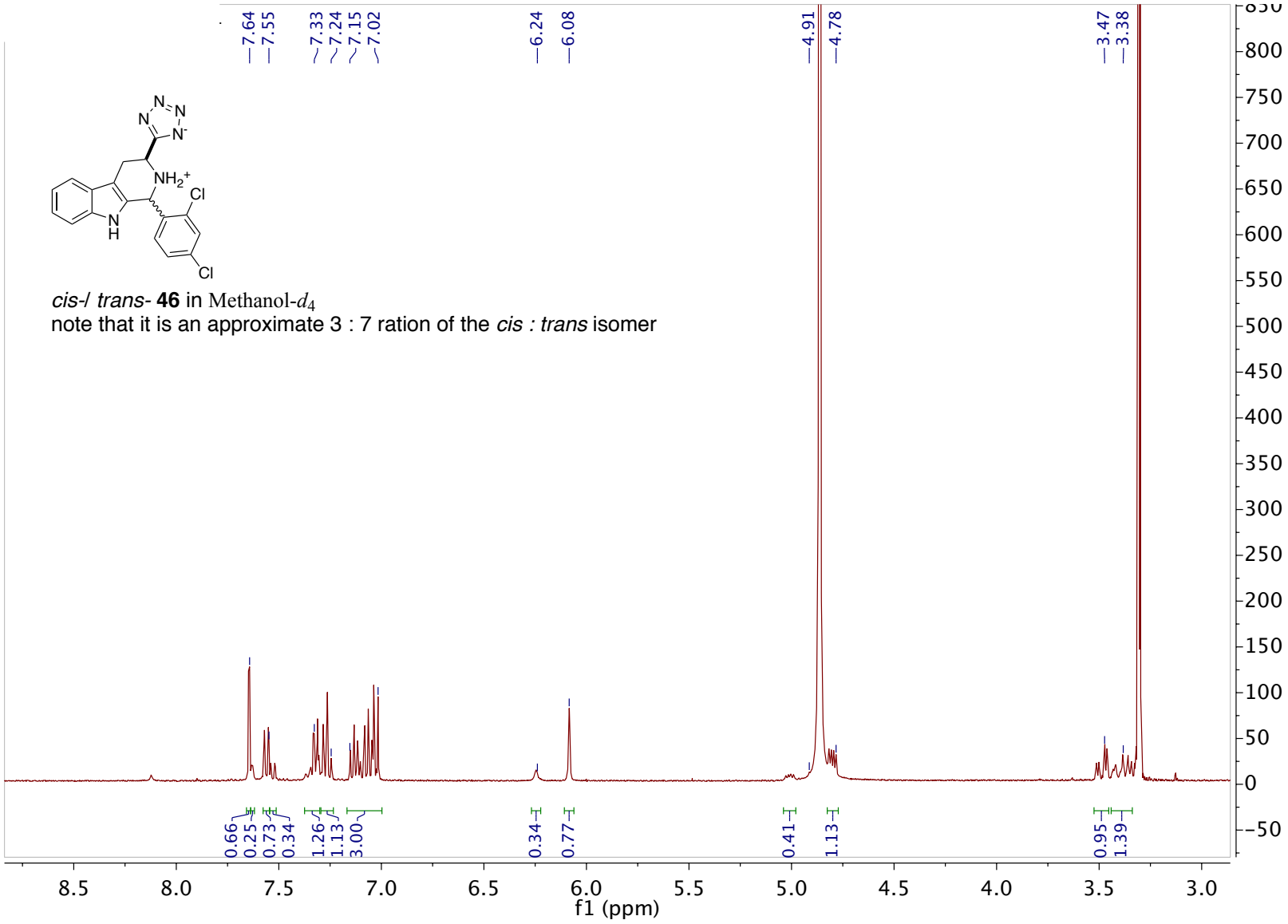

cis-/ *trans-* **46** in Methanol-d_4
note that it is an approximate 3 : 7 ration of the *cis : trans* isomer

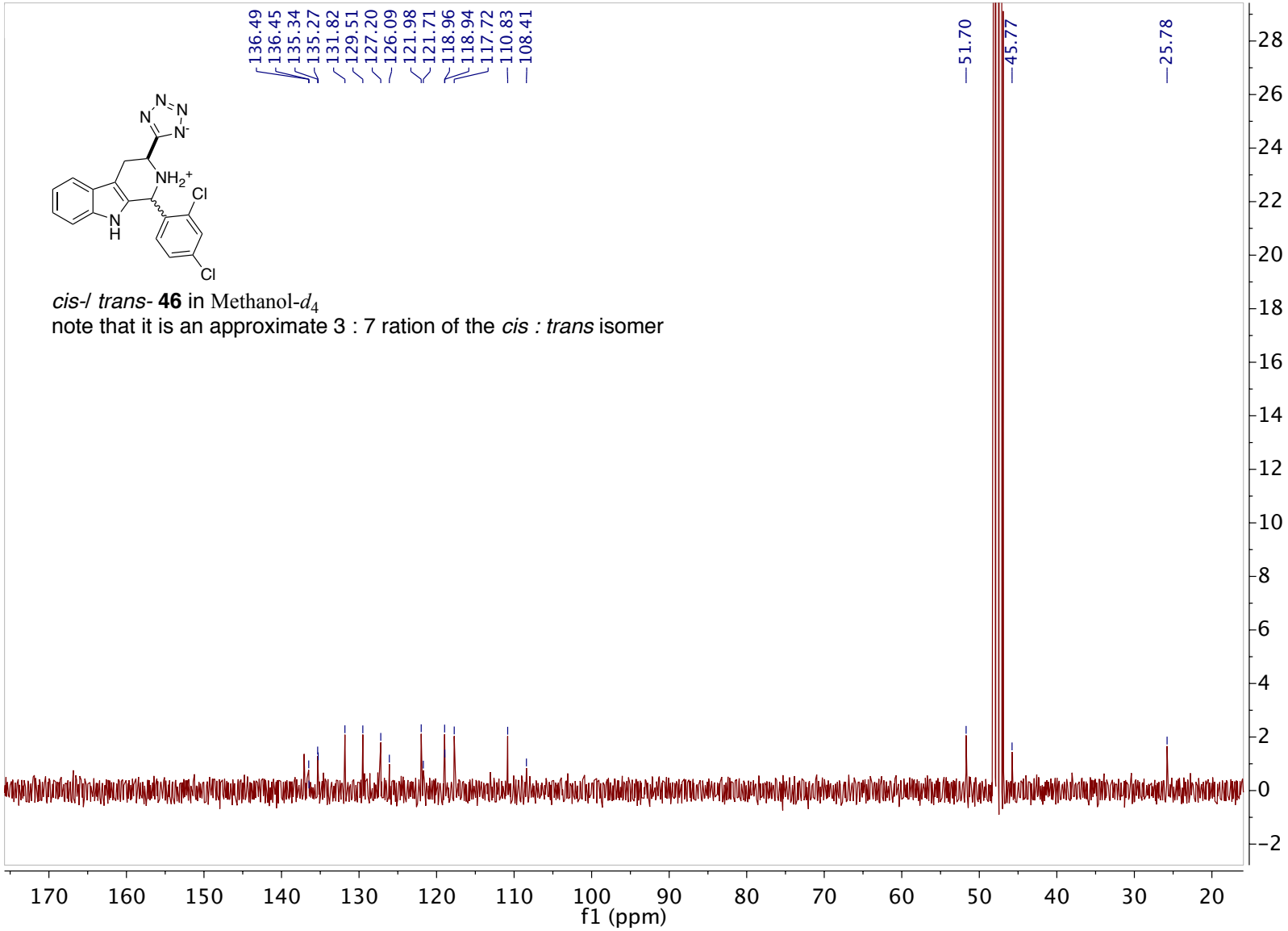

cis-/ *trans-* **46** in Methanol-d_4
note that it is an approximate 3 : 7 ration of the *cis : trans* isomer

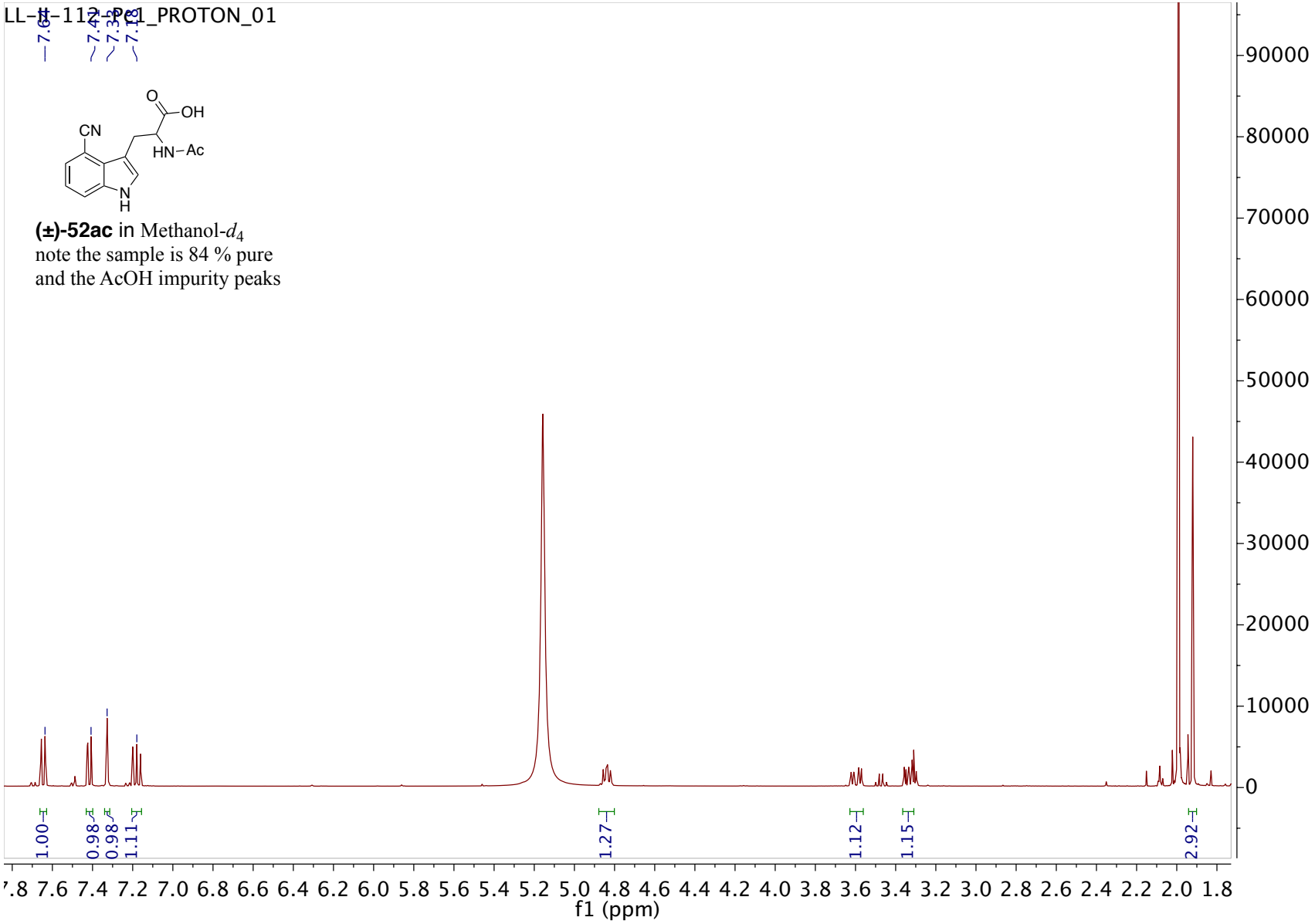
LL-II-112-PC1_PROTON_01
7.6
7.4
7.3
7.1
O
OH
CN
HN–Ac
N
H
(±)-52ac in Methanol-d4
note the sample is 84 % pure
and the AcOH impurity peaks
90000
80000
70000
60000
50000
40000
30000
20000
10000
0
1.00
0.98
0.98
1.11
1.27
1.12
1.15
2.92
7.8 7.6 7.4 7.2 7.0 6.8 6.6 6.4 6.2 6.0 5.8 5.6 5.4 5.2 5.0 4.8 4.6 4.4 4.2 4.0 3.8 3.6 3.4 3.2 3.0 2.8 2.6 2.4 2.2 2.0 1.8
f1 (ppm)

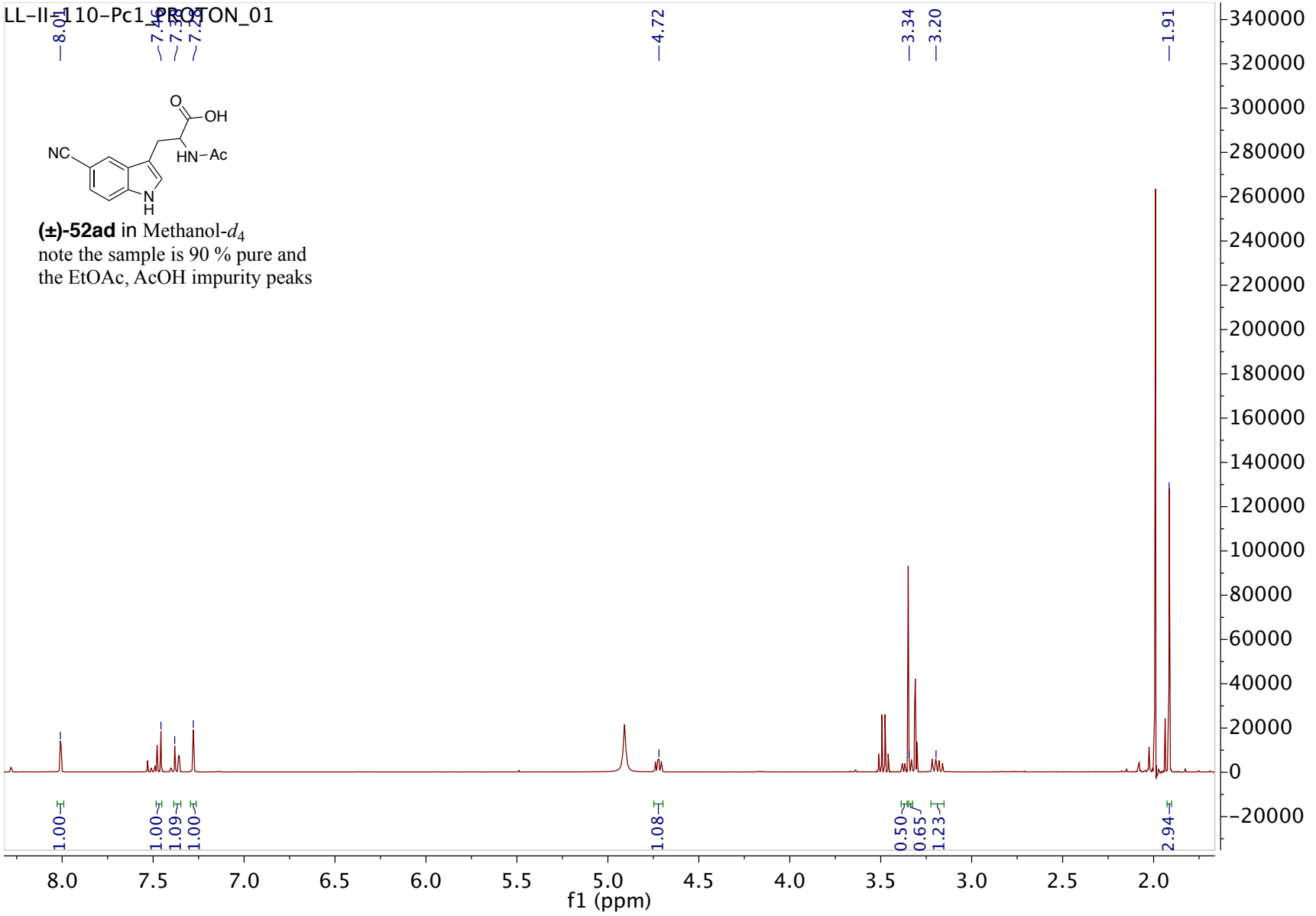
LL-II-110-Pc1_PROTON_01
8.01
7.46
7.33
7.27
4.72
3.34
3.20
1.91
O
OH
NC
HN–Ac
N
H
(±)-52ad in Methanol-d4
note the sample is 90 % pure and
the EtOAc, AcOH impurity peaks
1.00
1.00
1.09
1.00
1.08
0.50
0.65
1.23
2.94
340000
320000
300000
280000
260000
240000
220000
200000
180000
160000
140000
120000
100000
80000
60000
40000
20000
0
-20000
8.0
7.5
7.0
6.5
6.0
5.5
5.0
4.5
4.0
3.5
3.0
2.5
2.0
f1 (ppm)

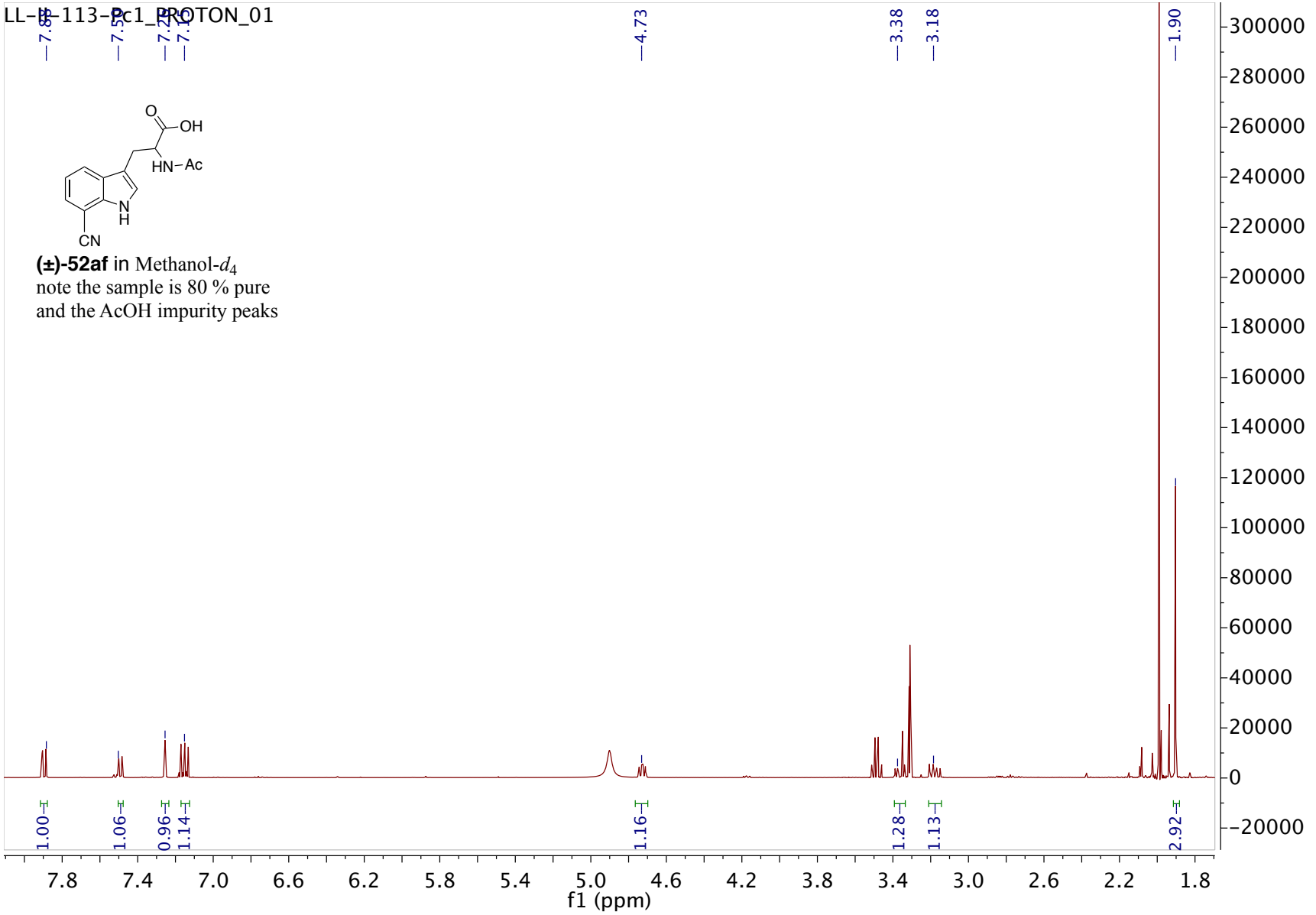
LL-II-113-Pc1_PROTON_01
7.88
7.55
7.24
7.17
4.73
3.38
3.18
1.90
O
OH
HN–Ac
N
H
CN
(±)-52af in Methanol-d4
note the sample is 80 % pure
and the AcOH impurity peaks
1.00
1.06
0.96
1.14
1.16
1.28
1.13
2.92
300000
280000
260000
240000
220000
200000
180000
160000
140000
120000
100000
80000
60000
40000
20000
0
-20000
7.8
7.4
7.0
6.6
6.2
5.8
5.4
5.0
4.6
4.2
3.8
3.4
3.0
2.6
2.2
1.8
f1 (ppm)

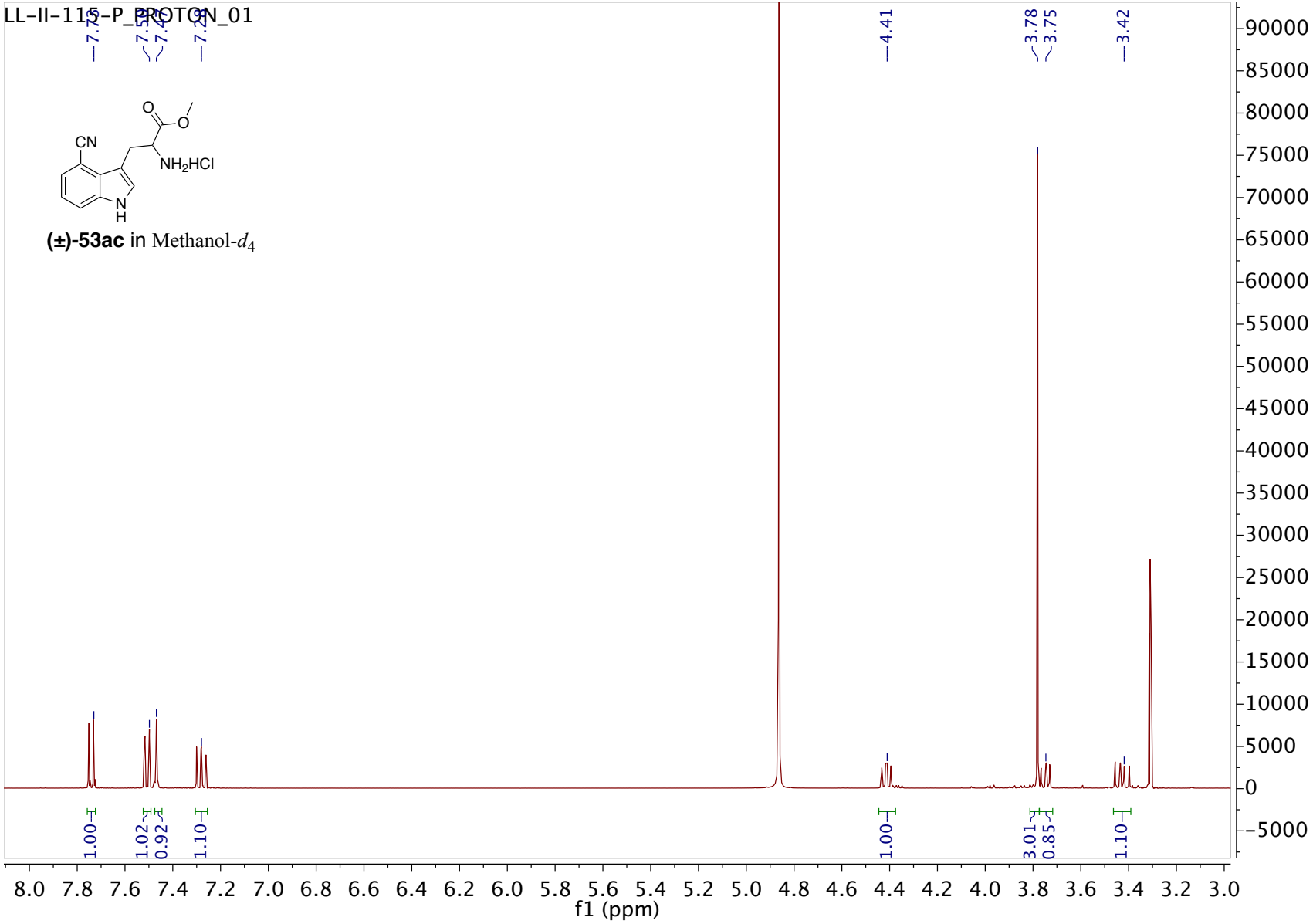
LL-II-115-P_PROTON_01
7.72
7.54
7.43
7.27
4.41
3.78
3.75
3.42
CN
O
O
NH2HCl
N
H
(±)-53ac in Methanol-d4
1.00
1.02
0.92
1.10
1.00
3.01
0.85
1.10
f1 (ppm)

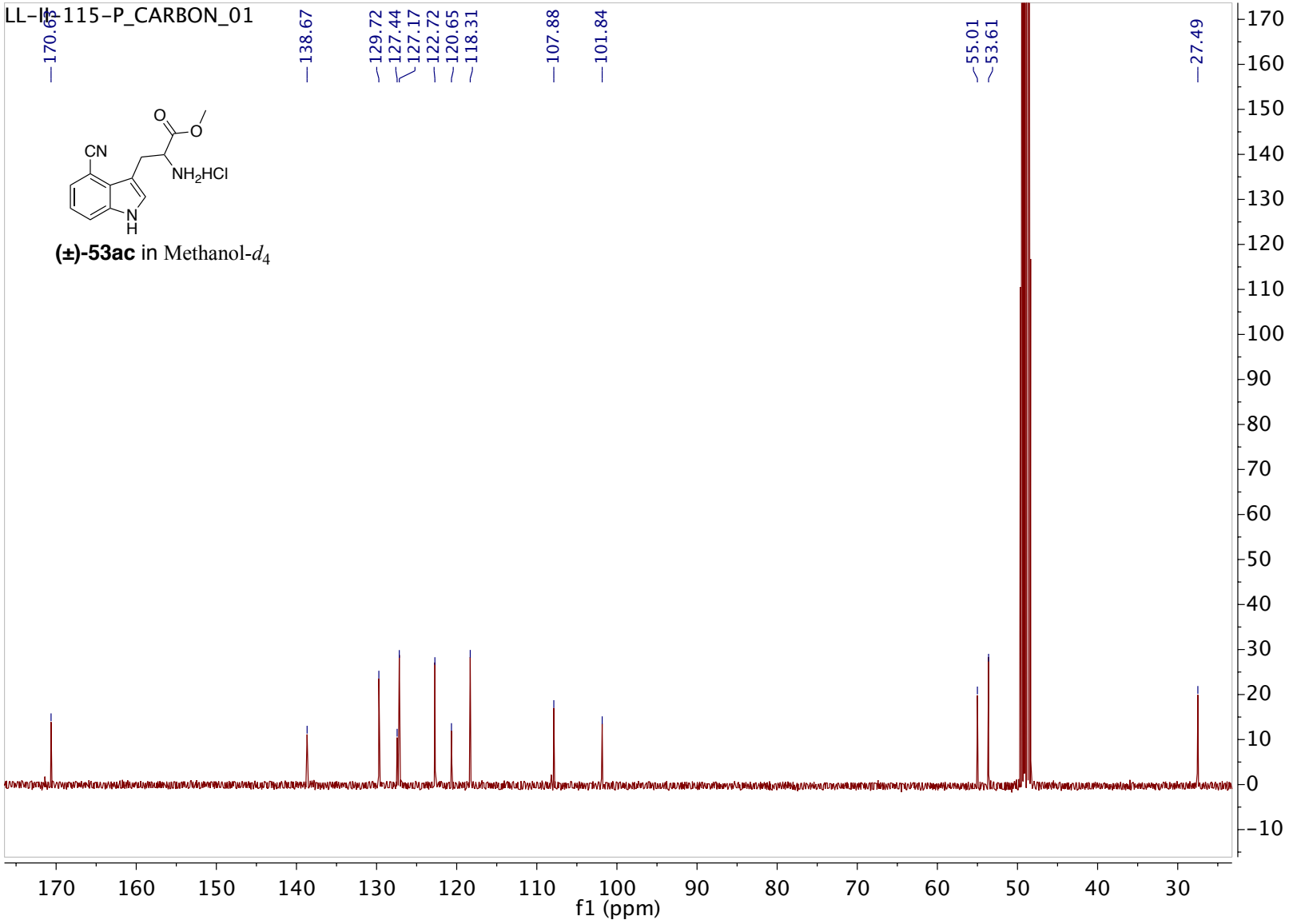
LL-IL-115-P_CARBON_01
170.65
138.67
129.72
127.44
127.17
122.72
120.65
118.31
107.88
101.84
55.01
53.61
27.49
CN
O
O
NH2HCl
N
H
(±)-53ac in Methanol-d4
f1 (ppm)

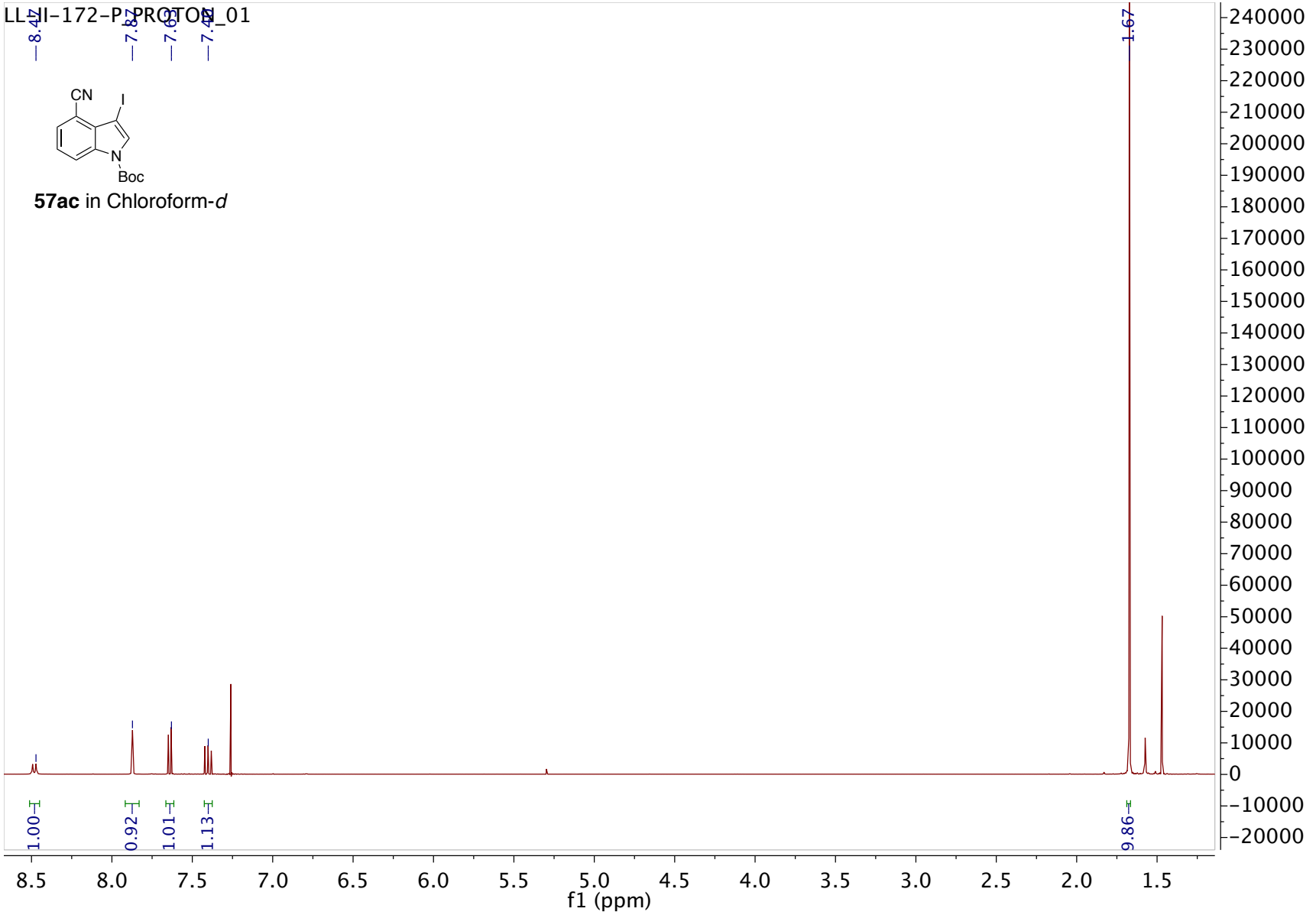
LL-II-172-P_PROTON_01
8.47
7.87
7.63
7.49
1.67
CN
I
N
Boc
57ac in Chloroform-d
1.00
0.92
1.01
1.13
9.86
f1 (ppm)

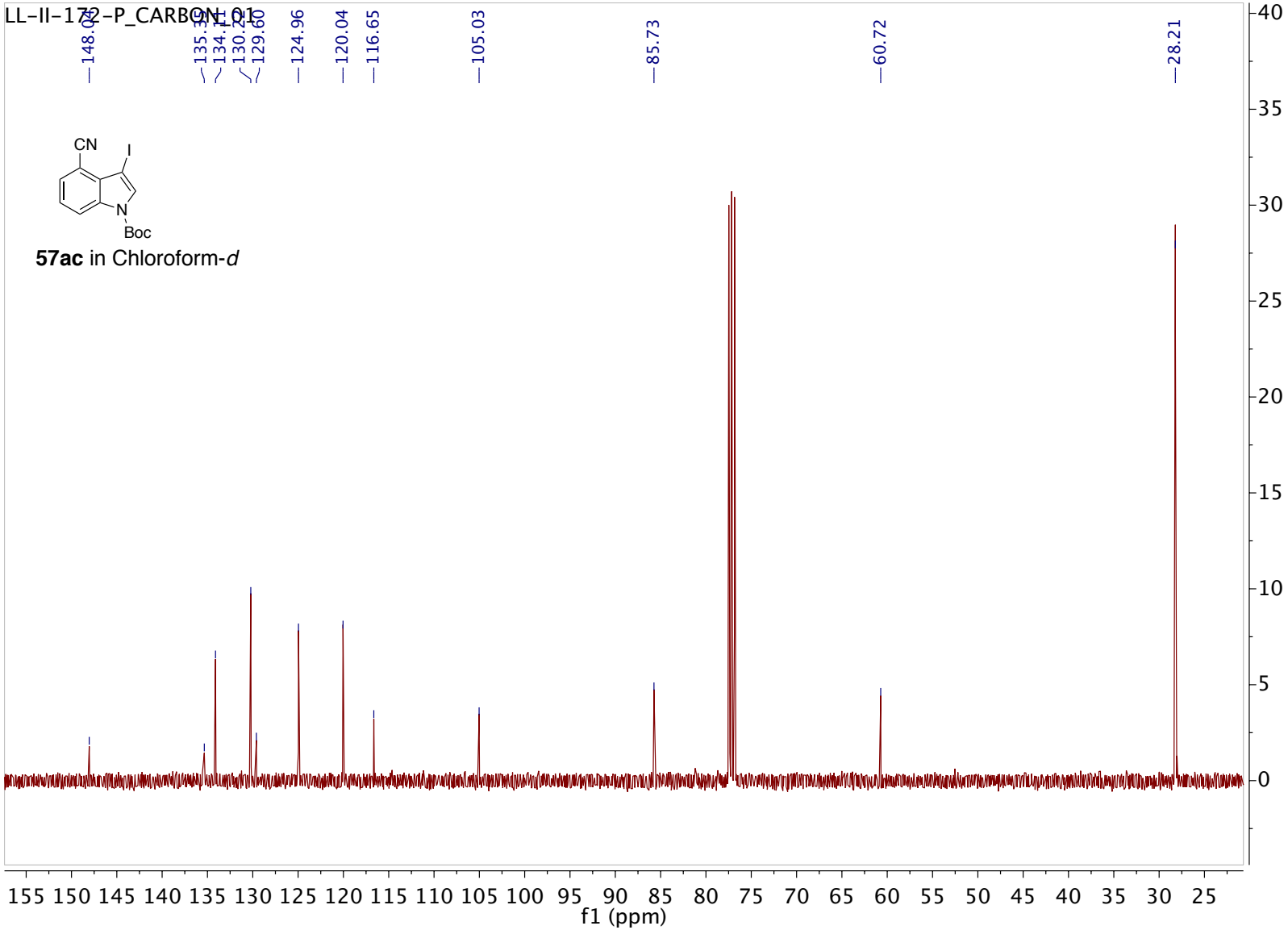
LL-II-172-P_CARBON_01
148.02
135.33
134.12
130.24
129.60
124.96
120.04
116.65
105.03
85.73
60.72
28.21
CN
I
N
Boc
57ac in Chloroform-d
40
35
30
25
20
15
10
5
0
155 150 145 140 135 130 125 120 115 110 105 100 95 90 85 80 75 70 65 60 55 50 45 40 35 30 25
f1 (ppm)

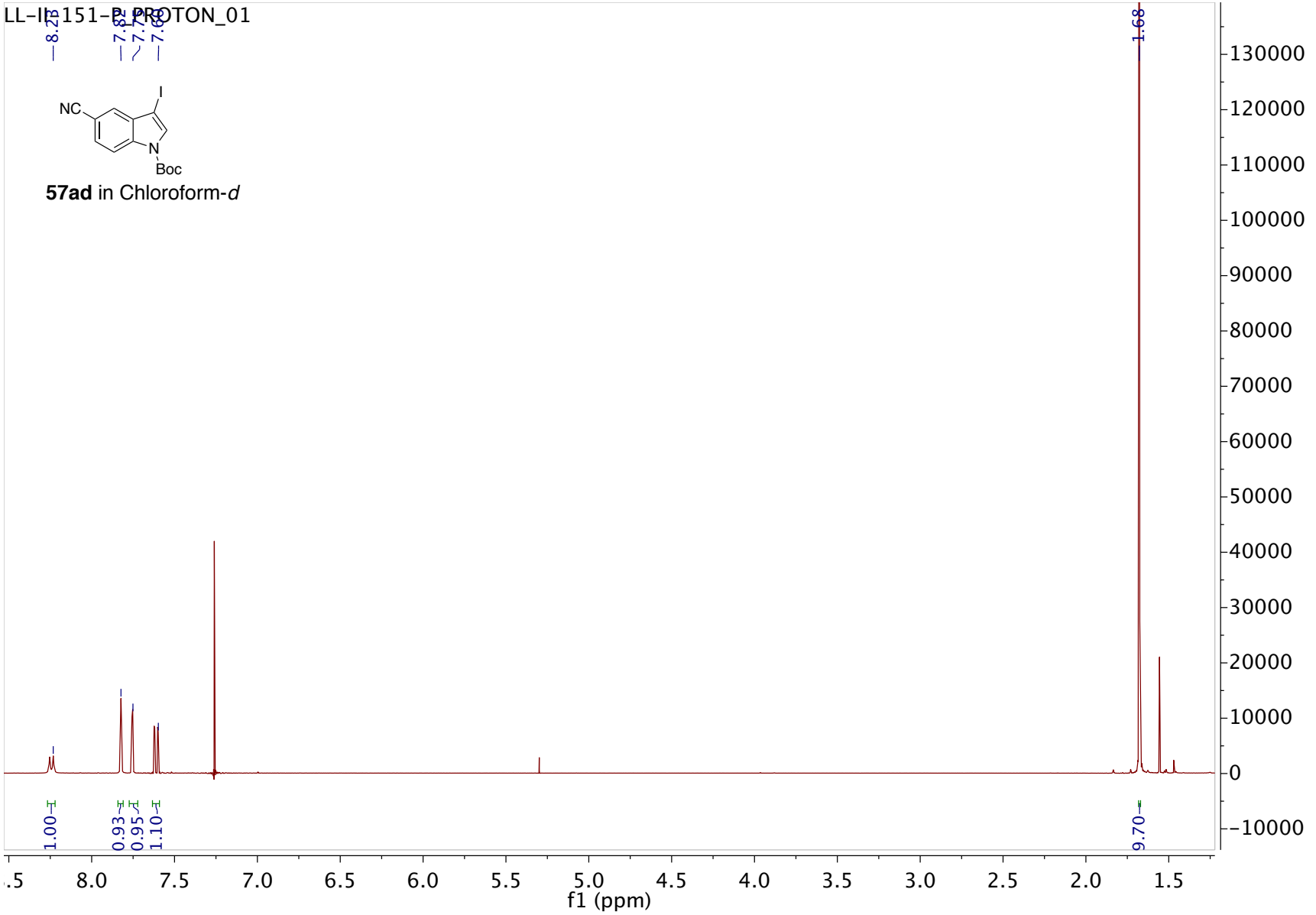
LL-IT-151-P1 PROTON_01
8.23
7.82
7.77
7.68
1.68
NC
I
N
Boc
57ad in Chloroform-d
1.00
0.93
0.95
1.10
9.70
130000
120000
110000
100000
90000
80000
70000
60000
50000
40000
30000
20000
10000
0
-10000
8.0
7.5
7.0
6.5
6.0
5.5
5.0
4.5
4.0
3.5
3.0
2.5
2.0
1.5
f1 (ppm)

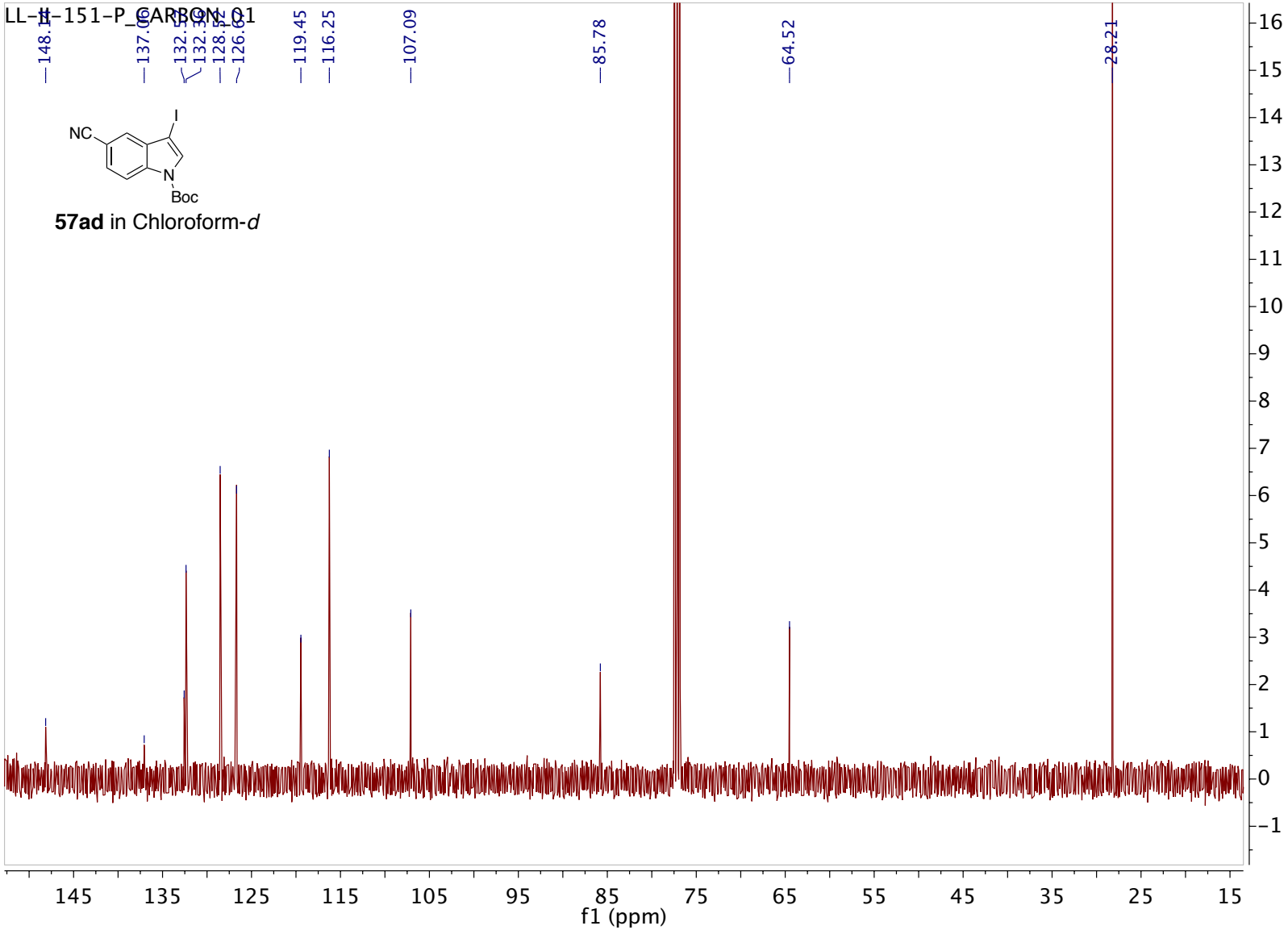
LL-II-151-P_CARBON_01
148.14
137.65
132.39
132.35
128.52
126.68
119.45
116.25
107.09
85.78
64.52
28.21
NC
I
N
Boc
57ad in Chloroform-d
f1 (ppm)

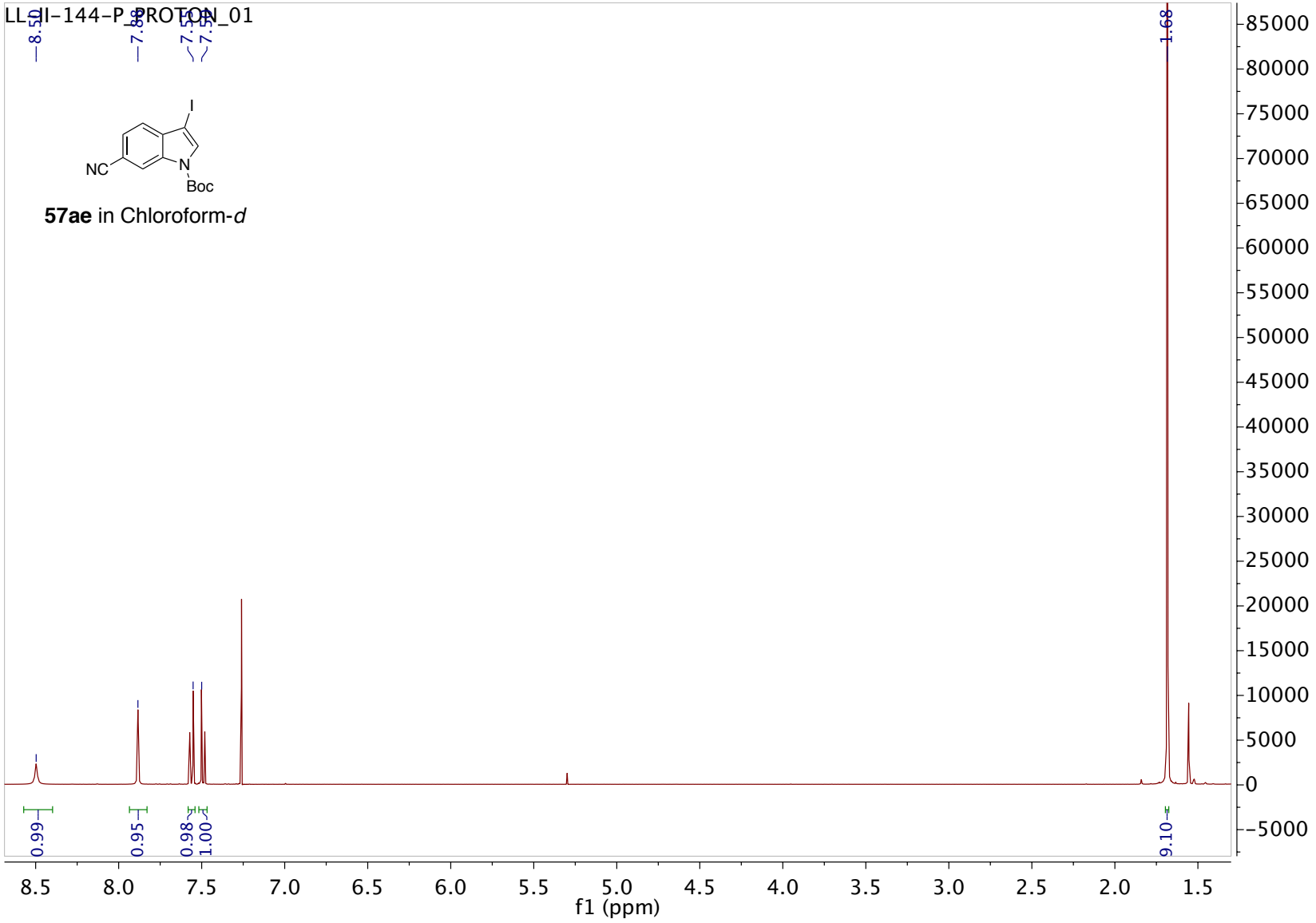
LL_II-144-P_PROTON_01
8.50
7.88
7.55
7.53
1.68
I
NC
N
Boc
57ae in Chloroform-d
85000
80000
75000
70000
65000
60000
55000
50000
45000
40000
35000
30000
25000
20000
15000
10000
5000
0
-5000
0.99
0.95
0.98
1.00
9.10
8.5
8.0
7.5
7.0
6.5
6.0
5.5
5.0
4.5
4.0
3.5
3.0
2.5
2.0
1.5
f1 (ppm)

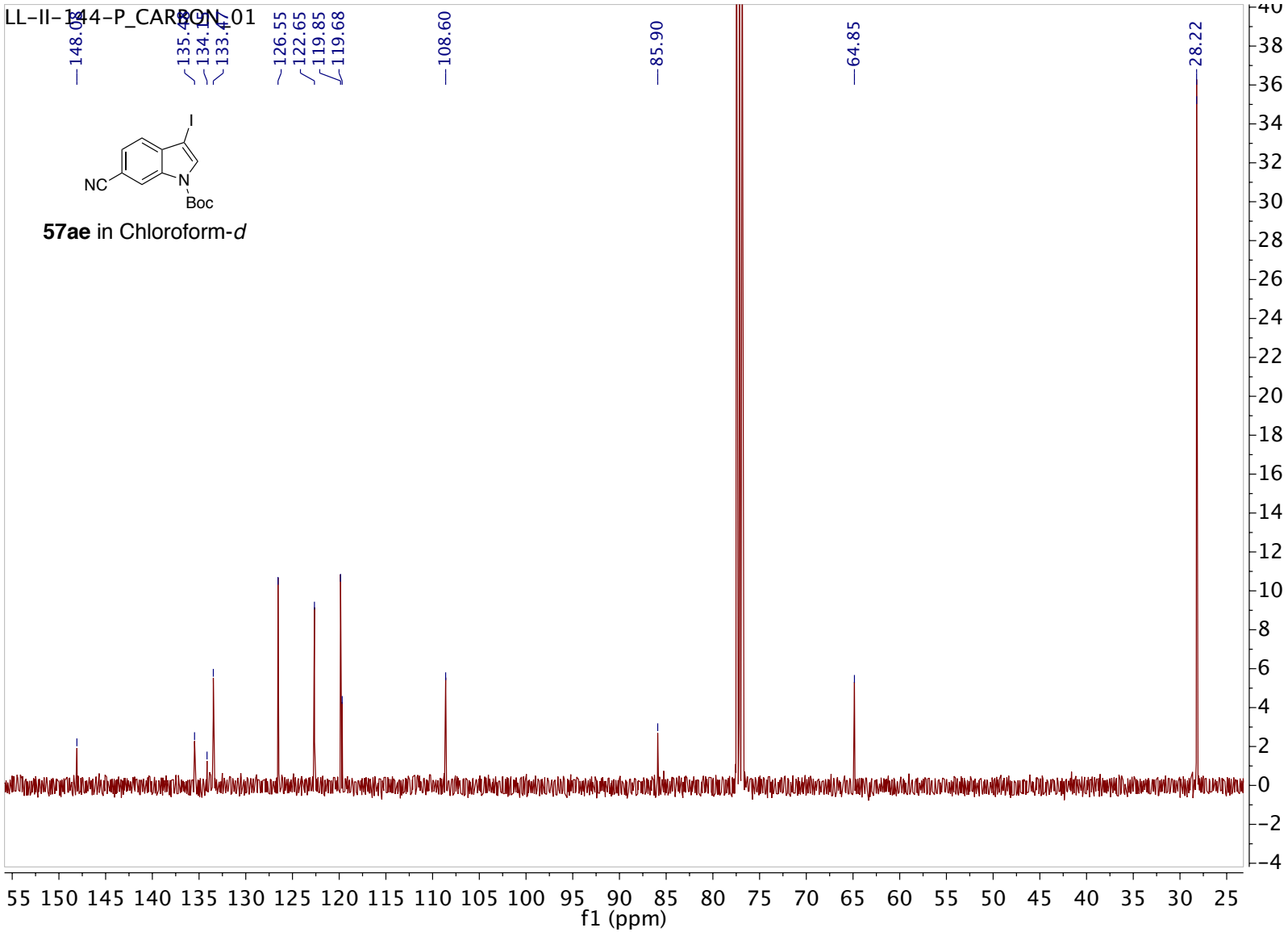
LL-II-144-P_CARBON_01
148.05
135.21
134.47
133.47
126.55
122.65
119.85
119.68
108.60
85.90
64.85
28.22
I
NC
N
Boc
57ae in Chloroform-d
f1 (ppm)

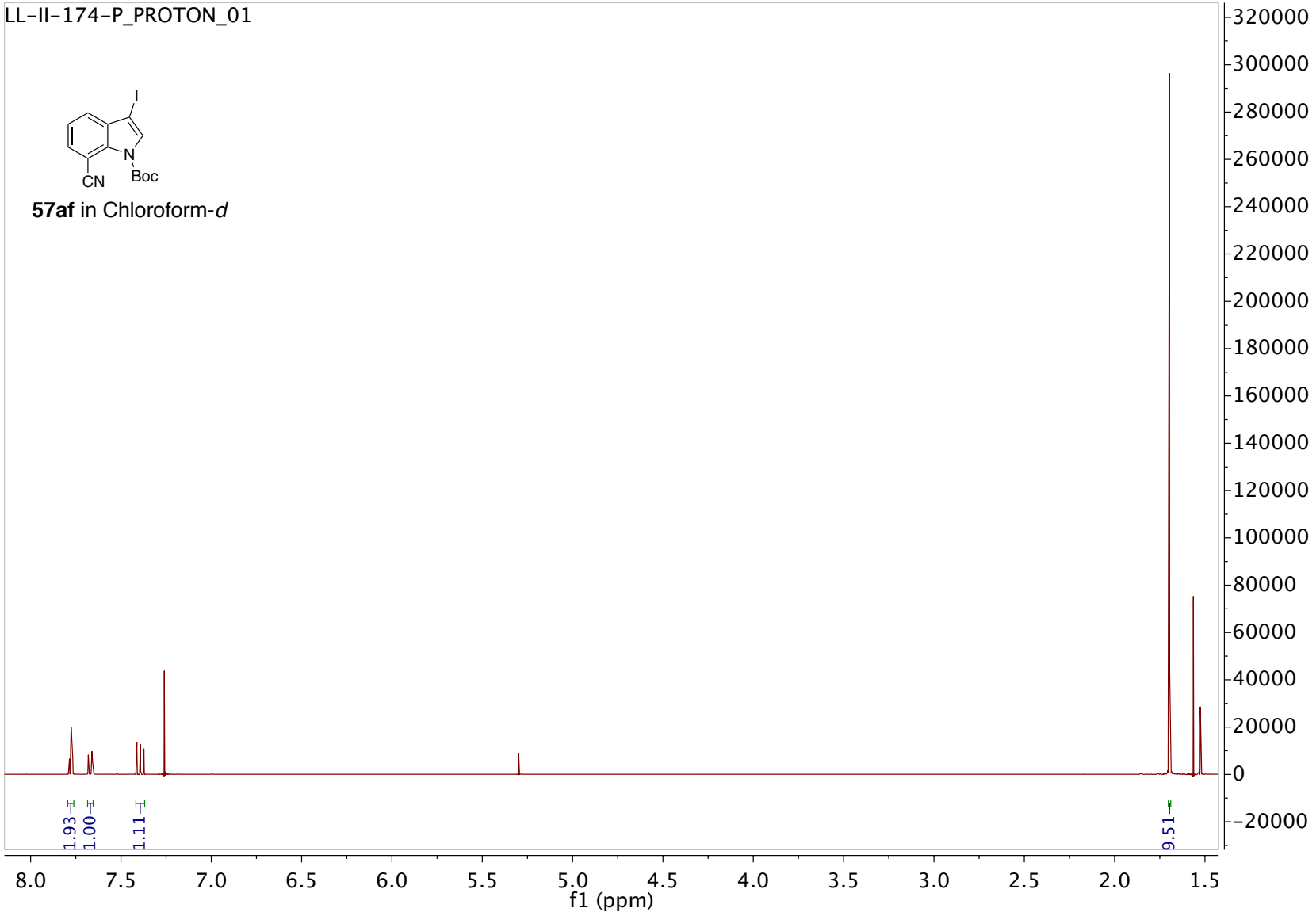
LL-II-174-P_PROTON_01
I
N
Boc
CN
57af in Chloroform-d
1.93
1.00
1.11
9.51
8.0
7.5
7.0
6.5
6.0
5.5
5.0
4.5
4.0
3.5
3.0
2.5
2.0
1.5
f1 (ppm)
320000
300000
280000
260000
240000
220000
200000
180000
160000
140000
120000
100000
80000
60000
40000
20000
0
-20000

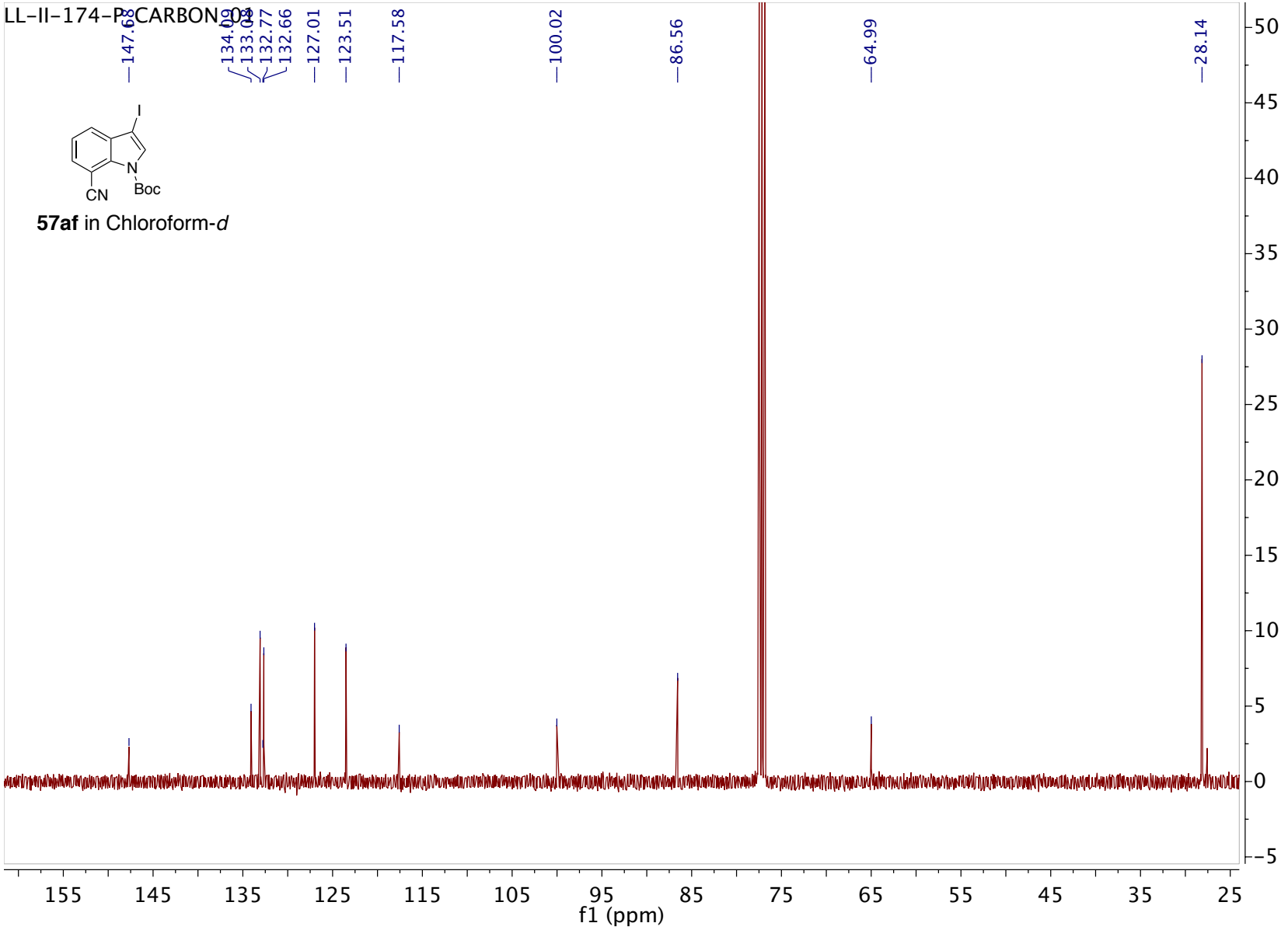
LL-II-174-P CARBON 01
147.68
134.09
133.03
132.77
132.66
127.01
123.51
117.58
100.02
86.56
64.99
28.14
I
N
CN
Boc
57af in Chloroform-d
50
45
40
35
30
25
20
15
10
5
0
-5
155
145
135
125
115
105
95
85
75
65
55
45
35
25
f1 (ppm)

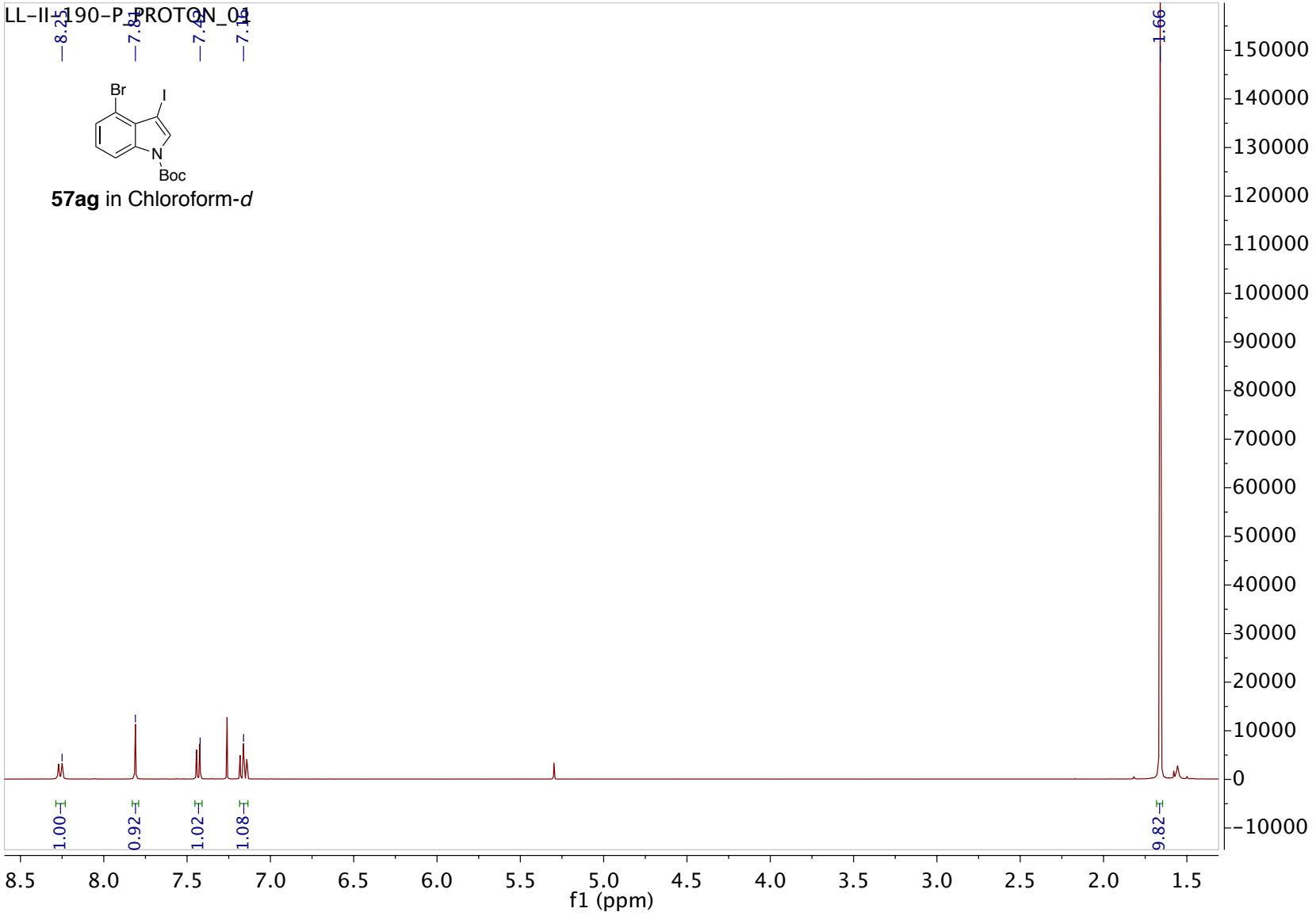
LL-II-190-P-PROTON_01
8.25
7.80
7.47
7.15
1.66
Br
I
N
Boc
57ag in Chloroform-d
1.00
0.92
1.02
1.08
9.82
150000
140000
130000
120000
110000
100000
90000
80000
70000
60000
50000
40000
30000
20000
10000
0
-10000
8.5
8.0
7.5
7.0
6.5
6.0
5.5
5.0
4.5
4.0
3.5
3.0
2.5
2.0
1.5
f1 (ppm)

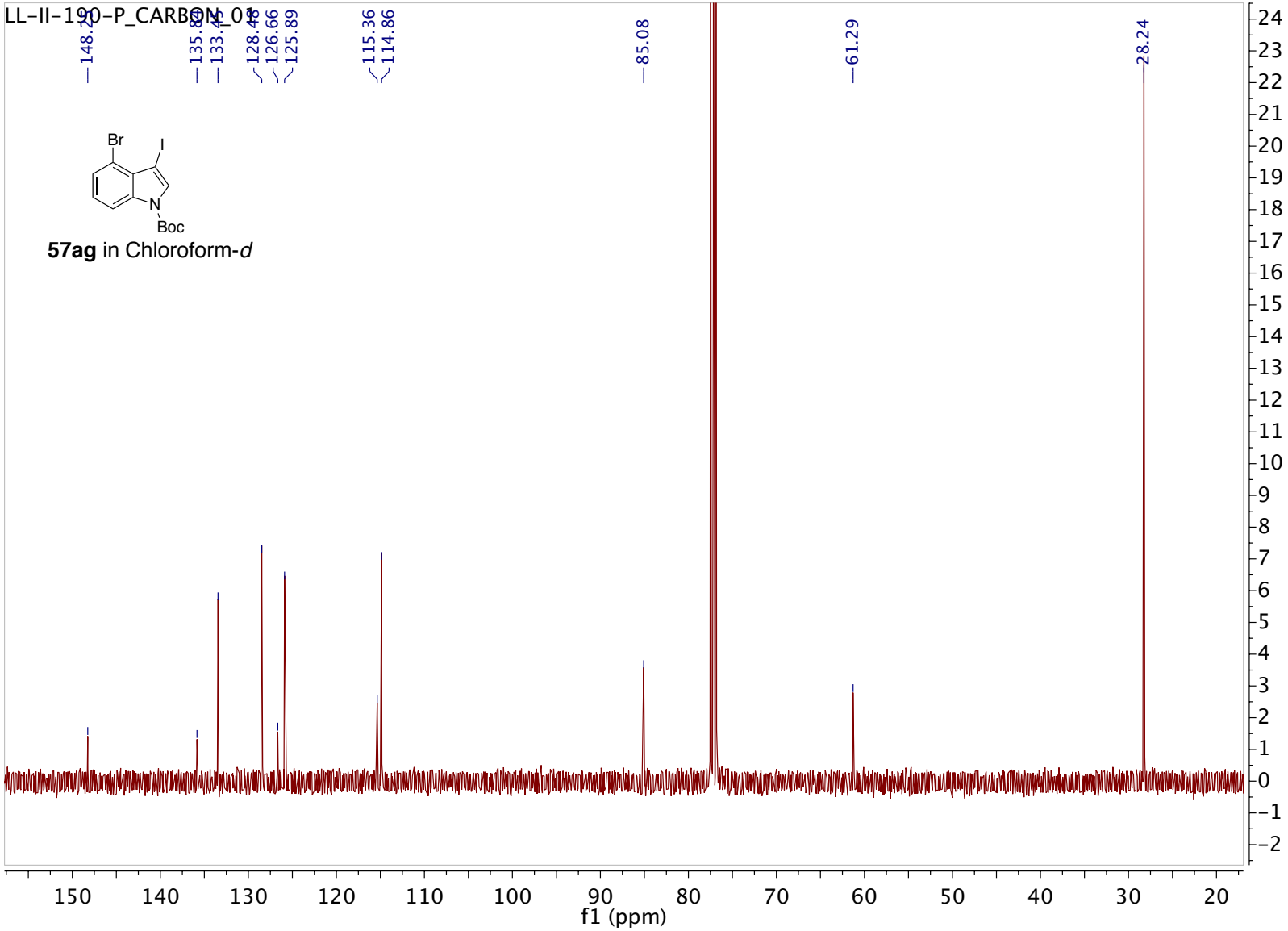
LL-II-190-P_CARBON_01
148.20
135.82
133.44
128.48
126.66
125.89
115.36
114.86
85.08
61.29
28.24
Br
I
N
Boc
57ag in Chloroform-d
f1 (ppm)

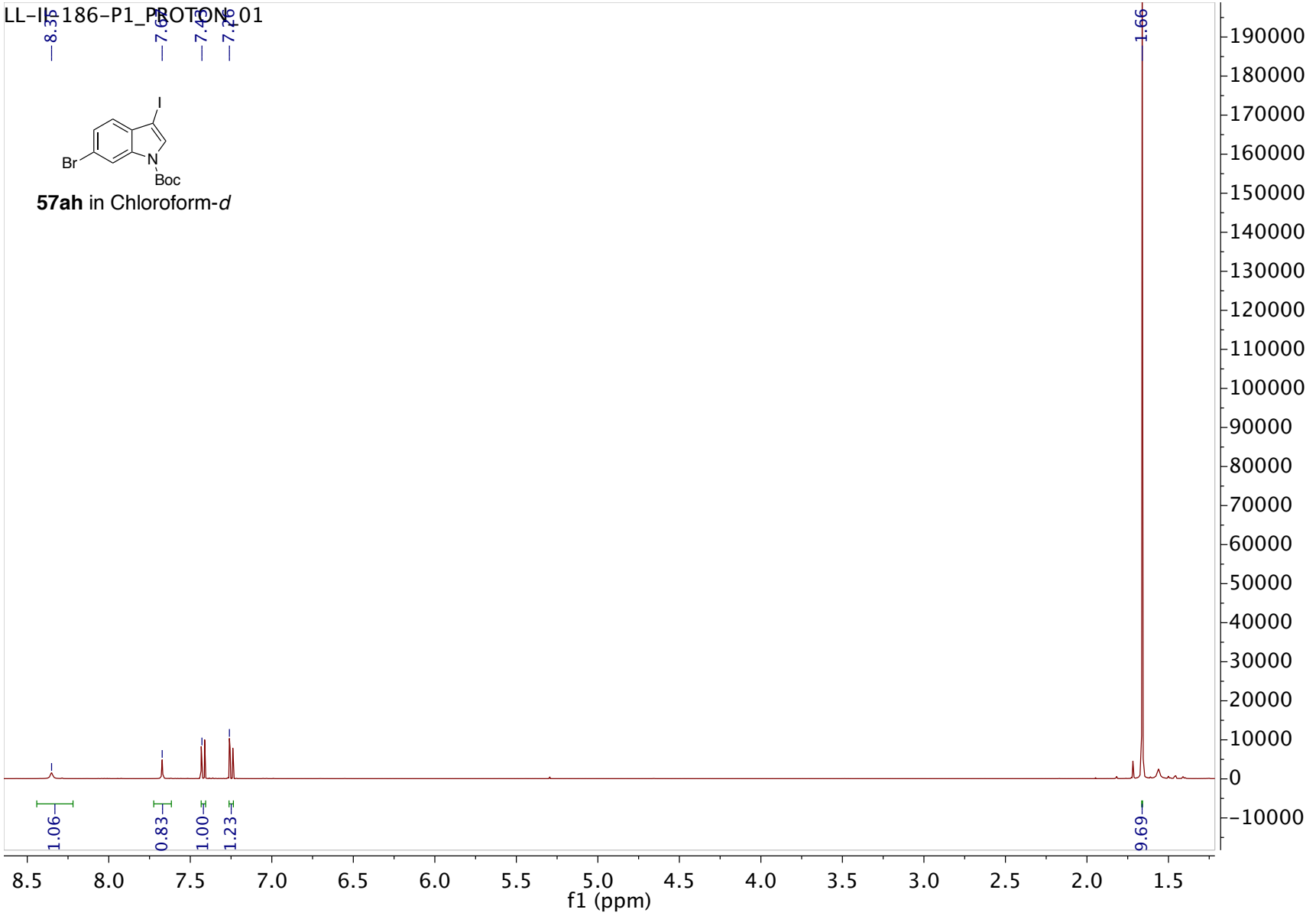
LL-II-186-P1_PROTON_01
8.35
7.68
7.43
7.42
1.66
I
Br
N
Boc
57ah in Chloroform-d
1.06
0.83
1.00
1.23
9.69
f1 (ppm)

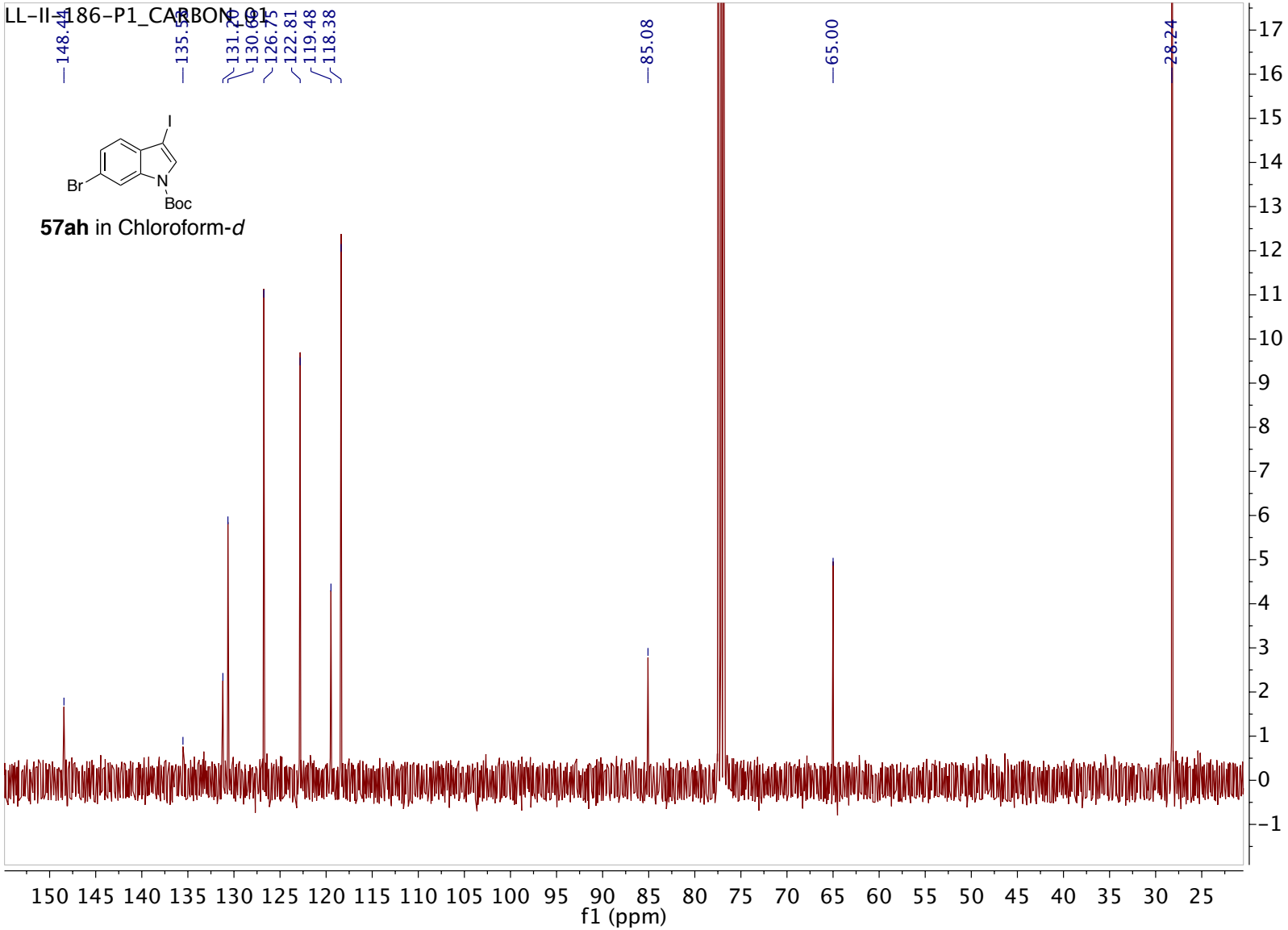
LL-II-186-P1_CARBON_01
148.41
135.58
131.70
130.67
126.75
122.81
119.48
118.38
85.08
65.00
28.24
I
Br
N
Boc
57ah in Chloroform-d
f1 (ppm)

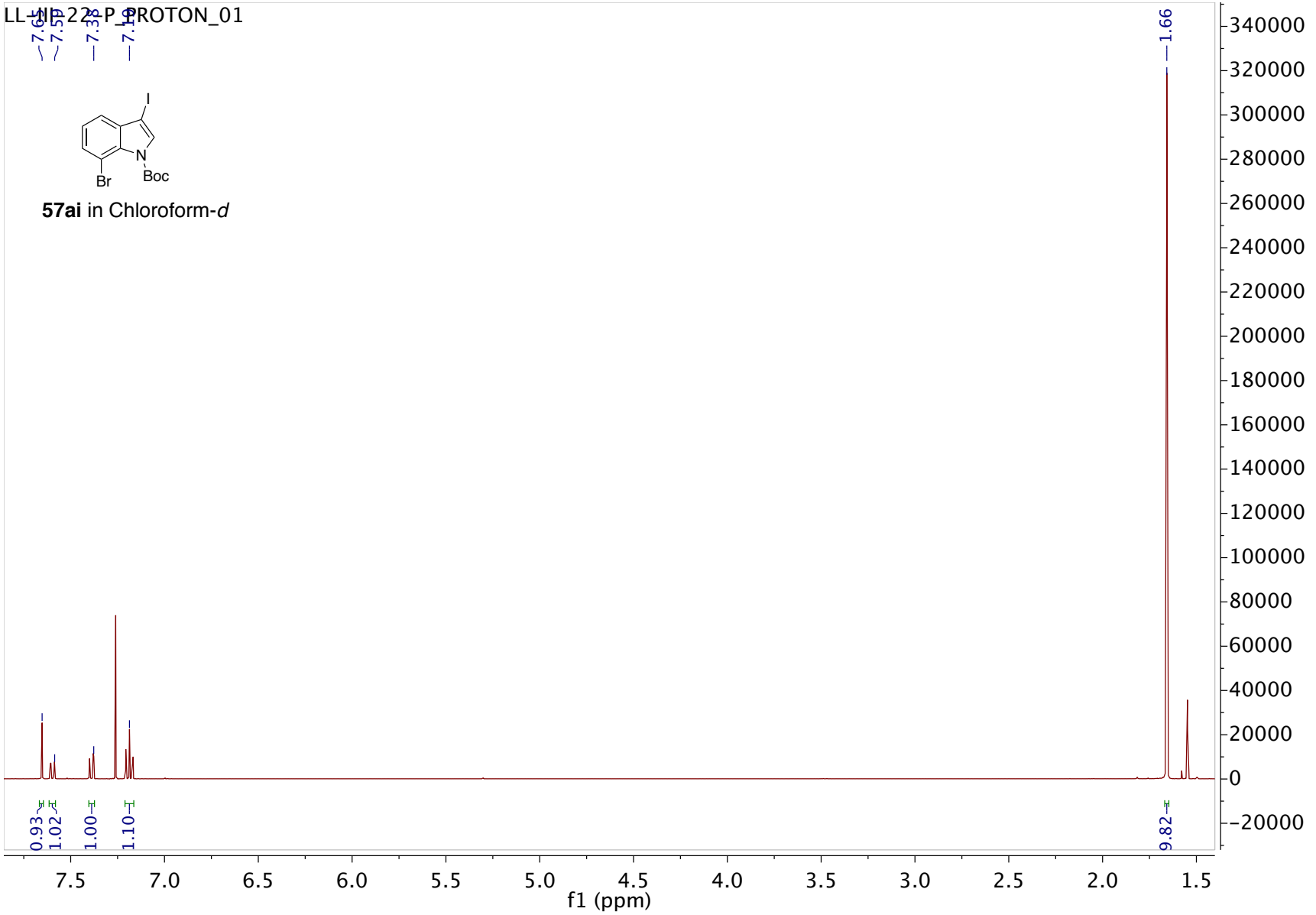
LL-HP-22-P_PROTON_01
7.62
7.55
7.38
7.19
1.66
I
N
Boc
Br
57ai in Chloroform-d
340000
320000
300000
280000
260000
240000
220000
200000
180000
160000
140000
120000
100000
80000
60000
40000
20000
0
-20000
0.93
1.02
1.00
1.10
9.82
7.5
7.0
6.5
6.0
5.5
5.0
4.5
4.0
3.5
3.0
2.5
2.0
1.5
f1 (ppm)

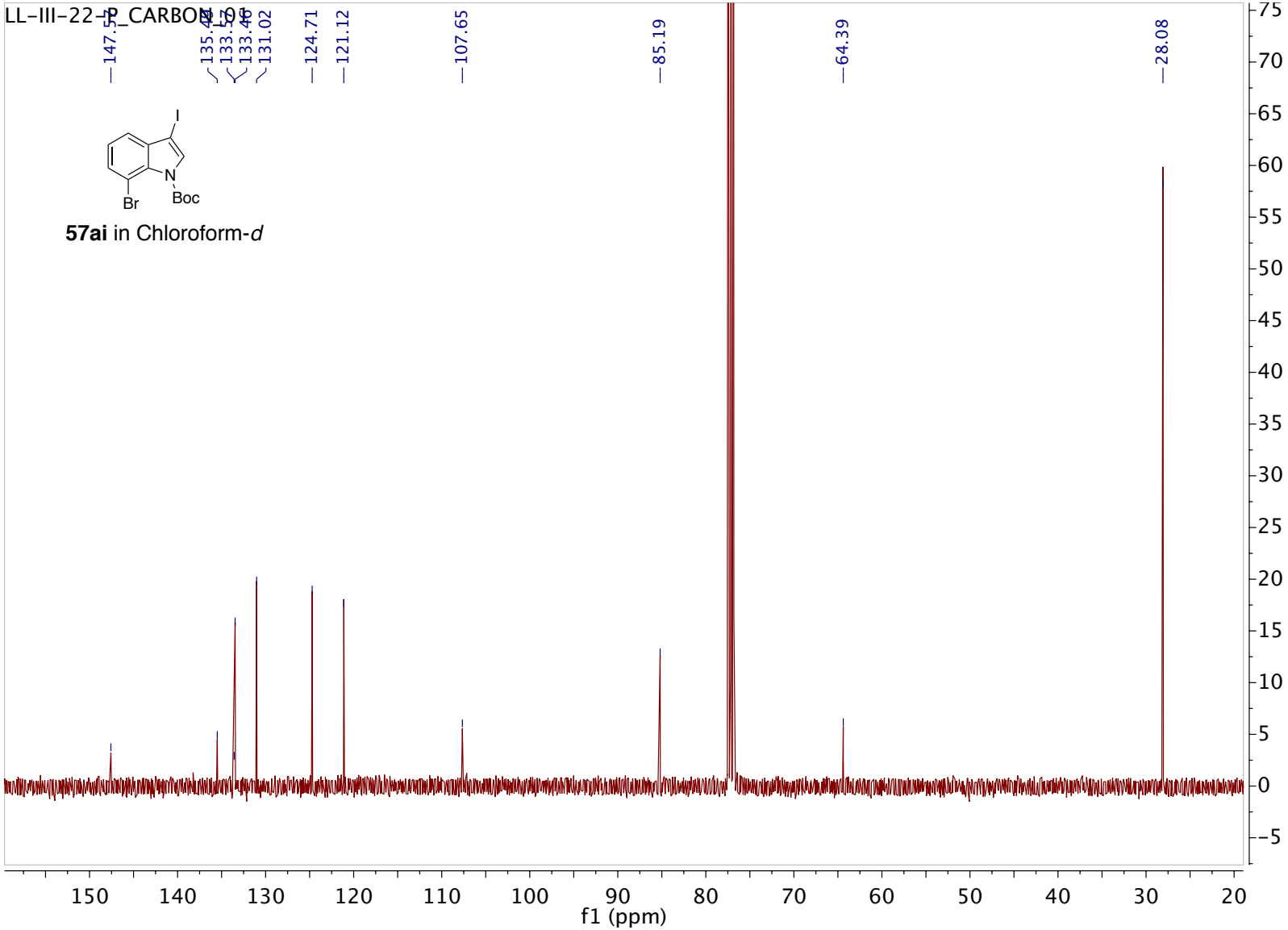
LL-III-22-P_CARBON_01
147.55
135.42
133.15
133.46
131.02
124.71
121.12
107.65
85.19
64.39
28.08
I
N
Br
Boc
57ai in Chloroform-d
f1 (ppm)

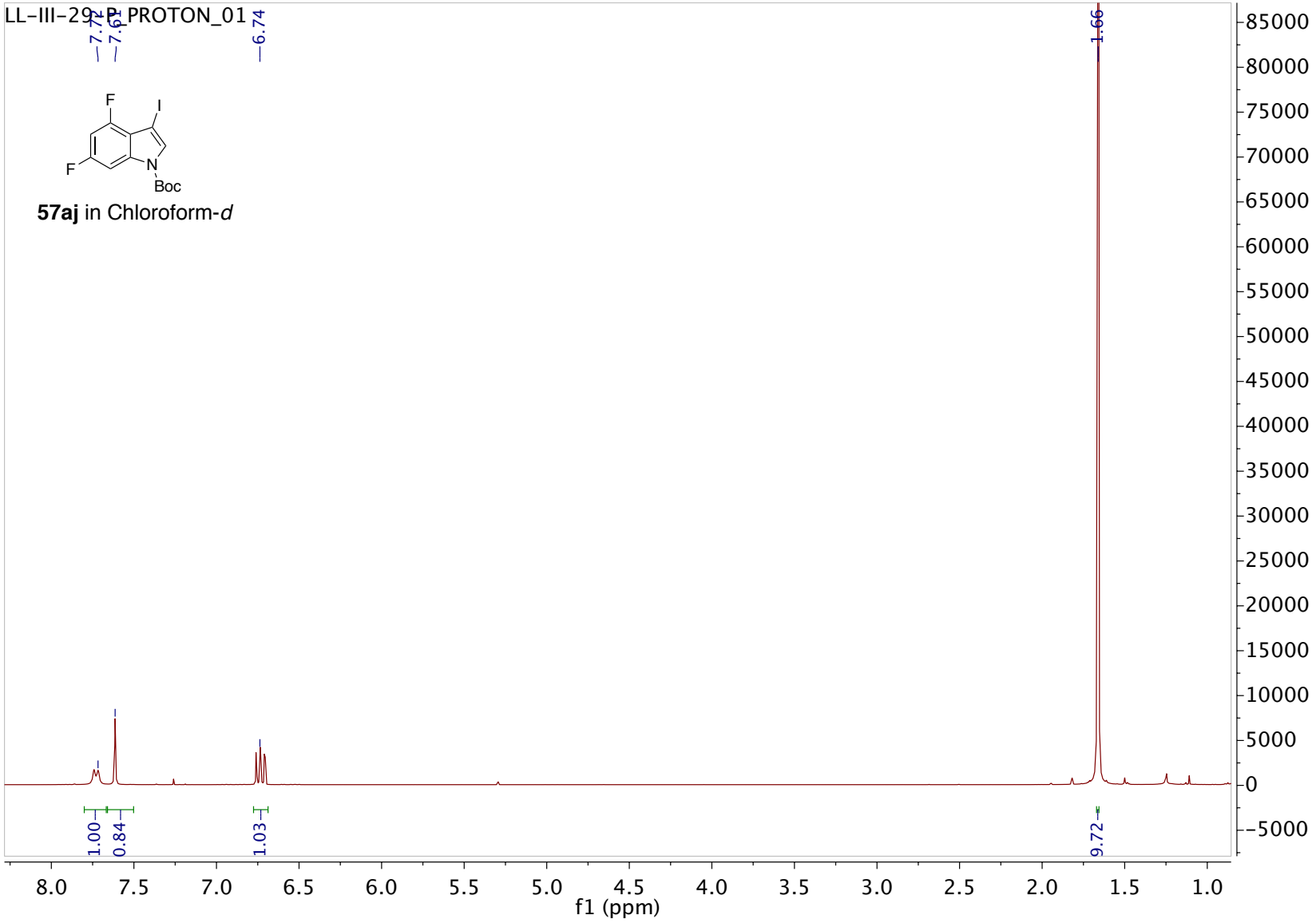
LL-III-29-P PROTON_01
7.72
7.61
6.74
1.66
F
I
F
N
Boc
57aj in Chloroform-d
1.00
0.84
1.03
9.72
f1 (ppm)

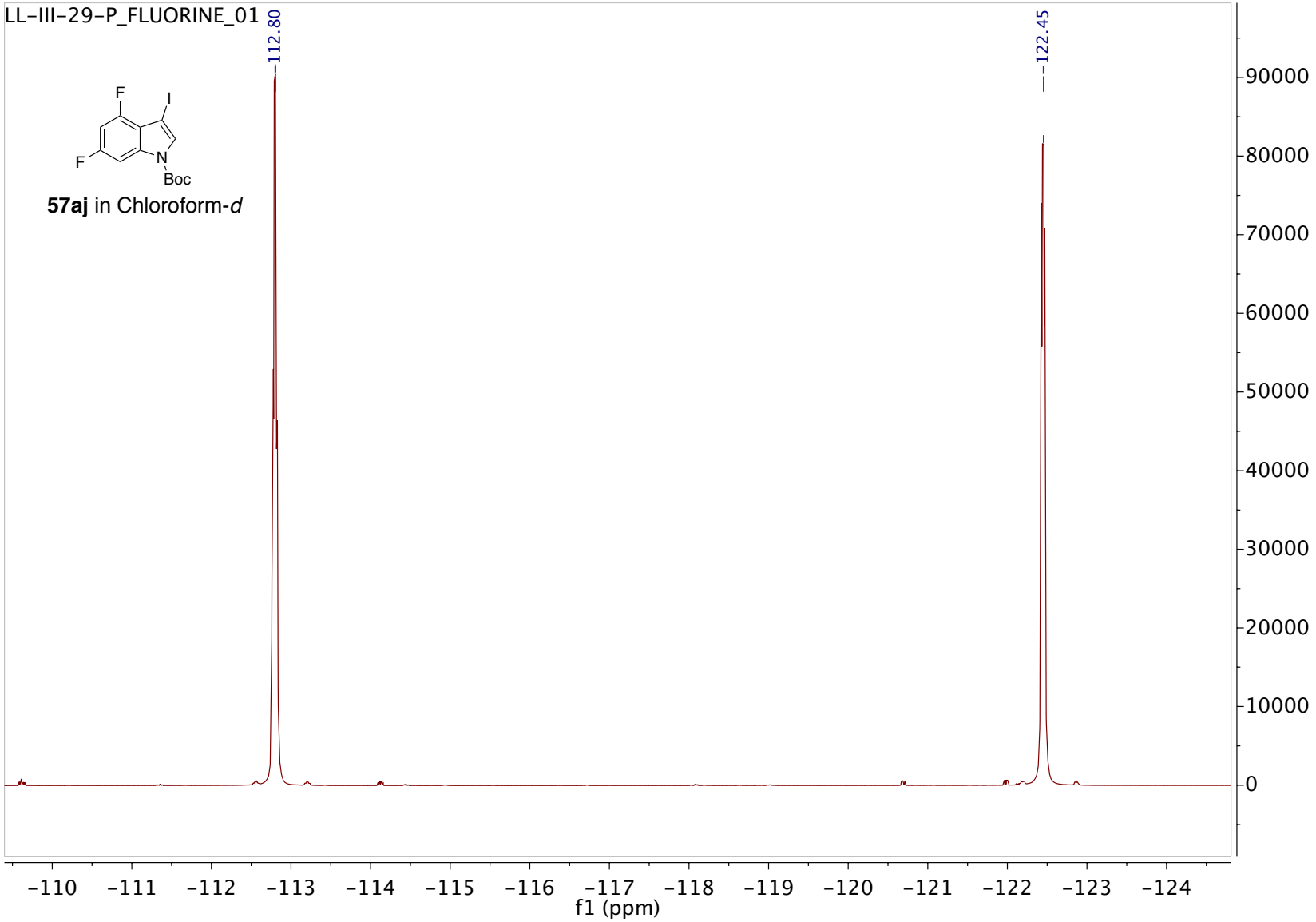
LL-III-29-P_FLUORINE_01
-112.80
-122.45
F
I
F
N
Boc
57aj in Chloroform-d
90000
80000
70000
60000
50000
40000
30000
20000
10000
0
-110
-111
-112
-113
-114
-115
-116
-117
-118
-119
-120
-121
-122
-123
-124
f1 (ppm)

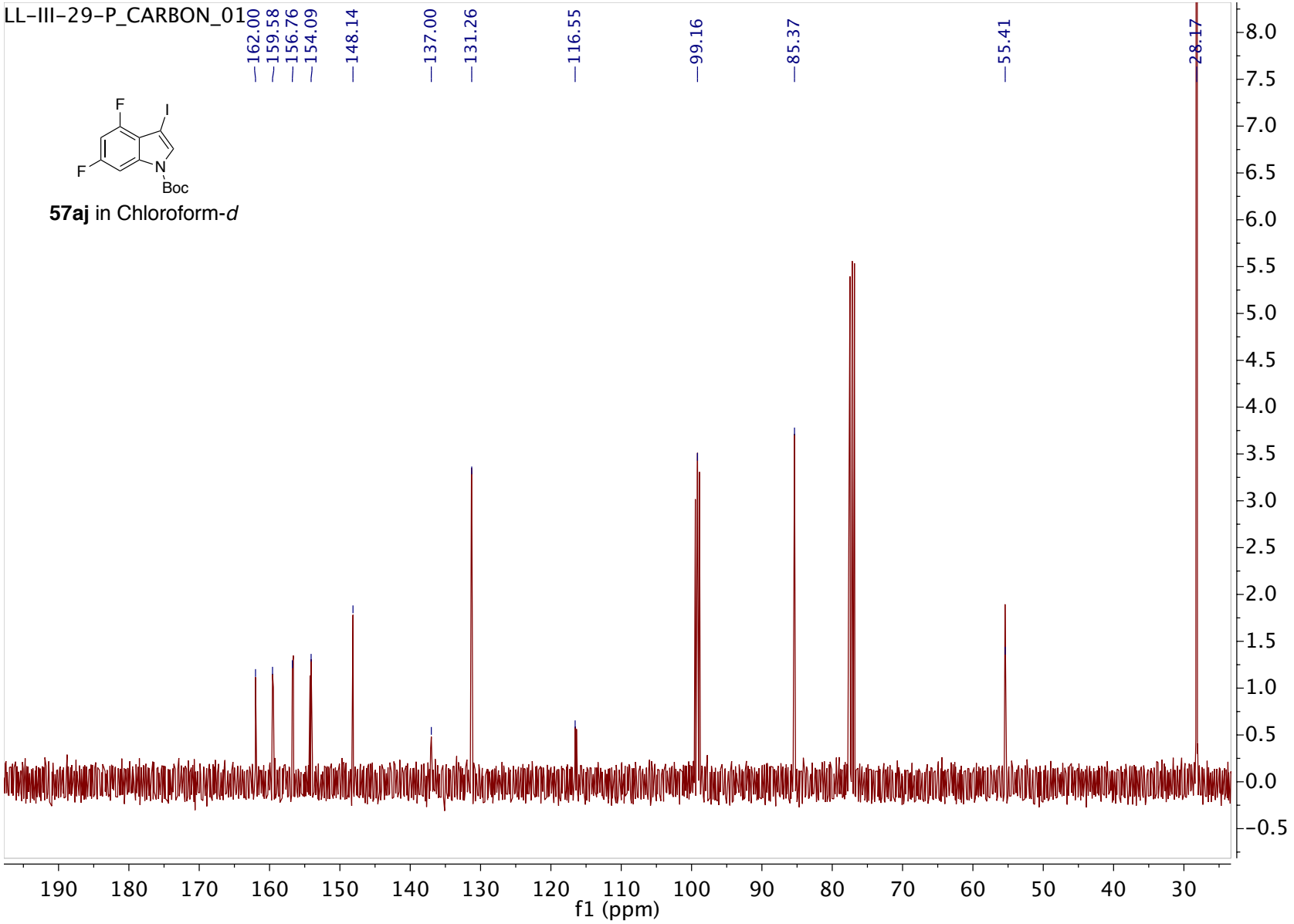
LL-III-29-P_CARBON_01
162.00
159.58
156.76
154.09
148.14
137.00
131.26
116.55
99.16
85.37
55.41
28.17
F
I
F
N
Boc
57aj in Chloroform-d
f1 (ppm)

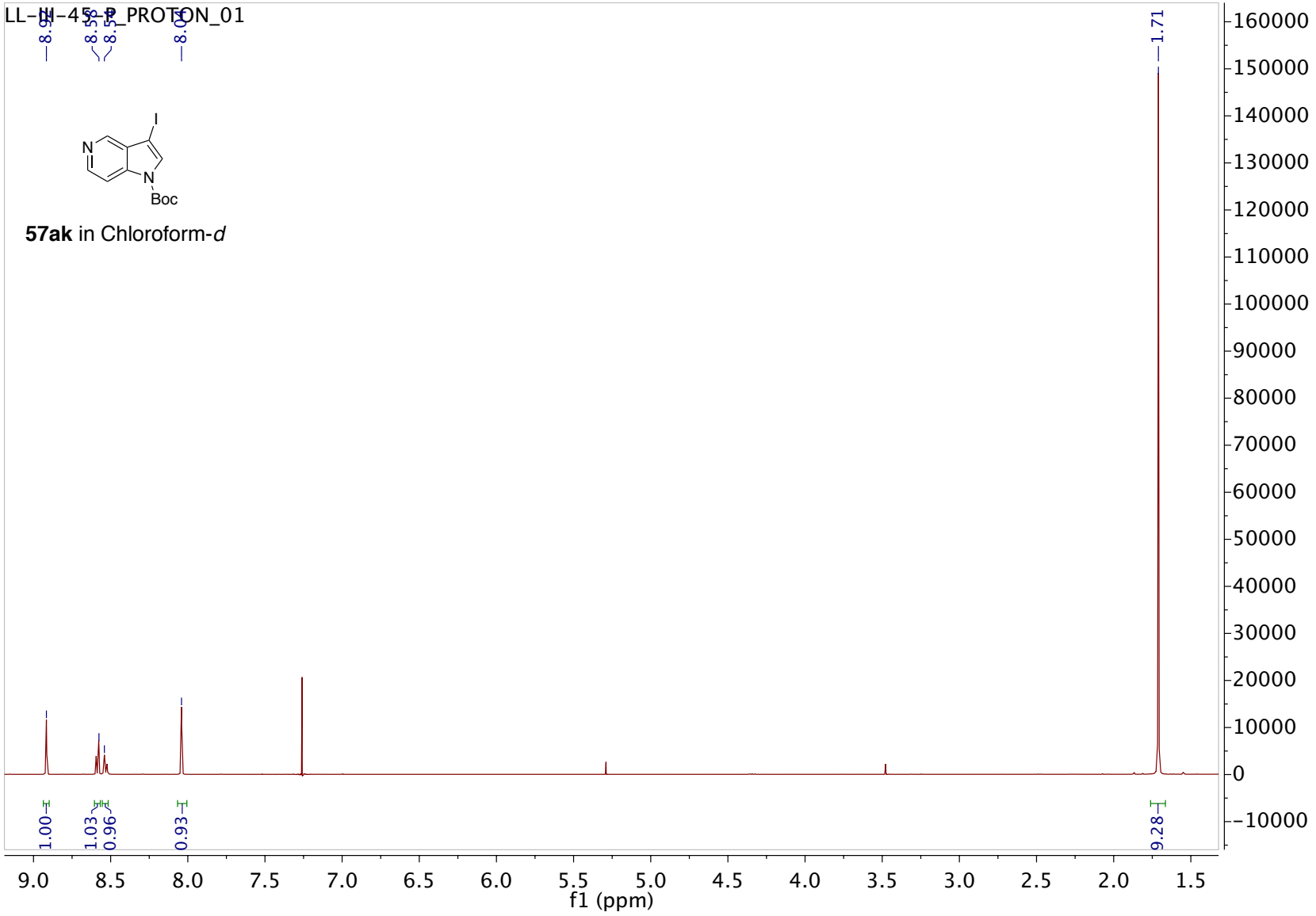
LL-IM-45-P_PROTON_01
8.99
8.55
8.54
8.02
1.71
I
N
N
Boc
57ak in Chloroform-d
1.00
1.03
0.96
0.93
9.28
160000
150000
140000
130000
120000
110000
100000
90000
80000
70000
60000
50000
40000
30000
20000
10000
0
-10000
9.0
8.5
8.0
7.5
7.0
6.5
6.0
5.5
5.0
4.5
4.0
3.5
3.0
2.5
2.0
1.5
f1 (ppm)

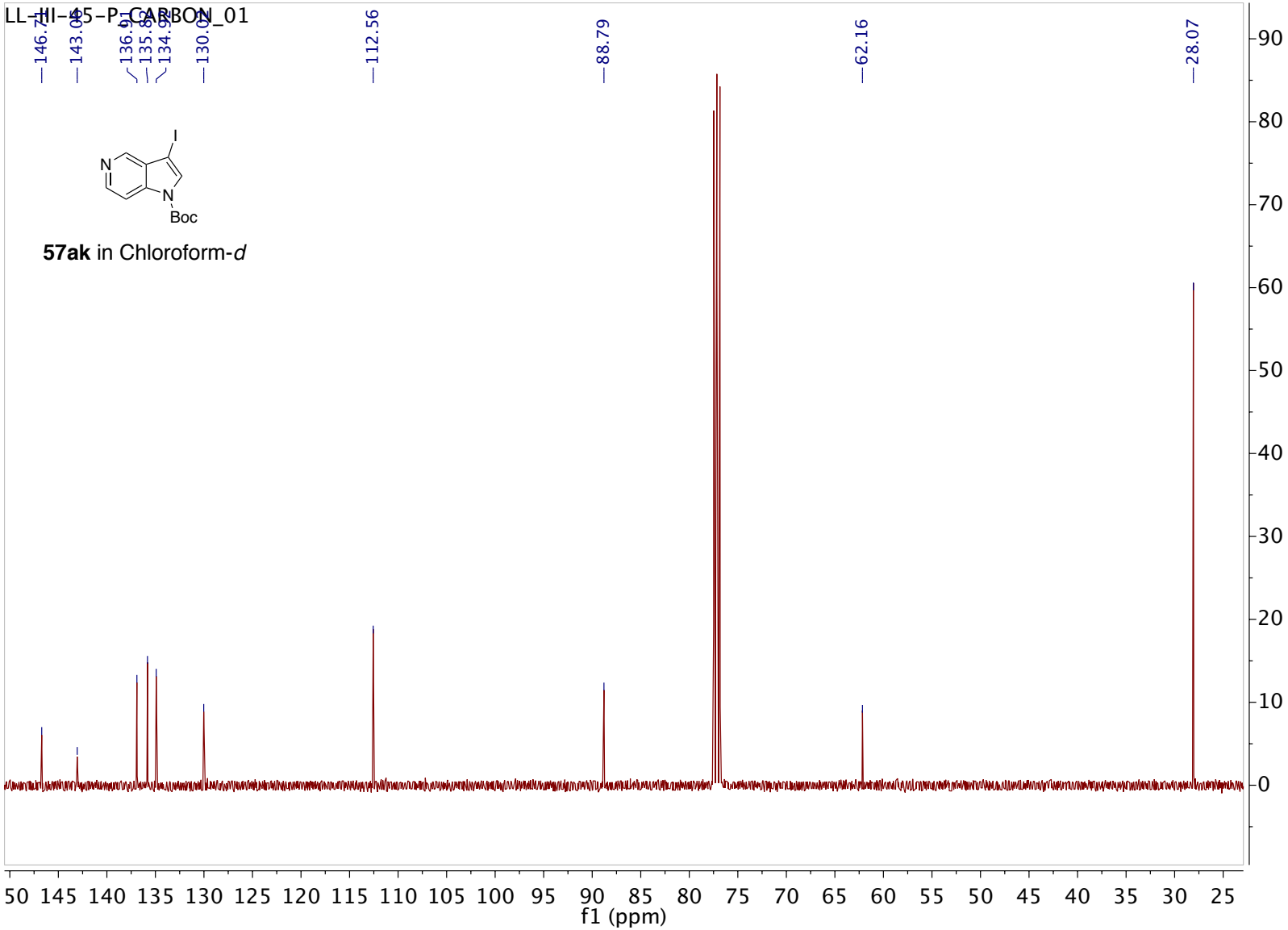
LL-III-45-P_CARBON_01
146.71
143.04
136.91
135.64
134.38
130.02
112.56
88.79
62.16
28.07
I
N
N
Boc
57ak in Chloroform-d
90
80
70
60
50
40
30
20
10
0
50 145 140 135 130 125 120 115 110 105 100 95 90 85 80 75 70 65 60 55 50 45 40 35 30 25
f1 (ppm)

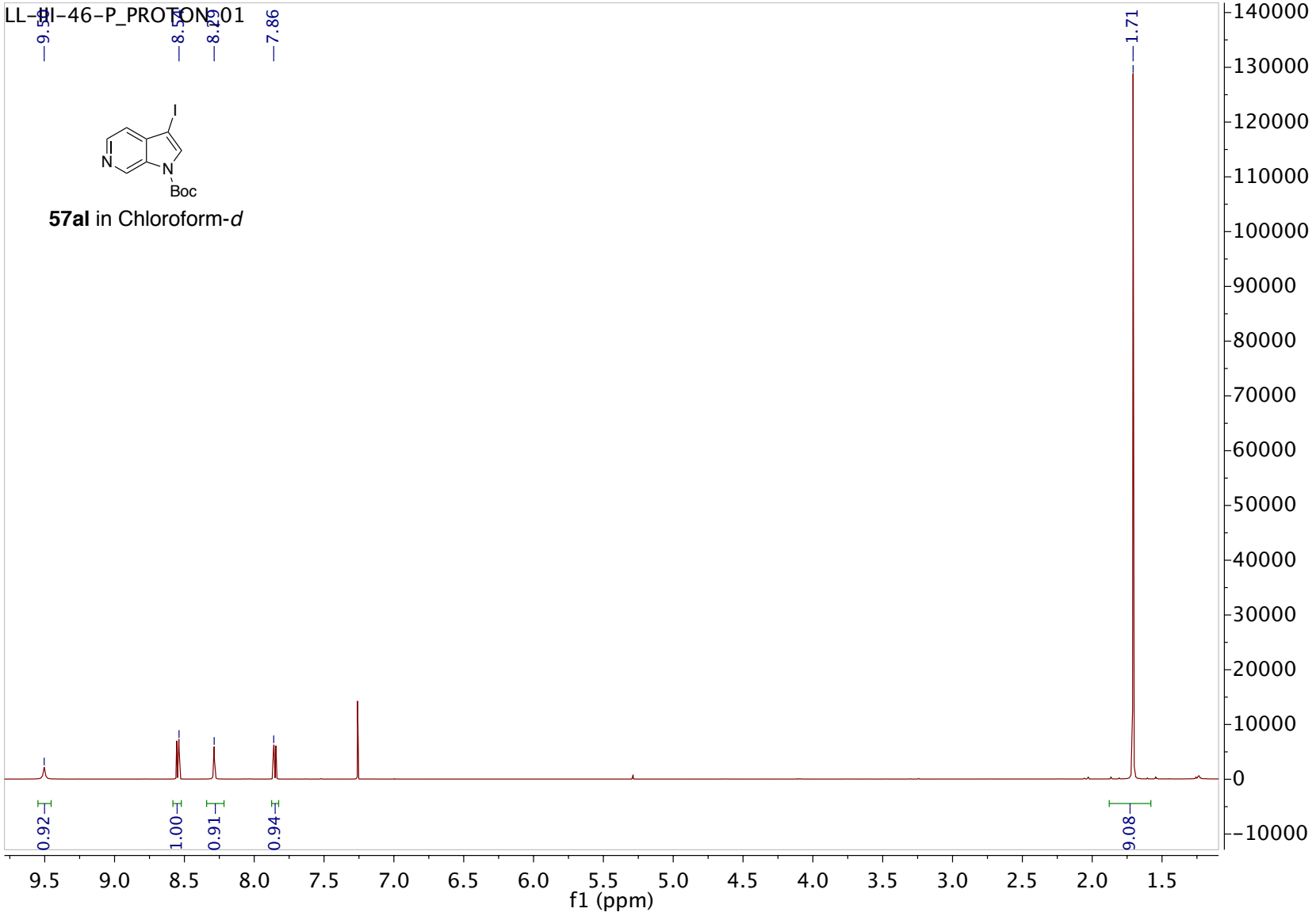
LL-HI-46-P_PROTON_01
9.50
8.55
8.29
7.86
1.71
I
N
N
Boc
57al in Chloroform-d
0.92
1.00
0.91
0.94
9.08
140000
130000
120000
110000
100000
90000
80000
70000
60000
50000
40000
30000
20000
10000
0
-10000
9.5
9.0
8.5
8.0
7.5
7.0
6.5
6.0
5.5
5.0
4.5
4.0
3.5
3.0
2.5
2.0
1.5
f1 (ppm)

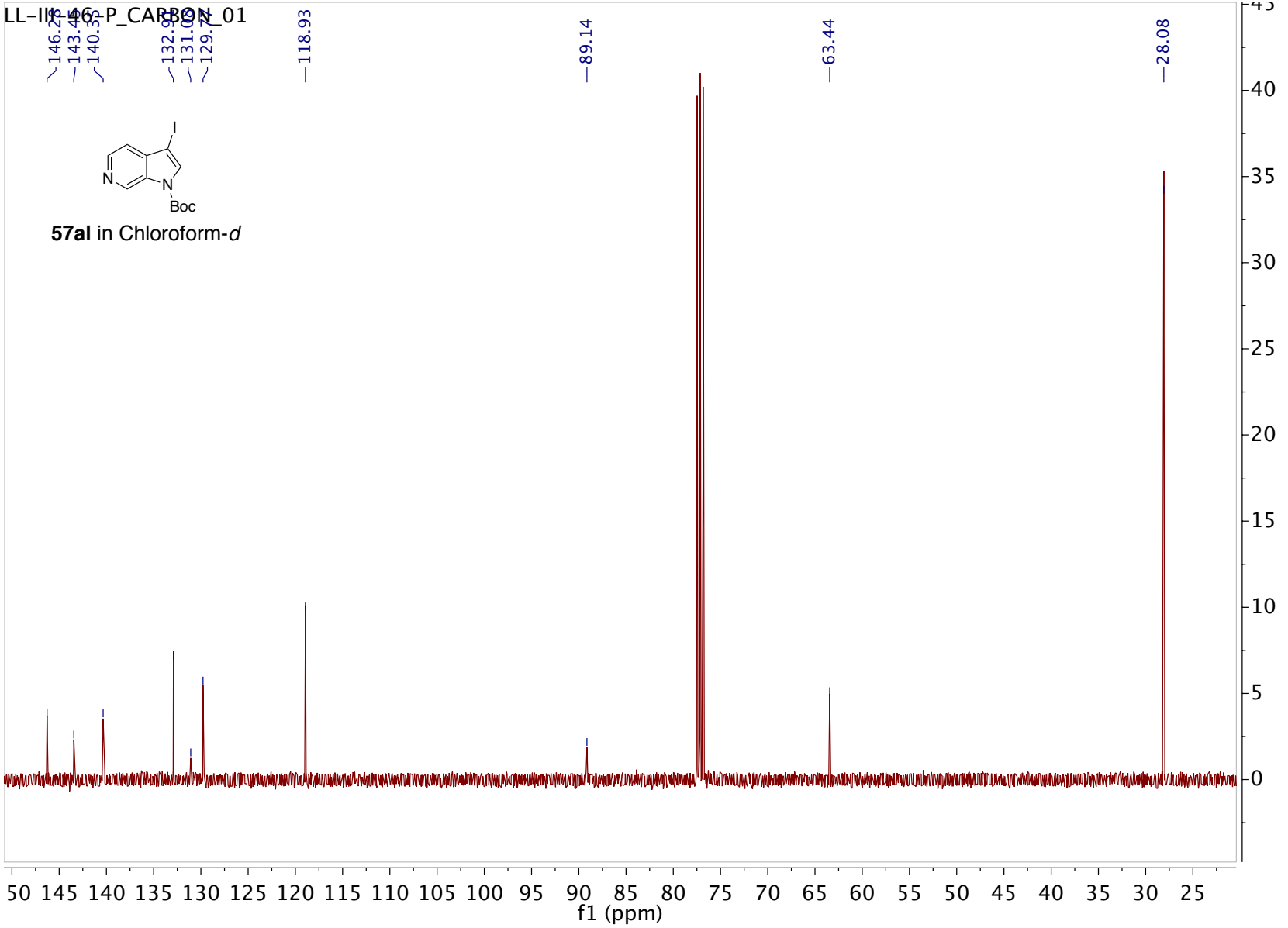
LL-II-46-P_CARBON_01
146.27
143.46
140.33
132.89
131.01
129.17
118.93
89.14
63.44
28.08
I
N
N
Boc
57al in Chloroform-d
40
35
30
25
20
15
10
5
0
50 145 140 135 130 125 120 115 110 105 100 95 90 85 80 75 70 65 60 55 50 45 40 35 30 25
f1 (ppm)

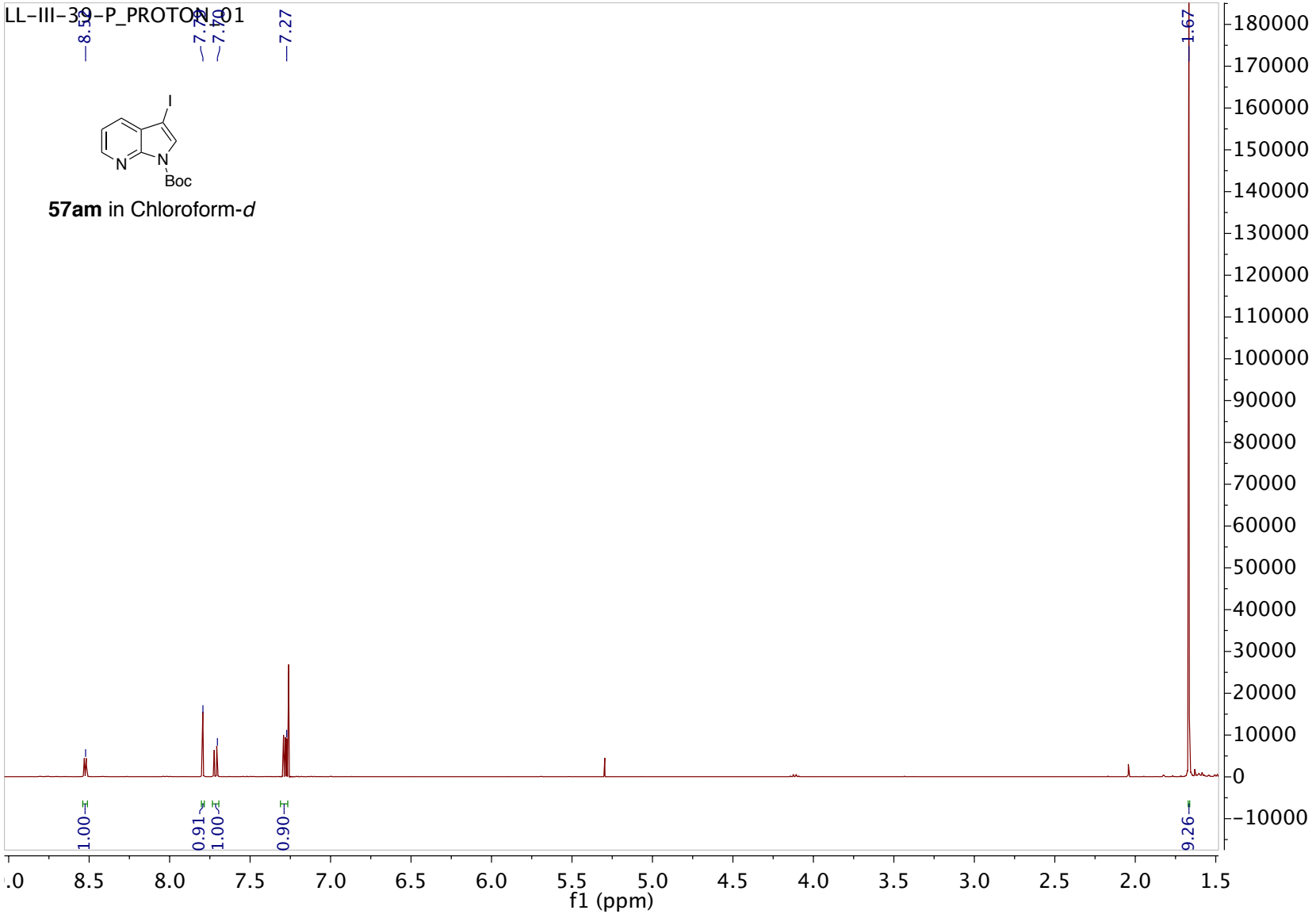
LL-III-39-P_PROTON_01
8.53
7.72
7.71
7.27
1.67
I
N
N
Boc
57am in Chloroform-d
1.00
0.91
1.00
0.90
9.26
180000
170000
160000
150000
140000
130000
120000
110000
100000
90000
80000
70000
60000
50000
40000
30000
20000
10000
0
-10000
8.5
8.0
7.5
7.0
6.5
6.0
5.5
5.0
4.5
4.0
3.5
3.0
2.5
2.0
1.5
f1 (ppm)

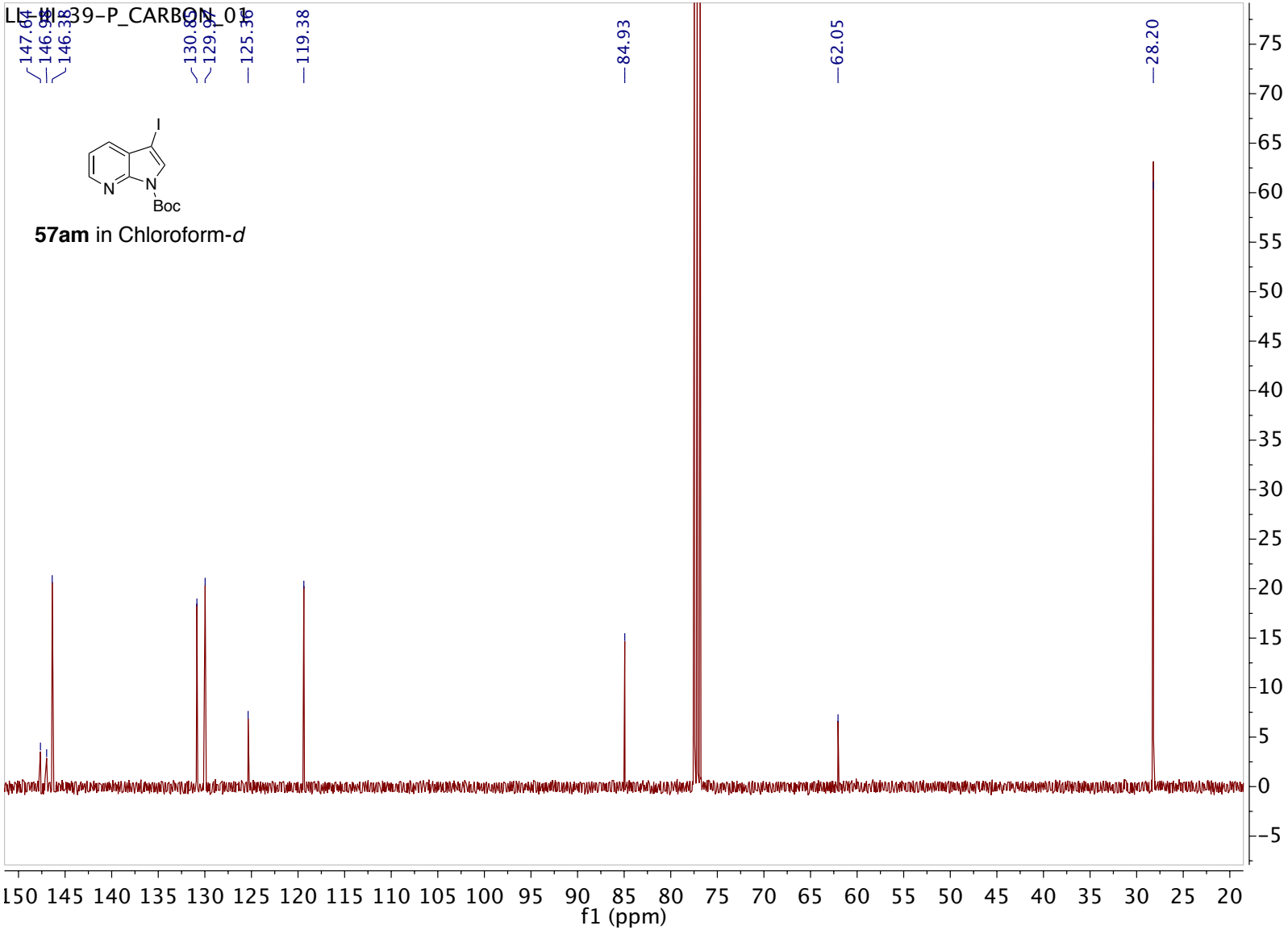
LL-III-39-P_CARBON_01
147.64
146.98
146.38
130.88
129.91
125.36
119.38
84.93
62.05
28.20
I
N
N
Boc
57am in Chloroform-d
150 145 140 135 130 125 120 115 110 105 100 95 90 85 80 75 70 65 60 55 50 45 40 35 30 25 20
f1 (ppm)
75 70 65 60 55 50 45 40 35 30 25 20 15 10 5 0 -5

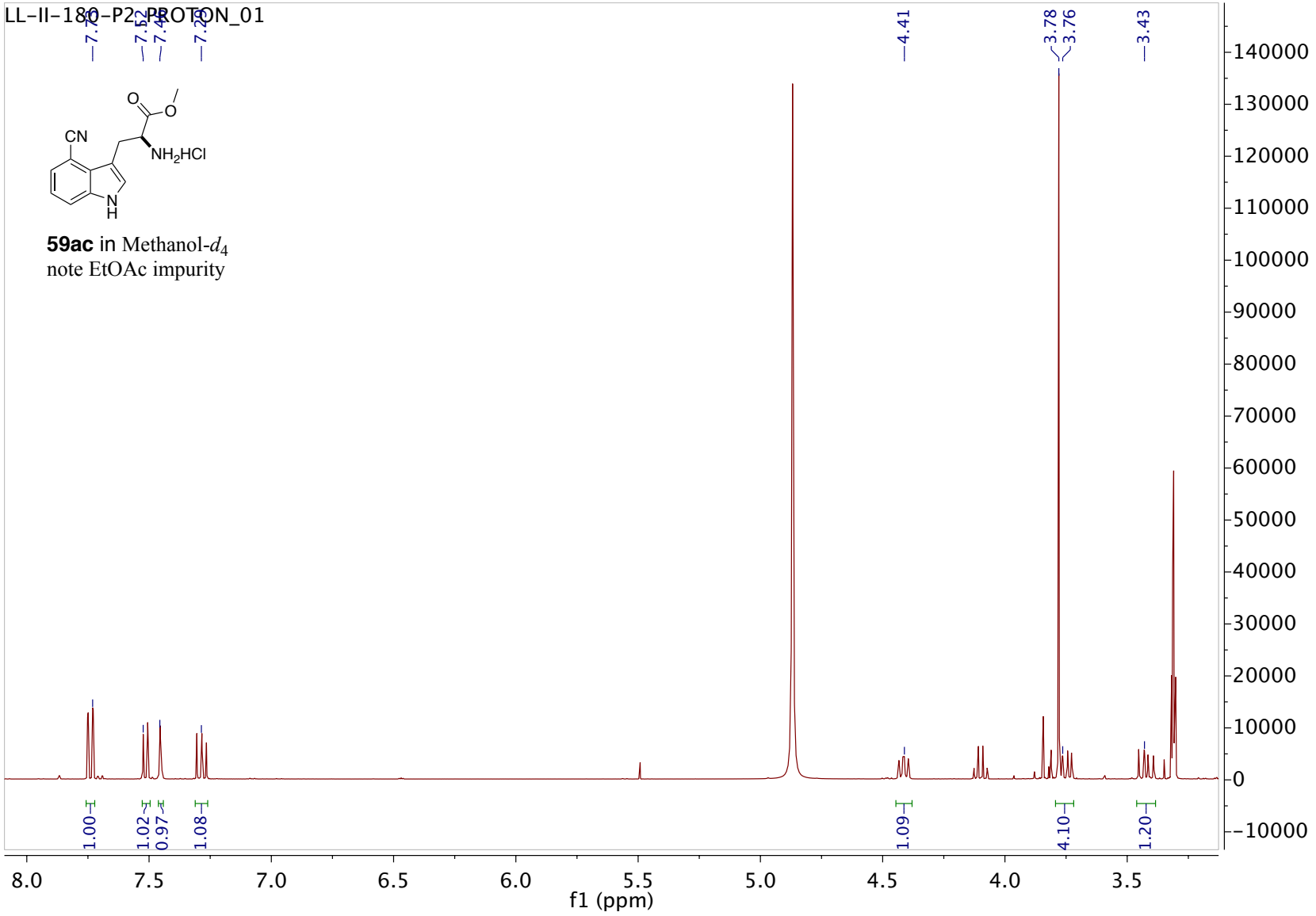
LL-II-180-P2-PROTON_01
7.75
7.52
7.44
7.29
4.41
3.78
3.76
3.43
O
O
CN
NH2HCl
N
H
59ac in Methanol-d4
note EtOAc impurity
140000
130000
120000
110000
100000
90000
80000
70000
60000
50000
40000
30000
20000
10000
0
-10000
1.00
1.02
0.97
1.08
1.09
4.10
1.20
8.0
7.5
7.0
6.5
6.0
5.5
5.0
4.5
4.0
3.5
f1 (ppm)

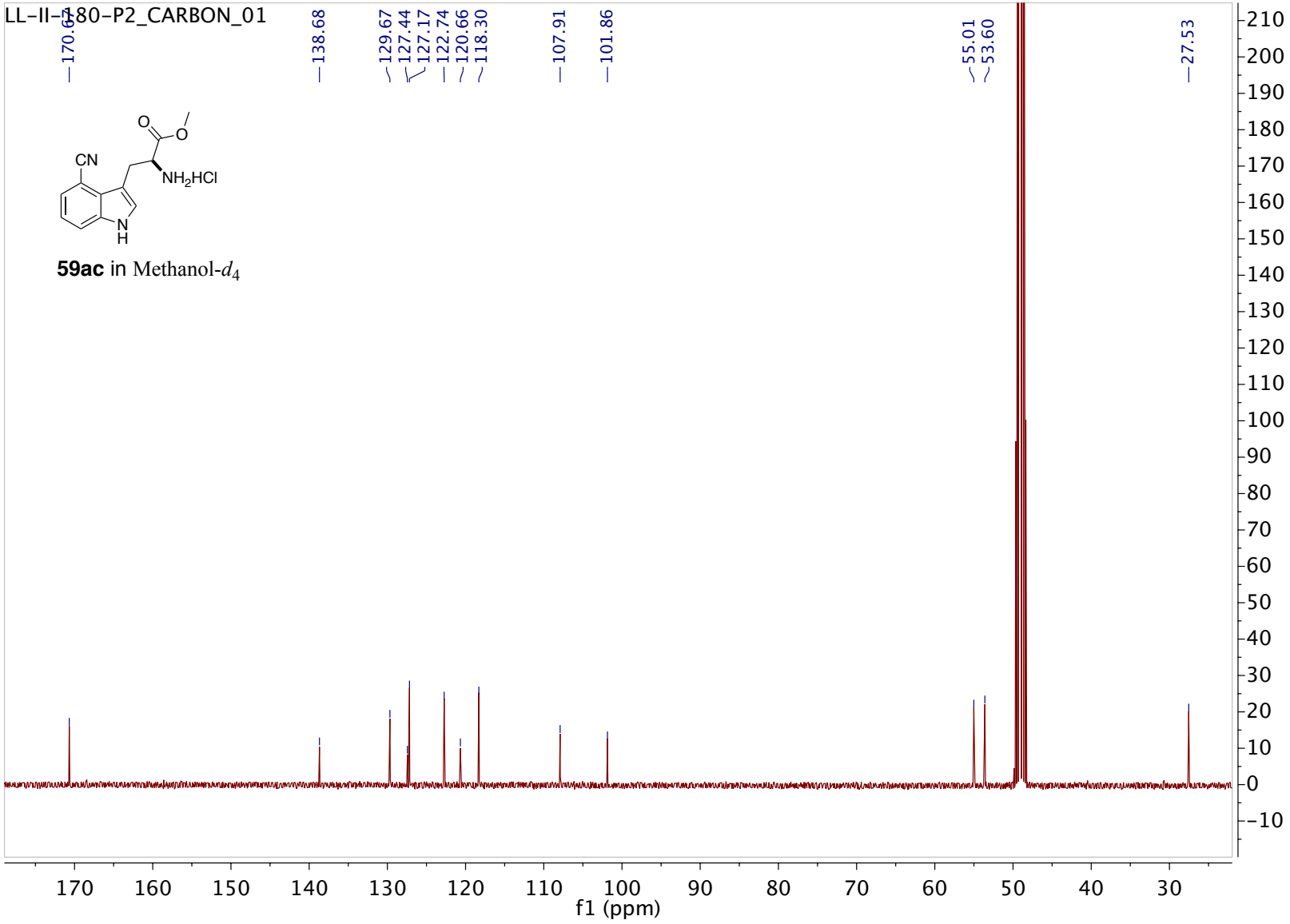
LL-II-180-P2_CARBON_01
170.67
138.68
129.67
127.44
127.17
122.74
120.66
118.30
107.91
101.86
55.01
53.60
27.53
CN
O
O
NH2HCl
N
H
59ac in Methanol-d4
f1 (ppm)

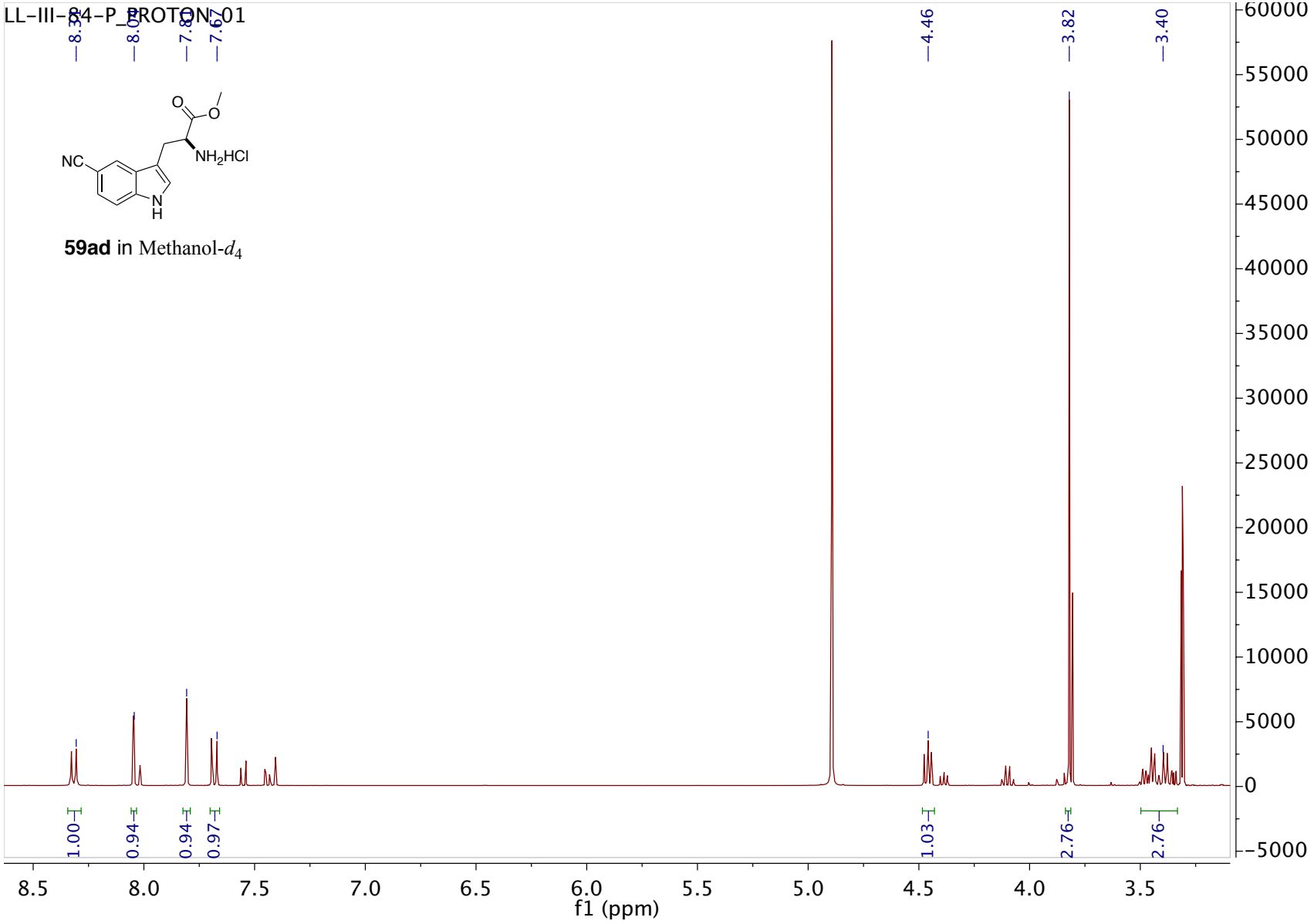
LL-III-84-P_PROTON_01
8.33
8.05
7.82
7.67
4.46
3.82
3.40
O
O
NC
NH2HCl
N
H
59ad in Methanol-d4
60000
55000
50000
45000
40000
35000
30000
25000
20000
15000
10000
5000
0
-5000
1.00
0.94
0.94
0.97
1.03
2.76
2.76
8.5
8.0
7.5
7.0
6.5
6.0
5.5
5.0
4.5
4.0
3.5
f1 (ppm)

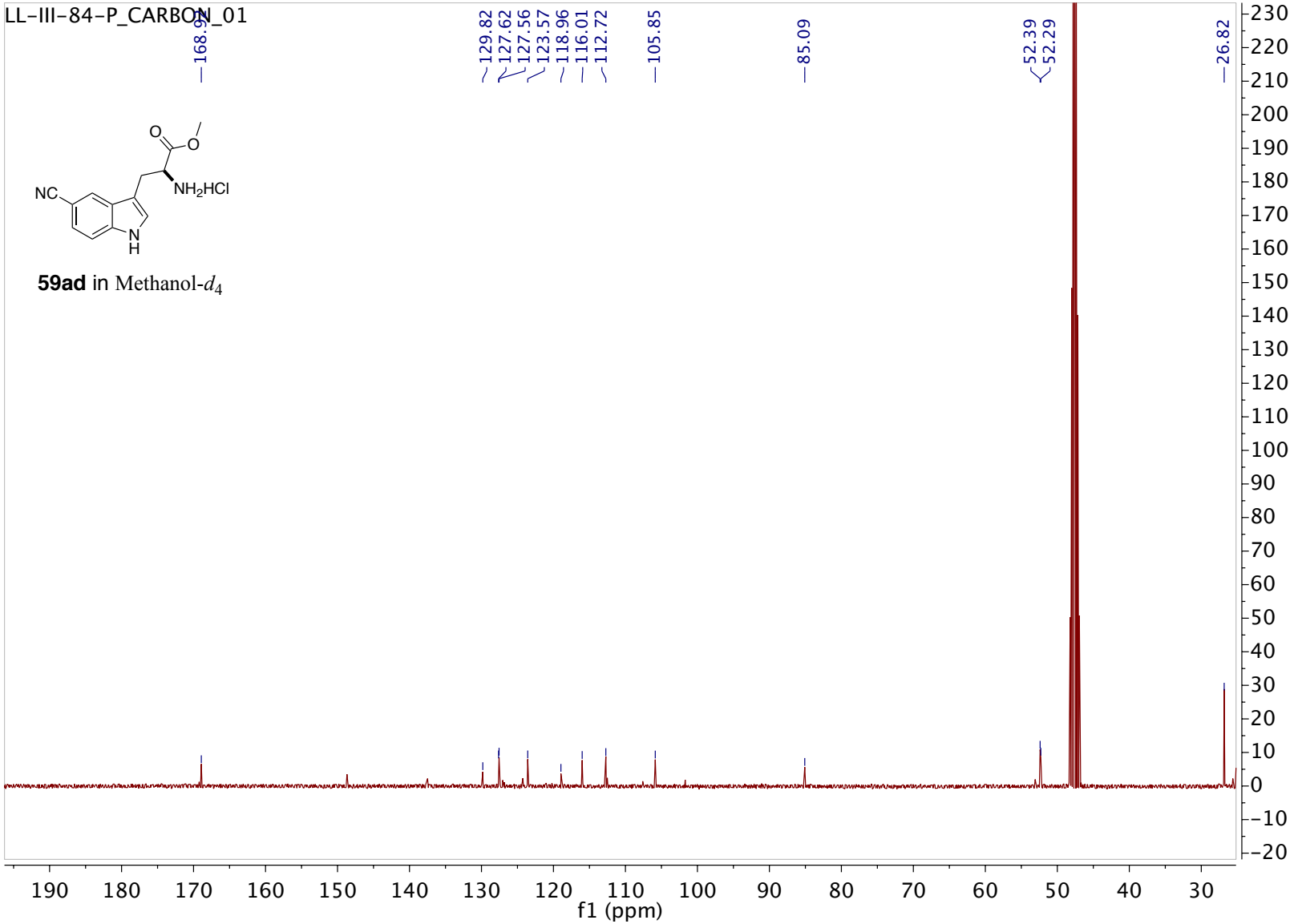
LL-III-84-P_CARBON_01
168.99
129.82
127.62
127.56
123.57
118.96
116.01
112.72
105.85
85.09
52.39
52.29
26.82
NC
O
O
NH2HCl
N
H
59ad in Methanol-d4
f1 (ppm)

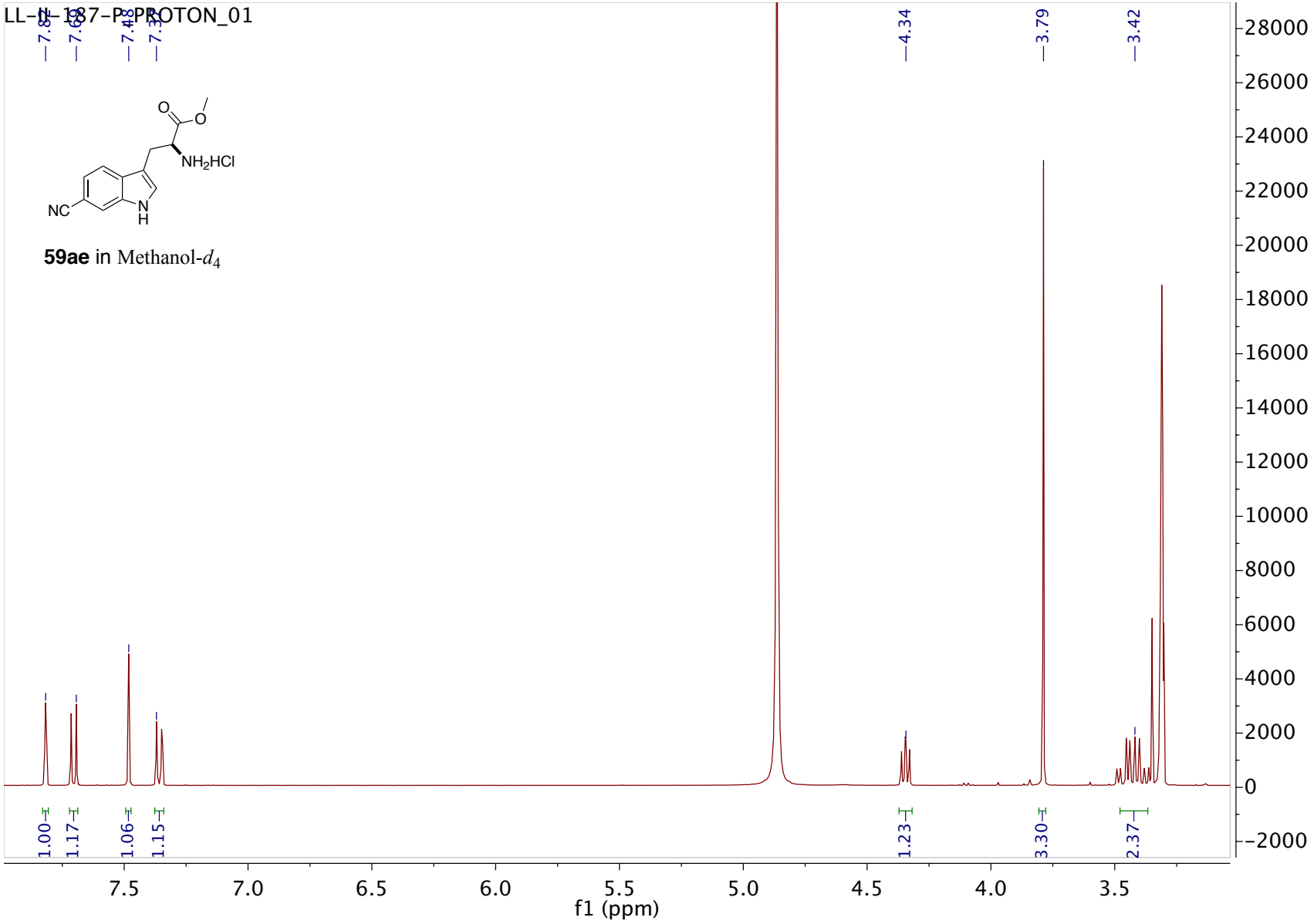
LL-IL-187-P PROTON_01
7.85
7.83
7.48
7.33
4.34
3.79
3.42
O
O
NH2HCl
NC
N
H
59ae in Methanol-d4
28000
26000
24000
22000
20000
18000
16000
14000
12000
10000
8000
6000
4000
2000
0
-2000
1.00
1.17
1.06
1.15
1.23
3.30
2.37
7.5
7.0
6.5
6.0
5.5
5.0
4.5
4.0
3.5
f1 (ppm)

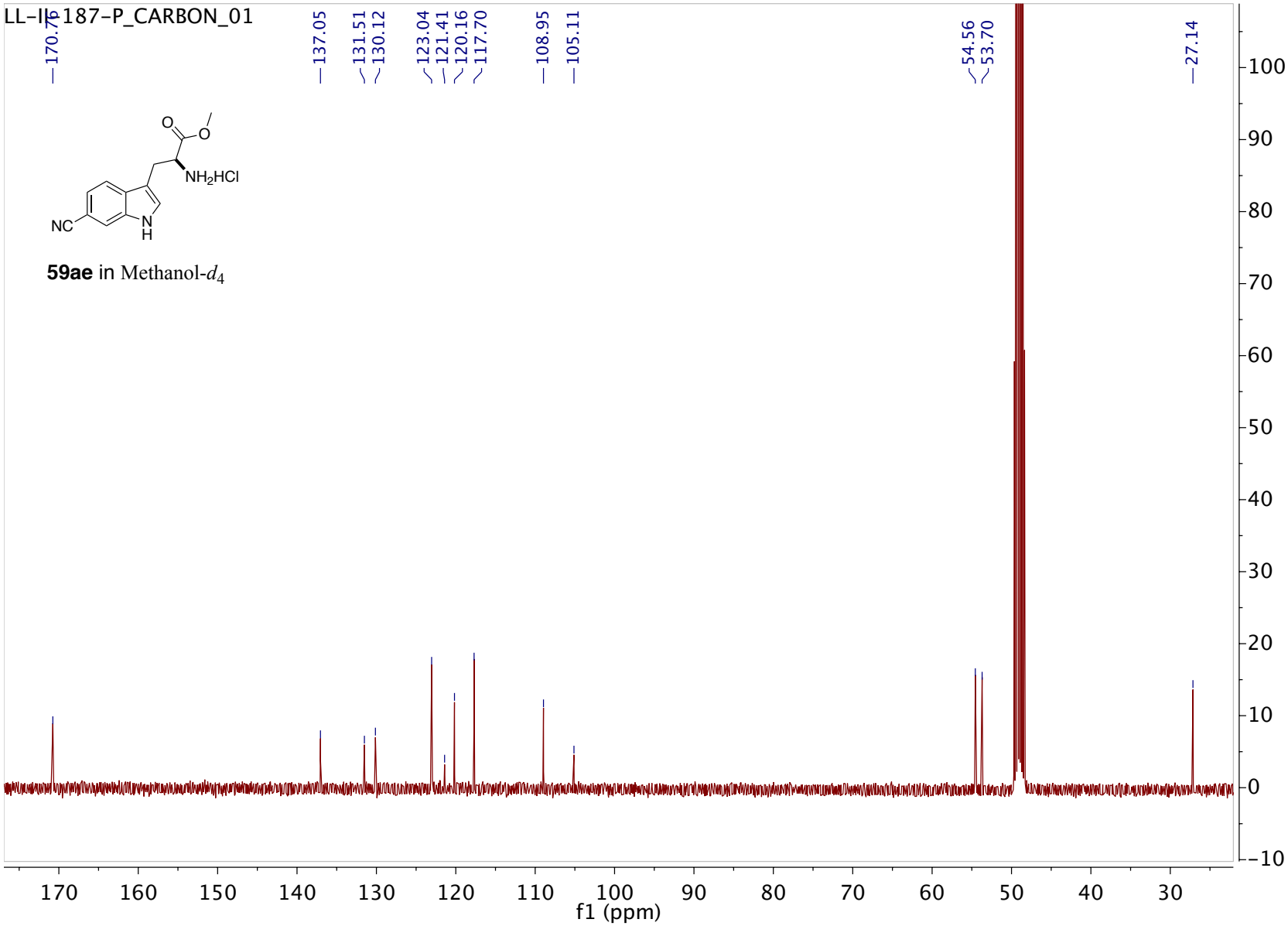
LL-IL-187-P_CARBON_01
170.76
137.05
131.51
130.12
123.04
121.41
120.16
117.70
108.95
105.11
54.56
53.70
27.14
O
O
NH2HCl
NC
N
H
59ae in Methanol-d4
f1 (ppm)

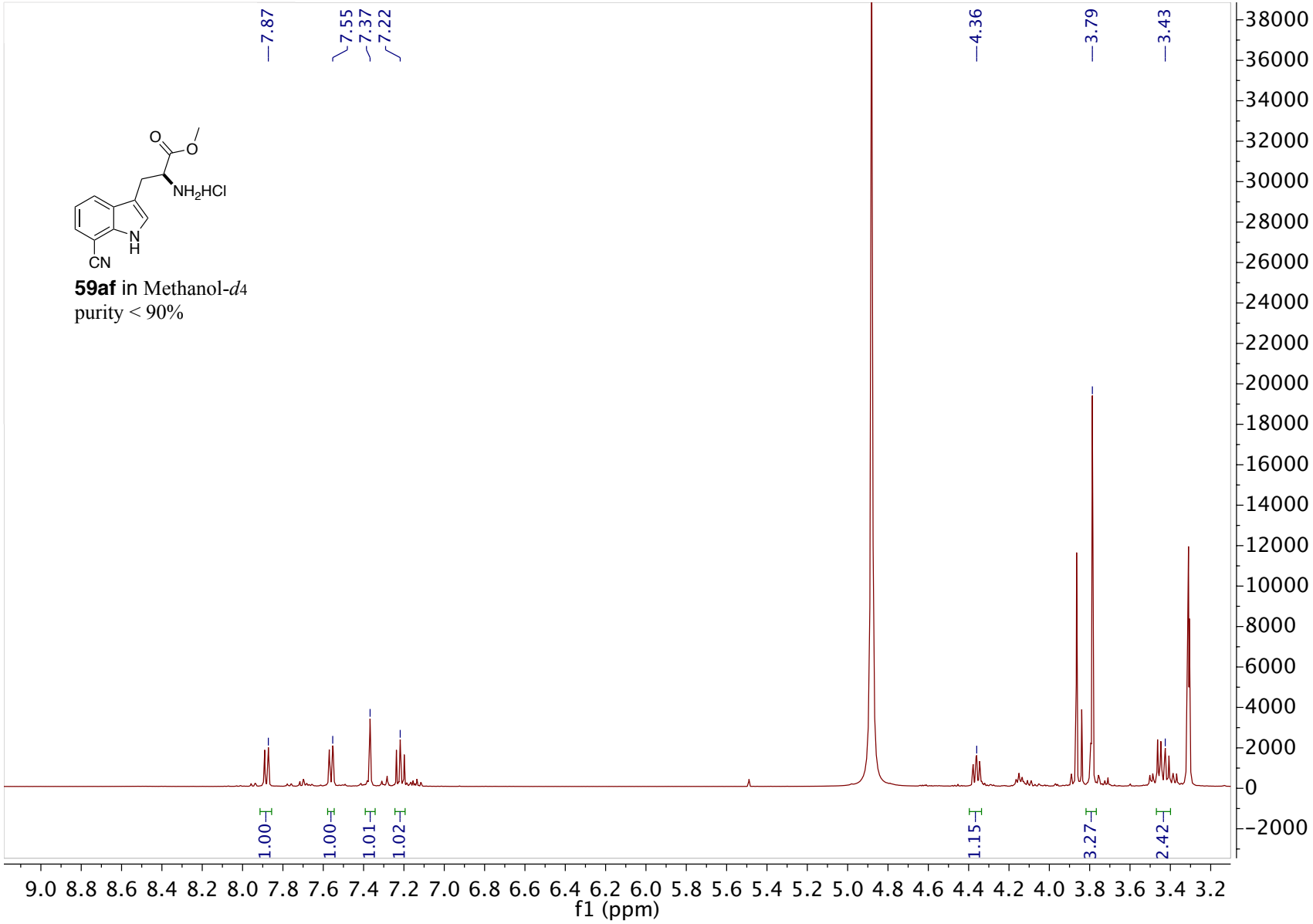

59af in Methanol-*d*4
purity < 90%

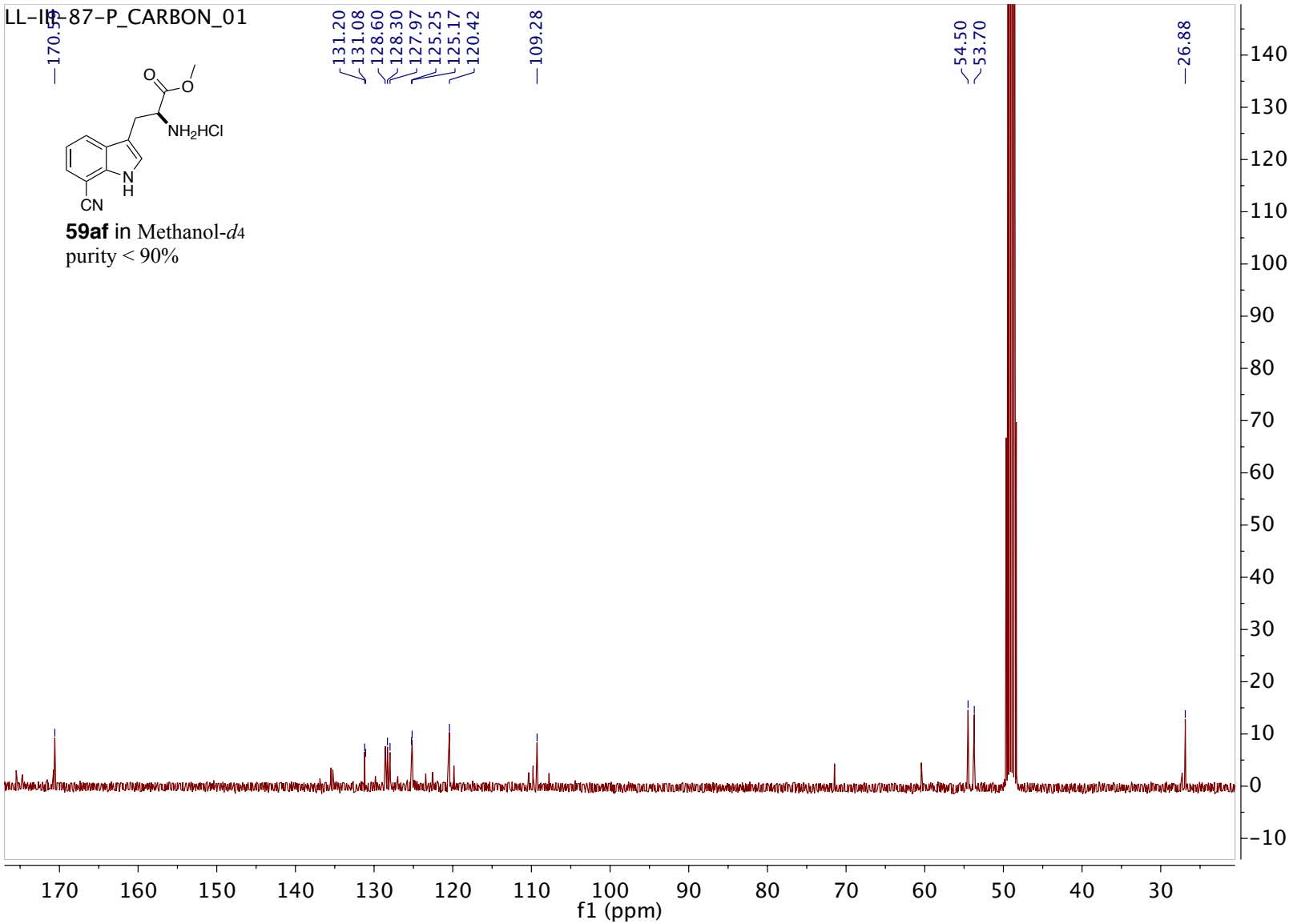
LL-IB-87-P_CARBON_01
170.57
131.20
131.08
128.60
128.30
127.97
125.25
125.17
120.42
109.28
54.50
53.70
26.88
O
O
NH2HCl
N
H
CN
59af in Methanol-d4
purity < 90%
f1 (ppm)

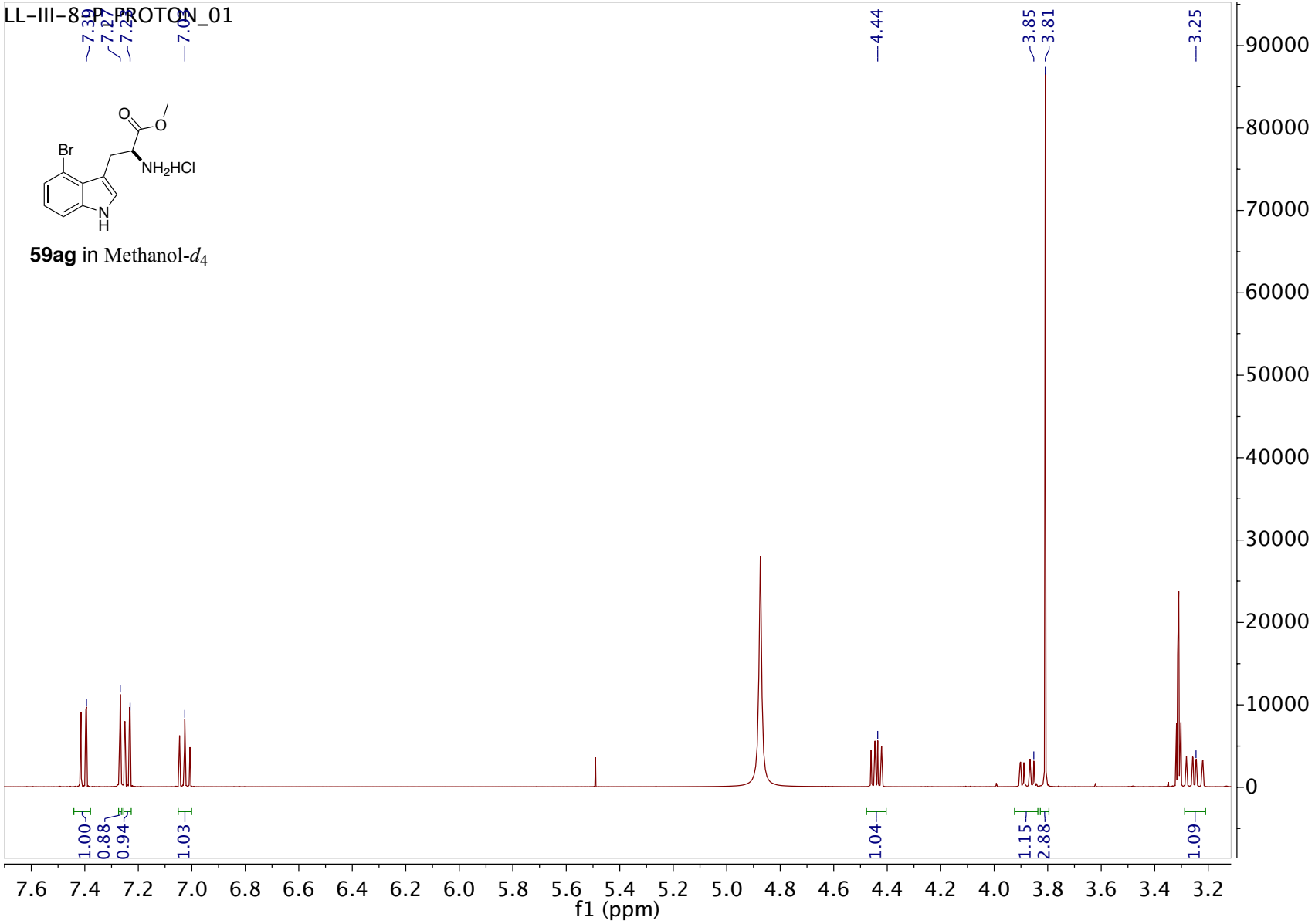
LL-III-8-P PROTON_01
7.39
7.27
7.22
7.05
4.44
3.85
3.81
3.25
Br
NH2HCl
N
H
59ag in Methanol-d4
1.00
0.88
0.94
1.03
1.04
1.15
2.88
1.09
f1 (ppm)

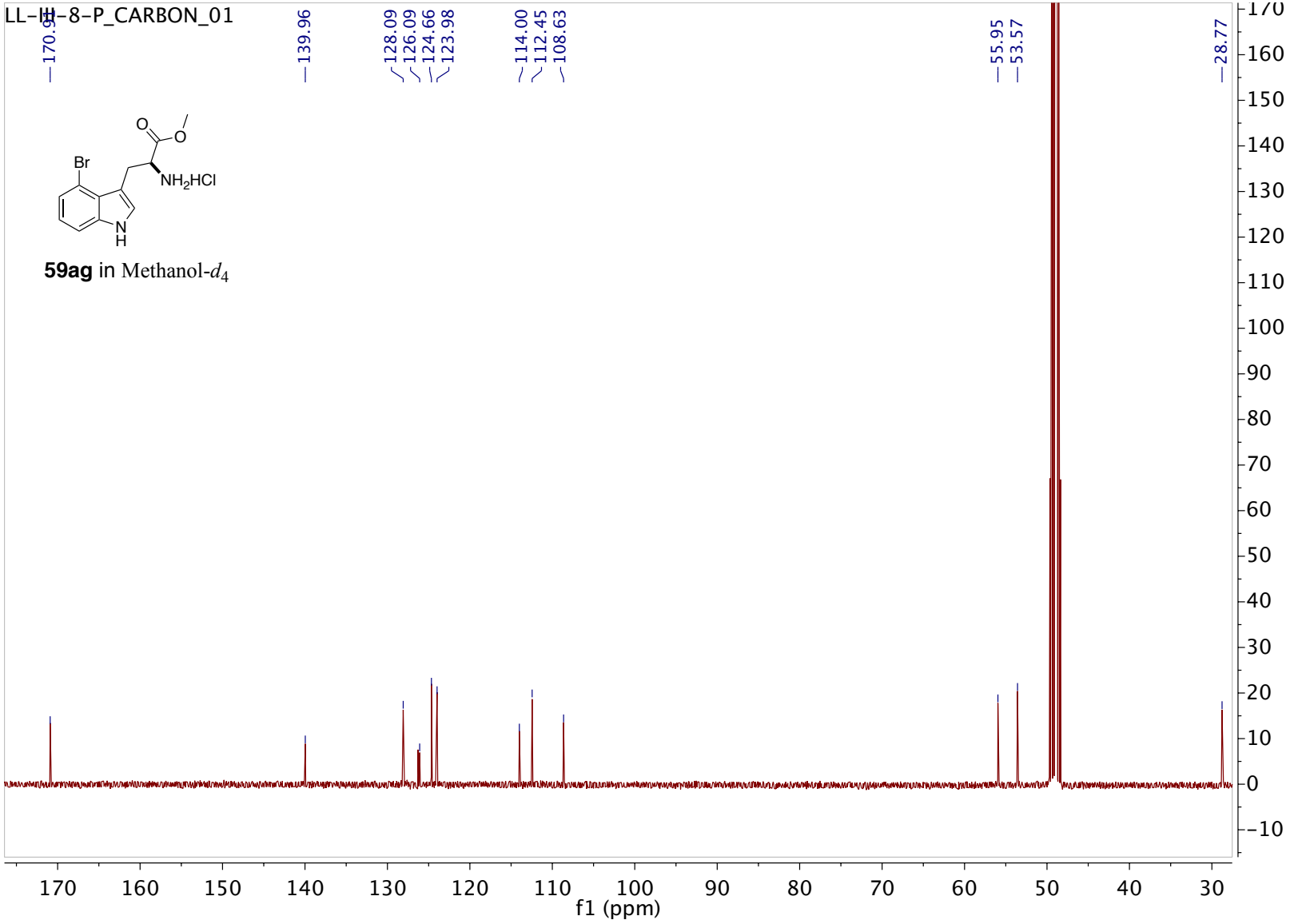
LL-IH-8-P_CARBON_01
170.93
139.96
128.09
126.09
124.66
123.98
114.00
112.45
108.63
55.95
53.57
28.77
Br
O
O
NH2HCl
N
H
59ag in Methanol-d4
f1 (ppm)

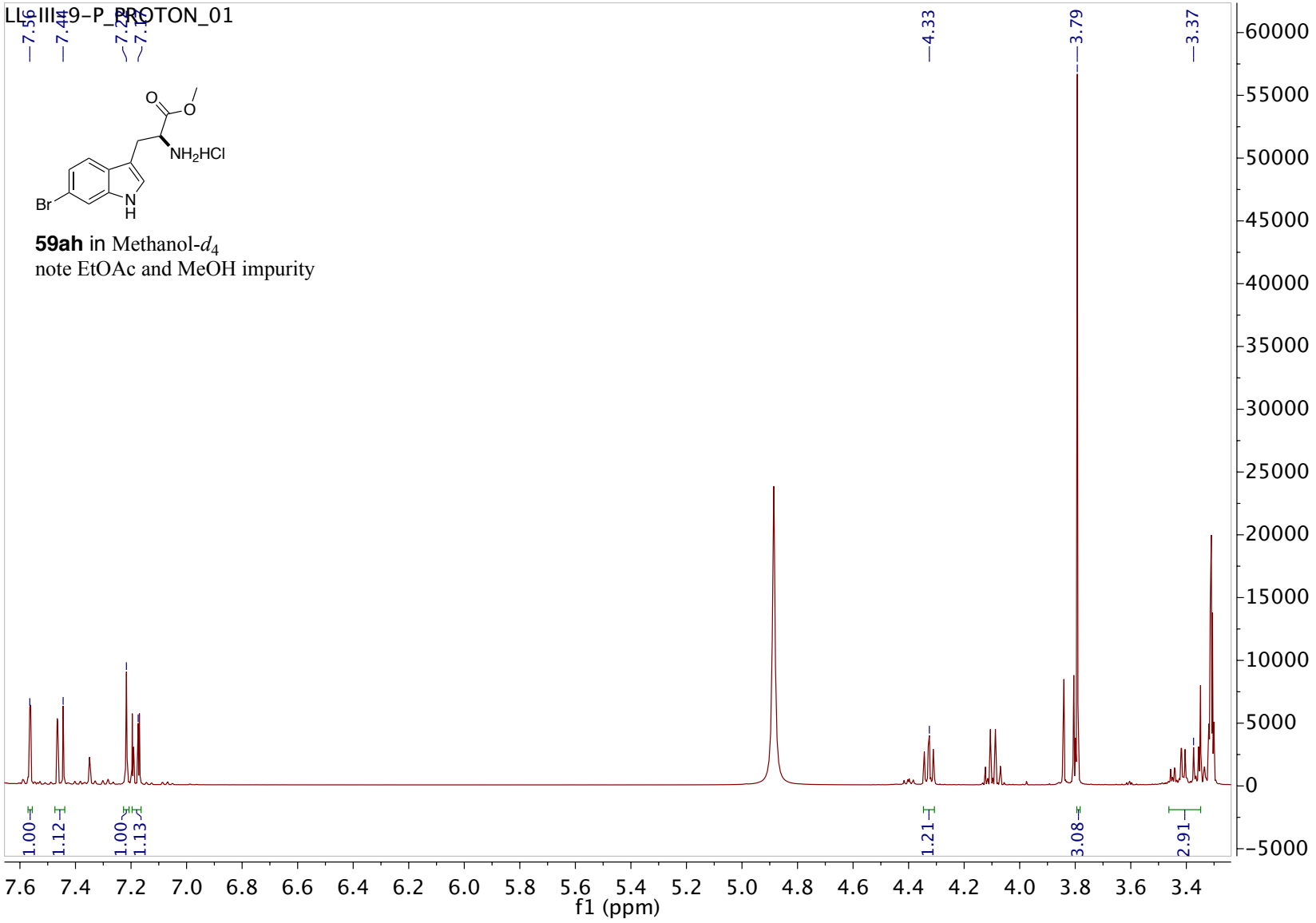
LL-III-9-P_PROTON_01
7.56
7.44
7.22
7.14
4.33
3.79
3.37
O
O
NH2HCl
Br
N
H
59ah in Methanol-d4
note EtOAc and MeOH impurity
1.00
1.12
1.00
1.13
1.21
3.08
2.91
60000
55000
50000
45000
40000
35000
30000
25000
20000
15000
10000
5000
0
-5000
7.6
7.4
7.2
7.0
6.8
6.6
6.4
6.2
6.0
5.8
5.6
5.4
5.2
5.0
4.8
4.6
4.4
4.2
4.0
3.8
3.6
3.4
f1 (ppm)

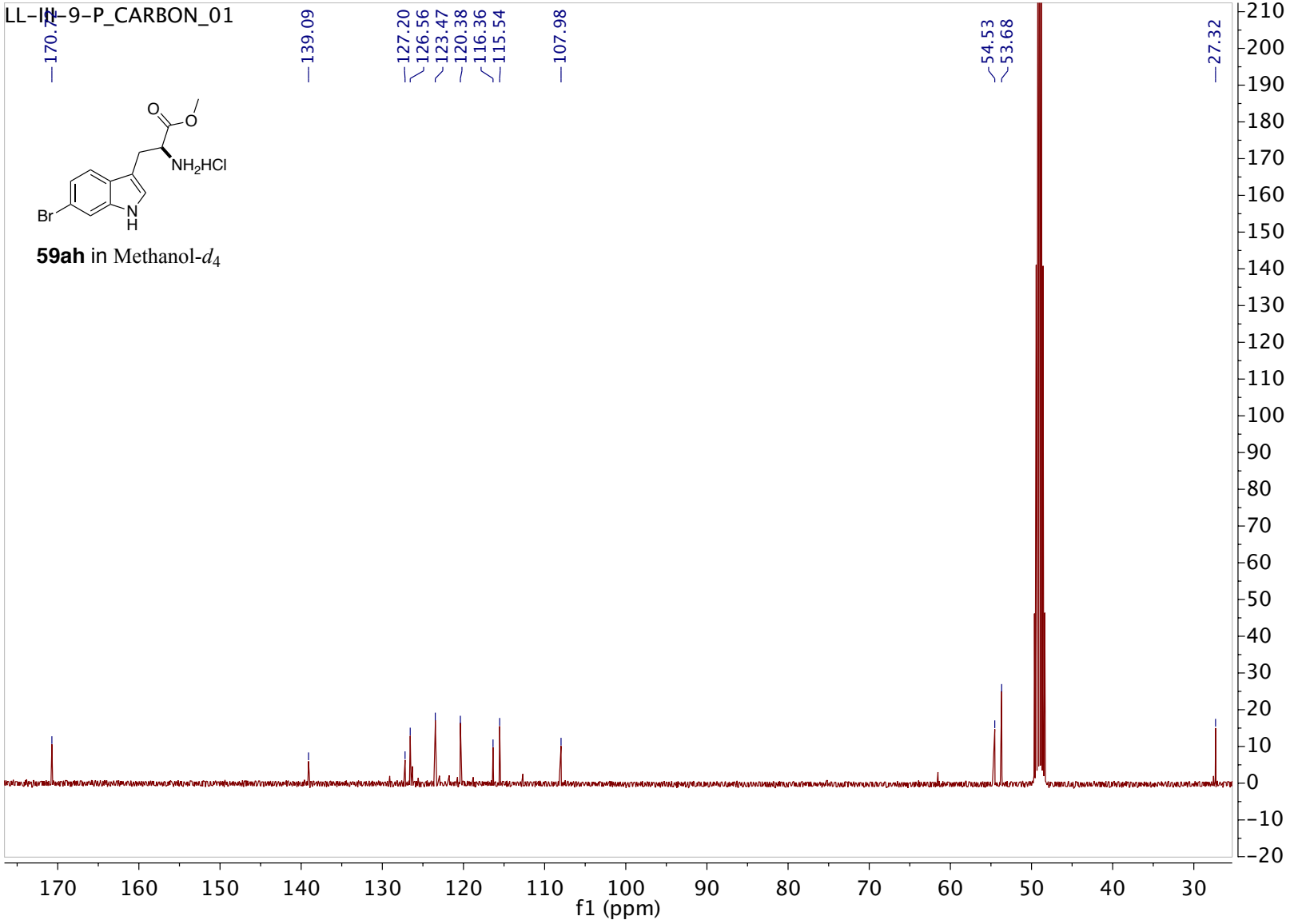
LL-IN-9-P_CARBON_01
170.77
139.09
127.20
126.56
123.47
120.38
116.36
115.54
107.98
54.53
53.68
27.32
O
O
NH2HCl
Br
N
H
59ah in Methanol-d4
f1 (ppm)

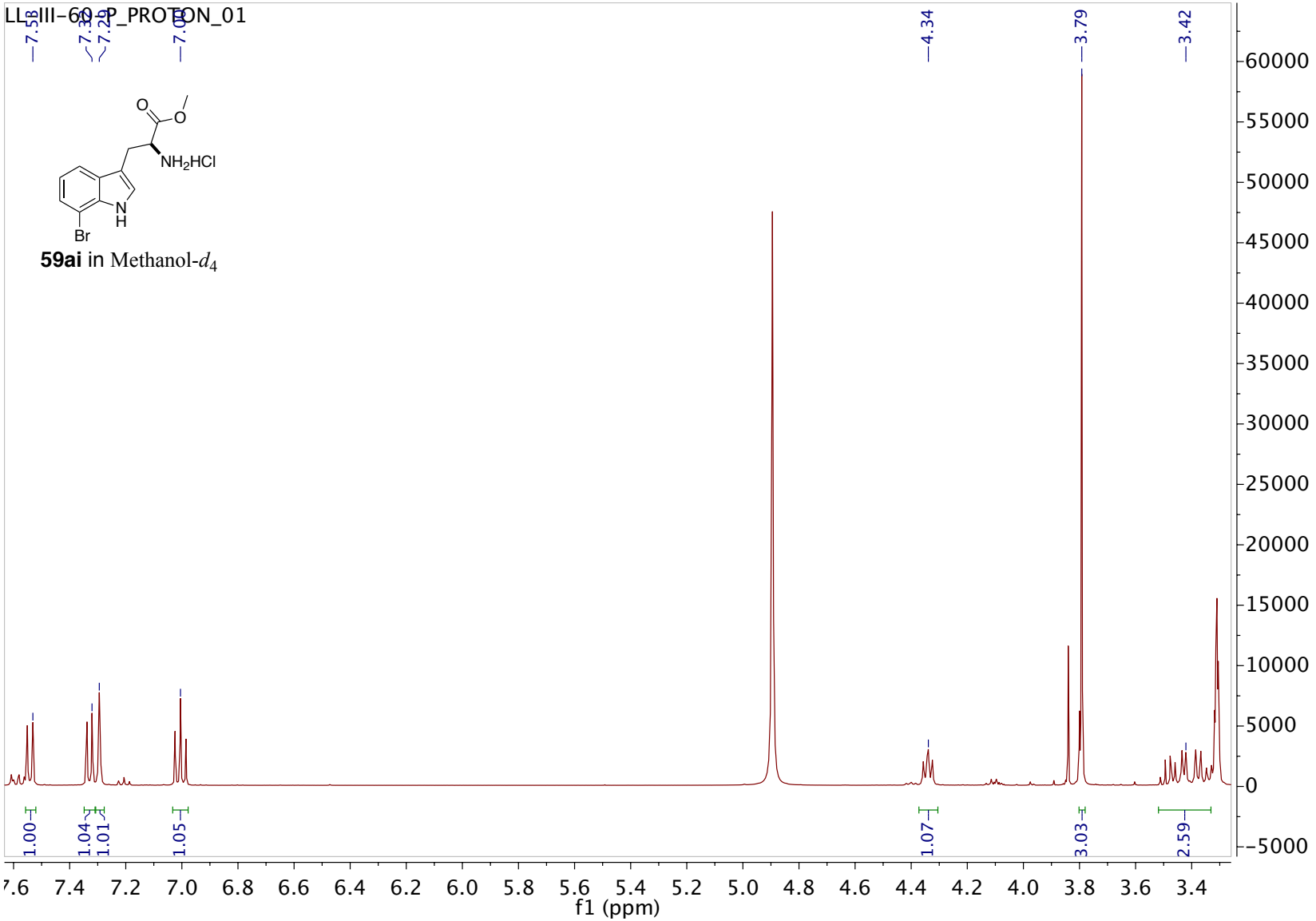
LL-III-60-P_PROTON_01
7.58
7.33
7.22
7.00
4.34
3.79
3.42
O
O
NH2HCl
N
H
Br
59ai in Methanol-d4
60000
55000
50000
45000
40000
35000
30000
25000
20000
15000
10000
5000
0
-5000
1.00
1.04
1.01
1.05
1.07
3.03
2.59
7.6
7.4
7.2
7.0
6.8
6.6
6.4
6.2
6.0
5.8
5.6
5.4
5.2
5.0
4.8
4.6
4.4
4.2
4.0
3.8
3.6
3.4
f1 (ppm)

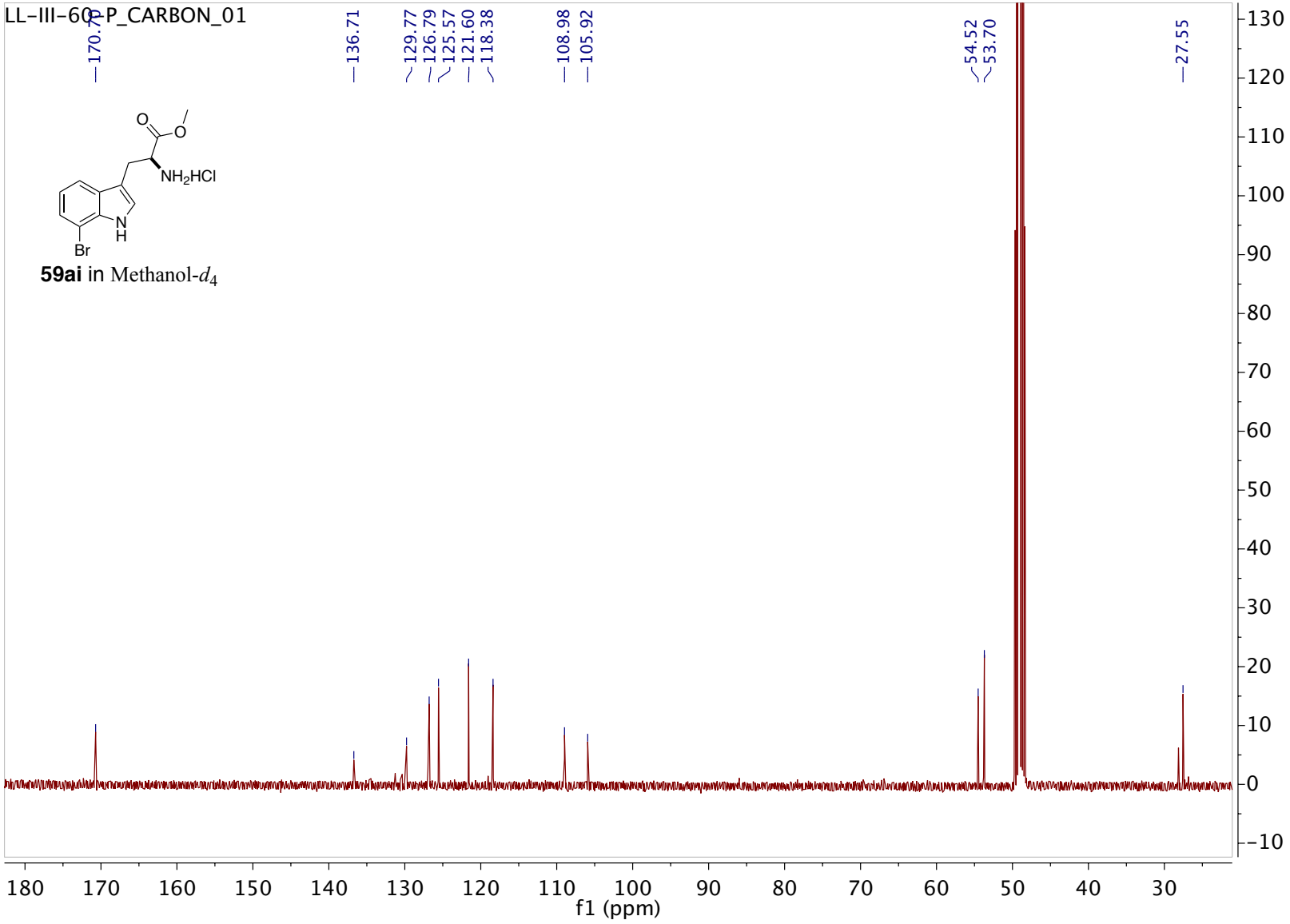
LL-III-60-P_CARBON_01
170.77
136.71
129.77
126.79
125.57
121.60
118.38
108.98
105.92
54.52
53.70
27.55
O
O
NH2HCl
N
H
Br
59ai in Methanol-d4
f1 (ppm)

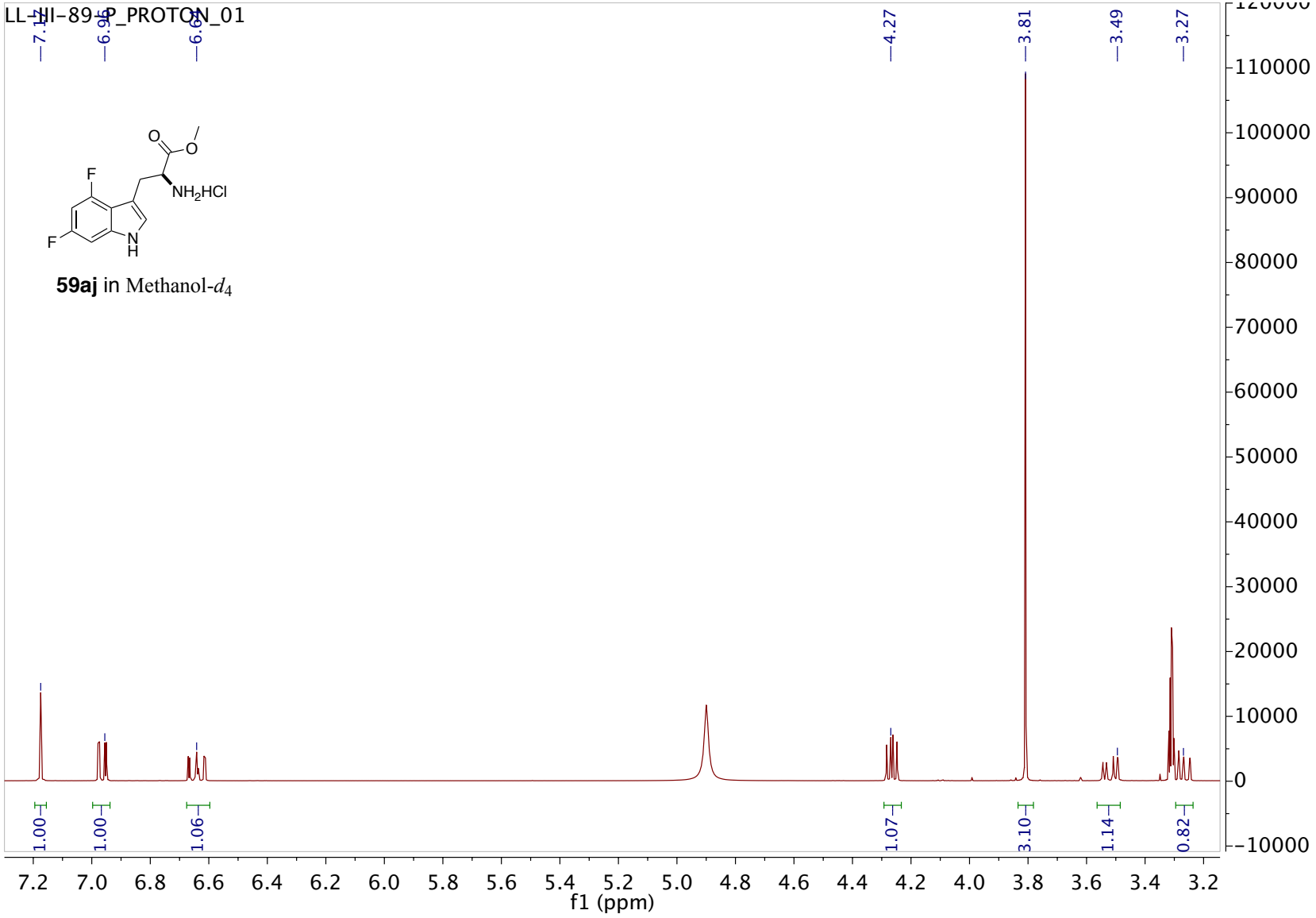
LL-JII-89-P_PROTON_01
7.19
6.96
6.82
4.27
3.81
3.49
3.27
O
O
F
NH2HCl
F
N
H
59aj in Methanol-d4
1.00
1.00
1.06
1.07
3.10
1.14
0.82
f1 (ppm)

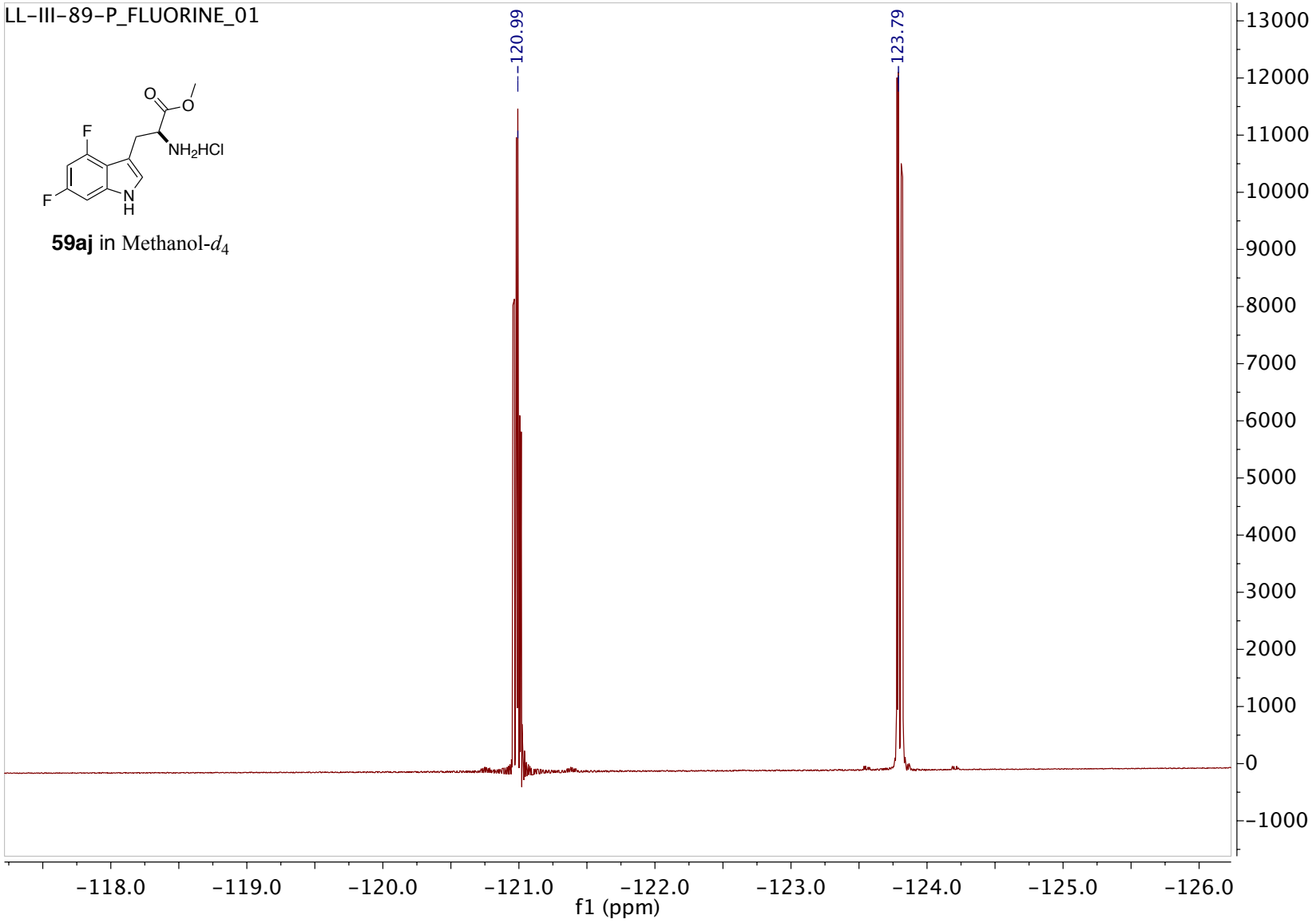
LL-III-89-P_FLUORINE_01
-120.99
-123.79
F
O
O
NH2HCl
F
N
H
59aj in Methanol-d4
13000
12000
11000
10000
9000
8000
7000
6000
5000
4000
3000
2000
1000
0
-1000
-118.0
-119.0
-120.0
-121.0
-122.0
-123.0
-124.0
-125.0
-126.0
f1 (ppm)

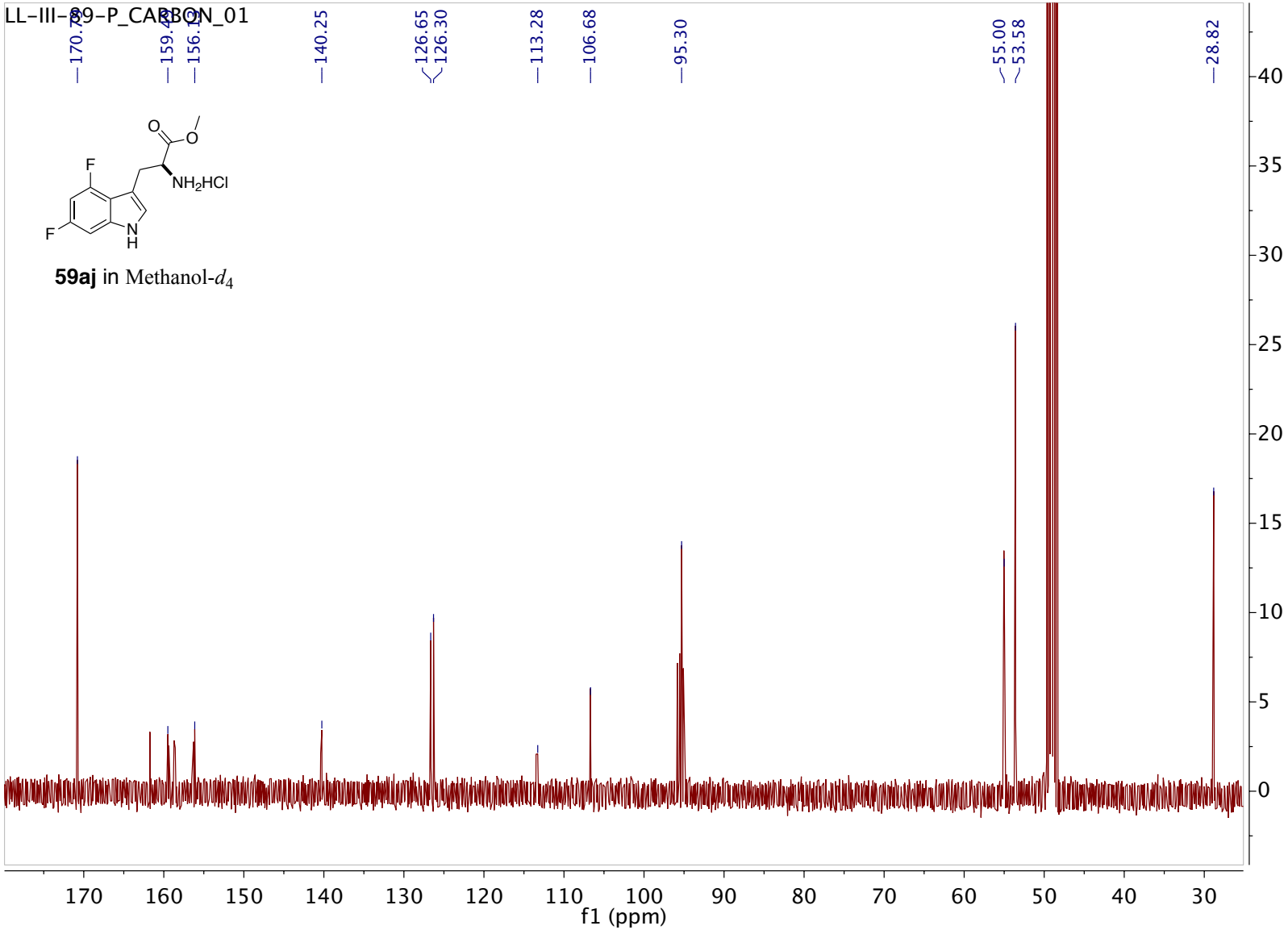
LL-III-89-P_CARBON_01
170.72
159.43
156.21
140.25
126.65
126.30
113.28
106.68
95.30
55.00
53.58
28.82
O
O
F
NH2HCl
F
N
H
59aj in Methanol-d4
40
35
30
25
20
15
10
5
0
170
160
150
140
130
120
110
100
90
80
70
60
50
40
30
f1 (ppm)

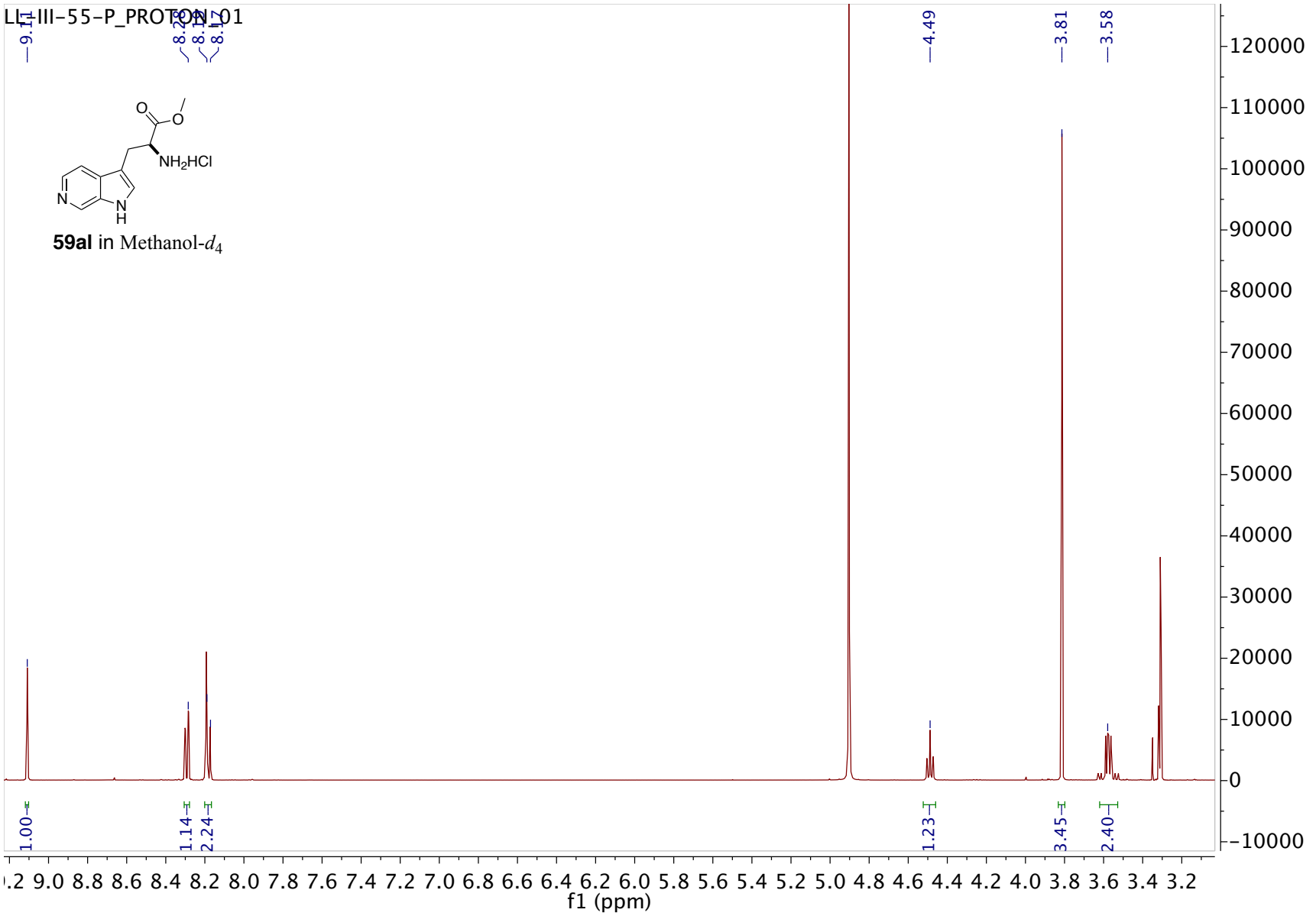
LL-III-55-P_PROTON_01
9.11
8.21
8.17
8.17
4.49
3.81
3.58
O
O
NH2HCl
N
N
H
59al in Methanol-d4
120000
110000
100000
90000
80000
70000
60000
50000
40000
30000
20000
10000
0
-10000
1.00
1.14
2.24
1.23
3.45
2.40
.2 9.0 8.8 8.6 8.4 8.2 8.0 7.8 7.6 7.4 7.2 7.0 6.8 6.6 6.4 6.2 6.0 5.8 5.6 5.4 5.2 5.0 4.8 4.6 4.4 4.2 4.0 3.8 3.6 3.4 3.2
f1 (ppm)

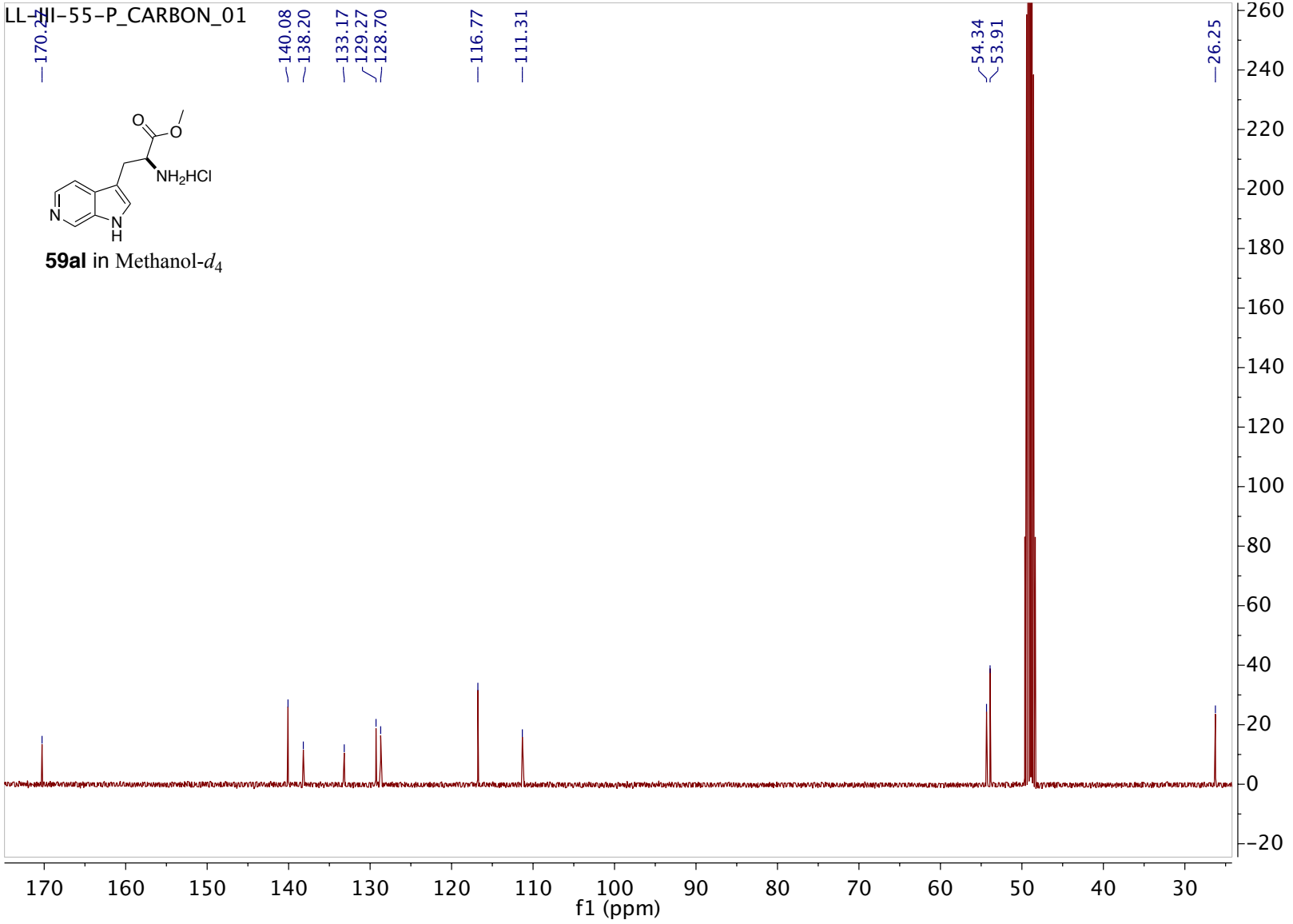
LL-JH-55-P_CARBON_01
170.22
140.08
138.20
133.17
129.27
128.70
116.77
111.31
54.34
53.91
26.25
O
O
NH2HCl
N
N
H
59al in Methanol-d4
260
240
220
200
180
160
140
120
100
80
60
40
20
0
-20
170
160
150
140
130
120
110
100
90
80
70
60
50
40
30
f1 (ppm)

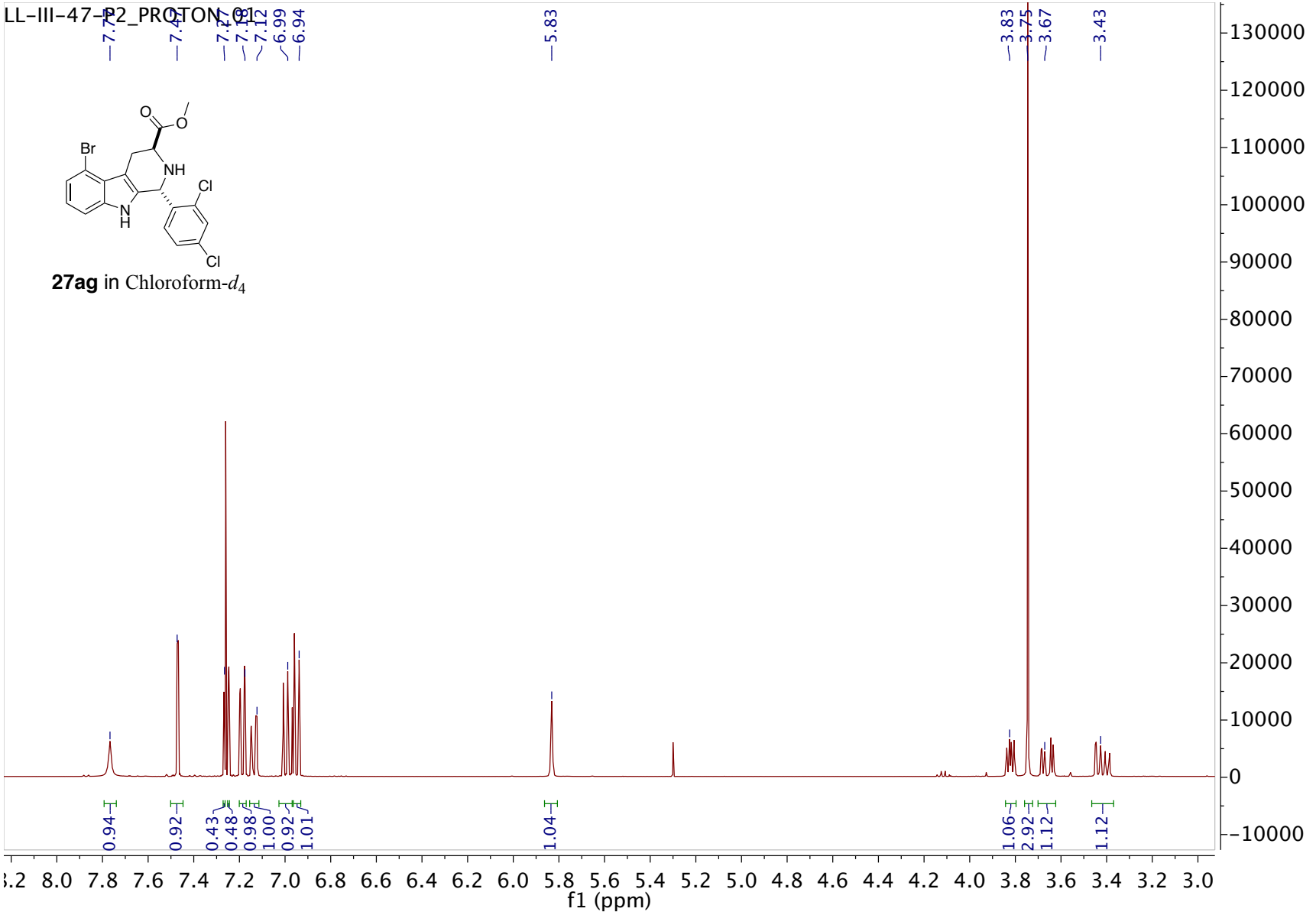
LL-III-47-P2_PROTON_01
7.77
7.43
7.41
7.12
7.12
6.99
6.94
5.83
3.83
3.75
3.67
3.43
Br
NH
Cl
N
H
Cl
O
O
27ag in Chloroform-d4
0.94
0.92
0.43
0.48
0.98
1.00
0.92
1.01
1.04
1.06
2.92
1.12
1.12
130000
120000
110000
100000
90000
80000
70000
60000
50000
40000
30000
20000
10000
0
-10000
8.2 8.0 7.8 7.6 7.4 7.2 7.0 6.8 6.6 6.4 6.2 6.0 5.8 5.6 5.4 5.2 5.0 4.8 4.6 4.4 4.2 4.0 3.8 3.6 3.4 3.2 3.0
f1 (ppm)

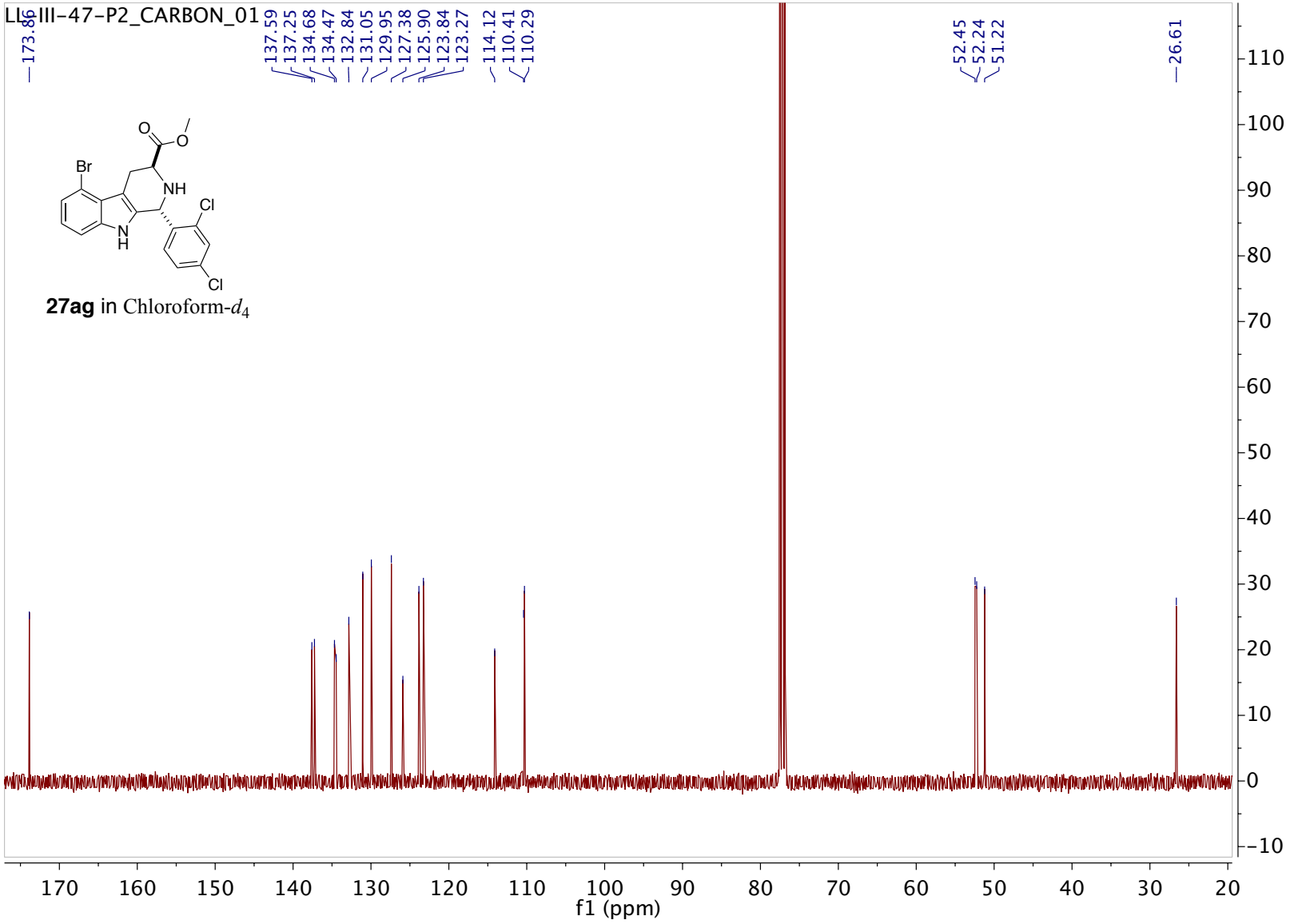
LL-III-47-P2_CARBON_01
173.86
137.59
137.25
134.68
134.47
132.84
131.05
129.95
127.38
125.90
123.84
123.27
114.12
110.41
110.29
52.45
52.24
51.22
26.61
Br
NH
N
H
Cl
Cl
O
O
27ag in Chloroform-d4
f1 (ppm)

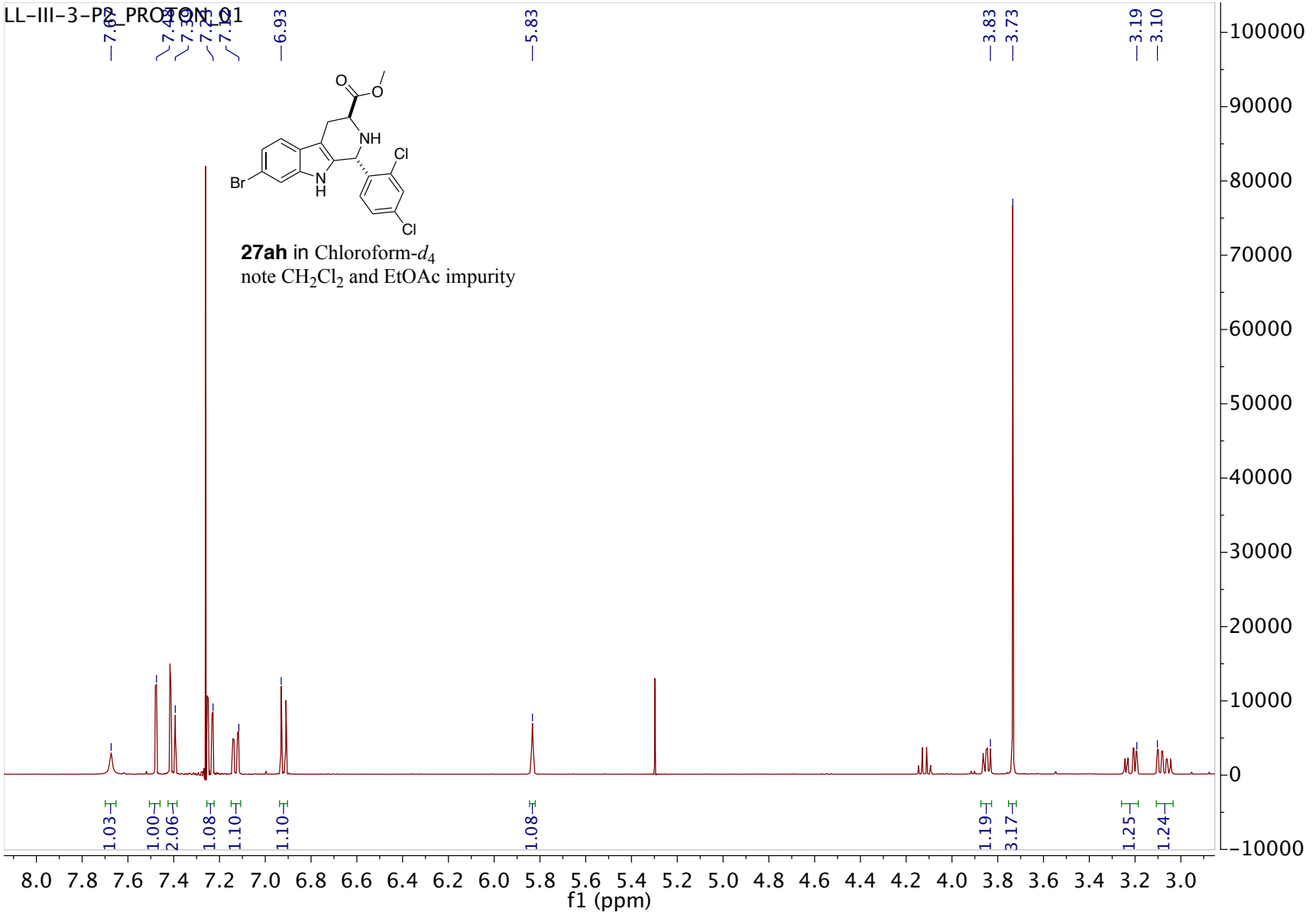
LL-III-3-P2_PROTON_01
7.61
7.43
7.33
7.24
7.14
6.93
5.83
3.83
3.73
3.19
3.10
O
O
NH
Cl
Br
N
H
Cl
27ah in Chloroform-d4
note CH2Cl2 and EtOAc impurity
1.03
1.00
2.06
1.08
1.10
1.10
1.08
1.19
3.17
1.25
1.24
100000
90000
80000
70000
60000
50000
40000
30000
20000
10000
0
-10000
8.0 7.8 7.6 7.4 7.2 7.0 6.8 6.6 6.4 6.2 6.0 5.8 5.6 5.4 5.2 5.0 4.8 4.6 4.4 4.2 4.0 3.8 3.6 3.4 3.2 3.0
f1 (ppm)

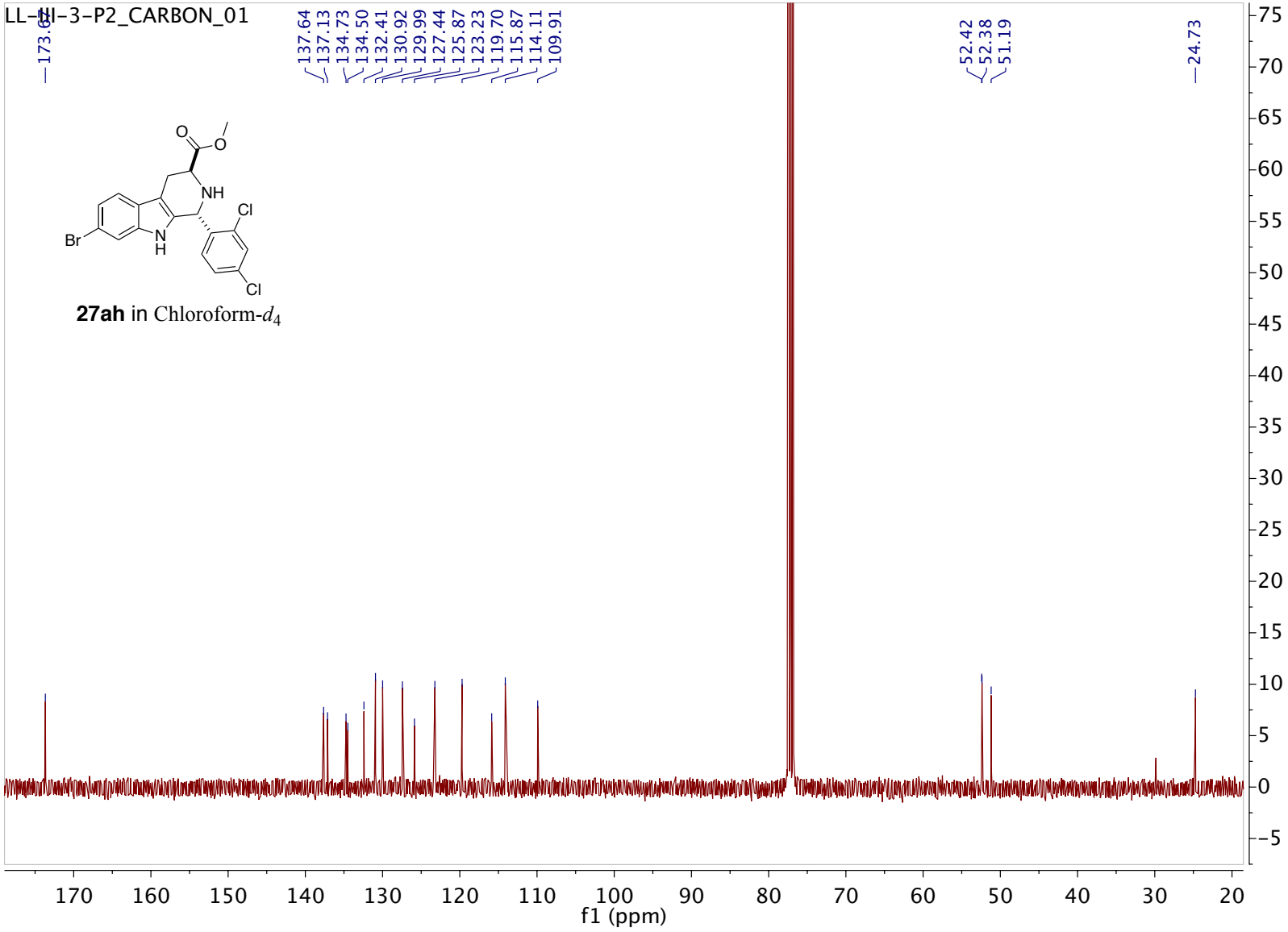
LL-III-3-P2_CARBON_01
173.62
137.64
137.13
134.73
134.50
132.41
130.92
129.99
127.44
125.87
123.23
119.70
115.87
114.11
109.91
52.42
52.38
51.19
24.73
O
O
NH
Br
N
H
Cl
Cl
27ah in Chloroform-d4
f1 (ppm)

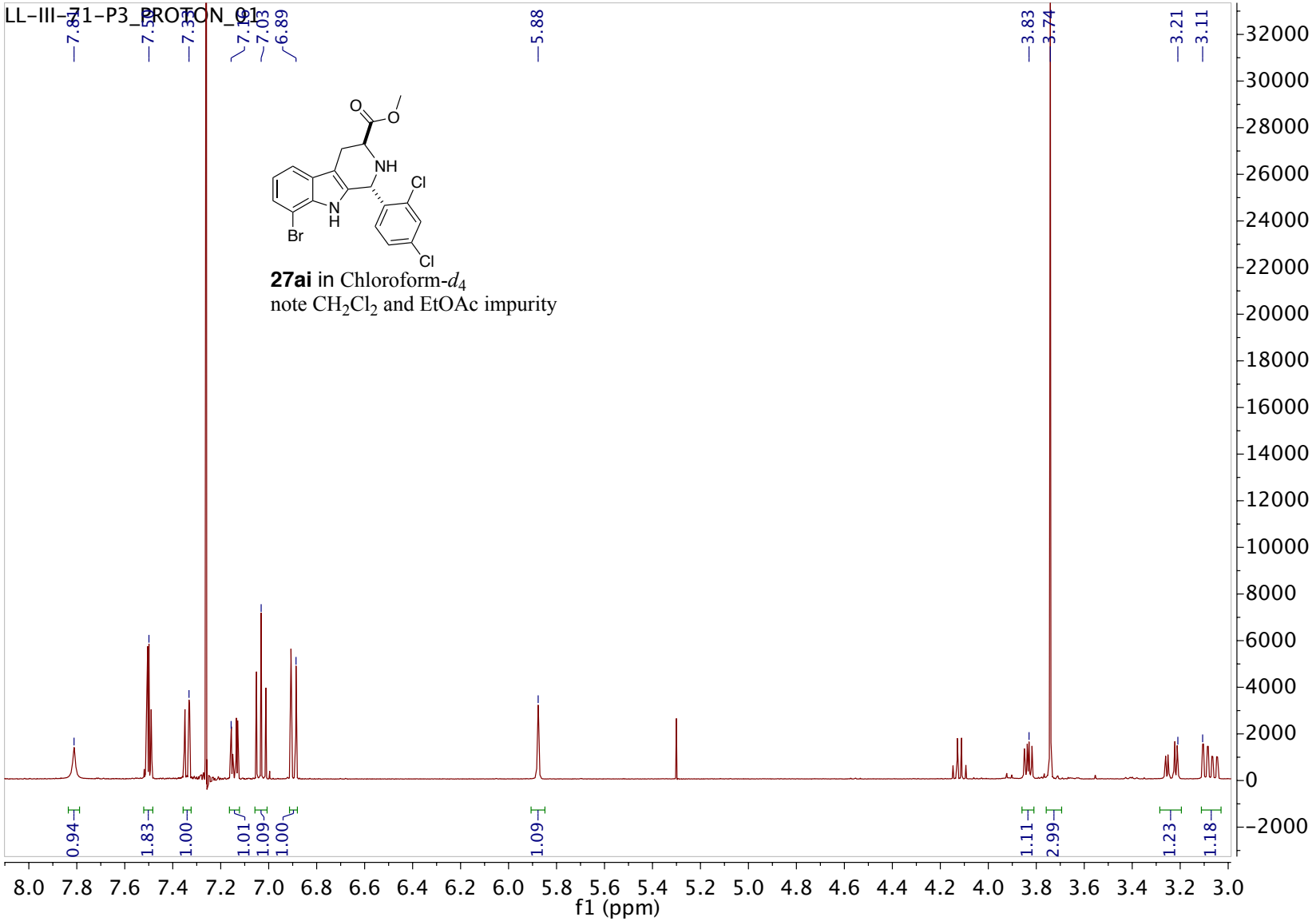
LL-III-71-P3_PROTON_01
7.81
7.55
7.33
7.13
7.03
6.89
5.88
3.83
3.74
3.21
3.11
O
O
NH
N
H
Br
Cl
Cl
27ai in Chloroform-d4
note CH2Cl2 and EtOAc impurity
0.94
1.83
1.00
1.01
1.09
1.00
1.09
1.11
2.99
1.23
1.18
32000
30000
28000
26000
24000
22000
20000
18000
16000
14000
12000
10000
8000
6000
4000
2000
0
-2000
8.0 7.8 7.6 7.4 7.2 7.0 6.8 6.6 6.4 6.2 6.0 5.8 5.6 5.4 5.2 5.0 4.8 4.6 4.4 4.2 4.0 3.8 3.6 3.4 3.2 3.0
f1 (ppm)

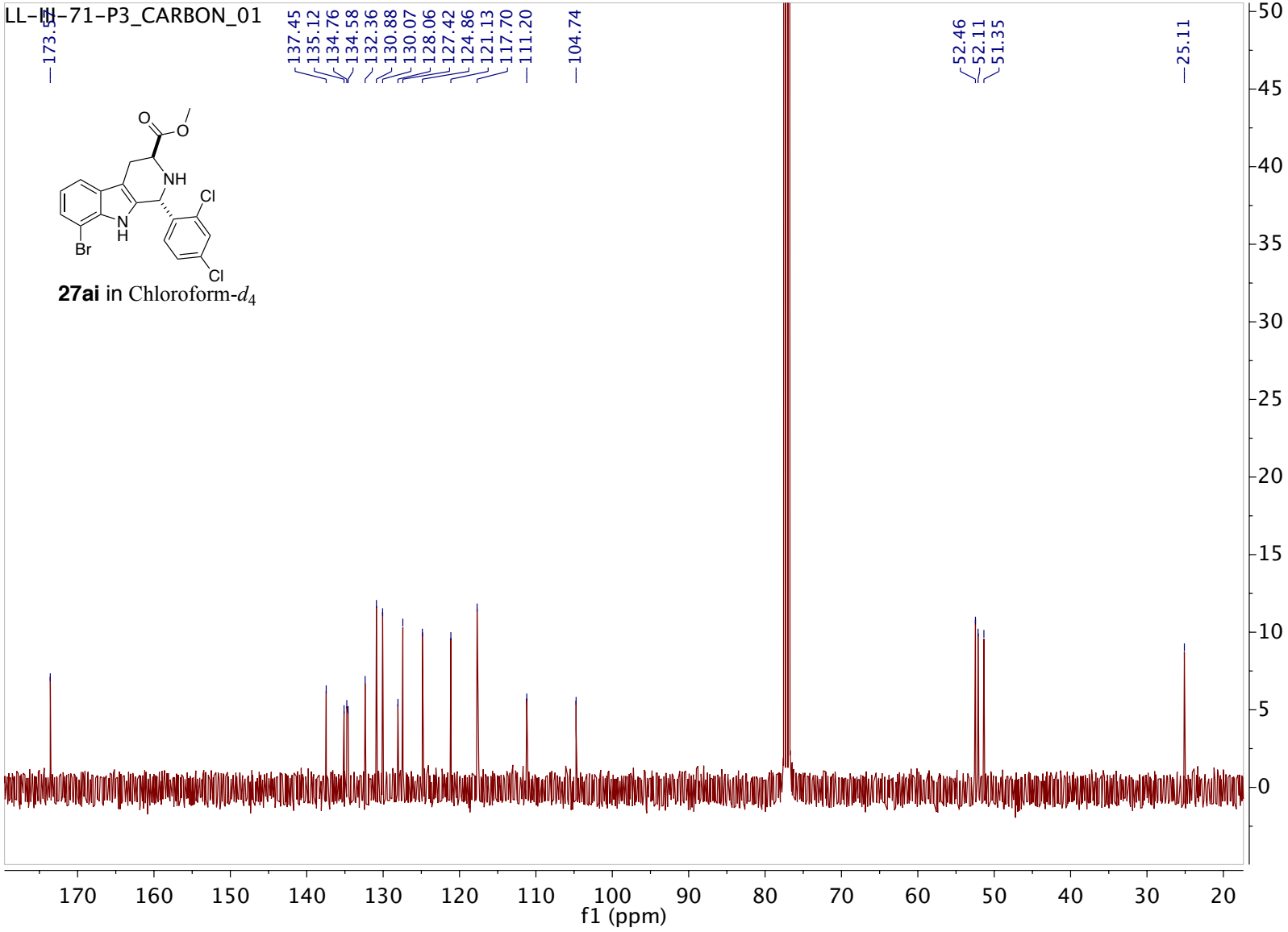
LL-IH-71-P3_CARBON_01
173.53
137.45
135.12
134.76
134.58
132.36
130.88
130.07
128.06
127.42
124.86
121.13
117.70
111.20
104.74
52.46
52.11
51.35
25.11
O
O
NH
Cl
N
H
Br
Cl
27ai in Chloroform-d_4
50
45
40
35
30
25
20
15
10
5
0
170
160
150
140
130
120
110
100
90
80
70
60
50
40
30
20
f1 (ppm)

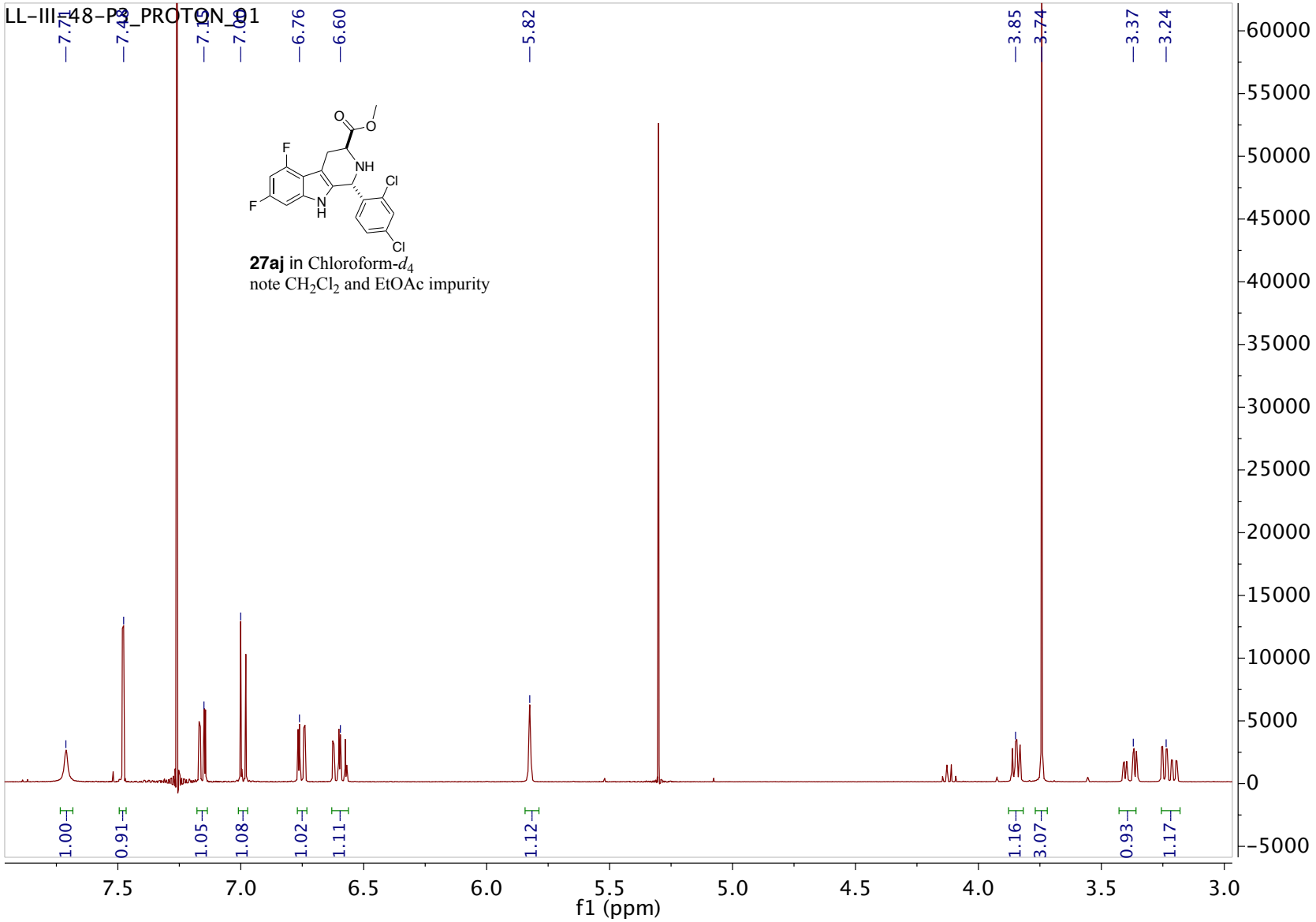
LL-III-48-P3_PROTON_01
7.71
7.43
7.14
7.00
6.76
6.60
5.82
3.85
3.74
3.37
3.24
O
O
F
NH
Cl
F
N
H
Cl
27aj in Chloroform-d4
note CH2Cl2 and EtOAc impurity
1.00
0.91
1.05
1.08
1.02
1.11
1.12
1.16
3.07
0.93
1.17
60000
55000
50000
45000
40000
35000
30000
25000
20000
15000
10000
5000
0
-5000
7.5
7.0
6.5
6.0
5.5
5.0
4.5
4.0
3.5
3.0
f1 (ppm)

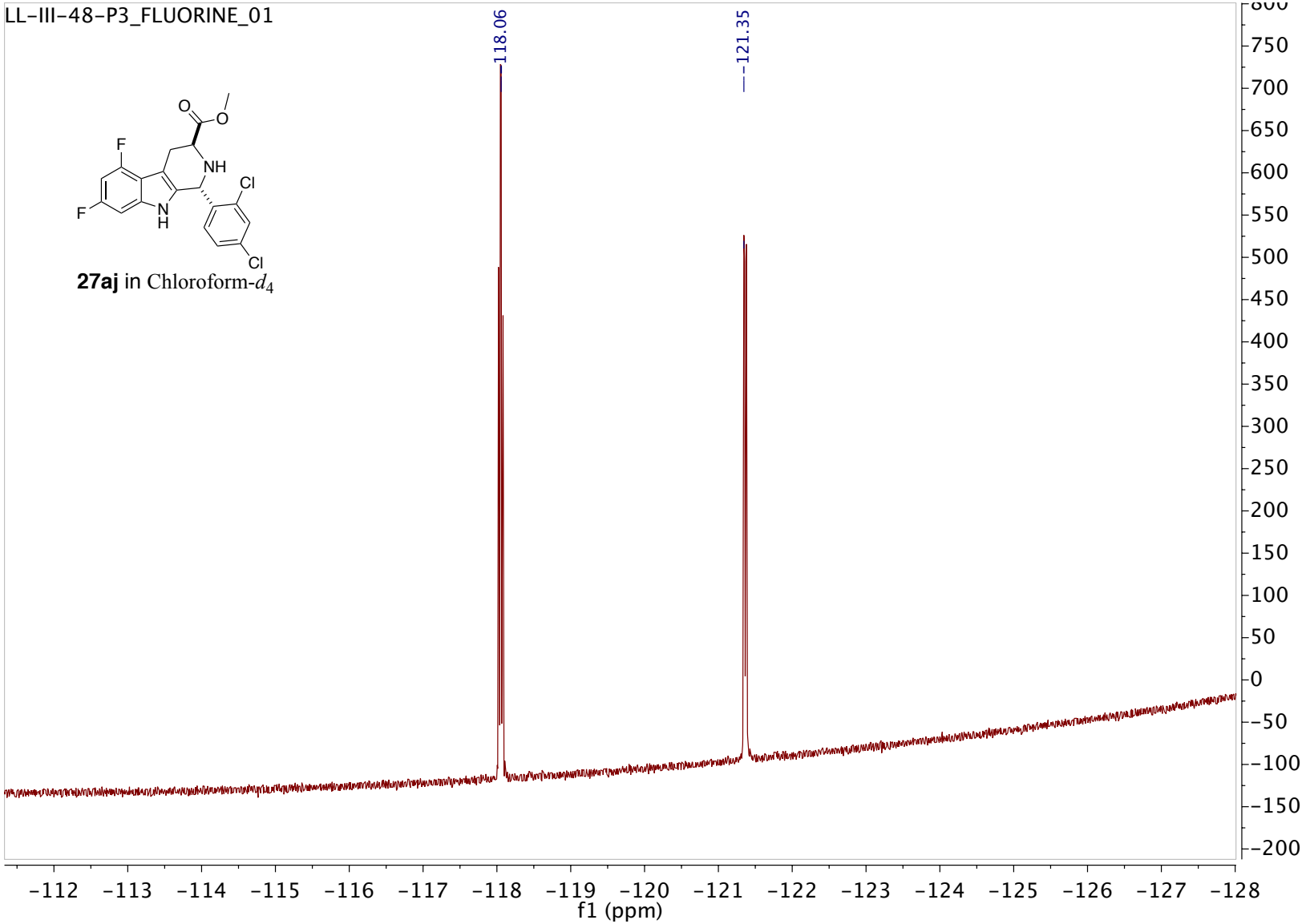
LL-III-48-P3_FLUORINE_01
118.06
121.35
O
O
F
NH
Cl
F
N
H
Cl
27aj in Chloroform-d4
750
700
650
600
550
500
450
400
350
300
250
200
150
100
50
0
-50
-100
-150
-200
-112 -113 -114 -115 -116 -117 -118 -119 -120 -121 -122 -123 -124 -125 -126 -127 -128
f1 (ppm)

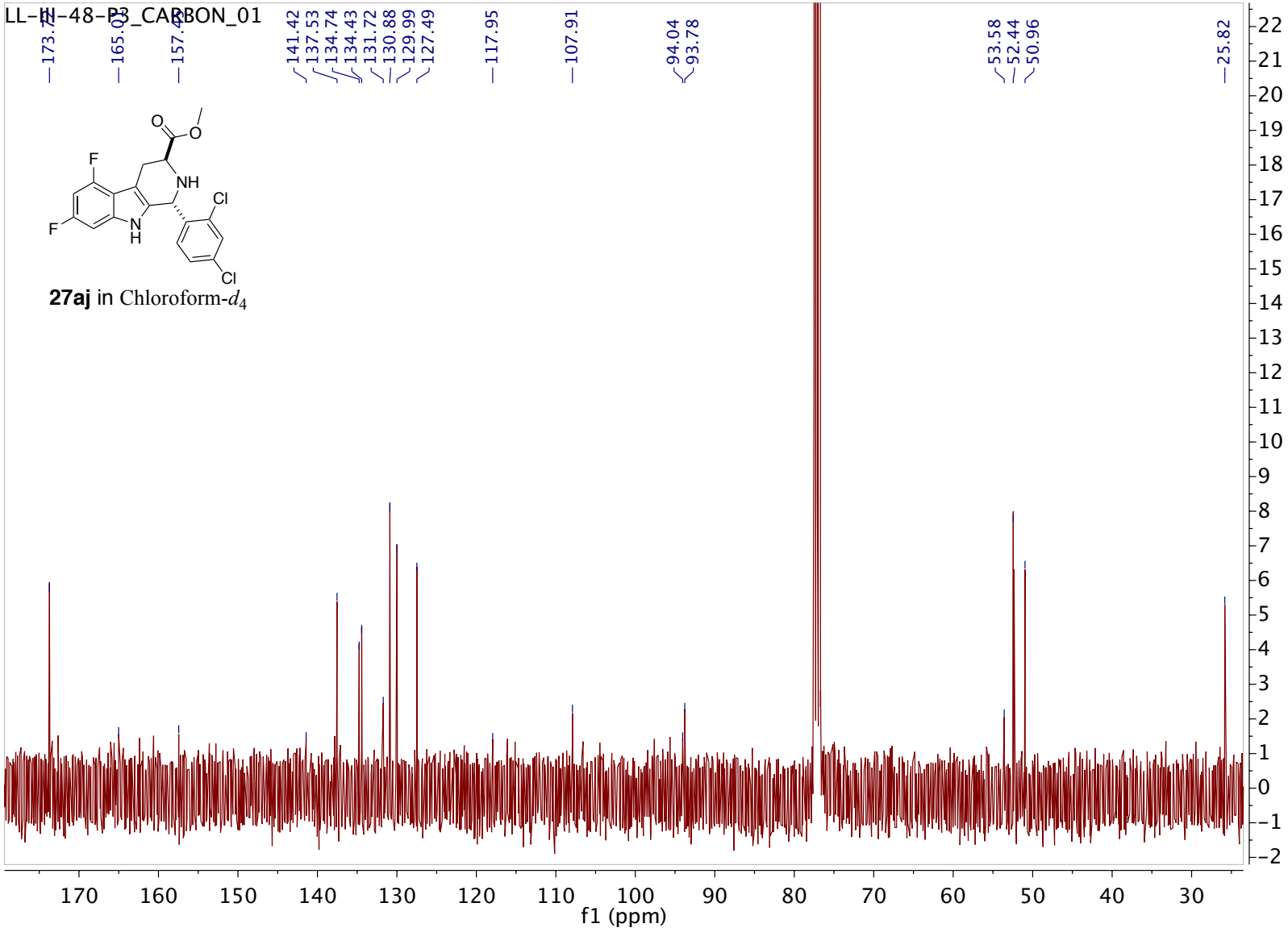
LL-IN-48-P3_CARBON_01
173.72
165.03
157.43
141.42
137.53
134.74
134.43
131.72
130.88
129.99
127.49
117.95
107.91
94.04
93.78
53.58
52.44
50.96
25.82
O
O
F
NH
Cl
F
N
H
Cl
27aj in Chloroform-d4
f1 (ppm)

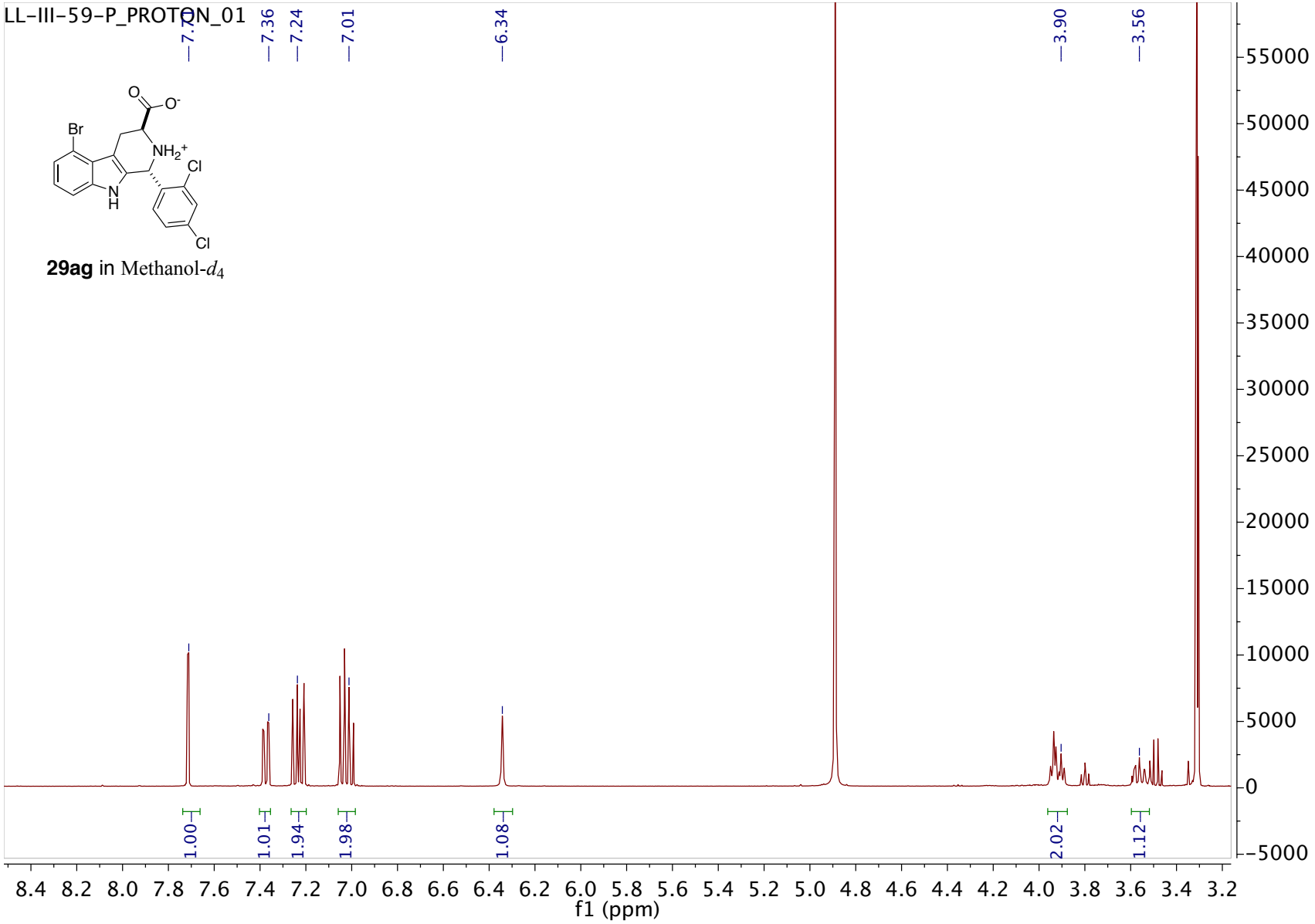
LL-III-59-P_PROTON_01
7.36
7.24
7.01
6.34
3.90
3.56
Br
O
O-
NH2+
Cl
N
H
Cl
29ag in Methanol-d4
55000
50000
45000
40000
35000
30000
25000
20000
15000
10000
5000
0
-5000
1.00
1.01
1.94
1.98
1.08
2.02
1.12
8.4 8.2 8.0 7.8 7.6 7.4 7.2 7.0 6.8 6.6 6.4 6.2 6.0 5.8 5.6 5.4 5.2 5.0 4.8 4.6 4.4 4.2 4.0 3.8 3.6 3.4 3.2
f1 (ppm)

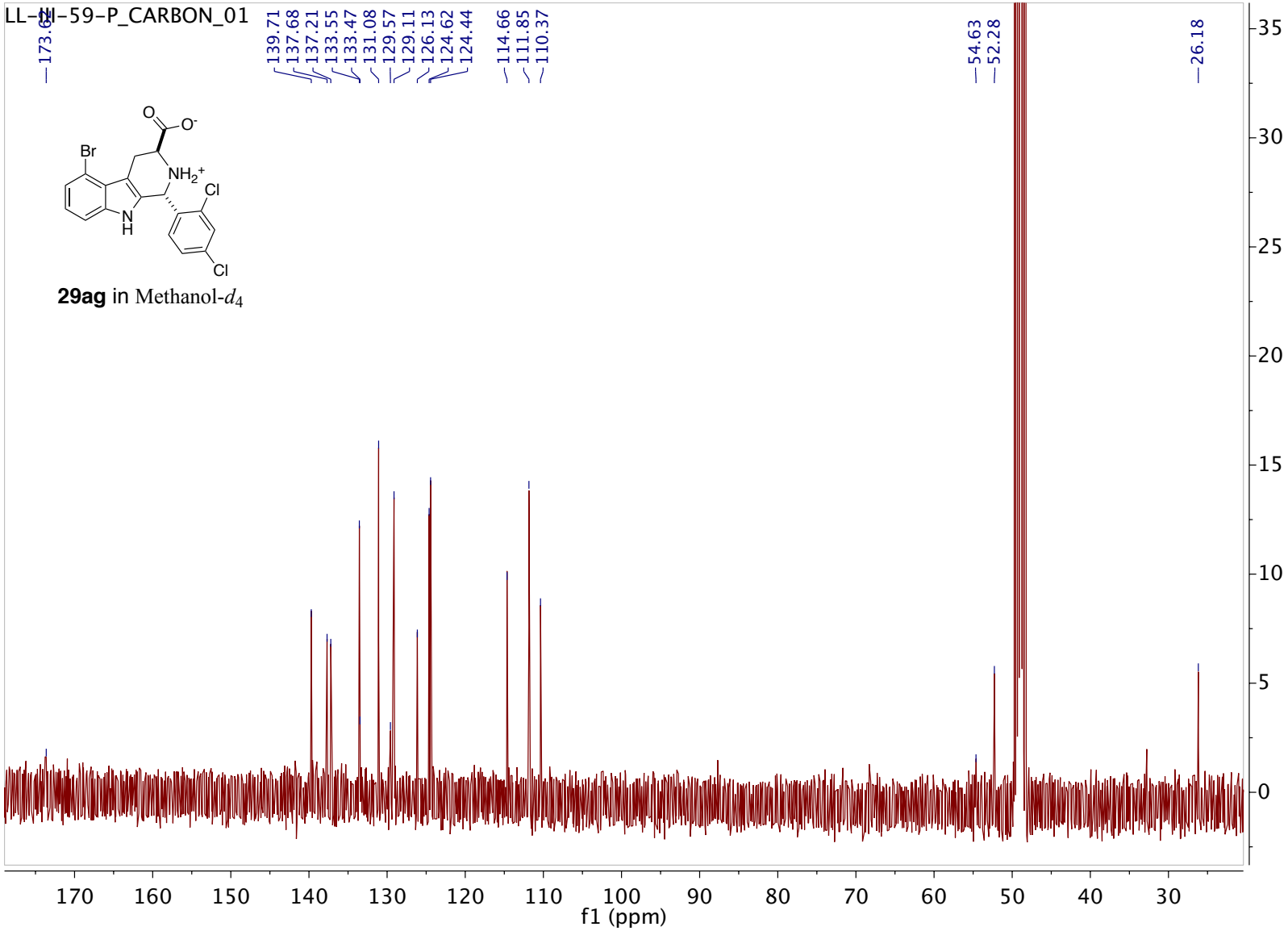
LL-NI-59-P_CARBON_01
173.62
139.71
137.68
137.21
133.55
133.47
131.08
129.57
129.11
126.13
124.62
124.44
114.66
111.85
110.37
54.63
52.28
26.18
Br
O
O-
NH2+
Cl
N
H
Cl
29ag in Methanol-d4
35
30
25
20
15
10
5
0
170
160
150
140
130
120
110
100
90
80
70
60
50
40
30
f1 (ppm)

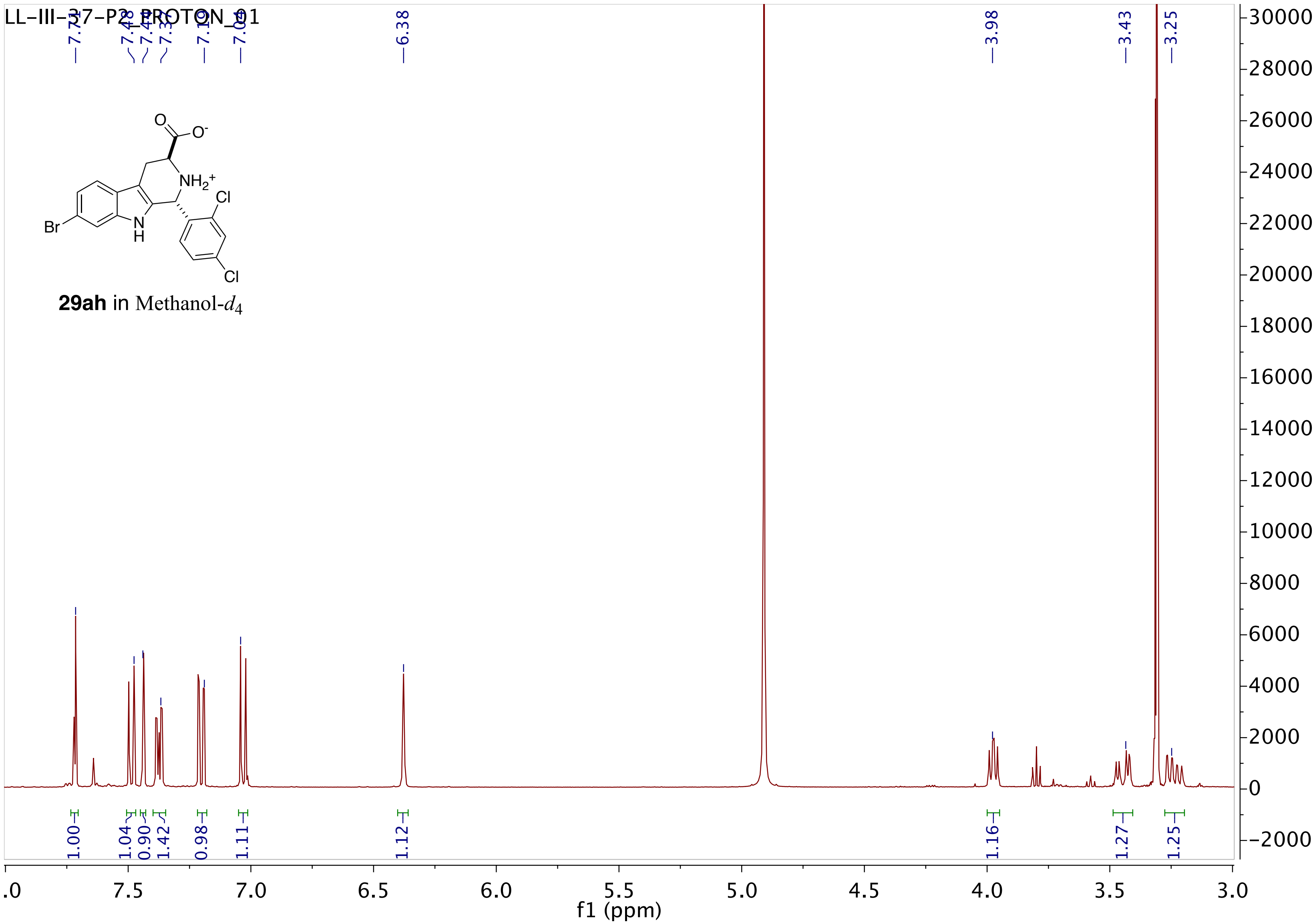
LL-III-37-P2_PROTON_01
6.38
3.98
3.43
3.25
O
O-
NH2+
Cl
Br
N
H
Cl
29ah in Methanol-d4
1.00
1.04
0.90
1.42
0.98
1.11
1.12
1.16
1.27
1.25
30000
28000
26000
24000
22000
20000
18000
16000
14000
12000
10000
8000
6000
4000
2000
0
-2000
7.5
7.0
6.5
6.0
5.5
5.0
4.5
4.0
3.5
3.0
f1 (ppm)

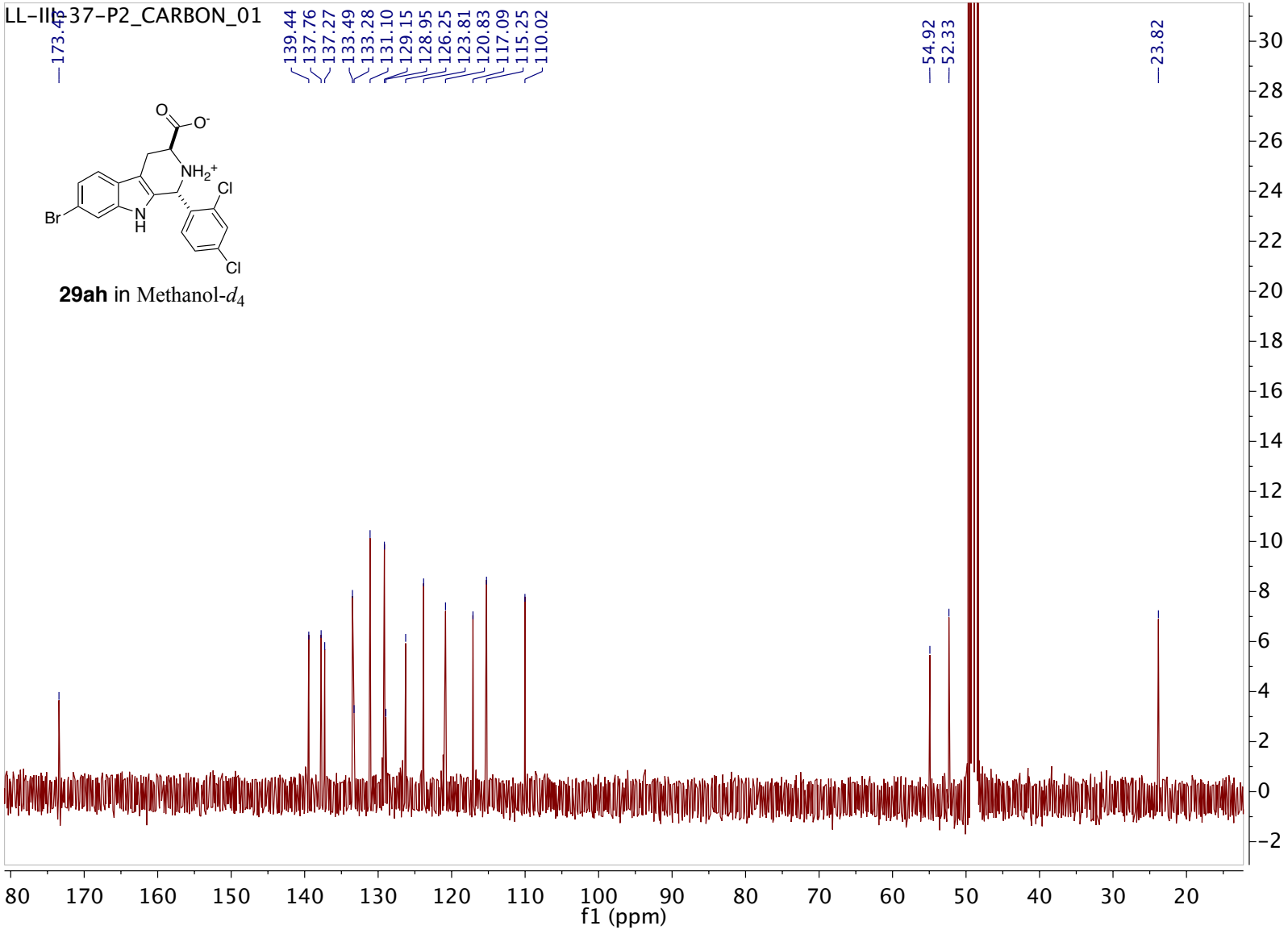
LL-III-37-P2_CARBON_01
173.47
139.44
137.76
137.27
133.49
133.28
131.10
129.15
128.95
126.25
123.81
120.83
117.09
115.25
110.02
54.92
52.33
23.82
O
O-
NH2+
Cl
Br
N
H
Cl
29ah in Methanol-d4
f1 (ppm)

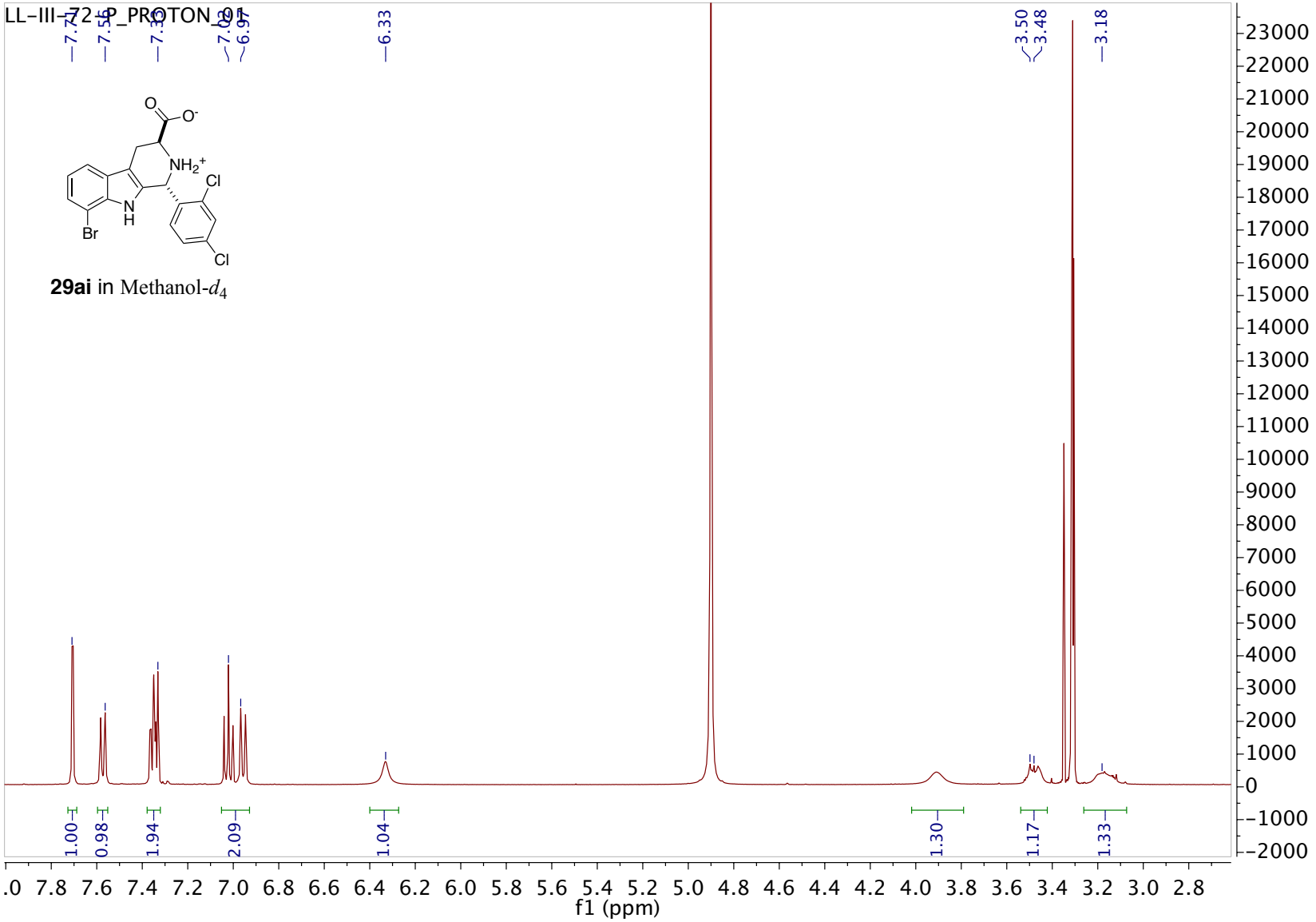
LL-III-72-P_PROTON_01
7.71
7.56
7.43
7.02
6.97
6.33
3.50
3.48
3.18
O
O-
NH2+
Cl
N
H
Br
Cl
29ai in Methanol-d4
1.00
0.98
1.94
2.09
1.04
1.30
1.17
1.33
23000
22000
21000
20000
19000
18000
17000
16000
15000
14000
13000
12000
11000
10000
9000
8000
7000
6000
5000
4000
3000
2000
1000
0
-1000
-2000
.0 7.8 7.6 7.4 7.2 7.0 6.8 6.6 6.4 6.2 6.0 5.8 5.6 5.4 5.2 5.0 4.8 4.6 4.4 4.2 4.0 3.8 3.6 3.4 3.2 3.0 2.8
f1 (ppm)

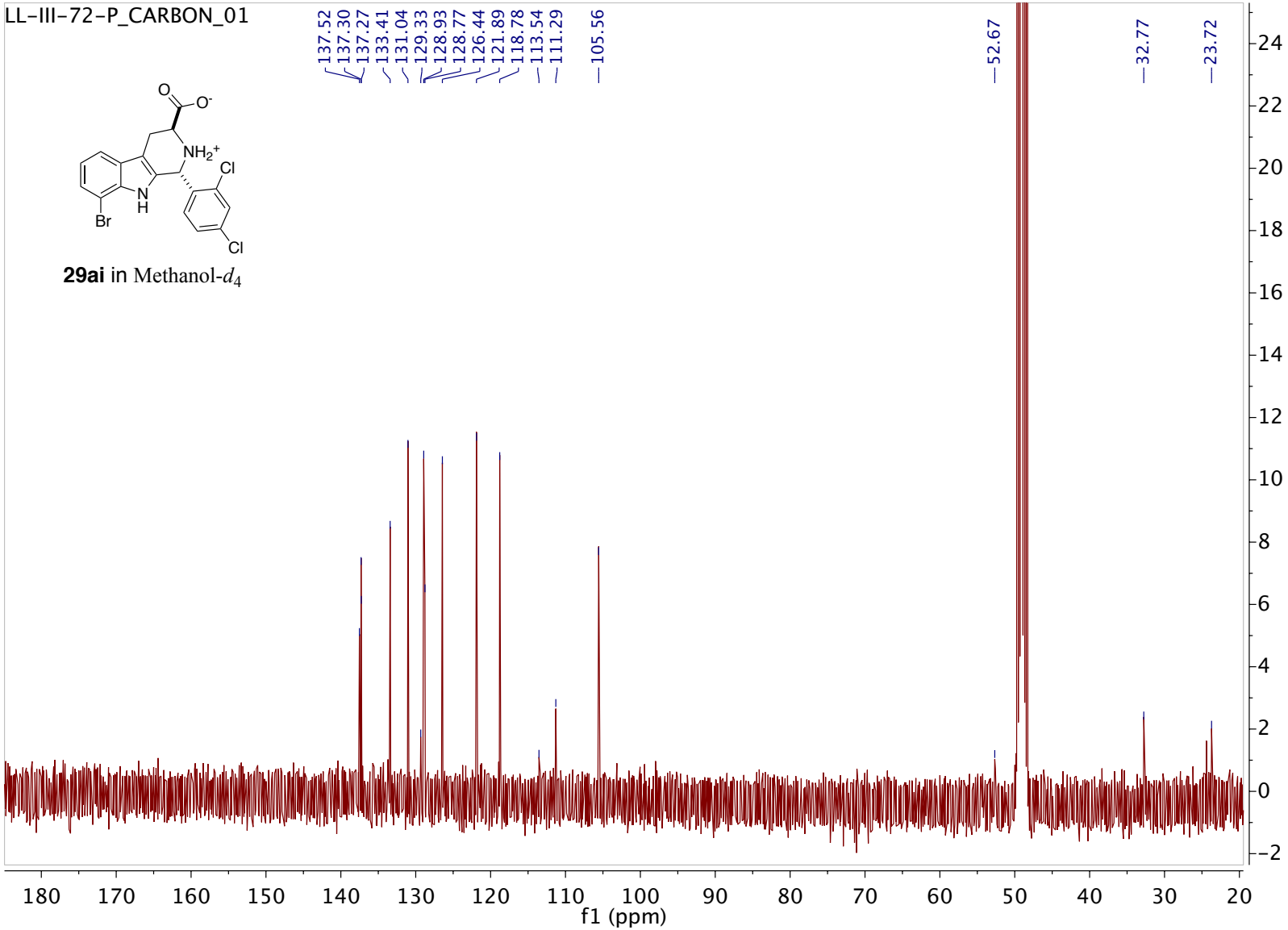
LL-III-72-P_CARBON_01
137.52
137.30
137.27
133.41
131.04
129.33
128.93
128.77
126.44
121.89
118.78
113.54
111.29
105.56
52.67
32.77
23.72
O
O-
NH2+
Cl
N
H
Br
Cl
29ai in Methanol-d4
f1 (ppm)

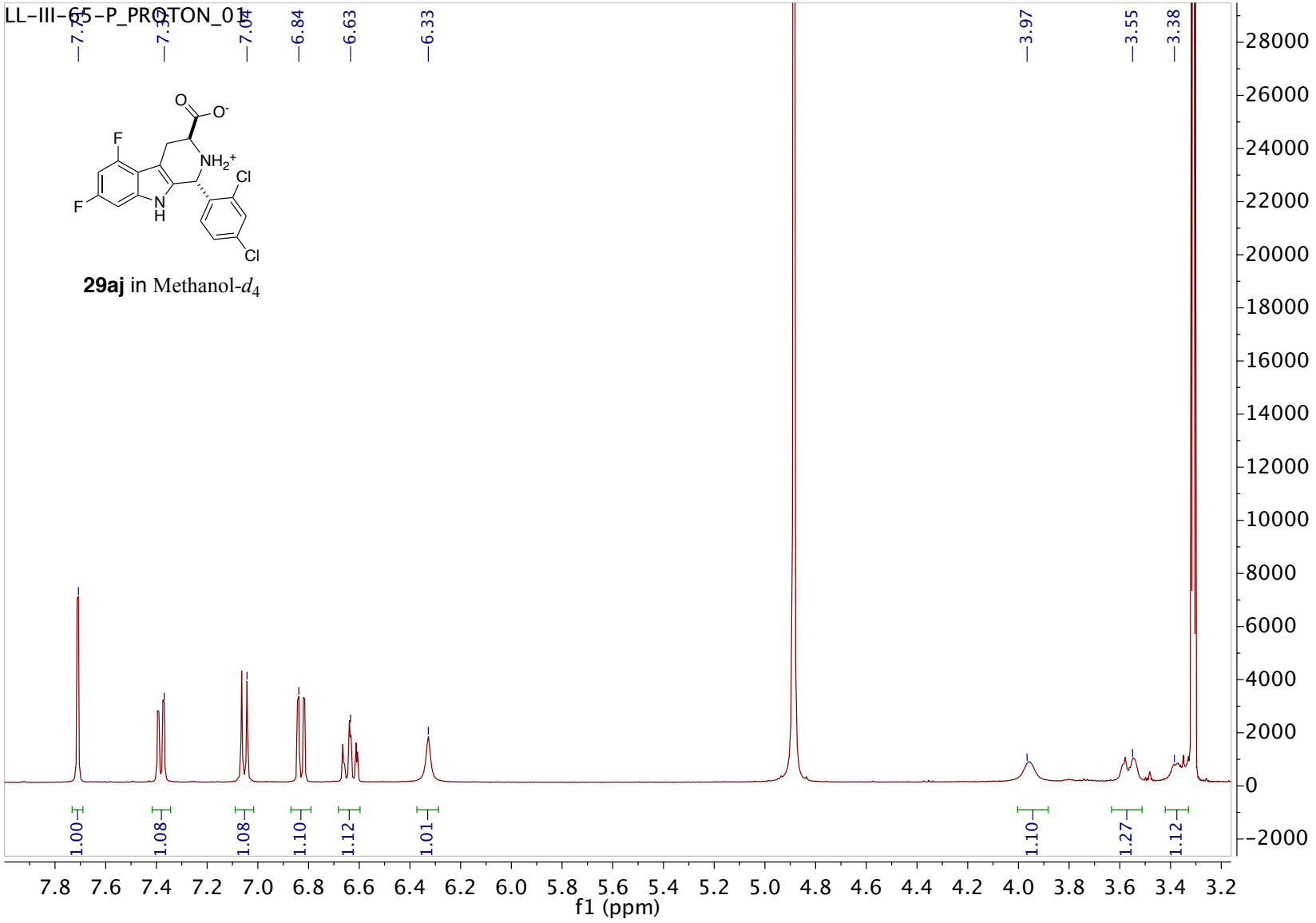

29aj in Methanol-d_4

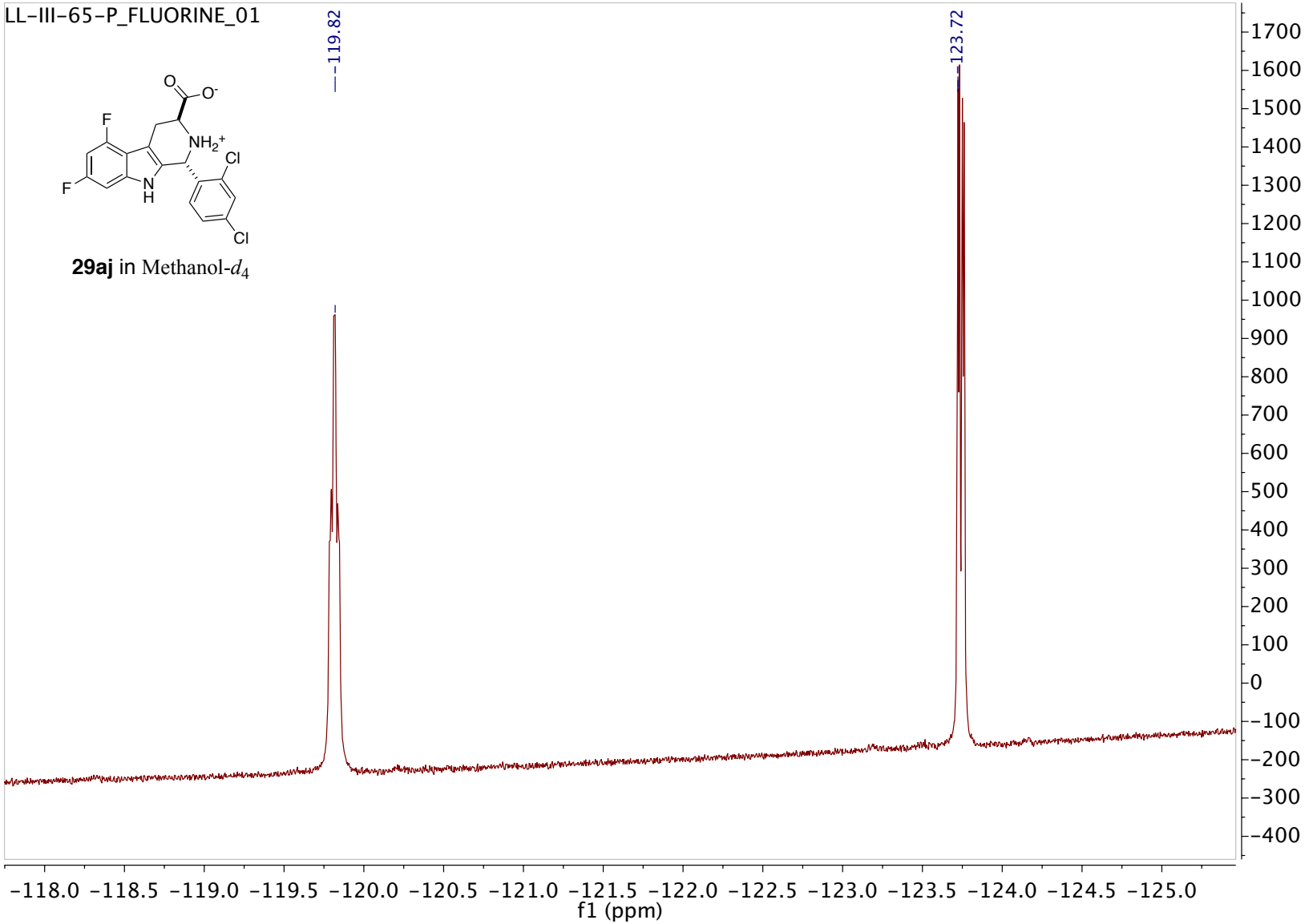
LL-III-65-P_FLUORINE_01
-119.82
-123.72
F
O
O-
NH2+
Cl
F
N
H
Cl
29aj in Methanol-d4
1700
1600
1500
1400
1300
1200
1100
1000
900
800
700
600
500
400
300
200
100
0
-100
-200
-300
-400
-118.0 -118.5 -119.0 -119.5 -120.0 -120.5 -121.0 -121.5 -122.0 -122.5 -123.0 -123.5 -124.0 -124.5 -125.0
f1 (ppm)

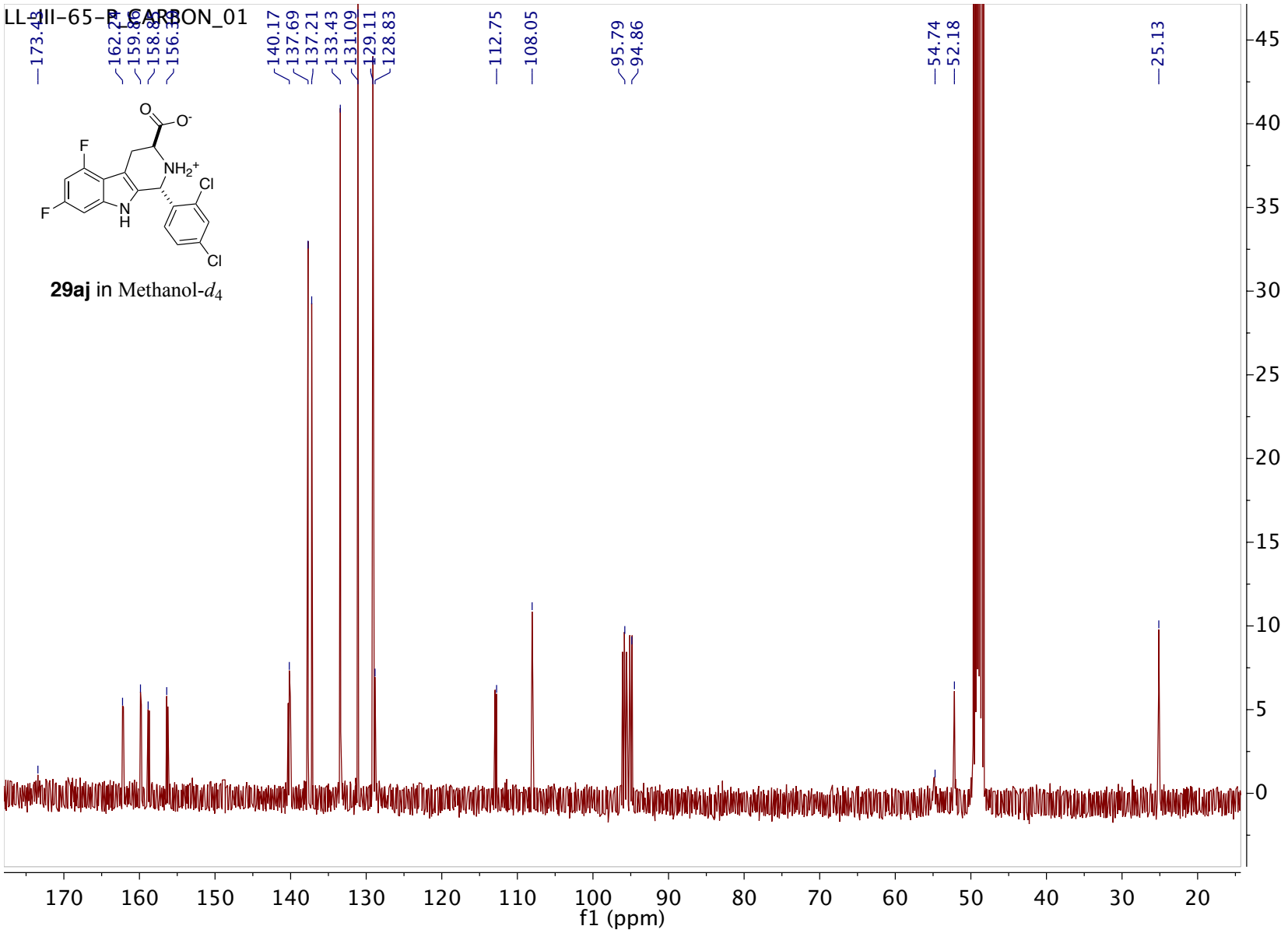
LL-III-65-P CARBON_01
173.41
162.78
159.89
158.89
156.89
140.17
137.69
137.21
133.43
131.09
129.11
128.83
112.75
108.05
95.79
94.86
54.74
52.18
25.13
F
F
O
O-
NH2+
N
H
Cl
Cl
29aj in Methanol-d4
45
40
35
30
25
20
15
10
5
0
170
160
150
140
130
120
110
100
90
80
70
60
50
40
30
20
f1 (ppm)